A study of langmuir-blodgett films of valinomycin

Howarth, Vaughan Antony

A STUDY OF LANGMUIR-BLODGETT
FILMS OF VALINOMYCIN

BY

VAUGHAN ANTONY HOWARTH
B.Sc., M.Sc.

A thesis submitted for the Degree of
Doctor of Philosophy in the
University of Durham

School of Engineering and Applied Science
University of Durham
September 1989

2 1 DEC 1990

This thesis is dedicated to my gran

DECLARATION

I hereby declare that the work reported in this thesis has not been previously submitted for any degree, and is not being currently submitted in candidature for any other degree.

Signed .

The work reported in this thesis was carried out by the candidate.

Si

Signed ..

STATEMENT OF COPYRIGHT

ACKNOWLEDGEMENTS

ABSTRACT

The deposition and characterisation of Langmuir-Blodgett (LB) films containing the ionophore valinomycin are described. In particular, the thesis concentrates on two specific mixed LB systems incorporating the ionophore, namely, arachidic acid/valinomycin and L-α-phosphatidic acid dipalmitoyl (DPPA)/valinomycin. The extremely sensitive spectroscopic technique of attenuated total reflection (ATR) Fourier transform infrared (FTRIR) spectroscopy is used to investigate the interaction of these ultra-thin LB structures with aqueous solutions containing potassium ions.

It is shown that LB layers of pure valinomycin do not complex with potassium ions and that, in order for complexation to occur, the ionophore must be mixed with a secondary component. The formation of the valinomycin-potassium (VM/K^+) complex in the arachidic acid/valinomycin system is demonstrated and the effects of the mole-fraction of arachidic acid, and of the potassium ion concentration upon complexation are described. The IR studies also reveal profound structural changes in the fatty acid matrix upon complexation, and the important result that dissociation of the VM/K^+ complex does not occur in this mixed system.

However, it is shown that if the fatty acid molecule is replaced by the phospholipid molecule, DPPA, then both formation and dissociation of the complex occur. The results, however, indicate that this system is unstable with loss of the LB film into the aqueous solution during immersion. A number of attempts to eliminate this problem are described.

The fabrication and characterisation of ion-selective-field-effect transistors (ISFETs) are also reported. One of the aims of the research is to develop a potassium-ion sensor, and with this in mind, the deposition of LB films onto the gate surface of the ISFET is demonstrated. The K^+-response of the LB film coated devices is described and the results interpreted in terms of the IR evidence.

CONTENTS

CHAPTER 1

INTRODUCTION

Over the past fifteen years, there has been a growing awareness of the potential for integrated circuit technology to provide a new generation of microsize sensors for the measurement of a variety of physical parameters. The possibility of integrating one or more sensors with the appropriate signal-processing circuitry on the same silicon chip will provide microtransducers having unique advantages over their conventional counterparts, particularly, with regard to size. In the field of electrochemical analysis, the integration of semiconductor devices with electrochemically active films makes possible chemical micro-transducers capable of challenging presently-used electrode systems, such as the ion-selective electrode. The most popular semiconductor device utilised for such applications has been the metal-insulator-semiconductor (MIS) transistor which has been modified by substituting an electrochemically active material for the gate metal, thus forming an ion-sensitive (chemical sensitive) field-effect transistor ISFET (ChemFET).

The first report of an active, ion-sensing microelectronic device was the description by Bergveld in 1970 [1,2] of an FET structure in which the SiO_2 gate dielectric was found to be responsive to both pH and sodium ions. Since then a variety of ISFETs have been fabricated with inorganic gate films including; sodium aluminosilicate glasses (for Na^+ devices) [3], silver halide films (for Ag^+, Br^- and Cl^- devices) [4] and lanthanum fluoride (for F^- ions) [5]. Poor selectivity is generally obtained for such devices, with interference from ions other than the sensed ion. However, very high specificity can be achieved using ion-exchanging materials supported in inert polymeric membranes. Such a device was first reported by Moss et al [6] in 1975, who incorporated the ionophore into a plasticised polymer matrix (PVC) forming a highly specific K^+-responsive sensor.

Valinomycin is a membrane-active cyclodepsipeptide that can selectively com-

plex with and transport potassium ions across both biological and synthetic membranes [7,8]. The Langmuir-Blodgett (LB) technique is a method for producing uniform, high quality organic thin films, and can be used to create novel structures with precisely defined symmetry. In the LB technique the substrate is passed through a water surface on which a monolayer of an organic material is floating. In general, a monomolecular layer of the organic is deposited onto the substrate with each traversal through the air-water interface. The LB film can therefore be built up by repeatedly depositing a series of monolayers. The physics of LB films [9] and their potential applications [10,11] are the subject of extensive literature reviews.

Artificial membrane structures can be conveniently fabricated on a suitable substrate using the LB technique. The classical fatty acids are examples of LB film forming materials and they can be used to represent the phospholipid molecules of the biological membrane. The incorporation of valinomycin into such an LB system then acts as a model for the natural environment of the ionophore. The LB technique provides an elegant method for engineering this molecular environment. Although this work concentrates on the potassium sensing application of valinomycin containing LB films it is possible to envisage more exotic LB films incorporating antibody/antigen materials and highly specific and reversible receptor proteins.

This thesis reports on the use of valinomycin-containing LB films as potassium ion sensors. The principal aims of the present work are summarised as follows:

(1) To demonstrate the feasibility of the deposition of LB films onto the gate surface of mounted ISFET structures.

(2) To investigate the interaction of valinomycin containing LB films with aqueous potassium solutions.

(3) To study the potential of these films for potassium ion sensing applications.

Chapter 2 introduces the ionophoric material valinomycin and covers the structure of valinomycin and the conformational changes occurring upon com-

plexation with a potassium ion. The environment of the biological membrane is also presented along with the concept of carrier (valinomycin)- mediated potassium ion transport across such membranes. Chapter 3 deals with the theoretical background of the ISFET as an extension of first-order MOSFET theory. The operation of the ISFET, based on the site dissociation theory is also discussed. In chapter 4 the various experimental techniques used during the course of this work are described. The theoretical background of each technique is presented and detailed descriptions are given of the equipment used and the procedures adopted.

Chapter 5 contains the results of experiments on LB film-coated ISFETs. Chapter 6 deals with the deposition and structural characterisation of valinomycin containing LB films using the techniques of infrared spectroscopy, electron diffraction, X-ray diffraction and ellipsometry. Chapter 7 contains a detailed examination of the interaction of the films described in chapter 6 with potassium containing solutions. Two systems are investigated: valinomycin/arachidic acid and valinomycin/phospholipid mixed LB layers. The structural changes upon complexation in these model membranes are discussed. Finally, chapter 8, summarises all the results, and suggests the direction in which future research should be aimed.

CHAPTER 2

VALINOMYCIN

2.0 INTRODUCTION

The Langmuir-Blodgett films described in this thesis are based on the membrane active antibiotic called valinomycin. This chapter introduces this material which, because of its ability to complex with alkali metal ions, has become an important model compound for studying ion selective transport in membranes. Section 2.1 concerns the structure of valinomycin, the conformational changes in structure upon complexation and how these changes may be observed. Section 2.2 introduces the biological membrane, the natural environment for valinomycin and section 2.3 describes the function of valinomycin in this environment and the concept of carrier-mediated ion transport.

2.1 THE STRUCTURE OF VALINOMYCIN

The antibiotic valinomycin, first isolated in 1955 by Brockmann *et al* [1] from the bacteria Streptomyces Fulvissimus, is known to complex with the alkali cations selectively in the order $Rb^+ > K^+ > Cs^+ > Na^+ > Li^+$ [2], and to facilitate the transport of alkali cations across mitochondrial membranes with the same selectively [3]. The conductance of lipid bilayers containing valinomycin is about 400 times greater for K^+ than for Na^+. Similar results have been obtained in model membrane systems. Early work on valinomycin and artificially synthesised analogues concluded that their antimicrobial activity, and effect on membrane permeability, were due to their unique molecular structure.

2.1.1 Uncomplexed conformation

Valinomycin is a 12-membered macrocyclic depsipeptide (cyclic dodecadepsipepitde) consisting of three units joined sequentially to form a ring. Each unit

4
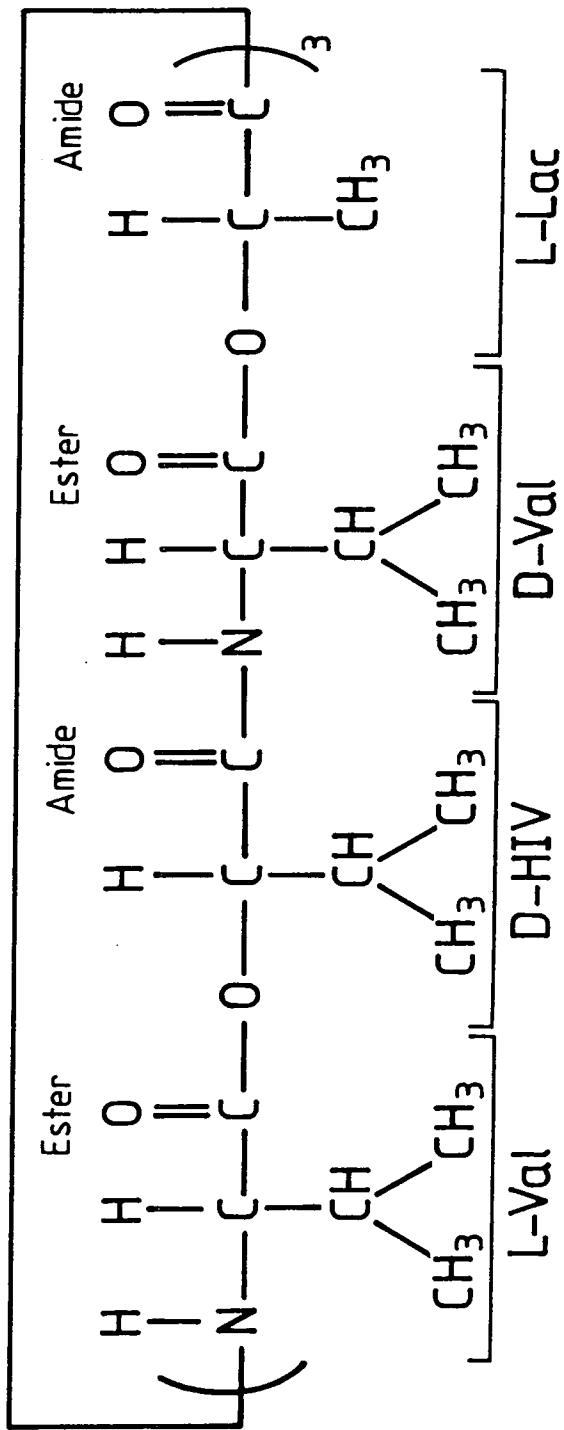
Figure 2.1 Primary structure of valinomycin showing the three peptide units and the alternating amide and ester linkages.
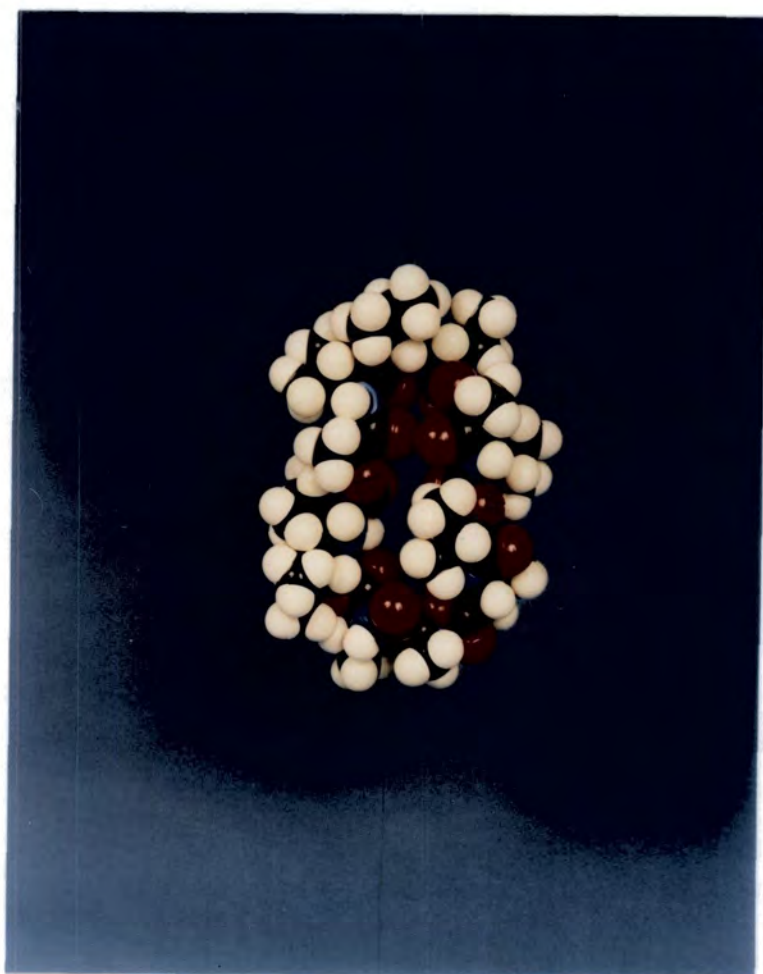
Figure 2.2 A photograph of a CPK model of valinomycin in its uncomplexed conformation (after ref. 6).
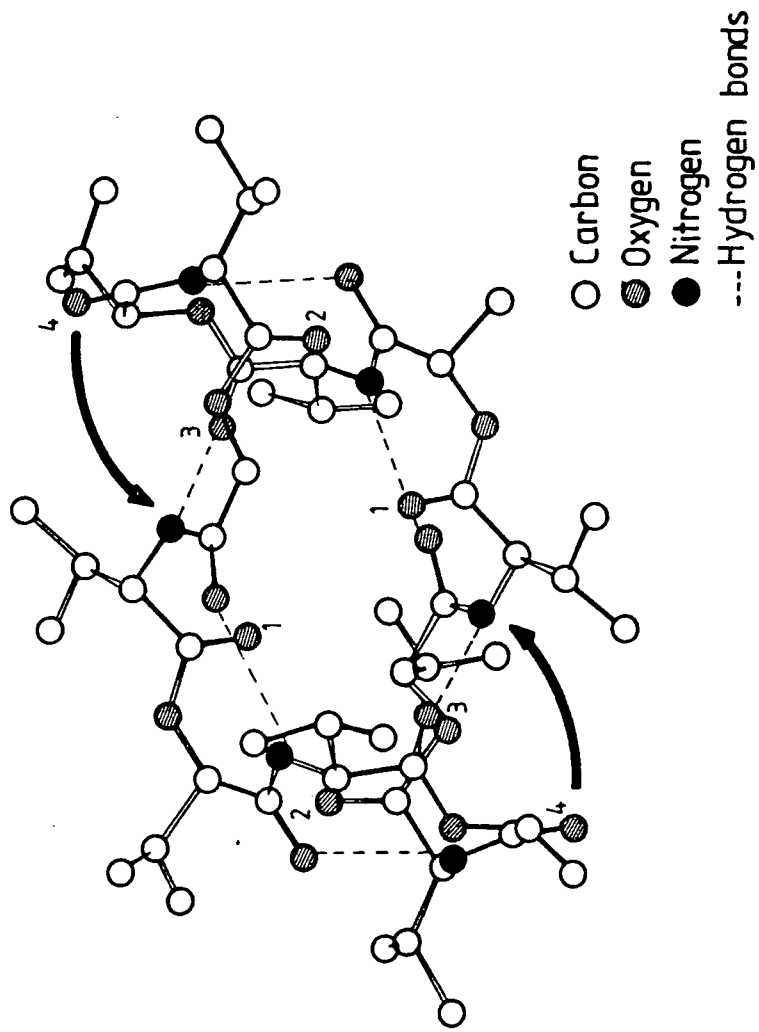
Figure 2.3 Structure of uncomplexed valinomycin crystallised from warm n-octane. Ester carbonyl oxygen pairs 1 and 2 are exposed, and pair 3 is hydrogen bonded and is replaced upon complexation by amide carbonyl pair 4.

consists of L-valine, L-lactic acid, D-valine and D-hydroxyisovaleric acid alternately joined by amide C=O and ester C=O linkages. The primary structure is shown in figure 2.1 and a photograph of this structure made from a CPK packing model is shown in figure 2.2. The ring shape is evident and the hole in the centre can be envisaged as accommodating the alkali metal ion. The ring diameter is important for the selectivity of the molecule. Work on valinomycin analogues [4], having larger rings (4 units), or smaller rings (2 units), has shown that they possess little antimicrobial activity or complexing ability. In the first case, the molecule becomes loose and unstable as a ring. In the second case, the ring is too small to accommodate the hydration shell of hydrated ions and too large to coordinate around the naked ion. The molecule has 12 polar C=O groups; of which there are six ester C=O groups and six amide C=O groups, and there are also six NH groups.

Smith et al [5] have examined the structure of crystalline uncomplexed valinomycin using X-rays and determined that the area of the molecule lies in the range 1.68 nm^2 to 1.88 nm^2. In addition, X-ray evidence [6] has revealed the complete structure of one form of valinomycin suggesting that, of the six ester C=O groups, two were hydrogen-bonded and the other four were free and highly mobile, and thus available to take part in complexation. Also all six NH groups are intra-molecularly hydrogen-bonded, four to amide C=O groups and two to the two ester C=O carbonyls. The structure is shown in figure 2.3.

An extensive Raman spectroscopic study of uncomplexed valinomycin in the solid state crystallised from a variety of polar and non-polar solvents has been carried out by Asher *et al* [7]. Their findings indicated that all their crystallised samples adopted the same structure as that proposed by Smith (i.e. crystallised from warm n-octane), except for one, crystallised from o-dichlorobenzene. This lacked any strongly hydrogen bonded ester C=O groups, a conformation of valinomycin only previously observed in solution. Complementary Raman spectroscopic studies of valinomycin in polar and non-polar solvents [8] has revealed a number
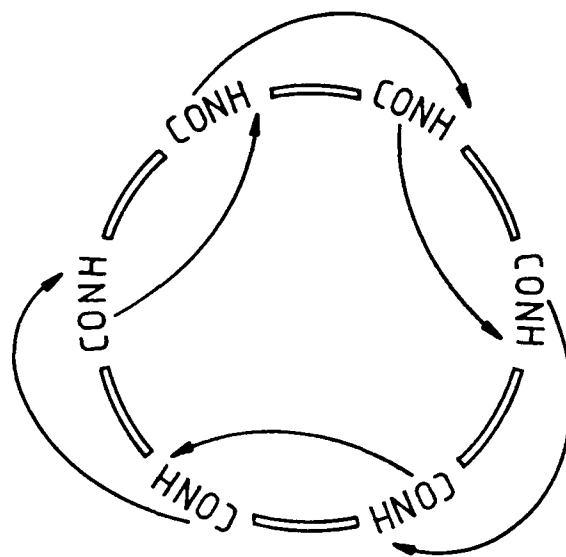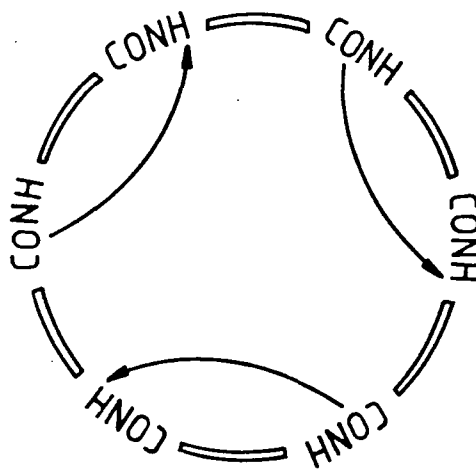
Figure 2.4 Hydrogen bonding schemes in (a) non-polar solvents, and (b) polar solvents.
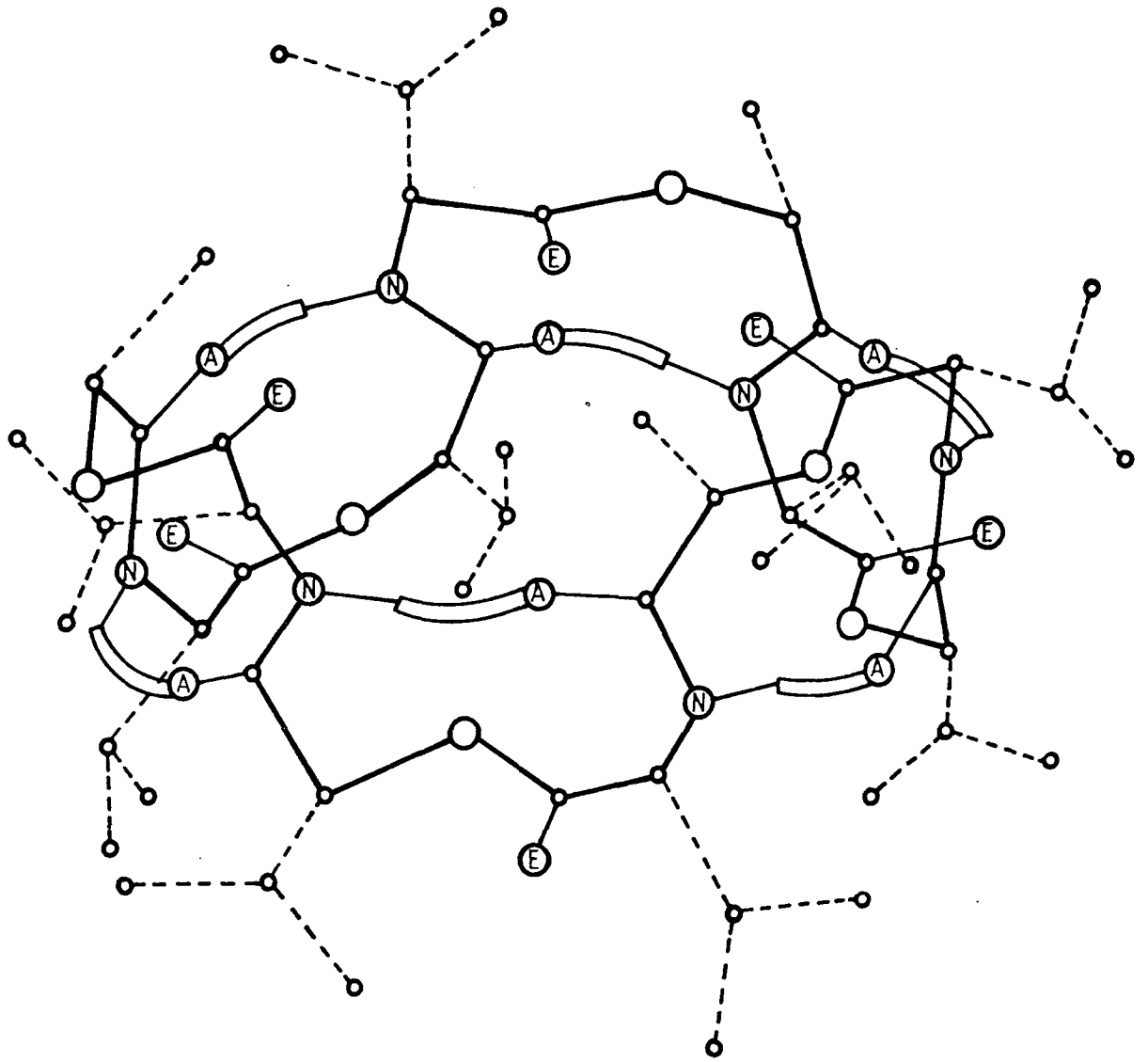
Conformation of valinomycin in nonpolar solvents.

o   Carbon

O   Oxygen

Ⓝ   Nitrogen

▭   H – bond

Ⓔ   Ester

Ⓐ   Amide Carbonyl

Figure 2.5 Structure of uncomplexed valinomycin in non-polar solvents showing the bracelet configuration of the hydrogen bonds.
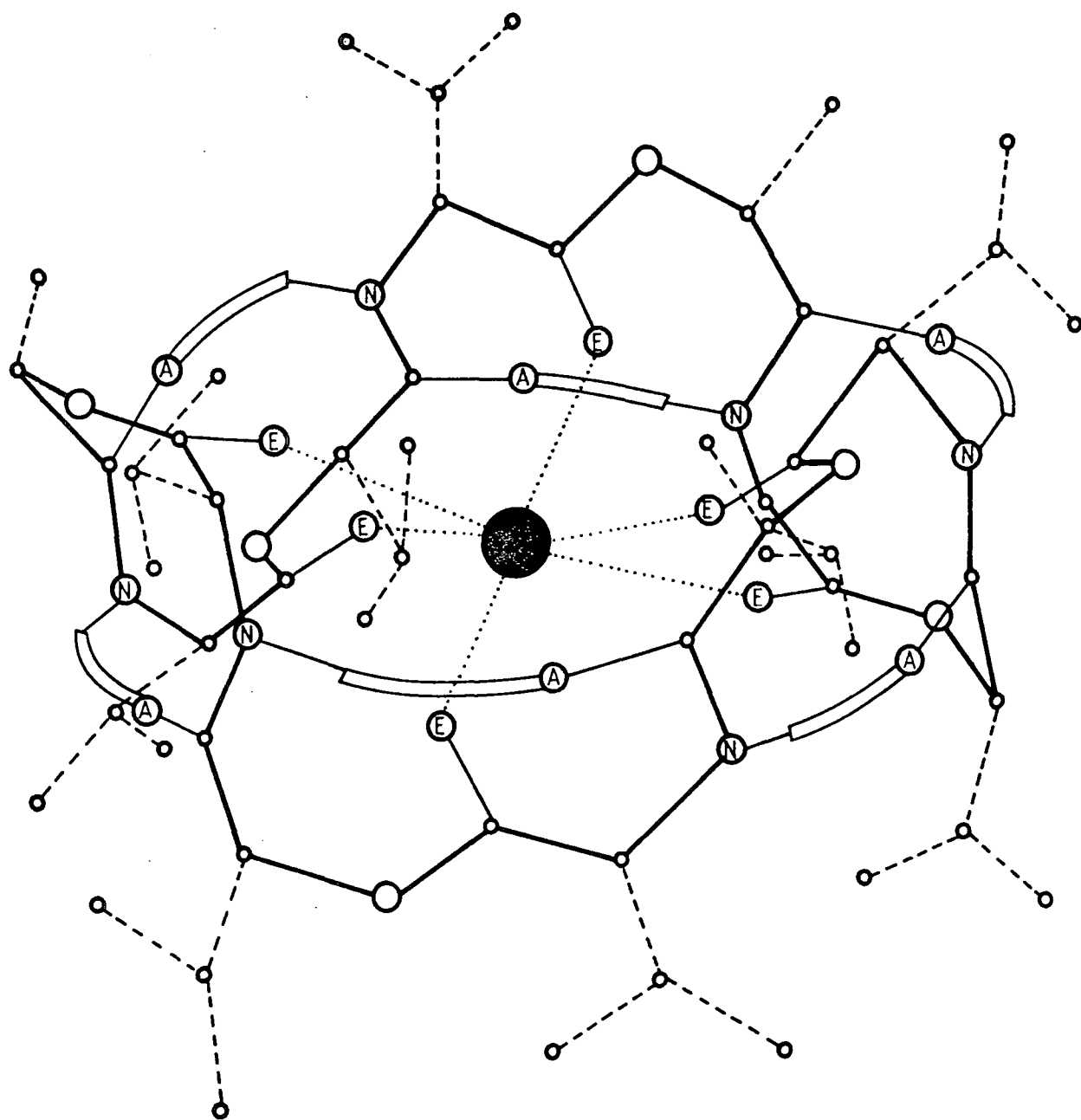
Conformation of the K⁺ complex of Valinomycin.

o   Carbon   ▭ H-bond

O   Oxygen   Ⓔ Ester

Ⓝ   Nitrogen   Ⓐ Amide Carbonyl

●   Potassium
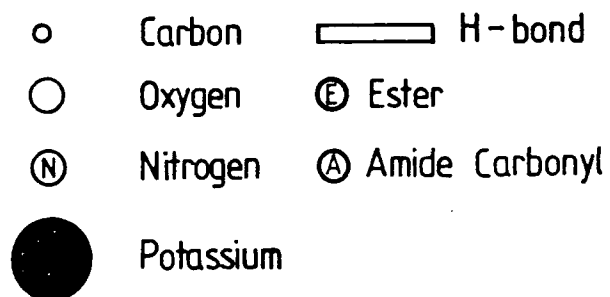
Figure 2.6 K⁺-complex conformation of valinomycin.

of different conformations. The evidence supports the co-existence of two forms of valinomycin in solution, the predominance of one over the other depending on the polarity of the solvent. For example; in carbon tetrachloride (CCl_4), a non-polar medium, all the amide groupings simultaneously participate in the formation of six intra-molecular hydrogen bonds (figure 2.4a). This leads to the conformation illustrated in figure 2.5, known as the "bracelet" configuration. Each hydrogen bond leads to the formation of a stabilising ten membered (ten atom) ring. Six rings are formed which equatorially circle the perimeter of the molecule giving considerable rigidity to the conformation. In low polarity solvents, the conformation described above is in equilibrium with one in which there are only three hydrogen-bonded amide groupings. The remaining NH groups probably prefer to associate with the solvent molecules. This hydrogen bonding scheme is also shown in figure 2.4b.

2.1.2 Complexed conformation

Newpert-Laves et al [9] have determined the dimensions of the unit cell for complexed valinomycin and have calculated from these data an area for the molecule of $1.45\,nm^2$. Thus the change in conformation as a result of complexation produces a change in molecular area from $1.88\,nm^2$ to $1.45\,nm^2$. The question of whether this change may be observed on a macroscopic scale using a surface pressure versus area isotherm will be addressed in a later chapter.

Analogous infra-red and Raman spectroscopic studies have been performed on the valinomycin-K^+ complex in polar and non-polar solutions [10]. In all cases, the results are consistent with a conformational reforming of the molecule on complexation. The hydrogen-bonded, stabilised framework (of the "bracelet" configuration in non-polar solutions) is retained. The ester carbonyls are oriented within the ring and are coordinated with the cation via ion-dipole interactions. The complexed conformation of valinomycin is represented schematically in figure 2.6 and a photograph of a CPK model is shown in figure 2.7. The potassium ion,

6
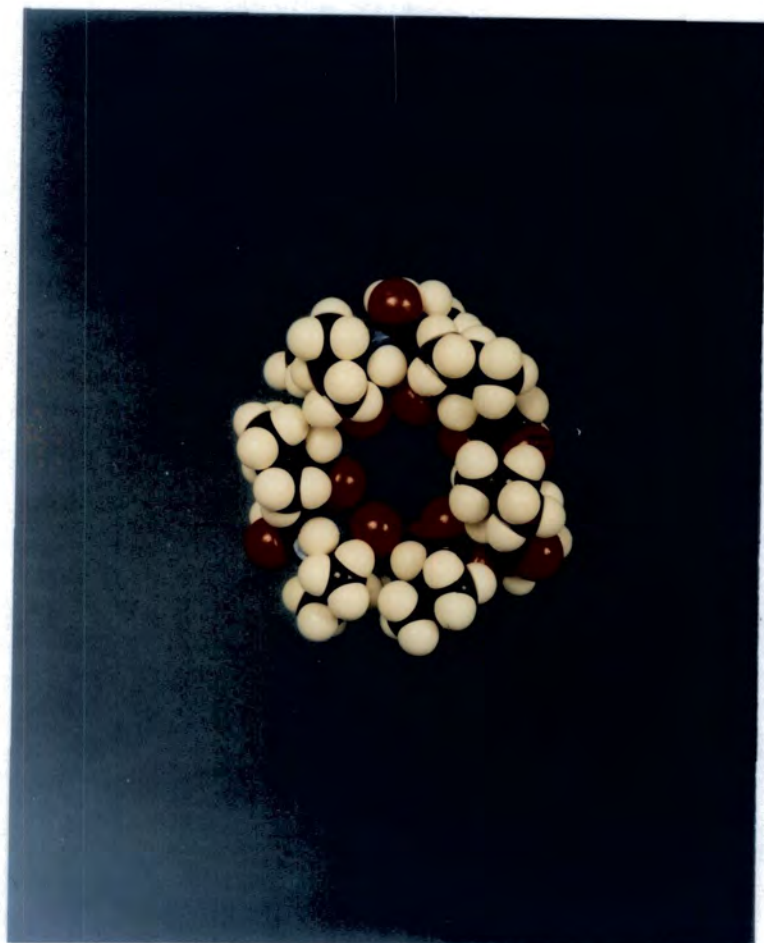
Figure 2.7 A photograph of a CPK model of the K$^+$-complex.

for example, sits at the centre of an octahedral, electrostatic field formed by the six oxygen atoms. The non-polar isopropyl and methyl residues can shield the K^+ ion from solvent interaction. The peripheral hydrocarbon side chains are also compatible with the hydrophobic interior of biological membranes and thus this conformaton might also facilitate diffusion through such membranes.

The effect of the polarity of the solvent is most evident on the ester $C=O$ groupings, whilst the amide groupings appear to be solvent independent. These results suggest that the complexed cation might not be completely shielded from the solvent molecules. The ion-release mechanism of ion-carrying molecules such as valinomycin is not fully understood, but solvent interactions with the cation have been proposed to play a part.

2.1.3 Observation of the valinomycin-cation complex

In this subsection the electrochemical experiments used to observe the complexing reaction and the structural techniques employed to elucidate the valinomycin conformations described in the two previous subsections are outlined. Valinomycin intially attracted much scientific interest because of its ability to specifically increase the alkali metal ion flow through artificial and biological membranes. These pioneering experiments were performed on experimental lipid membranes separating solutions of monovalent salts of two different concentrations [4].

Across a cell membrane there exists an electrical potential difference which depends on the ionic concentration gradients across the membrane, and its relative permeability to the ions present. Each individual permeant is subject to two gradients tending to drive it in or out of the cell, a concentration gradient and an electrical gradient. For potassium, which is much more concentrated in the cell cytoplasm than in the extracelluar fluid, the two gradients are nearly in balance. The tendency of potassium ions to move out of the cell along their concentration gradient is opposed exactly by the potential gradient tending to prevent such movement. The membrane potential at which there is no net potassium flux
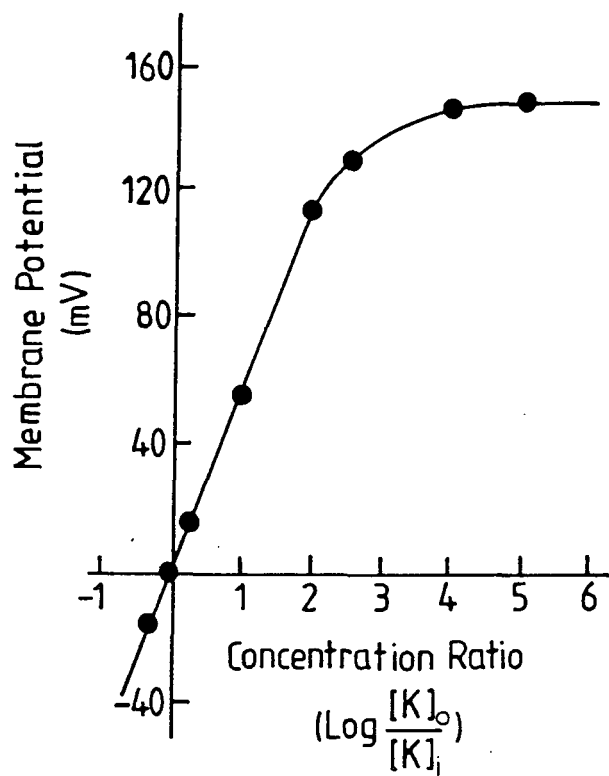
(a)

Figure 2.8 (a) membrane potential developed across a lipid membrane separating KCl and NaCl. 10^{-7} g cm^{-3} valinomycin added on outside of membrane. K_o/K_i is the ratio of the KCl concentration on the outside to the inside.
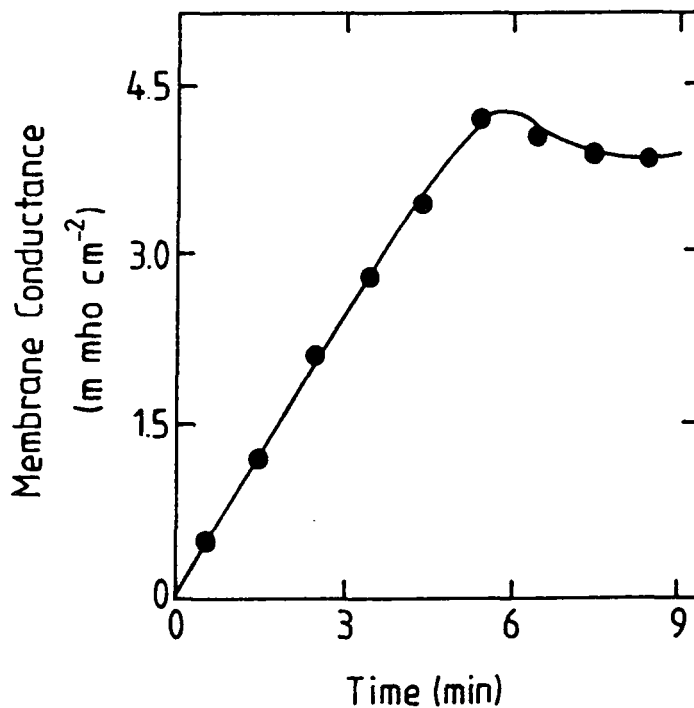
(b)

Figure 2.8 (b) time-conductance curve for a lipid bilayer with 10^{-7} g cm^{-3} valinomycin added at t=0 to both sides of the bilayer. 0.1 M KCl was intially present on both sides of the bilayer.

is called the potassium resting potential. The resting potential is related to the concentration ratio by the Nernst equation, $E_k = 58 \log_{10}(K_o/K_i)$ (in mV). When the cyclodepsipeptide is introduced to one or both sides of the membrane, resting membrane potentials, which are negative on the side of the higher concentration by values of 54-58 mV per decade, are induced (figure 2.8a). This is a result of the increase in membrane conductance (figure 2.8b), which is a measure of the valinomycin-induced membrane permeability to potassium ions. Typically the membrane conductance increases from 10^{-8} mho cm^{-2} to 10^{-3} mho cm^{-2}.

From simple experiments similar to this, the selectivity coefficients of valinomycin for different ions can be calculated. Also by combining steady state conductance measurements with electrical relaxation measurements the rate constants of valinomycin mediated transport across the lipid membrane can be evaluated. In relaxation experiments, a voltage pulse is applied to the membrane. After the intial charging of the membrane capacitance, the current decays exponentially with a characteristic time constant. This time constant is related to how quickly the valinomycin molecules are able to redistribute the stored charge so that the potassium resting potential is re-established.

Complexation can be conveniently studied by conductimetric methods. For example, when cyclodepsipeptides are added to ethanol solutions of alkali metal chlorides, there is a decrease in electroconductivity as a result of the low mobility of the complexed cation. Thus, the complexing reaction can be studied under different conditions such as solvent, temperature, concentration etc.

As well as the thermodynamic parameters of the complexing reaction, the molecular structure of valinomycin and its complexes are also of considerable interest. Nuclear magnetic resonance (NMR) [11], optical rotary dispersion (ORD) [2], and infrared absorption (IR) studies [2] have all been used to elucidate conformational structure.

ORD is a technique which looks at the optical rotation of plane polarised light after transmission through a medium as a function of wavelength. Plane polarised
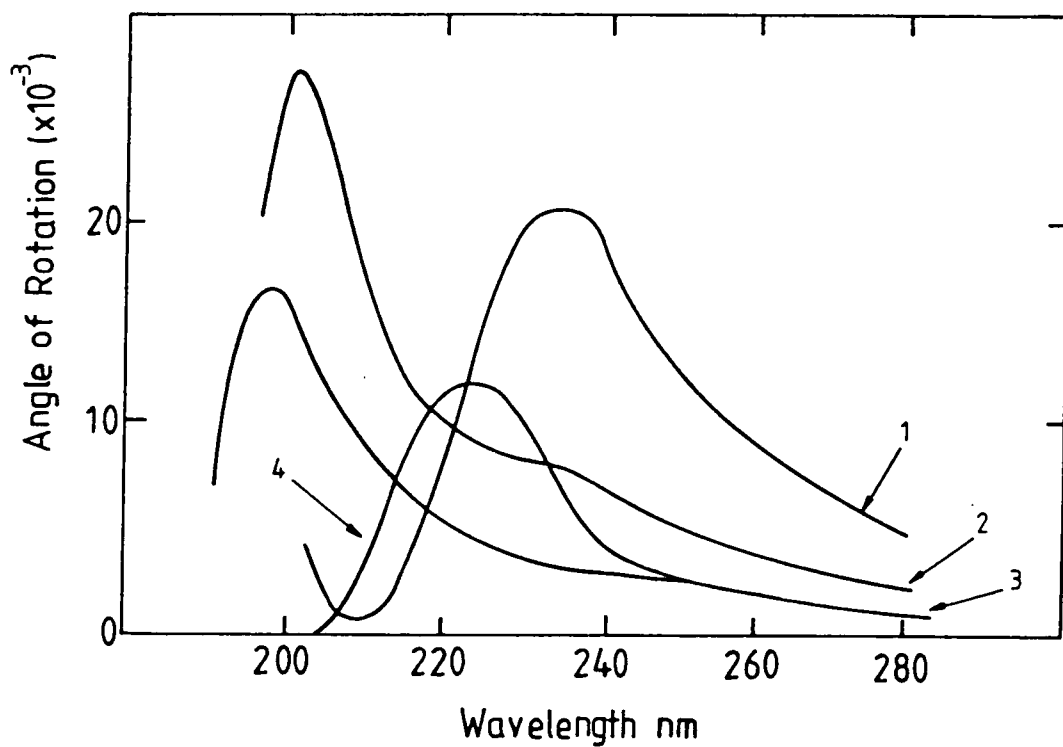
Figure 2.9 ORD curves for valinomycin: (1) heptane-dioxane (10:1); (2) ethanol; (3) trifluoroethane-water (1:2); and (4) K^+-complex (after ref. 2).
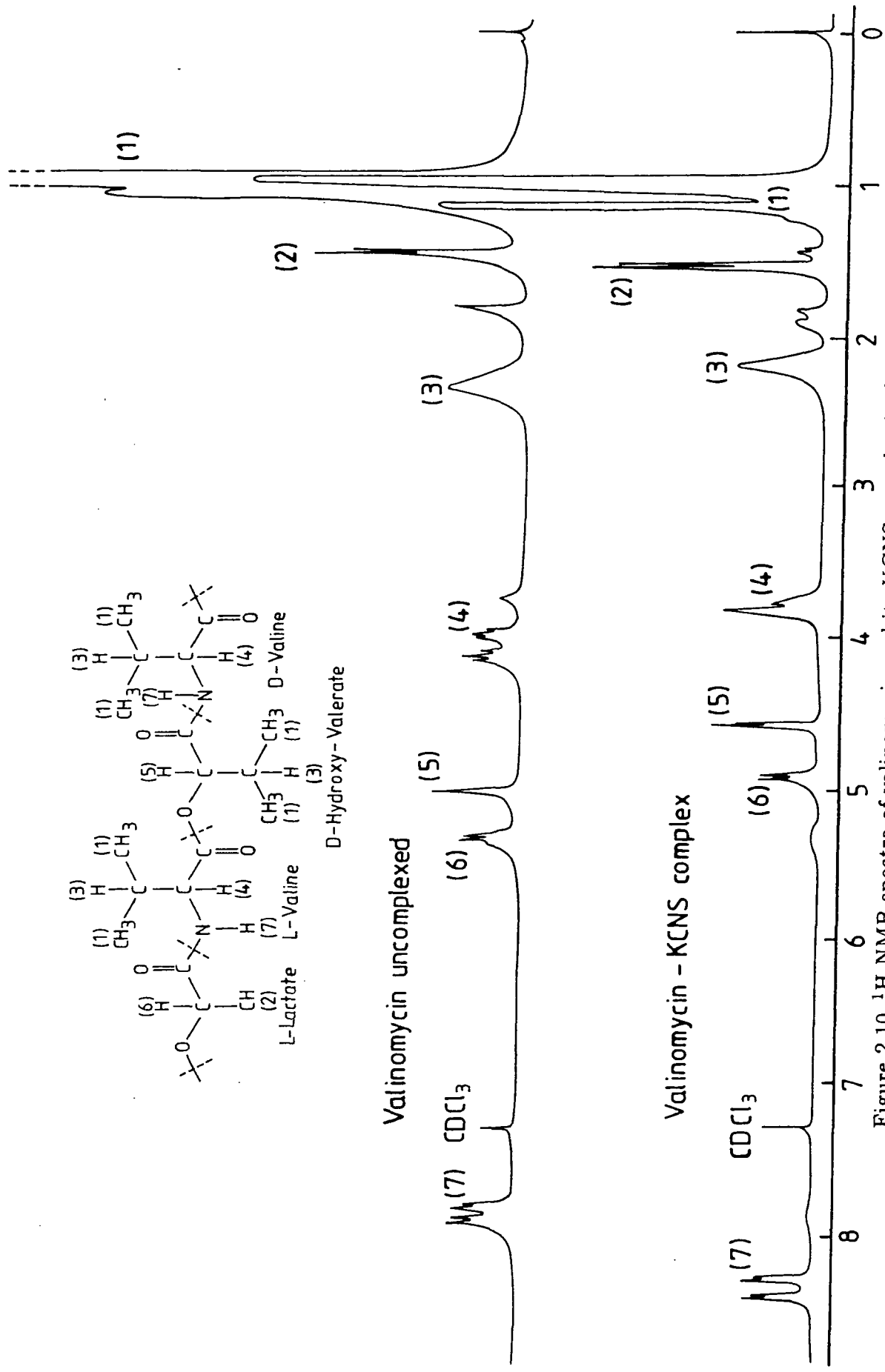
Figure 2.10 ^{1}H NMR spectra of valinomycin and its KCNS-complex in deuterated chloro-form ($CDCl_3$), the inset shows a unit of the valinomycin molecule.
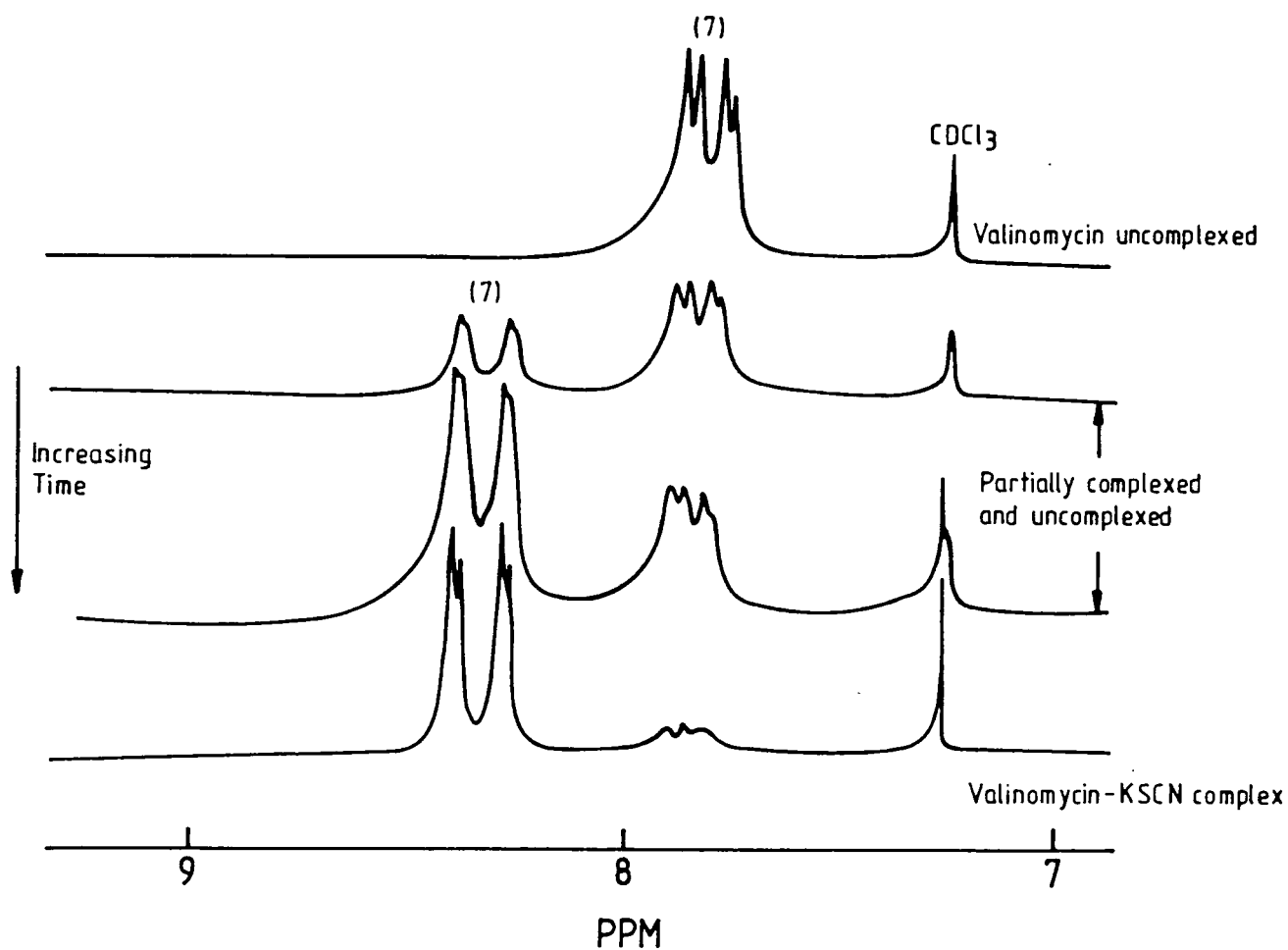
Figure 2.11 A portion of the NMR spectra of valinomycin in CDCl₃ showing the changes occurring in the NH proton signals as a function of time during complexation.
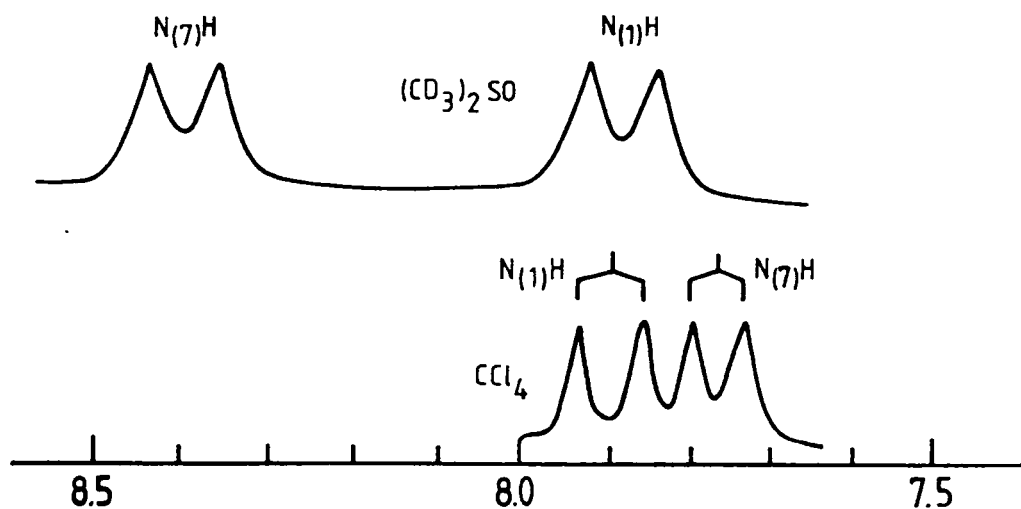
Figure 2.12 The affect of solvent polarity on the NH proton signals (after ref. 2).

light can be considered to be made up of a left and a right circularly polarised component. In general, these components will be transmitted with unequal velocities through the medium, and upon recombination, there will be a phase difference with the plane of polarisation of the emergent light rotated. In fact unequal absorption of the two components also occurs and this phenomenon is referred to as "circular dichroism". The effect of the polarity of the solvent on the conformation of valinomycin can clearly be seen from the set of ORD curves in figure 2.9, after Shemyakin *et al* [2]. The changes in the curves are due to conformational changes in the valinomycin. The ORD curve for the K^+ complex is also shown indicating the existence of a different conformer. A greater understanding of the polarity effect can be obtained from NMR and IR studies.

The resonant frequency of magnetic nuclei in a molecule is dependent on the different environments present in that molecule. In proton NMR, a short powerful radio pulse which behaves like a spread of frequencies, simultaneously excites a series of protons. The relaxation signals of all the excited protons are superimposed to form a combined signal which is known as the free induction decay (FID). By performing a Fourier transform on this signal an NMR spectra can be obtained, showing each nucleus in its unique electronic environment. The ^{1}H NMR spectra, for valinomycin and its complex in CDCl$_3$ (deuterated chloroform), are shown in figure 2.10. The assignments are labelled according to the inset which shows one unit of the valinomycin molecule. The most interesting changes in the spectra are those associated with the NH protons, and these changes are highlighted in figure 2.11. The top spectrum is that for the uncomplexed valinomycin and shows two doublets corresponding to two types of NH protons, one due to the L-valine residues (low-field signal) and the other due to the D-valine residues (high- field signal. The low field signal has been assigned to the L-valine NH protons by enriching the L-valine with radioactive ^{15}N [2]. Upon complexation there is a 0.5 ppm down-field shift of both doublets. In the two central spectra, the observation of two sets of doublets (at δ 7.80 and 8.3 ppm) suggests that both forms of vali-
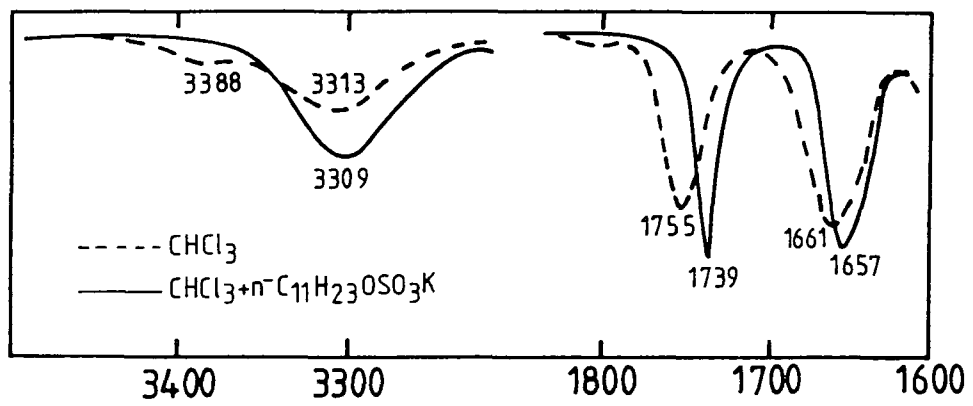
Figure 2.13 IR spectra of valinomycin and its KCNS complex in CHCl$_3$ (after ref. 2).

nomycin (complexed and uncomplexed) are present in the NMR tube. The final spectrum indicates that complexation is almost complete with the disappearance of the doublets at δ 7.80ppm. Figure 2.12 shows the effect of the polarity of the solvent on the uncomplexed ^{1}H NMR valinomycin spectrum. In the case of CCl$_4$, the doublets are quite close to each other, but for (CD$_3$)$_2$SO (a more polar solvent), the low-field signal is shifted downfield whereas the high-field signal remains constant. From this and with corroborative infrared evidence, it can be concluded that in the more polar solvent the NH protons are participating in hydrogen bonds with the solvent molecules, rather than in intra-molecular hydrogen bonds. In non-polar solvents (such as CCl$_4$), they are forming intra-molecular hydrogen bonds. The NMR spectrum of the complex in a variety of solvents is the same, and this evidence supports the characteristic "bracelet" structure of hydrogen bonds in the K$^+$-valinomycin complex.

The theory of IR spectroscopy and the collection of spectra are dealt with in chapter 4, and the IR spectra of valinomycin and its complex are discussed in detail in chapter 7. A brief discussion of results from the IR data of other workers [2,7] is included here for completeness. The IR spectra for valinomycin and its K$^+$ complex in CCl$_3$ (chloroform), are presented in figure 2.13. In the NH stretching region, a strong band due to intra-molecular hydrogen-bonded NH groups is evident at 3313 cm^{-1}, and in addition, a weaker band at 3388 cm^{-1} is also present. This corresponds to a free NH stretching mode. In the CO stretching region a band characteristic of non-hydrogen-bonded ester carbonyl is present at 1755 cm^{-1}. Both these pieces of data indicate that in low polarity solvents, such as chloroform, the two conformations illustrated in figure 2.4a and b are found. The changes in the IR spectrum upon complexation are marked. The free NH band disappears, indicating that all L-valine protons are hydrogen-bonded. Also the ester carbonyl band is shifted (to 1739 cm^{-1}) and narrowed suggesting that all the ester carbonyls are now involved with ion-dipole interactions with the K$^+$ ion.

2.2 THE BIOLOGICAL MEMBRANE

The principal function of the biological membrane is to maintain a constant internal environment for the cell, irrespective of changes that may occur outside. The membrane must also provide selective communication with the exterior such as the controlled passage of nutrients into the cell, and the removal of waste products from it. Plasma membranes, therefore, have associated with them a range of transfer systems which enable molecules to pass through in a specific manner. There are processes that do not require energy (passive transfer) and those that do (active transfer). Valinomycin-mediated cation transport, described in section 2.3, is an example of one of these transfer systems. The membrane potential results in an electrochemical gradient which is utilised by the cell as an energy source for processes such as solute transport and ATP synthesis. At the supermolecular level, membranes are the structural elements of cells and therefore, in multicelluar organisms, of the tissues. Membranes help to maintain the shape and form of the cell. At the molecular level, the membrane also provides an ordered array of sites for enzymes to locate, helping the chain-reaction-like series of coordinated reactions, taking place in biological systems, to proceed more readily.

2.2.1 Membrane components

The exact composition of membranes varies with their source but generally approximately 40% of their dry weight is lipid and 60% is protein, held together by non-covalent interactions. Membranes contain some 20% of their total weight as water, which is tightly bound and essential for the maintenance of their structure.

Lipids are water-insoluble organic substances which are amphipathic, meaning that they incorporate both a hydrophobic tail and a hydrophilic head group within the molecule. These two regions can be bridged by a glycerol moiety, as illustrated in figure 2.14. The chain length may vary and unsaturated acids also occur. The lipid component of membranes is predominantly of a type known as phospholipid. The term phospholipid is applied to any lipid containing phospho-

Hydrophilic
Head
Group
|
O
|
CH_2 — CH — CH_2
| |
O   O
| |
CO CO
| |
CH_2 CH_2
CH_2 CH_2
CH_2 CH_2
CH_2 CH_2
CH_2 CH_2
CH_2 CH_2
CH_2 CH_2 ⎫ Hydrophobic
CH_2 CH_2 Tail
CH_2 CH_2
CH_2 CH_2
CH_2 CH_2
CH_2 CH_2
CH_2 CH_2
CH_2 CH_2
CH_3 CH_3⎭

Figure 2.14 Polar lipid based on a glycerol backbone. Chain lengths may vary and unsaturated acids may occur.

(a)   (b)   (c)
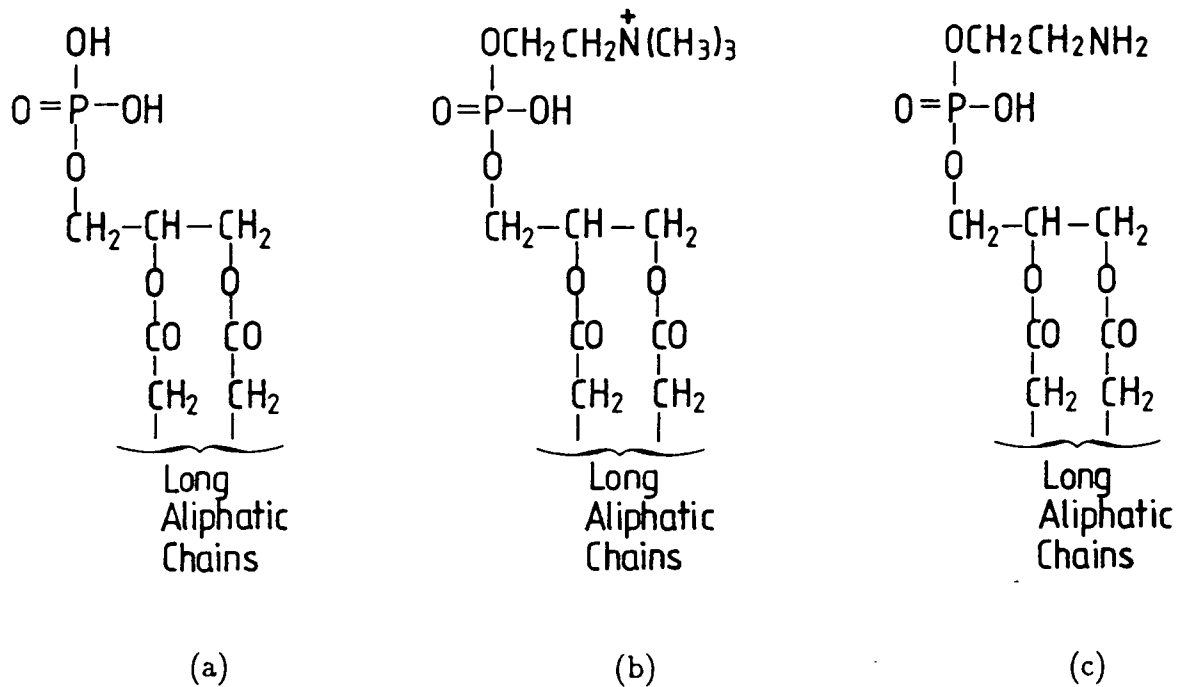
Figure 2.15 Glycerophospholipids (a) phosphatidic acid, (b) phosphatidylcholine and (c) phosphatidylethanolamine.
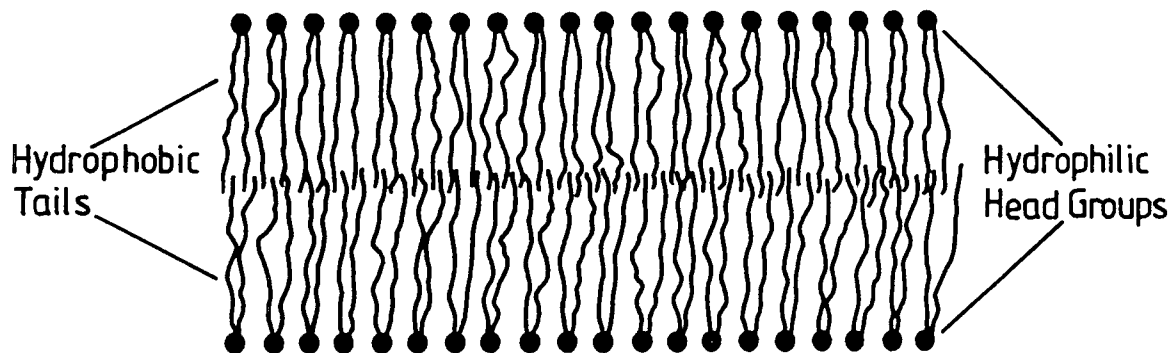
Figure 2.16 Bilayer arrangement of polar lipids.

ric acid as a mono- or di-ester. For the glycerophospholipids in figure 2.15 the hydrophilic head group is attached via a phosphate di-ester linkage. Phosphatidic acid plays a key role in the biosynthesis of most glycerophospholipids and is present (1-5%) in many tissues. Phosphatidylcholine is usually the major phospholipid in mammalian, plant and fungal membranes, but is rare in bacteria in which phosphatidylethanolamine is a major component. The phospholipids are the most polar of the lipids. They all carry a phosphate acidic grouping which has a negative charge at pH 7.0. Choline and ethanolamine have additional amino groups which are positively charged at neutral pH, giving rise to dipolar zwitterions with no net charge.

The other major component of membranes are proteins. The important membrane functions such as enzymic, receptor and transport activities are largely mediated by proteins. The protein content of a particular membrane therefore reflects the level of activity of that membrane. Membrane proteins are classified into two categories, peripheral and integral. Peripheral proteins also referred to as extrinsic proteins are relatively easily dissociated by mild treatment such as modification of pH or ionic strength. Integral (or intrinsic) proteins are isolated by treatments involving extensive disruption of the membrane by detergents.

2.2.2 Structural organisation of the membrane

Most models proposed for membrane structures incorporate a lipid bilayer arrangement, shown schematically in figure 2.16. The long aliphatic chains are sequestered within the interior of the membrane and the hydrophilic head groups are in contact with the aqueous environments.

The lipid bilayer is thermodynamically stable and is the major structural unit of phospholipid-water systems. Phosphatidylcholine with low water content exists in a lamellar phase consisting of stacked bilayers separated by aqueous layers, figure 2.17a. As the water content is increased, the width of the aqueous layers increases until above 40% water, a system of multilamellar vesicles dispersed in

12
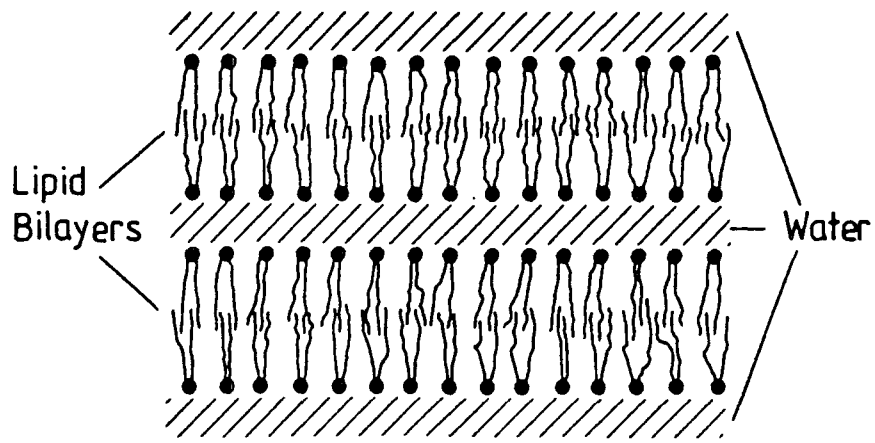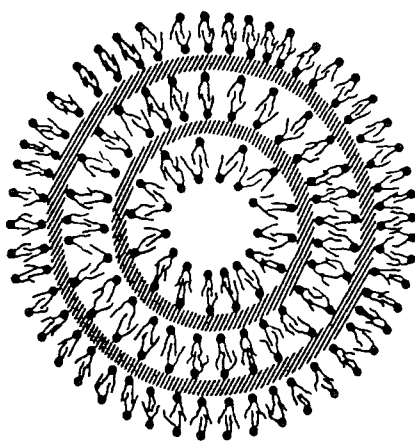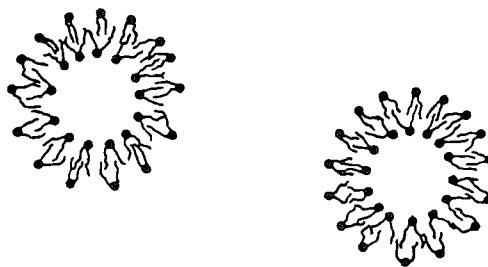
Figure 2.17 Lamellar phases: (a) bulk lamellar phase of phosphatidylcholine-water system, (b) multilamellar vesicle showing three concentric bilayers, and (c) single-bilayer-bounded vesicles.

water results, figure 2.17b. Ultrasonication of this system promotes the formation of single-bilayer-bounded vesicles, figure 2.17c. In figure 2.17 the basic structural unit of the lipid bilayer is evident in every system.

Gorter and Grendel in 1925 were first to propose the lipid bilayer model of figure 2.16. The idea was later elaborated upon by Danielli, Davson and Robertson [12] in 1935 who postulated that the lipid core of natural membranes was sandwiched between two layers of protein, figure 2.18. The Davson-Danielli-Robertson model was supported largely by electron microscopic and X-ray diffraction evidence which showed a trilaminar structure for the membrane. The electron density distribution across the membrane consisted of two fairly broad maxima separated by a trough. Davson interpreted the electron dense outer humps as arising from the protein layers, which are relatively rich in oxygen and nitrogen atoms, and the central trough represented the carbon and hydrogen atoms of the hydrocarbon chains. However, it is now believed that this structure is representative of the hydrophilic-hydrophobic-hydrophilic sequence across a lipid bilayer rather than the protein-lipid-protein structure proposed in the Davson-Danielli-Robertson model. The evidence comes from the fact that micrographs from artificial bilayers are remarkably similar to those of natural membranes. Also in the Davson-Danielli model, the polar and non-polar residues in the protein are effectively buried in non-polar and polar environments, respectively, resulting in a system of relatively high free energy. A system of lower free energy would result if the hydrophobic groupings could gather in a non-polar environment, leaving the polar residues in contact with the aqueous environments.

The mosaic model describes such a situation and was proposed by Singer and Wallach [13,14] as a result of experimental data suggesting that sometimes proteins penetrate the bilayer. The model is illustrated in figure 2.19. The protein is shown embedded in, and occasionally crossing a lipid bilayer core. In such a structure the polar groups of lipid and protein are in direct contact with the aqueous surroundings while the non-polar residues of both molecules are buried
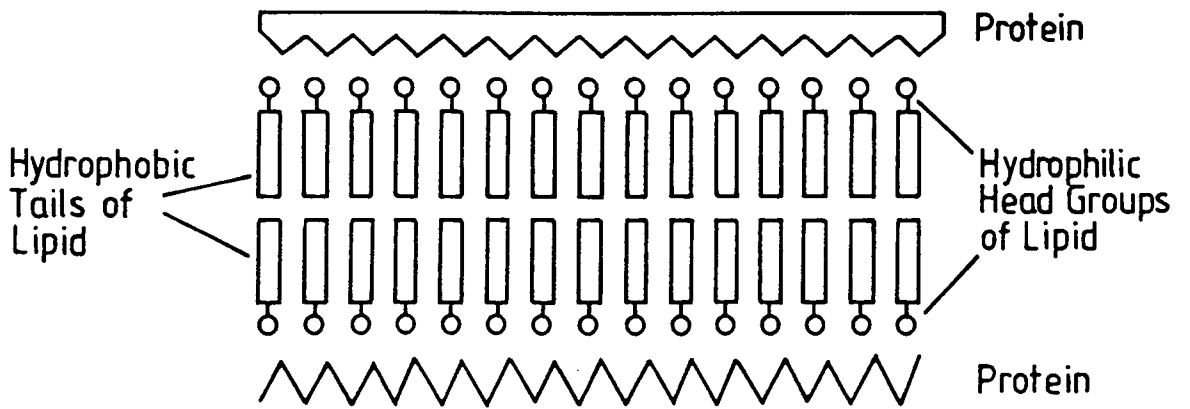
Figure 2.18 Schematic diagram of the Davson-Danielli-Robertson model (after ref. 12).
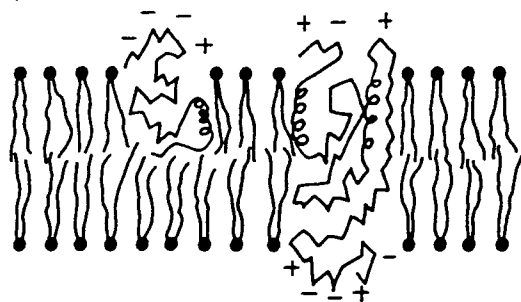
Figure 2.19 The mosaic model of membrane structure. The integral proteins are shown as globular molecules partially embedded in the lipid bilayer. The protruding parts carry the ionic residues of the protein, while the apolar residues are largely embedded (after ref. 14).
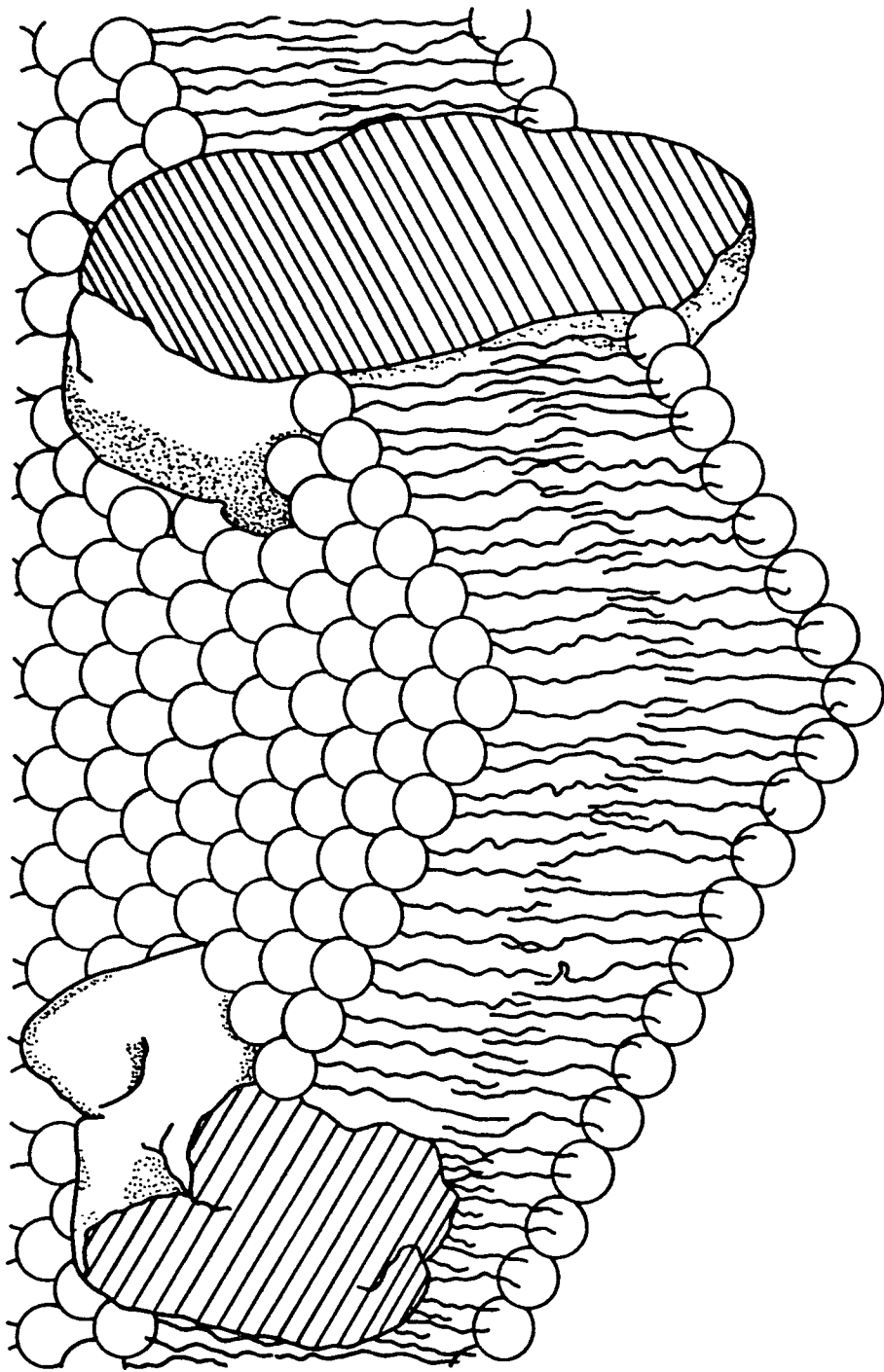
Figure 2.20 The fluid mosaic model. The globular proteins are shown immersed in and occasionally crossing a lipid bilayer matrix (after ref. 15).

in the hydrophobic interior. As well as being thermodynamically more favourable than previously proposed models, the mosaic model is also attractive because of its transmembrane proteins which offer a potential route through the bilayer, and serve to explain certain membrane transport mechanisms. The mosaic model requires that some protein molecules be embedded in the lipid bilayer. Convincing evidence for this is provided from freeze-fracture electron microscopy in which a membrane specimen is rapidly frozen and separated along its hydrophobic, interior surface. The topography of this surface, as revealed by electron microscopy, is that of a smooth matrix interrupted by a large number of fairly uniform particles. These particles are attributed to integral proteins which cross the mid-plane of the membrane. The smooth matrix are regions of the hydrophobic aliphatic chains unpenetrated by proteins.

In 1972 the mosaic model was further refined by Singer and Nicolson [15] to stress the dynamic aspects of membrane structure. In figure 2.20, the potential mobility of the integral proteins is stressed. The mobility of the proteins arises from the fluidity of the lipid matrix. At physiological temperatures the hydro-carbon chains are highly mobile, and proteins and individual lipids are free to move laterally. Lateral motion of the complete phospholipid molecule is much faster than that of the proteins, as might be expected from a consideration of size. Intra-molecular motion (as opposed to inter-molecular lateral motion) of the phospholipids is also possible and this can include; a pendulum-like motion of the aliphatic chains, segmental motion about each C-C bond within the chain, and also rotation of the entire molecule about its long axis.

As the temperature of a pure phospholipid is raised, a characteristic transition temperature is reached at which there is a sharp rise in heat absorption. The mobility of the aliphatic chains increases abruptly giving rise to a liquid-crystalline state. Below the transition temperature a gel state exists, with crystalline hydrocarbon chain regions. Both NMR and ESR techniques reveal relatively greater mobility for the hydrocarbon chains furthest removed from the polar head groups

14

i.e. in the hydrophobic centre of the bilayer.

2.3 VALINOMYCIN-MEDIATED ION-TRANSPORT MECHANISM

Membranes have associated with them a range of transport systems which enable molecules to pass through in a specific manner. The movement of molecules across the membrane may be the result of a passive mechanism such as simple diffusion, or an active mechanism drawing upon the energy yielding metabolic processes of the cell.

Diffusion in the bulk phase of a solution relies on a net movement of solute from higher concentration areas to lower concentration areas, the rate of diffusion being directly proportional to the concentration gradient and this is described by Fick's law, see figure 2.21a. It can be seen that the flux increases with increasing solute concentration. The introduction of a membrane presents a barrier to the free movement of solute molecules, and the permeability of the membrane as well as the concentration gradient of the solute must be considered. However, the transport of most solutes across membranes involves processes other than simple diffusion, known collectively as mediated transport mechanisms. Simple diffusion is an example of a non-mediated process.

In mediated transport, Fick's law no longer holds and the system exhibits saturation kinetics i.e. increasing the concentration gradient increases the flux up to an asymptotic value, figure 2.21b. The implication is that the transport of molecules is facilitated by their interaction with a finite number of specific membrane components or active molecules. The evidence points to membrane proteins being the key elements in mediated transport mechanisms [16].

Two mechanistic models [17,18] have been proposed to explain how such transport systems might function. The first of these is termed the pore hypothesis and the transport system is envisaged as a specific pore through the membrane, and is illustrated in figure 2.22. The pores are lined with proteins and are permanent structures. Specificity to a metabolite M may depend on the pore diameter,

15
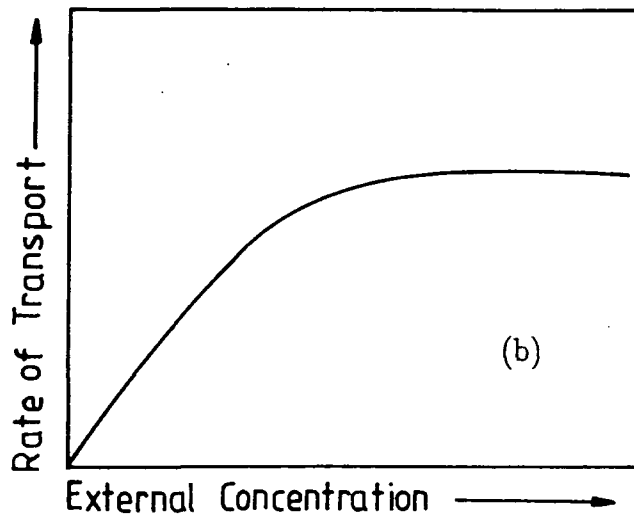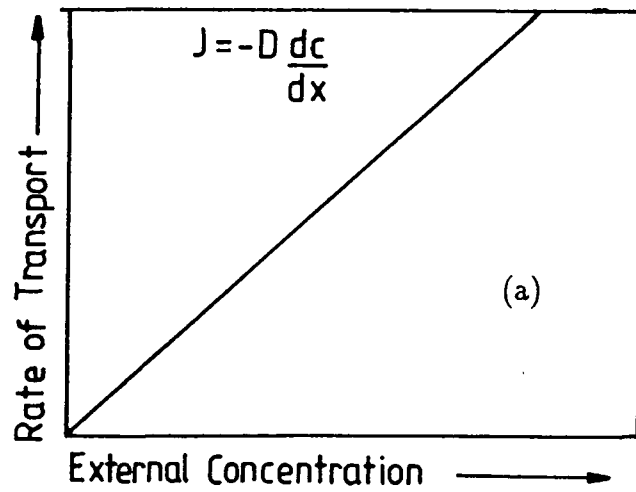
Figure 2.21 (a) Non-mediated and (b) facilitated or mediated transport.
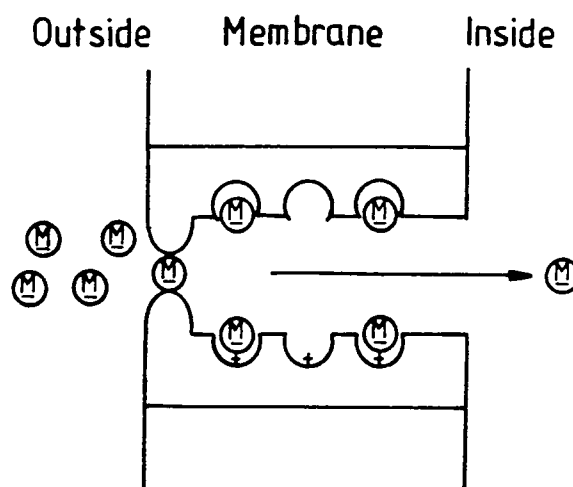
Figure 2.22 The pore hypothesis, trans-membrane proteins constitute a specific pore or channel through the membrane.

charge distribution and the presence of specific binding sites within the pore. A second interpretation of this model describes the active molecules stacked together to form a channel, completely spanning the membrane. Transport of, for example, an ionic species from one side of the membrane to the other is envisaged as occurring by a succession of intermediary complexes with molecules of the channel.

The second scheme, and the most likely candidate for describing the mechanism of valinomycin mediated cation transport, is called the mobile carrier hypothesis. The passage of the ion across the membrane involves three distinct steps: (i) the formation of the ion carrier (for example K^+-valinomycin) complex in the membrane surface, (i.i) translocation of the complex through the membrane interior to the other surface and (i.i.i) release of the ion into the aqueous environment. This sequence of steps is illustrated in figure 2.23a. Shemyakin *et al* [2] have inferred, from studies with phosphatidylcholine bilayers, that valinomycin molecules accumulate on the bilayer surface. Complexation therefore presumably takes place at the membrane/solution interface with the inner hydration shell of the ion being replaced by the ester carbonyl oxygens of the valinomycin ring. The ion which is normally extremely insoluble in the membrane is thus provided with a polar environment similar to that which it experiences in the aqueous environment. Valinomycin, because of its hydrophobic covering of aliphatic side chains, is soluble in the lipid environment and is able to cross the membrane.

Stark and Benz [19] have addressed the question of the rate determining step of the transport mechanism; i.e. is the overall rate of ion transport determined by the rate of association, dissociation or translocation of the complex? The model they used is illustrated in figure 2.23b. The association-dissociation reaction of the complex taking place at the membrane-solution interface is described by the following equation:

$$K^+_{(a)} + VM_{(m)} \underset{K_D}{\overset{K_A}{\rightleftharpoons}} VMK^+_{(m)}$$
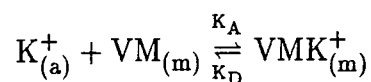
where a and m denote the aqueous and membrane environments, respectively and K_A and K_D are the rate constants for the association and dissociation of the

Membrane (m)

Aqueous
Phase
(a)

$$VM \xrightleftharpoons[]{K_{VM}} VM$$

K_A

K_D

K^+

$$VMK^+ \xrightleftharpoons[K_{VMK}]{} VMK^+$$

Aqueous
Phase
(a)

(b)

Outside   Membrane   Inside

(a)
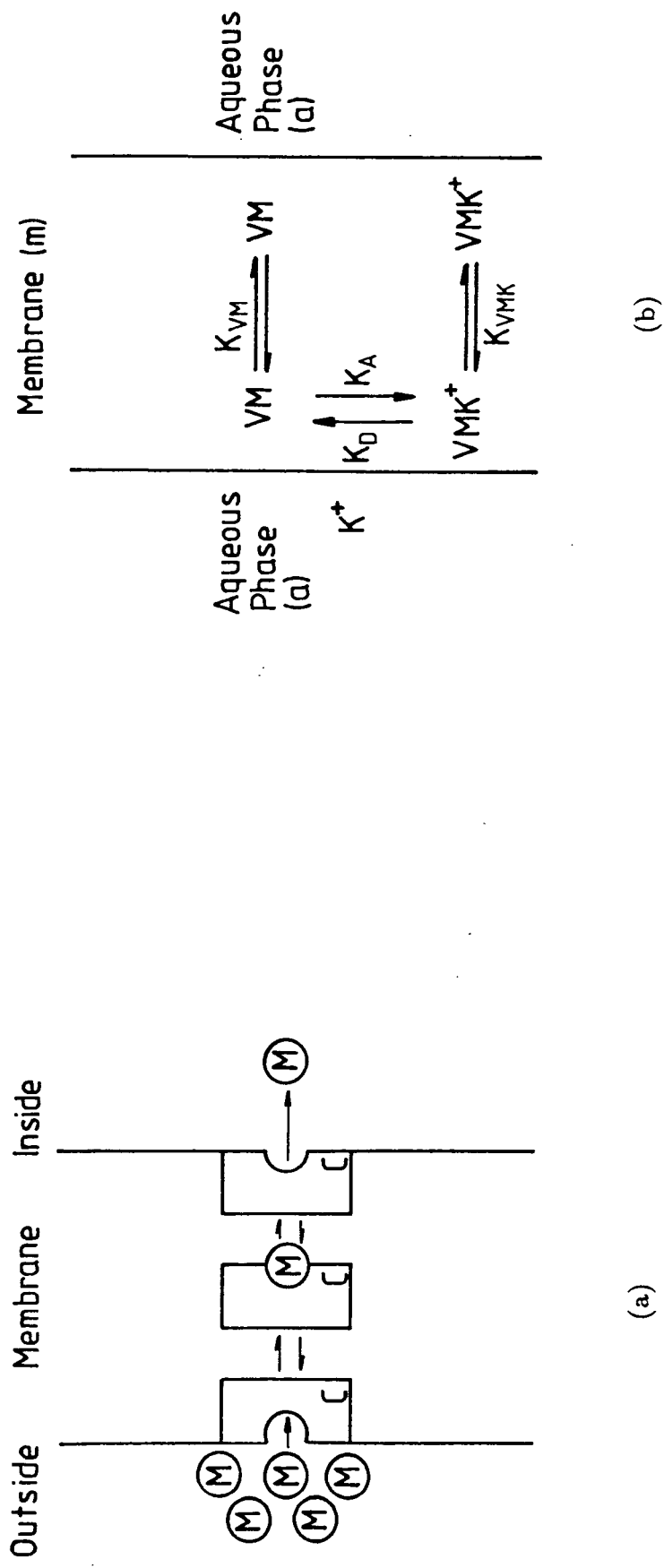
Figure 2.23 The mobile carrier hypothesis, (a) transport steps across the membrane, and
(b) transport model (after ref.19).

complex, respectively. In figure 2.23b, K_{VM} and K_{VMK} are the rate constants for the translocation across the membrane of the neutral carrier VM and the charged complex VMK^+, respectively. The model assumes that VMK^+ must surmount a symmetrical energy barrier within the membrane in order to translocate from one aqueous/membrane interface to the other. The potential energy of the VMK^+ complex is a minimum inside the membrane near the interface.

From steady-state conductance measurements [19] on phosphatidylinositol bilayers and electrical relaxation studies of the membrane current to voltage pulses, Stark and Benz determined K_{VM}, K_{VMK}, K_A and K_D. Despite the fact that the charged VMK^+ complex must surmount the potential energy barrier in the centre of the membrane, they discovered that K_{VM} and K_{VMK} were approximately the same. This result was interpreted in terms of the mechanism of complexation proposed by Shemyakin *et al* [2]. Here valinomycin, in the uncomplexed conformation, is adsorbed at the membrane/solution interface with its polar carbonyl residues in contact with the aqueous environment, and the apolar moieties embedded in the membrane interior. If the uncomplexed VM was able to translocate across the membrane in this conformation the exposed carbonyls would come into contact with the hydrophobic interior of the membrane. This is an energetically unfavourable situation resulting in a relatively high activation energy for the desorption of VM from the membrane surface into the interior. However, the desorption of the VMK^+ complex is relatively easier. This is because of the conformational change in the valinomycin structure taking place upon complexation, namely that, the ester carbonyl groups turn inward towards centre of the molecule to coordinate with the potassium ion. The polar nature of the molecule is thus "lost" and the isopropyl and methyl apolar groups ensure an energetically favourable compatibility with the membrane interior. The result that $K_{VM} \sim K_{VMK}$ indicates that the activation energies for the desorption of uncomplexed VM from the surface, and for VMK^+ to surmount the potential energy barrier, are of comparable magnitude.

17

The rate of formation of the VMK^+ complex in the interface described by K_A, and the dissociation rate constant K_D, were both found to be much lower than the corresponding rates for valinomycin and K^+ in ethanolic solutions. The reason for this is unclear but it might be due to two effects. Firstly, it is known that the stability of the complex diminishes with increasing polarity of the solvent. Therefore the polar surroundings of valinomycin in the membrane environment (i.e. the aqueous solution and the hydrophilic head groups of the phosphatidylinositol lipid) might have a deleterious effect on complexation. Secondly, the valinomycin molecule may be adsorbed in a conformation which is less favourable for complexation than the conformation in ethanolic solutions.

Finally, it is worth noting that in the past, proponents of the channel hypothesis have argued their case for the transport mechanism of valinomycin. However, the results of a nuclear magnetic resonance study of conformational changes in valinomycin during complexation, performed by Haynes et al [11], have indicated the unlikelihood of the transfer of cations by the channel mechanism. The channel mechanism would require several valinomycin molecules to stack or associate with each other across the membrane. A study of the fine structure of the NMR spectra as a function of the concentration of valinomycin, in a non-polar solvent, revealed no structural changes which might be interpreted as arising from the interactions between associating valinomycin molecules. Therefore, association in a non-polar medium such as the membrane interior seems unlikely. The second piece of evidence supporting the mobile carrier hypothesis concerns the exchange rate of the complex in a non-polar medium. In the channel mechanism, the potassium ion would undergo a series of exchanges with successive valinomycin molecules as it passes through the interior of the membrane. Comparison of the exchange rates for the reaction:

$$VM_AK^+ + VM_B \rightleftharpoons VM_A + VM_BK^+$$
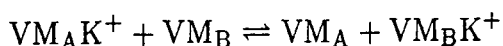
in non-polar and polar solvents reveals the inability of the complex to undergo exchange in a low dielectric medium. This is consistent with the mobile carrier

18

hypothesis in which complexation takes place at the membrane/solution interface (a polar/high dielectric medium), translocation through the membrane interior (a non-polar/low dielectric medium) without dissociation taking place , and finally, release of the cation at the opposite interface.

2.4 SUMMARY

The macrocyclic depsipeptide valinomycin has been introduced. Its ability to complex with the alkali metal cations has been described in terms of its unique molecular conformation. Methods for studying the conformation of valinomycin have been outlined and, in particular, the technique of IR spectroscopy (because of its relevance to this thesis) has been discussed. The biological membrane which forms the natural environment for valinomycin has been described, especially its structure and components. Finally, the concept of carrier mediated ion transport across a membrane has been examined for the case of valinomycin and potassium ions.

CHAPTER 3

ISFET THEORY

3.0 INTRODUCTION

In this chapter all aspects of the theory of the ion sensitive field effect transistor (ISFET) are addressed. The ISFET can be thought of as a special case of the normal metal oxide semiconductor field effect transistor (MOSFET) with the oxide replaced by an oxide-electrolyte system; thus first order MOSFET theory is summarised in section 3.1. Section 3.2 deals with the ISFET structure and the modification of the MOSFET theory to include the reference electrode, which acts as the gate electrode of the ISFET system. Section 3.3 briefly describes the operation and function of the reference electrode. Section 3.4 deals with the ion selective electrode (ISE) and introduces the well-known Nernst equation. Site dissociation theory which describes the generation of a surface charge at an electrolyte/oxide interface is presented in section 3.5, and section 3.6 derives the relationship between surface charge and surface potential using the Gouy-Chapman-Stern theory. The question of the measurement of the surface potential is addressed in section 3.7. Finally to conclude the chapter, section 3.8 concerns ISFETs incorporating an organic film membrane for the gate material, and in particular, describes the generation of a surface dipole moment in a valinomycin-doped hydrocarbon layer in contact with an aqueous potassium environment.

3.1 MOS TRANSISTOR FIRST-ORDER THEORY

A diagrammatic cross-section through an aluminium gate, n-channel MOS (NMOS) transistor is shown in figure 3.1a. The device consists of a lightly doped p-type substrate into which heavily doped n^+ regions, the source and the drain, are implanted. The area between the source and drain diffusions is referred to as the channel region which is overlaid with an intrinsic dielectric formed on the
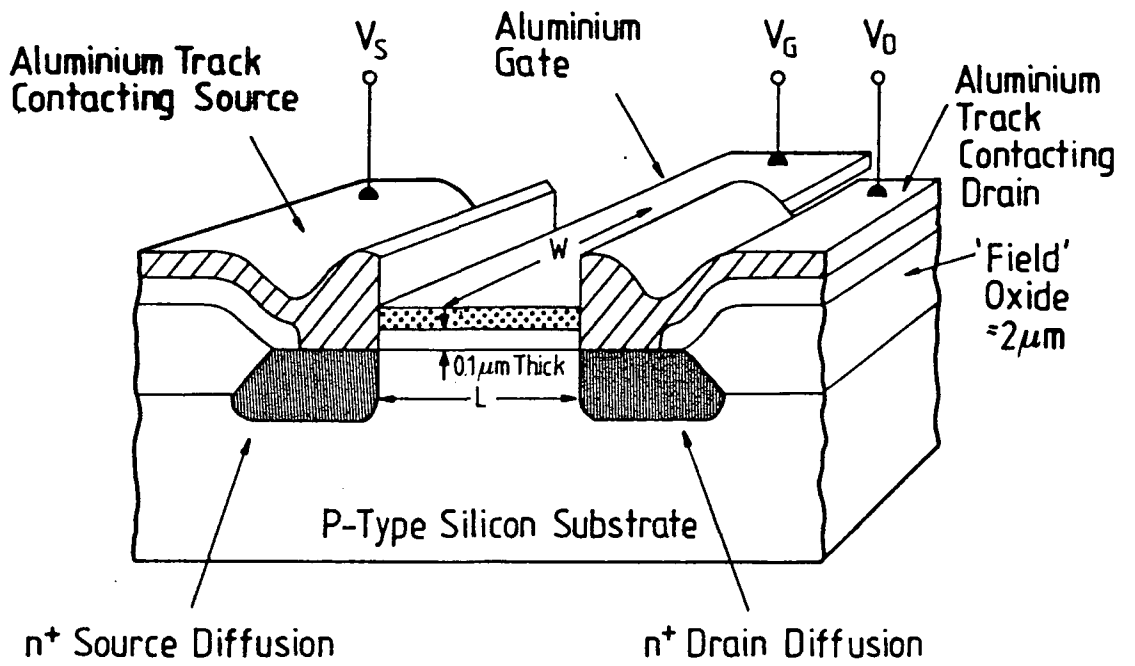
(a)
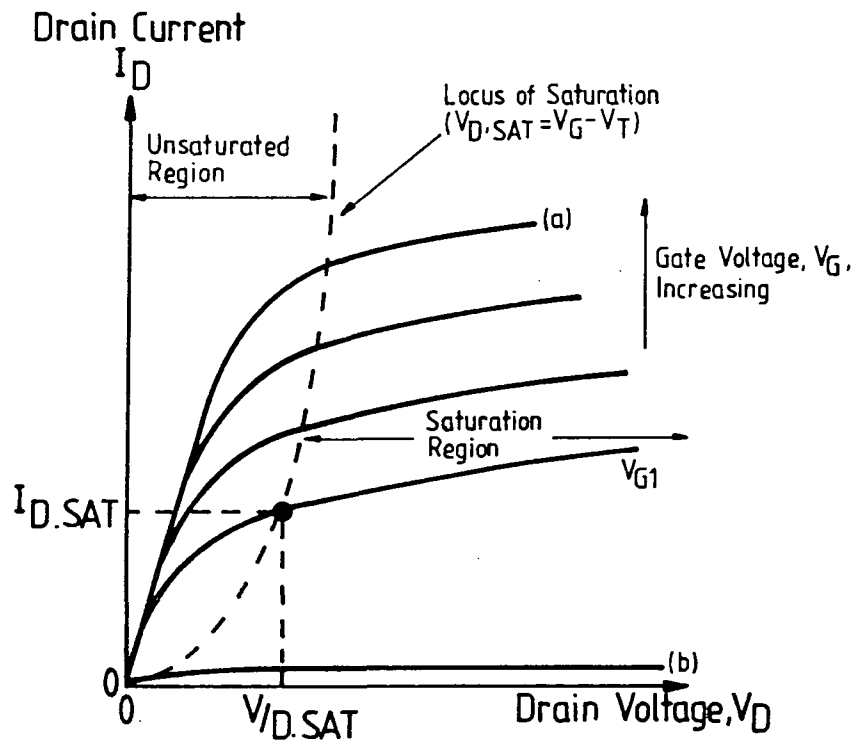
(b)

Figure 3.1 Aluminium gate NMOS transistor (a) cross section (not to scale) showing source and drain, and (b) I_D versus V_{DS} output characteristics.

substrate. The dielectric is a thermally grown, very pure silicon dioxide layer and capacitively couples the aluminium gate electrode to the silicon bulk. In operation, the channel conductivity is modulated by charges induced at the Si/SiO$_2$ interface by the applied potential (relative to the bulk substrate) across the gate insulator. For a sufficiently positive gate potential (greater than the threshold voltage) the electron density locally at the surface exceeds the hole density and the surface region is inverted. The inversion region bridges the source and drain diffusions and a channel current flows. The equation for the drain current I_D as a function of the gate and drain potentials (V_G, V_D) can be derived [1] and for small values of V_D it is

$$I_D = \mu C_{ox} \frac{W}{L} \left[(V_G - V_T)V_D - \frac{1}{2}V_D^2 \right] \tag{1}$$

where μ is the electron mobility in the channel, C_{ox} the oxide capacitance per unit area, $\frac{W}{L}$ the channel width-to-length (aspect ratio), V_G and V_D are the gate-source and drain-source voltages, respectively, and V_T is the threshold voltage. The dependence of the MOS transistor performance on the aspect ratio is the fundamental reason for the elegance of MOS circuit engineering.

Equation (1) gives the drain current in the unsaturated region $(V_D < V_G - V_T)$, see figure 3.1b. Referring to figure 3.1b, if the applied drain bias V_D is increased further, then at some point the voltage across the gate insulator (at the drain end of the channel) drops to exactly V_T i.e. $V_{D,Sat} = V_{G1} - V_T$ for a constant V_{G1}. Channel inversion thus ceases (figure 3.2a), and the channel is "pinched off" by the drain depletion region that now extends right up to the Si/SiO$_2$ interface. Further increase of V_D causes the "pinch-off" point to retreat towards the source as illustrated in figure 3.2b. At this stage the device is said to be "saturated" with the drain current being essentially independent of V_D, figure 3.1b. In the saturated region equation (1) has to be replaced by

$$I_D = \frac{1}{2}\mu C_{ox}\frac{W}{L}(V_G - V_T)^2 = \frac{1}{2}\mu C_{ox}\frac{W}{L}V_{D,Sat}^2 \tag{2}$$

21
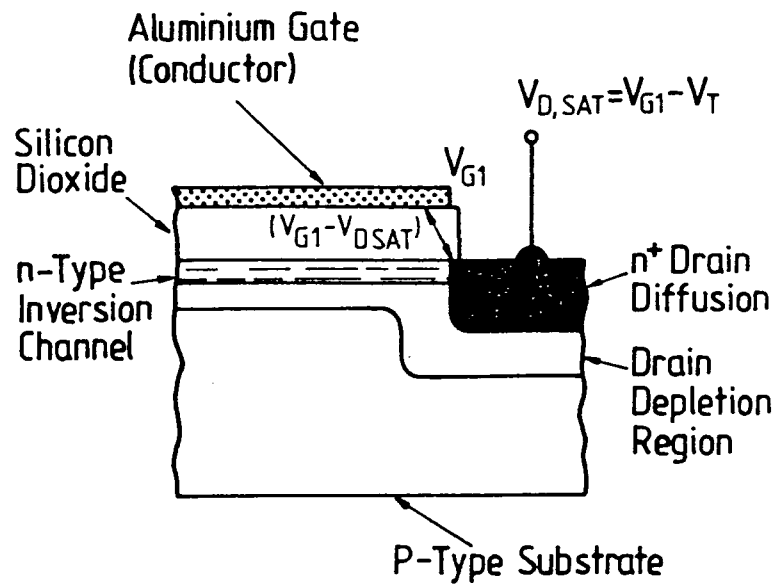
(a)
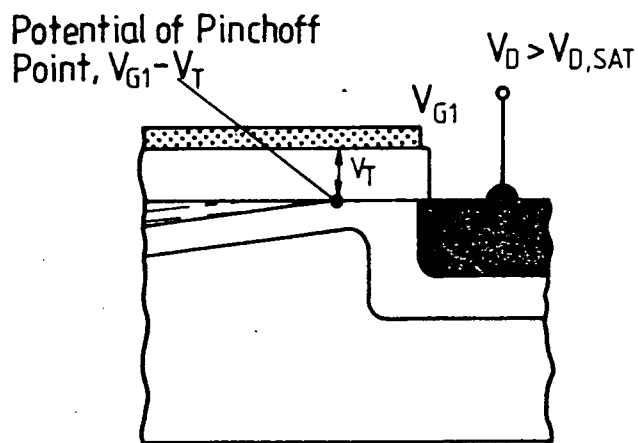
(b)

Figure 3.2 Saturation conditions for an MOS transistor (a) at saturation: $V_{G1} - V_{D,Sat} = V_T$, and (b) into saturation: $V_{G1} - V_D < V_T$.

The threshold voltage V_T in both equations (1) and (2) can be described as follows

$$V_T = V_{FB} - \frac{Q_B}{C_{OX}} + 2\phi_F \qquad (3)$$

where Q_B is the charge per unit area in the depletion region, ϕ_F is the Fermi potential classifying the concentration and the doping of the substrate, and V_{FB} is the flat band voltage. V_{FB} is the voltage shift in the energy bands of the semiconductor as a result of the unequal work functions of the semiconductor and the metal, Φ_{Si} and Φ_M, respectively, and any charge due to interface traps, Q_{IT}, or fixed oxide charge, Q_{OX}. V_{FB} is given by

$$V_{FB} = \underbrace{\frac{\Phi_M}{q} + \frac{\Phi_{Si}}{q}}_{\phi_{ms}} - \frac{Q_{IT} + Q_{OX}}{C_{OX}} \qquad (4)$$

If the parameters in the equation for the MOSFET drain current can be influenced by an external quantity then the MOS device can be used as a direct sensor for that quantity. The MOSFET configuration as shown in figure 3.1a can be used directly, for example, in the hydrogen sensitive palladium-gate MOS device of Lundström et al [2]. The catalytically active gate metal adsorbs hydrogen from the ambient causing a change in ϕ_{ms} which can then be monitored by observing the change in drain current. However, most MOSFET-based sensors incorporate simple modifications of the conventional MOSFET configuration, such as, removal of the gate metal entirely or the use of a gate at a certain distance. In the latter case, the distance between the oxide and the gate is bridged by a specific material. Changes in various parameters of this material, due to either chemical or physical quantities, results in sensors which are specific to these quantities. The ISFET falls into this latter category of FET-based sensors. An excellent paper describing FET-based sensors and their structures has been published recently by Bergveld [3].

3.2 ISFET THEORY AS MODIFIED FIRST-ORDER MOSFET THEORY

The structure of an oxide-nitride gate ISFET is shown in figure 3.3a. Five differences from the MOSFET structure are apparent; the removal of the gate metallisation, the inclusion of a dual-gate dielectric, an electrolyte, a reference electrode, and an encapsulant. It can be seen that the ISFET is a special type of MOSFET with the gate at a certain distance. The oxide has been replaced by an oxide-nitride-electrolyte system, and the metal part of the reference electrode can be seen as the actual gate of the ISFET system.

The use of an oxide-nitride overlayer has a dual role: firstly, to act as an ion-barrier so that no significant charge transfer can occur between the electrolyte and the gate oxide, and secondly, to increase C_{OX} and hence the transconductance per unit area of the device. Coincidentally, Si_3N_4 also behaves as a stable, pH-responsive surface. The fabrication of ISFETs is similar to that of MOSFETs therefore making it compatible with IC technology and mass fabrication.

In conventional MOSFET operation the gate potential is referenced to that of the semiconductor bulk, and similarly in ion-sensitive measurements, the bulk is connected to the electrolyte via a reference electrode. The reference electrode which is described in the next section is able to make a stable, ohmic electrical connection to the electrolyte which is essentially independent of its chemical composition, and therefore provides an electrical datum for measurements.

Since the ISFET is now operating in an electrically hostile environment it is necessary that the device is electrically isolated from the electrolyte, and this is achieved using an encapsulant. If residual leakage currents are greater than a few tens of pA, parasitic electrochemical processes occur which destabilise the device response and therefore lead to further degradation of the encapsulant.

As mentioned above, the actual gate of the ISFET system can be considered to be the metal part of the reference electrode, and the original MOSFET equation (1) of the last section can still be applied with V_G now taken as the

23

V_{Bias}

Reference Electrode

Analyte

Encapsulant

Source Metallization

Encapsulant

Drain Metallization

Bulk Metallization

Si_3N_4 Ion-Barrier

SiO_2

n^+

n^+

p Substrate

G

Reference Electrode

S

Electrolyte

H_+

D

Well encapsulated against leakage currents

n^+

n^+

p-Si

(a)

Si | SiO_2 | Si_3N_4 | Electrolyte | Reference Electrode | Metal

Insulator

Si

Si
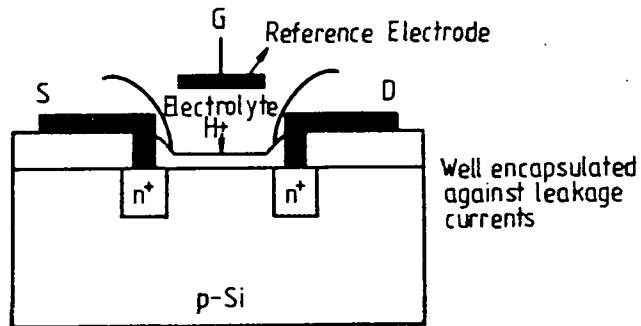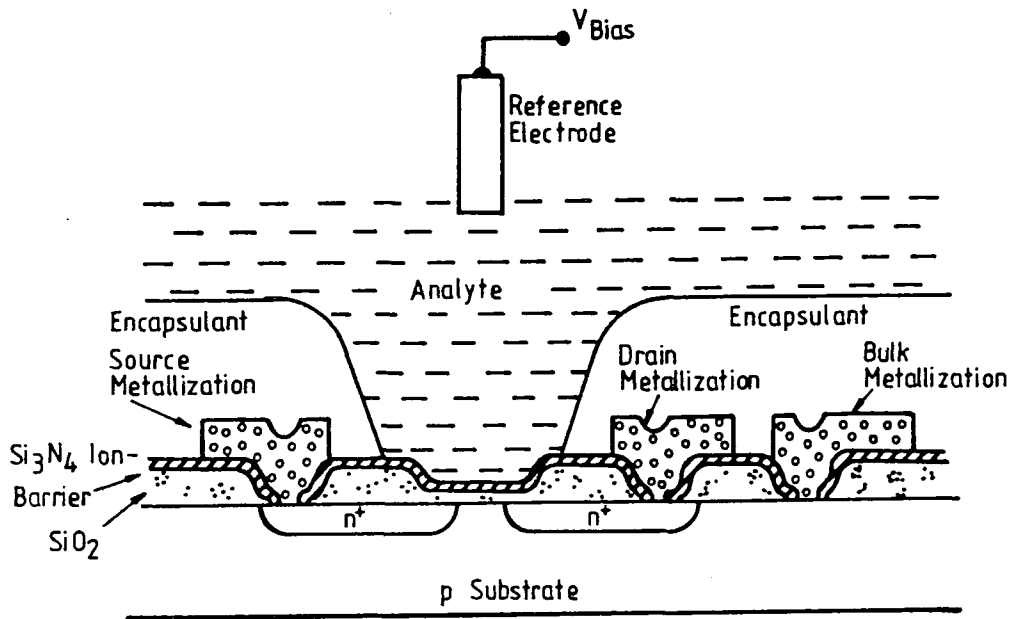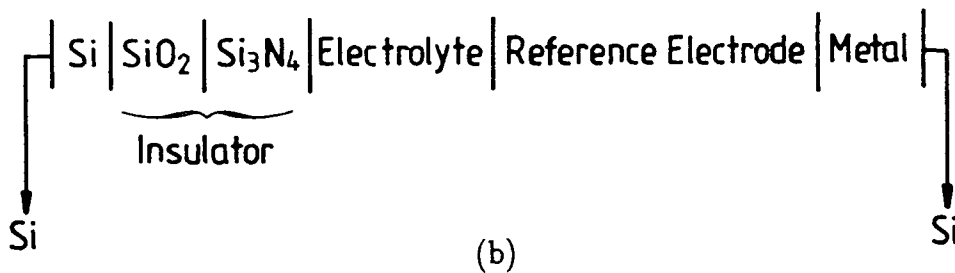
(b)

Figure 3.3 Dual dielectric ISFET (a) cross section showing oxide-nitride gate, and schematic representation, and (b) electrochemical representation

bias applied to the reference electrode. For the ISFET, however, the flat-band voltage (equation (4)) is altered to contain some additional terms which describe the interfacial potential developed at the electrolyte/insulator surface. At this stage, it is helpful, in visualising the potentials developed in the system, to write down the electrochemical representation of the ISFET system and this is given in figure 3.3b. It differs from the representation of the MOSFET system by the electrolyte/reference electrode term and this potential will modify the flat band voltage V_{FB} of the ISFET system as

$$V_{FB} = E_{ref} - \psi_0 + \chi^{sol} + \frac{\Phi_M}{q} - \frac{\Phi_{Si}}{q} - \frac{Q_{IT} + Q_{OX}}{C_{OX}} \qquad (5)$$

E_{ref} is the potential developed across the various phases constituting the reference electrode. The other additional term $(-\psi_0 + \chi^{sol})$ describes the interfacial potential at the oxide surface/electrolyte interface. χ^{sol} is the surface dipole moment of the solution and ψ_0 represents the surface potential at the oxide surface. The relation between surface charge σ_0 and ψ_0 is developed in section 3.6, and from this, the ψ_0/pH relation for the ISFET can be derived.

3.3 THE REFERENCE ELECTRODE

The reference electrode provides an electrical "ground" for the ion-sensitive measurements and is ideally independent of the analyte composition. This allows electrolyte-induced changes in ψ_0 to be assessed directly. The reference electrode can be considered to be an electrochemical half-cell against which the ISFET (the other half-cell) potential is measured. It is interesting to note that Bergveld, the pioneer of the ISFET, performed his early work without an external reference electrode and reported this as an advantage of ISFETs [4]. However, a theoretical treatment by Janata et al [5] argued that a reference electrode was essential for both thermodynamic and electrical stability, and operation without a reference was equivalent to measuring a single half-cell potential which was thermodynamically impossible. Janata suggested that Bergveld's devices were unintentionally

self-referenced via a leakage path, through the encapsulant, from the semiconductor bulk to the solution. This seems likely because of the recurrent problems involved in ISFET encapsulation due to their inherent small size and complicated encapsulant patterning.

The reference electrode used in the work reported in this thesis is of the saturated calomel, porous-frit variety shown in figure 3.4a. A thermodynamical representation of its structure is shown in figure 3.4b. The construction of the electrode consists of a mercury-calomel electrode immersed in a saturated potassium chloride solution which is allowed to diffuse slowly through the porous ceramic frit into the analyte. An electrostatic junction potential, E_J, is developed across this frit, between the inner KCl solution and the analyte, as a result of diffusion of the ionic species. By a correct choice of the inner solution, E_J can be reduced to a small value (typically 1-2 mV), and since it is common to all analytes it may be treated as a common factor and therefore may be ignored. The electrostatic potentials E_1, E_2, and E_3 are invariant and depend only on the activity of the mobile charge carriers common to adjacent phases. For example, E_3 depends on the activity of the Cl^- ion and because the saturated KCl has a fixed chloride activity, E_3 is constant. Thus, E_{ref}, the sum of the liquid junction potential and the electrostatic potentials can be considered as effectively independent of analyte composition thus providing a reference potential for the ISFET system. A consequence of a good liquid junction is that there is a slow escape of KCl into the test solution. This is a distinct disadvantage when potassium or chloride ions are being measured. To overcome this, a double-junction reference electrode was used (figure 3.4a), in which the escaping KCl is retained in a second chamber containing a noninterfering electrolyte. The latter escapes into the test solution through the second junction.
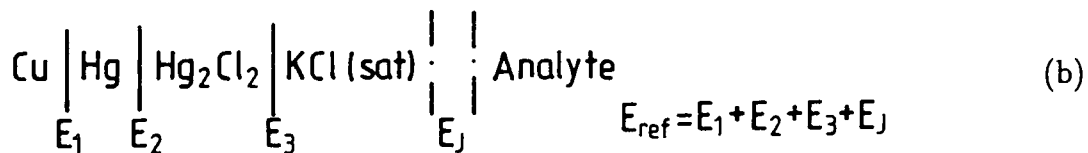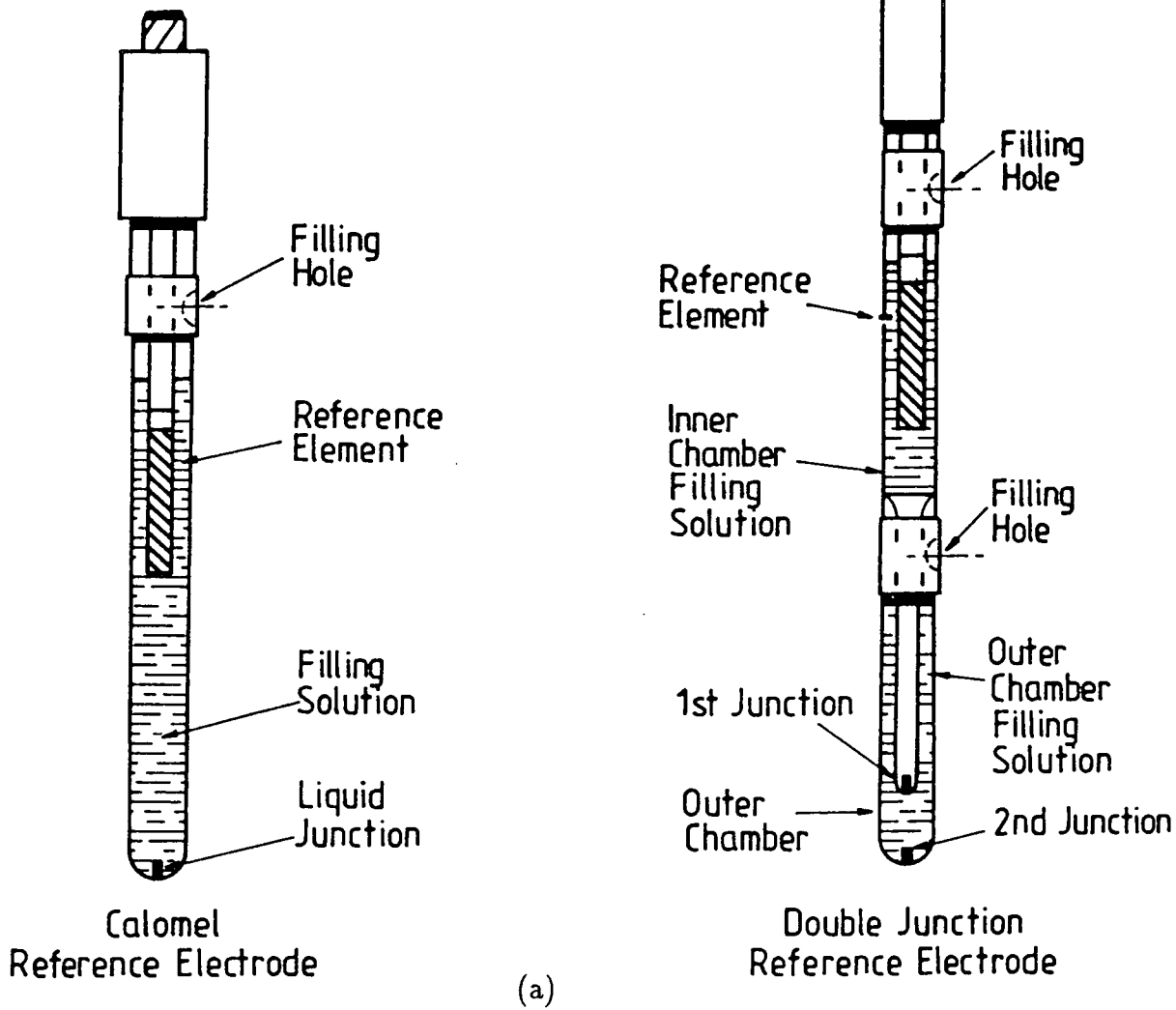
Figure 3.4 Reference electrodes (a) standard calomel and double junction electrodes, and (b) thermodynamical representation.

$$\text{Cu} \left| \text{Hg} \right| \text{Hg}_2\text{Cl}_2 \left| \text{KCl (sat)} \right| \text{Analyte}$$

$$E_1 \quad E_2 \quad\quad E_3 \quad\quad E_J$$

$$E_{ref} = E_1 + E_2 + E_3 + E_J$$

(b)
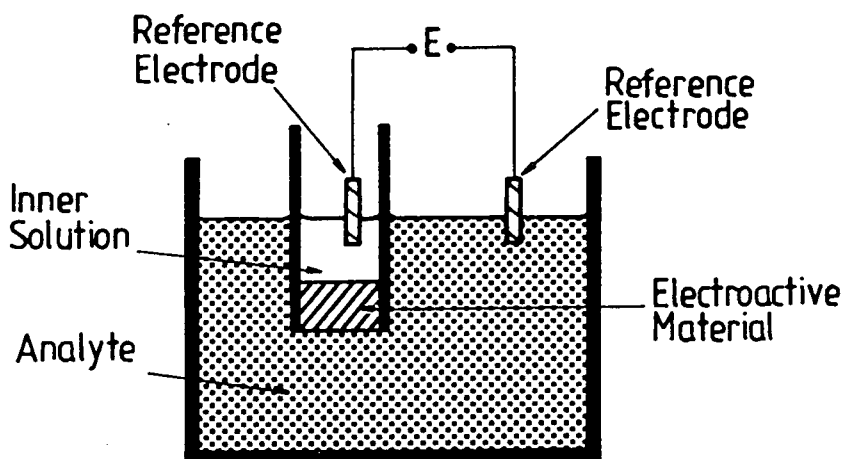
Figure 3.5 Conventional ISE measurement system.

3.4 ION-SELECTIVE ELECTRODES

The ion-selective electrode (ISE) is widely used for the detection and measurement of ionic species in solution [6]. A conventional ISE system is shown in figure 3.5 and is constructed in the following manner. A membrane containing the ion selective (electroactive) material is interposed between the unknown test analyte and an internal reference solution. The internal reference solution is of a known fixed chemical composition and is such that a reversible charge transfer can occur between it and the electroactive material. An internal reference electrode makes contact to the reference solution (and hence to the electroactive material), and the measurement system is completed by a second (external) reference electrode system contacting the analyte. This reference electrode serves the same purpose as that described in the previous section i.e. it forms an electrochemical cell against which the potential at the electroactive material/analyte interface is measured.

In figure 3.5, the ion sensing process takes place at the interface between the outer surface of the membrane and the analyte solution. An ion-exchange reaction between the solution and the surface layers of the membrane leads to a reversible transfer of charge, which gives rise to an interfacial potential between the two phases. If the charge transfer process is selective to the ion to be measured, with respect to other ions in the analyte, then the system behaves as an ISE. Contact to the inner surface of the membrane (via the inner reference solution) and contact to the reference solution (via the inner reference electrode) is achieved using the same type of charge transfer processes. Measurements using this system are possible when these charge-transfer reactions have reached a state of thermodynamic equilibrium. Using the membrane/analyte charge transfer reaction as an example, the equilibrium interfacial potential as a function of analyte concentration can be derived.

Thermodynamic equilibrium between the analyte (phase α) and the membrane (phase β) requires that the electrochemical potential $\bar{\mu}_i$ for the transferable species

26

i (involved in the ion-exchange reaction) be equal in both phases. In phase α,

$$\bar{\mu}_i{}^\alpha = \mu_i^{o\alpha} + RT \ln a_i{}^\alpha + z_i F \phi^\alpha \tag{6}$$

where $\mu_i^{o\alpha}$ is the standard chemical potential, $a_i{}^\alpha$ is the activity of species i in phase α, z_i is the charge on species i, ϕ^α is the Galvani potential of phase α, and R, T and F are the gas constant, absolute temperature and Faraday constant, respectively. The activity $a_i{}^\alpha$ is related to the concentration c_i^α, but takes into consideration the importance of the electrostatic interactions between ions at high ionic concentrations. At high ionic concentrations, electrostatic interaction of ion i with its neighbours reduces its ability to participate in any chemical reaction and so the effective concentration of the solution is reduced. For dilute solutions, concentration and activity are essentially equivalent.

A similar equation can be written for phase β, and applying the thermodynamic criterion for equilibrium

$$\bar{\mu}_i{}^\alpha = \mu_i^{o\alpha} + RT \ln a_i{}^\alpha + z_i F \phi^\alpha = \bar{\mu}_i{}^\beta = \mu_i^{o\beta} + RT \ln a_i{}^\beta + z_i F \phi^\beta \tag{7}$$

The interfacial potential between phases α and β is equal to $(\phi^\beta - \phi^\alpha)$, that is,

$$\Delta\phi = \phi^\beta - \phi^\alpha = \frac{(\mu_i^{o\alpha} - \mu_i^{o\beta})}{z_i F} + \frac{RT}{z_i F} \ln\left(\frac{a_i{}^\alpha}{a_i{}^\beta}\right) \tag{8}$$

The first term is a constant and is usually referred to as E_0 and therefore,

$$\Delta\phi = E_0 + \frac{RT}{z_i F} \ln\left(\frac{a_i{}^\alpha}{a_i{}^\beta}\right) \tag{9}$$

A similar equation can be derived for the interfacial potential developed between the inner membrane surface and the inner reference solution. $a_i{}^\beta$ can be eliminated and the total membrane potential, E_I, can be expressed in terms of $a_i{}^\alpha$ and $a_i{}^\gamma$, where $a_i{}^\gamma$ is the activity of species i in phase γ (the inner reference solution). $a_i{}^\gamma$ is known and a constant, and therefore E_I can be written as

$$E_I = \frac{RT}{z_i F} \ln\left(\frac{a_i{}^\alpha}{a_i{}^\gamma}\right) \tag{10}$$

27

For a singly charged ion at room temperature (298K), a graph of E_I against $\log_{10} a_i{}^\alpha$ is linear with a slope of 58 mV per decade change in activity. This is the well-known "Nernst equation" and is closely obeyed for conventional ISEs.

The membrane/solution interface of an ISE is an example of an "unblocked" interface i.e. charge transport can freely occur across the interface. Charge transfer occurs via an ion-exchange reaction which is the dominant process responsible for the generation of the electrode potential. An interface at which there is a absence of such reactions, and where no charge transport can occur, is termed "charge-blocked" or "blocked" [7,8]. The electrolyte/insulator interface of the ISFET described in sections 3.5 and 3.6 can be described as "blocked" and "reversible". That is, no charge transport occurs <u>across</u> the interface, but the electrolyte interacts with the insulator via reversible surface adsorption processes <u>at</u> the interface. These processes are also in equilibrium with the diffuse charges in the bulk of the electrolyte, and the system's response is determined by both the reversible electrochemical phenomena and the total ionic strength of the analyte.

3.5 THE INSULATOR/ELECTROLYTE INTERFACE AND SITE DISSOCIATION THEORY

The aim of this section is to describe the reactions taking place at the insulator/electrolyte surface, and to derive the surface charge σ_0 in terms of the pH of the electrolyte. σ_0 corresponds to the potential difference ϕ_0 between the gate surface and the bulk solution. Section 3.6 derives the relation between σ_0 and ϕ_0, and from this, σ_0 in terms of pH can be evaluated.

The origin of the interfacial potential, which determines the response of the ISFET, is the interaction of the insulator with the H^+ and OH^- ions in the solution. These ions are the so-called potential determining ions. The gate surface is covered with hydrophilic hydroxy OH groups which are amphoteric in nature i.e. the site can act as a proton donor or acceptor. The oxide surface thus contains three possible forms of site: negatively charged $Si - O^-$, neutral Si-OH and pos-

28

itively charged $Si - OH_2^+$. The degree of adsorption of the potential determining ions is dependent on their relative activities, and thus the oxide surface charge is pH dependent. The site dissociation theory [7,8] describes the dissociation and association of the amphoteric Si-OH sites in the form of two dissociation reactions, characterised by two equilibrium constants. The Si-OH groups interact directly with the H^+ ions located directly near the surface, H_s^+. The reactions then read as:

$$Si - OH_2^+ \rightleftharpoons Si - OH + H_s^+, \quad K_1 = \frac{[Si - OH][H^+]_s}{[Si - OH_2^+]} \quad (11)$$

$$Si - OH \rightleftharpoons Si - O^- + H_s^+, \quad K_2 = \frac{[Si - O^-][H^+]_s}{[Si - OH]} \quad (12)$$
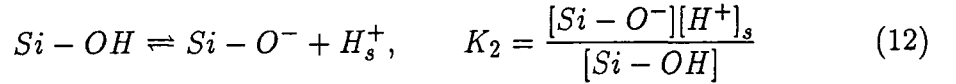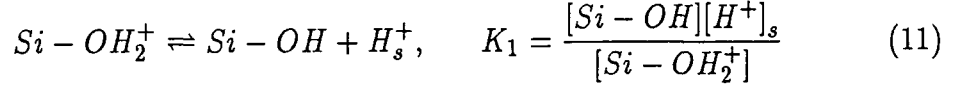
where $[Si - OH_2^+], [Si - OH]$ and $[Si - O^-]$ are the number of sites per unit surface area and $[H^+]_s$ is the surface concentration. The Boltzmann equation relates the surface concentration of H^+ ions, $[H^+]_s$, to the bulk concentration, $[H^+]_b$, and therefore

$$[H^+]_s = [H^+]_b \exp\left(\frac{-q\psi_0}{kT}\right) \quad (13)$$

where q is the elementary charge, k is Boltzmann's constant, T is the absolute temperature and ψ_0 is the potential difference between the bulk solution and the ISFET surface generated by the surface charge σ_0.

The surface charge is clearly:

$$\sigma_0 = q\{[Si - OH_2^+] - [Si - O^-]\} = q[Si - OH]\left\{\frac{[H^+]_s}{K_1} - \frac{K_2}{[H^+]_s}\right\} \quad (14)$$

and substituting for $[H^+]_s$ using (13) we have:

$$\sigma_0 = q[Si - OH]\left\{\frac{[H^+]_b \exp(-q\psi_0/kT)}{K_1} - \frac{K_2}{[H^+]_b \exp(-q\psi_0/kT)}\right\} \quad (15)$$

One more equation relating the surface species concentrations can be formulated, namely, the conservation of the number of surface sites

$$N_s = [Si - OH] + [Si - O^-] + [Si - OH_2^+] \quad (16)$$

Combining equations (11) to (16) Dousma *et al* [9] obtained a first relation between ψ_0, σ_0 and $pH = -\log[H^+]_b$, resulting in

$$2.303pH = 2.303(K_1/K_2)^{\frac{1}{2}} + \frac{q\psi_0}{kT} + \sinh^{-1}\left\{\frac{\sigma_0}{2qN_s(K_1K_2)^{\frac{1}{2}}}\right\} \quad (17)$$

Dousma made the assumptions that; $K_1K_2 \ll 1$ for inorganic insulators, which is justified according to tabulated values, and also that saturation of the pH response i.e. $\sigma_0 = qN_s$ can never occur with the pH range available in aqueous solutions. The pH of zero charge pH_{pzc} is the pH which results in a net zero charge (i.e. $\sigma_0 = \psi_0 = 0$) and from equation (17) it is clear that $pH_{pzc} = (K_1/K_2)^{\frac{1}{2}}$ and (17) can be rewritten as:

$$2.303(pH - pH_{pzc}) = \frac{q\psi_0}{kT} + \sinh^{-1}\left\{\frac{\sigma_0}{2qN_s(K_1K_2)^{\frac{1}{2}}}\right\} \quad (18)$$

To obtain the relationship between ψ_0 and pH, a ψ_0/σ_0 relation must be considered. The interfacial potential ψ_0 actually measured with an ISFET is related to the surface charge density σ_0 using the Gouy-Chapman-Stern theory.

3.6 RELATIONSHIP BETWEEN σ_0 AND ψ_0 USING GOUY-CHAPMAN-STERN THEORY

The Gouy-Chapman-Stern (GCS) model describes the charge distribution at a metal-solution interface. It is a refinement of the Gouy-Chapman theory, which is itself, an elaboration on the earlier "electric-double layer" model proposed by Helmholtz. In applying the GCS model to the electrolyte-insulator-semiconductor system it is worthwhile describing the origin of the model.

Helmholtz proposed that the counter charge to the excess charge residing at the metal surface was distributed in an "infinitely thin" planar sheet on the adjacent surface of the solution. The Helmholtz double layer is shown in figure 3.6a. However, the model predicts a double layer capacitance which is independent of applied voltage; and this is not found experimentally.

Gouy and Chapman [10] recognised that the solution charge distribution would not be uniform, but distorted. Since charge is attracted towards the electrode,
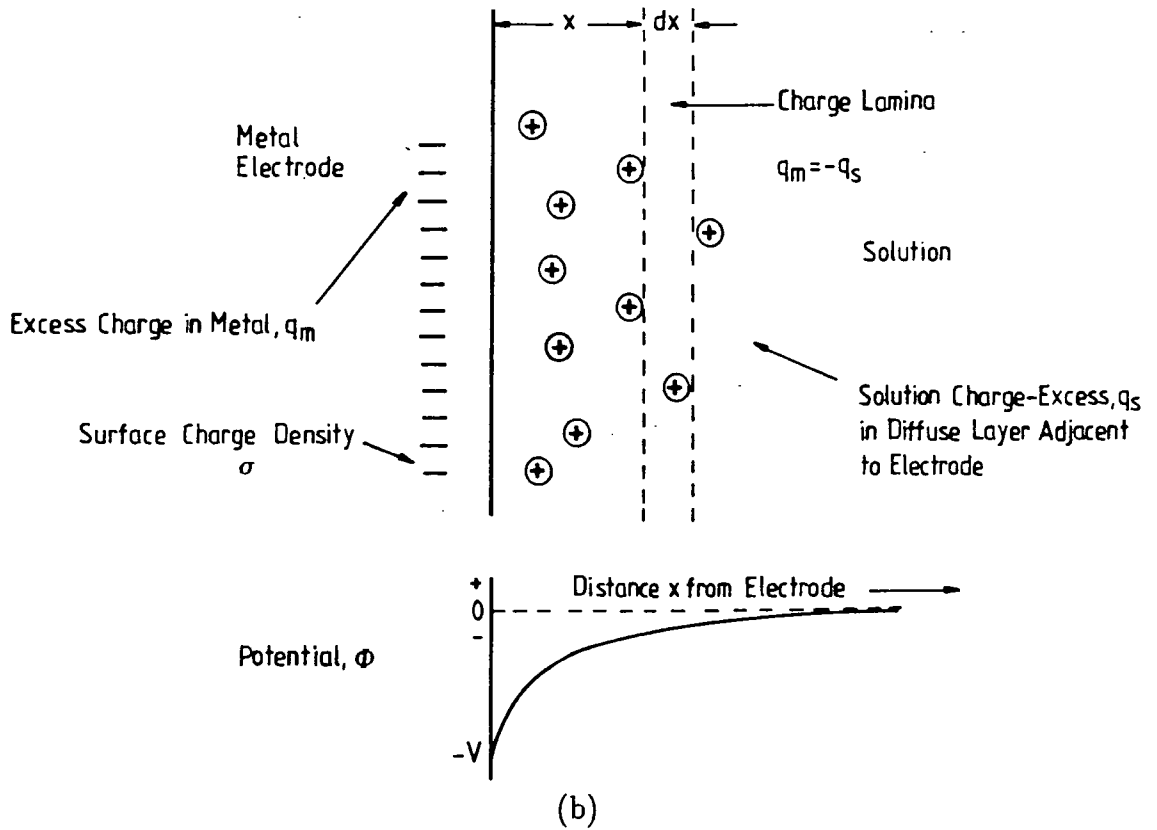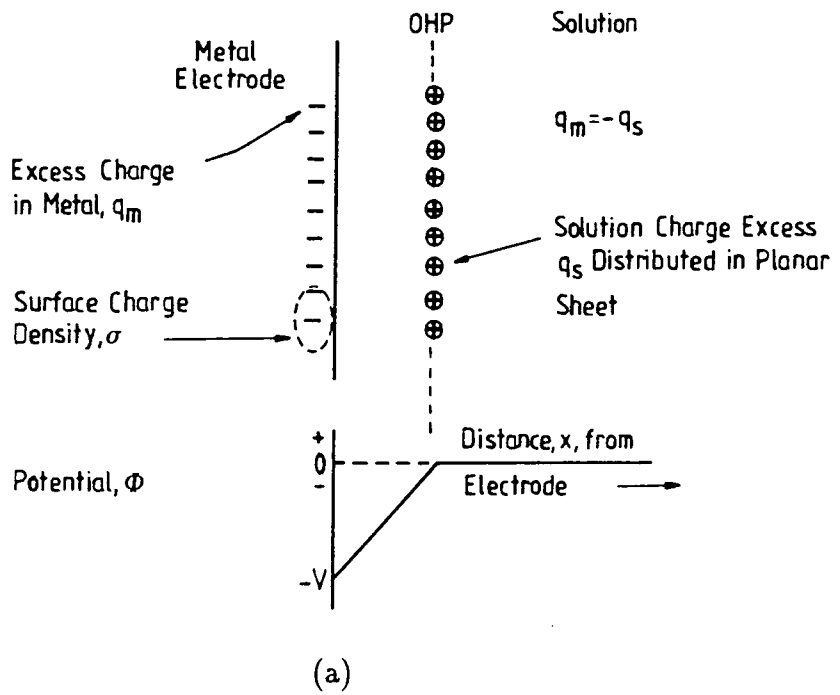
Figure 3.6 Models for the metal-electrolyte interface (a) Helmholtz double layer, and (b) the Gouy-Chapman diffuse charge model and potential profile.

IHP OHP

Metal Electrode

O Water Molecule

Electrolyte

Solvated Positive Ion

(a)

Hydrated Positive Ion

Partially Desolvated
Contact Adsorbed
Positive Ion

0 x_2 Distance x from Electrode →

Potential

Φ_{x_2}

(b)

Φ_0

σ_a

σ_d

$\sigma_a + \sigma_d = \sigma_s = -\sigma_m$

Charge
Density

0

σ_m

(c)
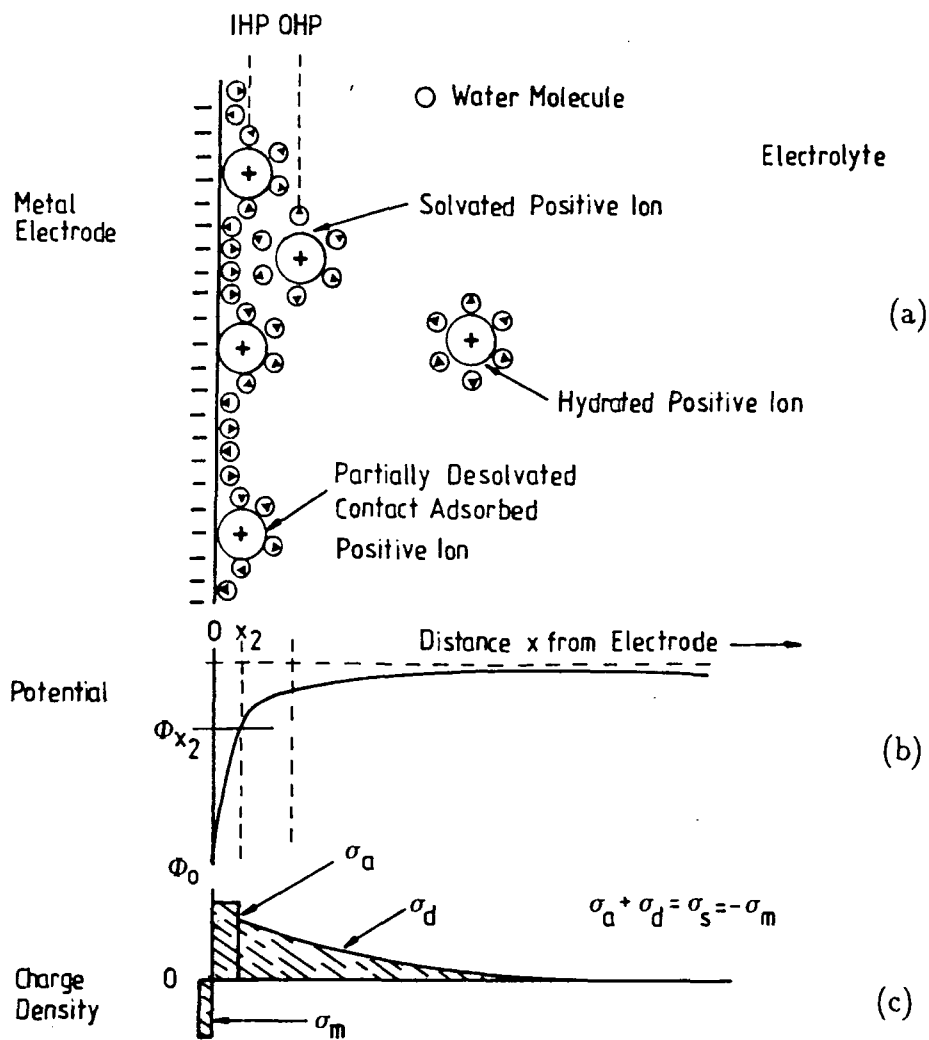
Figure 3.7 GCS model of the metal-electrolyte interface showing (a) the adsorbed, solvated ions and partially desolvated, contact adsorbed ions, and (b) potential profile, and (c) excess charge distribution.

charge concentration, and therefore electric field, decrease with increasing distance from the electrode. Therefore, the effects of random thermal processes which lead to distortions become more noticeable further away from the metal surface. The charge was envisaged to form a diffuse layer, and its potential profile is indicated in figure 3.6b. The diffuse layer can be represented as a discrete capacitance, C_d, characterised by a plate separation of d. As the ionic concentration increases, a thinner diffuse layer is required to counter the excess charge on the metal surface, and hence C_d increases. Similarly d decreases as the interfacial potential increases.

The potential distribution $\psi(x)$ in the diffuse layer can be obtained by combining Boltzmann's and Poisson's equations. By using Gauss's law applied to the electrode surface, the potential difference ψ across the Gouy-Chapman layer can be related to the solution excess charge density σ. The result is as follows:

$$\psi = \frac{2kT}{q} \sinh^{-1} \left\{ \frac{\sigma}{(8\epsilon_r \epsilon_0 kTC)^{\frac{1}{2}}} \right\} \tag{19}$$

where $\epsilon_r \epsilon_0$ is the permittivity and C is the ionic concentration of the solution, respectively.

Stern [11] later realised that the ions are prevented from fully approaching the electrode surface by their hydration sheaths, and took this into account in modifying the Gouy-Chapman model. He proposed that the charge distribution should be divided into three regions depicted in figure 3.7. The first extends from the metal to the plane through the centres of the specifically adsorbed (partially solvated) positive ions. This is called the inner Helmholtz plane (IHP). The second region is bounded on one side by the IHP and on the other by the outer Helmholtz plane (OHP). The OHP is defined by the centres of the hydrated ions at their distance of closest approach. The third region extending from the OHP into the bulk of the solution is the diffuse layer of the Gouy-Chapman model. This is the so-called GCS model and it can be applied to the electrolyte-insulator-semiconductor (EIS) system of the ISFET to relate ψ_0 and σ_0. The charge and potential distributions for the EIS system as well as an equivalent circuit are shown
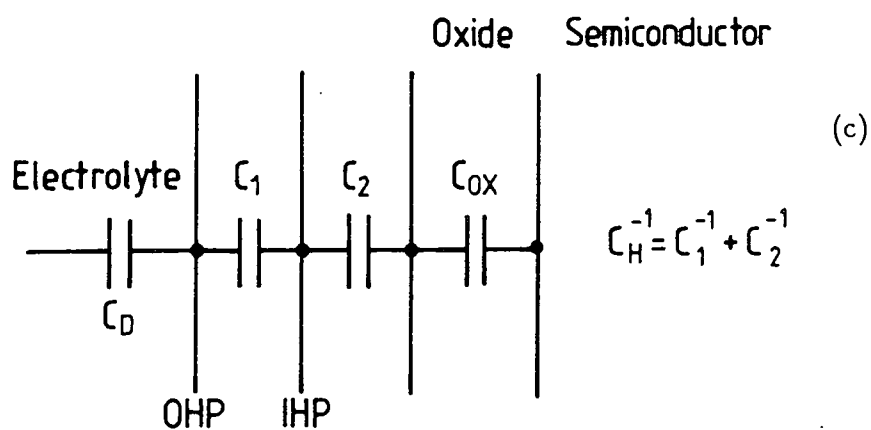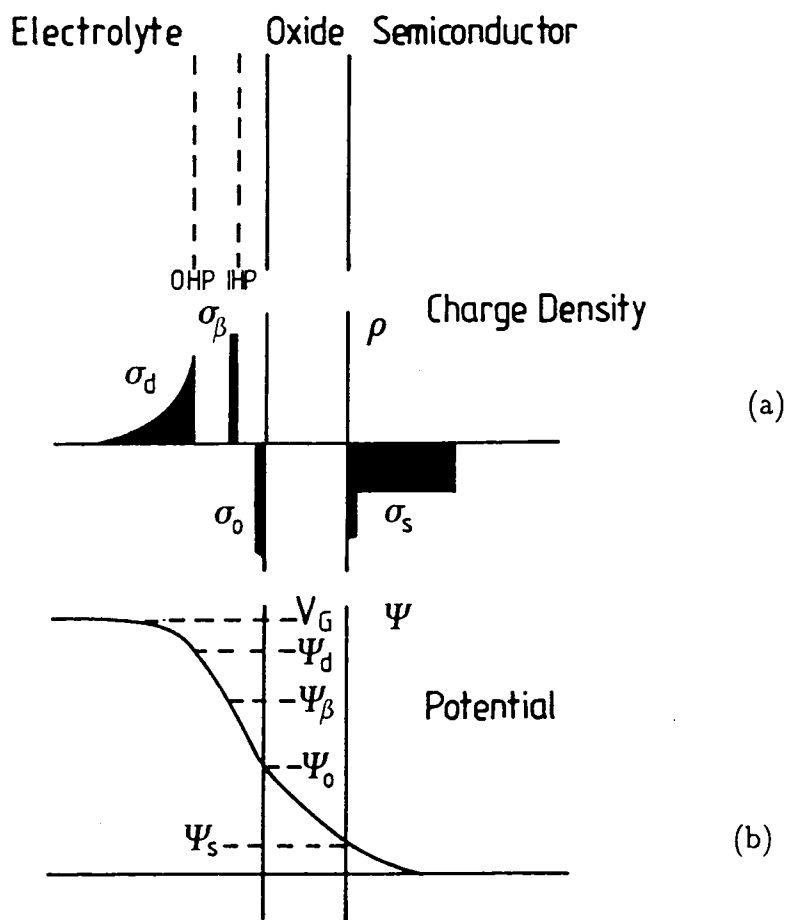
Figure 3.8 The EIS system showing (a) the charge, and (b) potential distributions, and
(c) the equivalent circuit.

in figures 3.8a, b, and c, respectively. C_H and C_{OX} are the capacitances (per unit area) of the Helmholtz layer and the oxide, respectively. ψ_0 can be partitioned into two components (referring to figure 3.8b)

$$\psi_0 = (\psi_0 - \psi_d) + \psi_d$$

where $(\psi_0 - \psi_d) = \sigma_0 / C_H$ and ψ_d is the potential difference across the diffuse layer capacitance given by

$$\psi_d = \frac{2kT}{q} \sinh^{-1} \left\{ \frac{\sigma_d}{(8\epsilon_r \epsilon_0 kTC)^{\frac{1}{2}}} \right\} \qquad \text{from} \quad (19)$$

where σ_d is the diffuse layer surface charge. Hence,

$$\psi_0 = \frac{2kT}{q} \sinh^{-1} \left\{ \frac{\sigma_d}{(8\epsilon_r \epsilon_0 kTC)^{\frac{1}{2}}} \right\} + \frac{\sigma_0}{C_H} \qquad (20)$$

Bousse $et\ al$ [12] have fully discussed the solution of this equation and have demonstrated that the deviations between the exact solution and an approximate one (with $\sigma_d = \sigma_0$ are very slight, and become even smaller as C increases). Therefore equation (20) can be rewritten approximately as

$$\psi_0 = \frac{2kT}{q} \sinh^{-1} \left\{ \frac{\sigma_0}{(8\epsilon_r \epsilon_0 kTC)^{\frac{1}{2}}} \right\} + \frac{\sigma_0}{C_H} \qquad (21)$$

This is the relationship between ψ_0 and σ_0 for the ISFET system. Combining (21) with (15) (which is the ψ_0, σ_0 and pH relation) and (16) Bousse obtained an exact solution for σ_0 as a function of pH. The derivation is complicated and beyond the scope of this thesis. However, a simpler solution can be obtained if ionic concentrations greater than or equal to 0.1 M are considered. Taking the total number of sites per unit area, N_s, for SiO$_2$ to be 5×10^{-14} cm^{-2}, so that for a fully ionised surface, $\sigma_{0,\text{max}} = qN_s \simeq 10^{-4}$ C cm^{-2}, then the argument of the sinh^{-1} function is $\simeq 2.5 \times 10^{-7}$ and thus the function can be replaced by its argument. Therefore (21) can be rewritten as

$$\psi_0 = \frac{\sigma_0}{C_D} + \frac{\sigma_0}{C_H} = \frac{\sigma_0}{C_R} \qquad C_D = \frac{q}{2kT}(8\epsilon_r \epsilon_0 kTC)^{\frac{1}{2}} \qquad (22)$$

$pK_1 = 9$
$pK_2 = 10$

$N_S = 10^{12} cm^{-2}$
10^{13}
10^{14}
10^{15}

$\Delta\psi_o$

$100\,mV$

pH
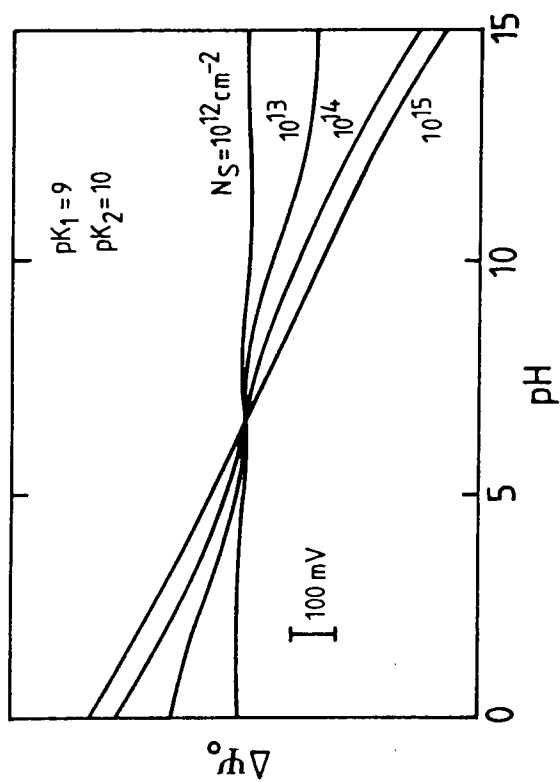
Figure 3.9 Theoretical pH response according to the site binding model (showing dependence on N_S). For $N_S = 10^{15}$ cm^{-2}, the response is virtually Nernstian.

and $C_R^{-1} = C_D^{-1} + C_H^{-1}$ and C_D is the diffuse layer capacitance. It can be seen from (22) that the EIS system can be represented as a pair of capacitors in series. One component C_D is the diffuse layer capacitance and the other, C_H, is the Helmholtz layer capacitance. This combined capacitance determines the surface potential ψ_0 generated by the surface charge density σ_0

A final ψ_0/pH relation can now be obtained by combining equation (22) and equation (21) from the last section, and eliminating σ_0 hence

$$2.303(pH - pH_{pzc}) = \frac{q\psi_0}{kT} + \sinh^{-1}\left\{\frac{\psi_0 C_R}{2qN_s(K_1K_2)^{\frac{1}{2}}}\right\} \qquad (23)$$

Introducing a dimensionless sensitivity parameter β,

$$\beta = 2q^2 N_s (K_1 K_2)^{\frac{1}{2}} / kT C_R$$

which reflects the chemical sensitivity of the surface in terms of the site density N_s of the hydroxyl groups and the surface reactivity. The surface reactivity is characterised by the equilibrium constants K_1 and K_2. The last equation now reads,

$$2.303(pH - pH_{pzc}) = \frac{q\psi_0}{kT} + \sinh^{-1}\left\{\frac{q\psi_0}{kT\beta}\right\} \qquad (24)$$

For $\beta \gg q\psi_0/kT$, the equation can be simplified by approximating the $\sinh^{-1}$ function by its argument and rearranging to give the final relationship,

$$\psi_0 = 2.303\frac{kT}{q}\left(\frac{\beta}{\beta+1}\right)(pH - pH_{pzc}) \qquad (25)$$

pH_{pzc} is simply equal to $(pK_1 + pK_2)/2$. The characteristics of the gate surface, and hence the ψ_0/pH curve are dependent on the parameters K_1, K_2 and N_s.

Van den Berg et al [13] have analysed the effect on the ψ_0/pH as a function of K_1, K_2 and N_s. Increases in K_1^{-1}, K_2 and N_s all lead to a shift from non-Nernstian to Nernstian behaviour. N_s largely influences the response as can be seen in figure 3.9. For N_s values $\leq 10^{14}$ cm^{-2} a saturation effect at $pH \geq pH_{pzc}+3$ is observed. The next section addresses the question of the measurement of the ψ_0/pH response.
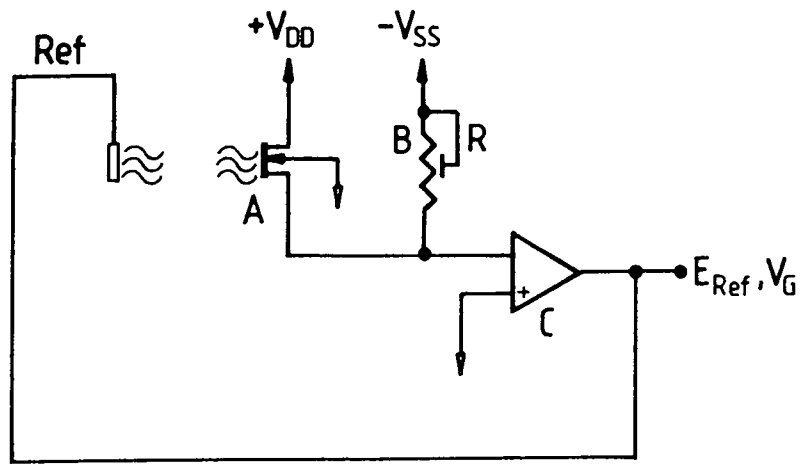
Figure 3.10 ISFET operating mode at constant drain current.

1- Before pH change.
2- After pH change.
3- After pH change
   for fixed reference
   electrode voltage.
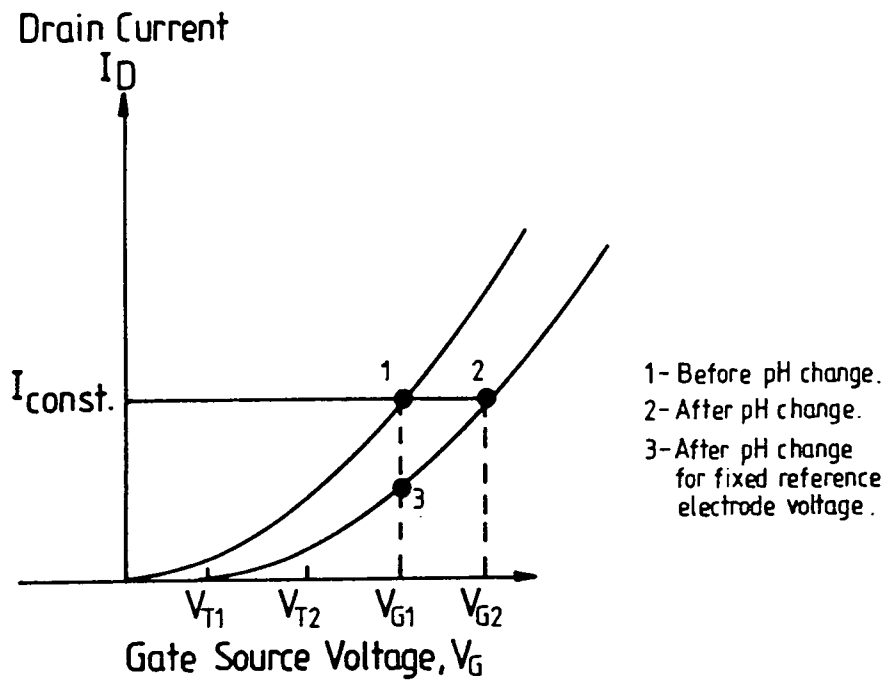
Figure 3.11 Operation of the electronic circuitry in terms of a shift (at constant drain current) from one threshold characteristic to another.

3.7 ψ_0/pH RESPONSE DETERMINATION

It is worthwhile summarising the equations so far derived in this chapter in order to see how the ψ_0/pH response might be measured. The equations describing the basic operation of the ISFET are:

$$I_D = \mu C_{OX} \frac{W}{L} \left[(V_G - V_T)V_D - \frac{1}{2}V_D^2 \right] \tag{1}$$

$$V_T = V_{FB} - \frac{Q_B}{C_{OX}} + 2\phi_F \tag{3}$$

$$V_{FB} = E_{ref} - \psi_0 + \chi^{sol} + \frac{\Phi_M}{q} - \frac{\Phi_{Si}}{q} - \frac{Q_{IT} + Q_{OX}}{C_{OX}} \tag{5}$$

$$\psi_0 = 2.303\frac{kT}{q}\left(\frac{\beta}{\beta+1}\right)(pH - pH_{pzc}) \tag{25}$$

Following this "equation-tree" the ISFET can be considered to have a threshold voltage V_T which is dependent on pH. One method of observing the effect of a change in pH is to directly measure the corresponding change in drain current I_D. However, a more elegant method, which allows the direct determination of the change in ψ_0 as a function of pH, has been used for the ψ_0/pH measurements described in this thesis.

From equation (1), it can be seen that a pH-induced change in V_T could be offset by an equal and opposite change in V_G (i.e. $V_G - V_T$ is unchanged), thus keeping the drain current I_D constant. The change in V_T (and hence the change in surface potential ψ_0) equals the change in V_G required to keep I_D constant. Therefore keeping I_D constant, by adjusting V_G, provides a direct means of measurement of ψ_0. The electronic circuitry required to control I_D is shown in figure 3.10. The drain current I_D flowing through the ISFET A is set by the current source B, and the purpose of the amplifier C (remembering that no

34

current flows into C) is to maintain I_D through the ISFET. The output V_G of the amplifier is applied to the reference electrode. When the ISFET is placed in solution the amplifier automatically adjusts V_G according to the pH of the solution so that a drain current of I_D flows through the ISFET. A pH-induced change in V_T ordinarily means a change in I_D, but in the feedback system of figure 3.10 this would involve the amplifier either sinking or sourcing (depending on the change in V_T) current. However, C adjusts its output V_G so that the ISFET sources or sinks the required amount of current. Thus the amplifier acts in such a way that the current I_D flows completely through the ISFET. The operation of the circuit can be appreciated by referring to figure 3.11. Intially, the ISFET is described by the (I_D, V_G) transfer characteristics with a threshold voltage of V_{T1} and an operating point of (V_{G1}, I_{const}). On a pH-induced threshold voltage change to V_{T2} the transfer characteristic moves, and V_G must be controlled to V_{G2} in order to maintain the drain current I_{const}. The response of the system to a change in pH is governed by the electrochemical processes at the surface/electrolyte interface. It is not limited by the response of the amplifier (typically μs which is determined by the amplifier transfer characteristics).

3.8 THE ISFET WITH AN ORGANIC FILM MEMBRANE AS THE GATE

The ISFET structure described so far in this chapter has utilised inorganic gate materials (e.g. SiO_2, Si_3N_4) which are well known in MOS technology. Coincidentally, these materials are also pH sensitive, however, very few materials are known that are both compatible with MOS technology and also have selectivity for ions other than H^+. However, with the development of conventional ion-selective electrodes (ISEs), it is known that a variety of ion-exchange materials can be entrapped within an organic matrix to form solid-state membrane electrodes. The matrix normally consists of a combination of an organic material such as PVC and a plasticiser. If it is possible to incorporate an ion-exchanging, organic membrane

V_{Bias}

Reference
Electrode

Encapsulant

Source
Metallization

Drain
Metallization

Bulk
Metallization

Analyte

Electroactive
Gate Material

Si_3N_4 Ion-
Barrier

SiO_2

n^+ n^+

p Substrate

(a)

G   Reference Electrode

Electrolyte

S $\downarrow I$ D

n^+ n^+

$\Delta \varphi = E_o + \dfrac{RT}{F} \ln a_i$

p-Si
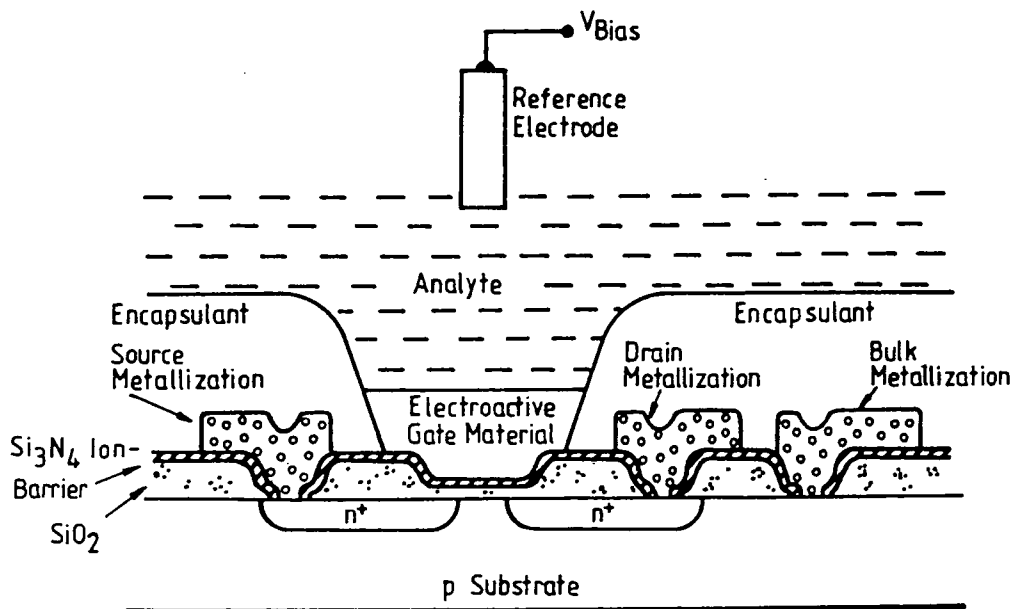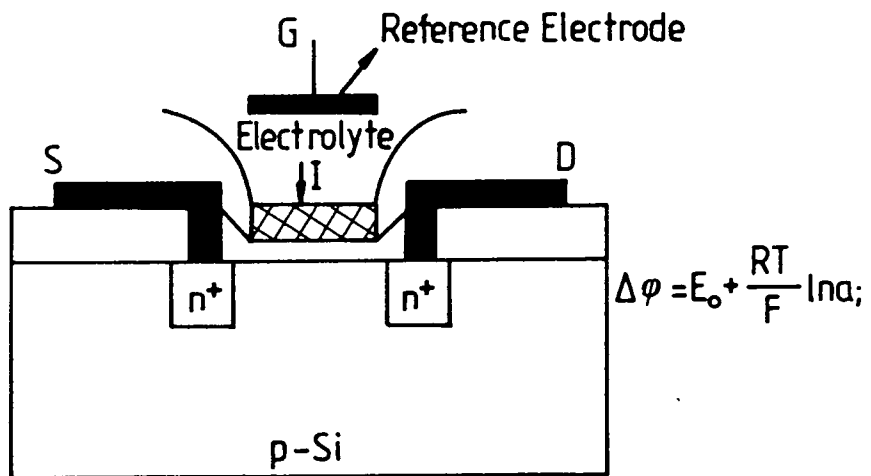
I = ion exchanger in matrix
organic material

(b)

Figure 3.12 Dual dielectric ISFET with an electroactive gate film showing (a) cross section, and (b) schematic with the Nernst equation.

with the ISFET, a CHEMFET might be realised. The CHEMFET is simply a combination of a chemically sensitive layer and the potential-sensitive FET structure. A well-known example is the potassium-sensitive CHEMFET which utilises a plasticiser/polyvinylchloride (PVC) membrane and contains valinomycin as the ion-exchanger. The first report of such a device was by Moss *et al* [14] in 1975 and since then much work has been done concerning the ion-exchanging materials used and the type of polymer used as the substrate. Very high specificity can be obtained using ionophoric materials such as valinomycin, and a triple-function chemical sensing CHEMFET for K^+, H^+ and Ca^{2+} has been described by Sibbald *et al* [15].

A cross-section through the ISFET structure coated with an electroactive gate film is shown in figure 3.12. The ISFET structure is charge-blocked and the potential determining processes at the membrane/solution interface are thought to be similar to those occurring in ion-selective electrodes. That is, the membrane/solution interface is thought to be non-blocked, and the threshold voltage V_T depends on the ionic activity, a_i, according to the Nernst equation, given in figure 3.12b (equation (9)).

A critical point in the construction of a CHEMFET is the attachment of the gate membrane to the underlying inorganic material. Normally application is by dip-coating or spinning of a suspension which contains the membrane material. This relies on a physical bond for the attachment and is not ideal, and loosening of the chemically sensitive layer whilst in solution has a deleterious effect on the lifetime of the device. Loosening of the electroactive gate will allow the solution to reach the dielectric/membrane interface and hence its potential will be altered. This potential is expected to behave according to the site-binding theory and will modify the threshold voltage dependence as outlined in section 3.2. For an ideal CHEMFET the dielectric/membrane potential should be constant, but Fogt *et al* [16] have demonstrated that it is possible for CO_2 and organic acids to diffuse through polymeric membranes resulting in local pH changes at the interface, and

36
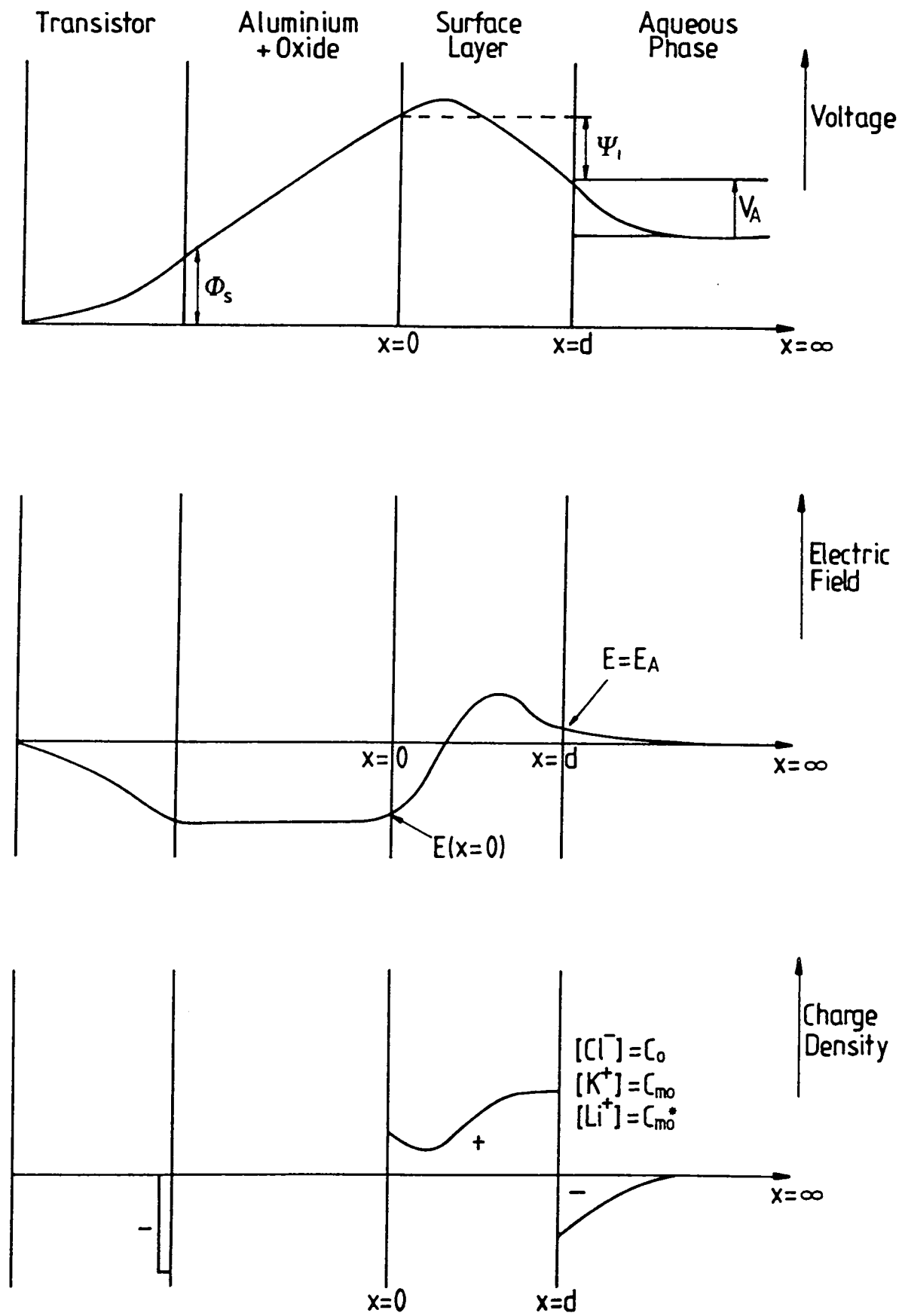
Figure 3.13 Three abutting phases of the LB-film gate ChemFET showing the potential, electric field and charge distributions (after ref. 17).
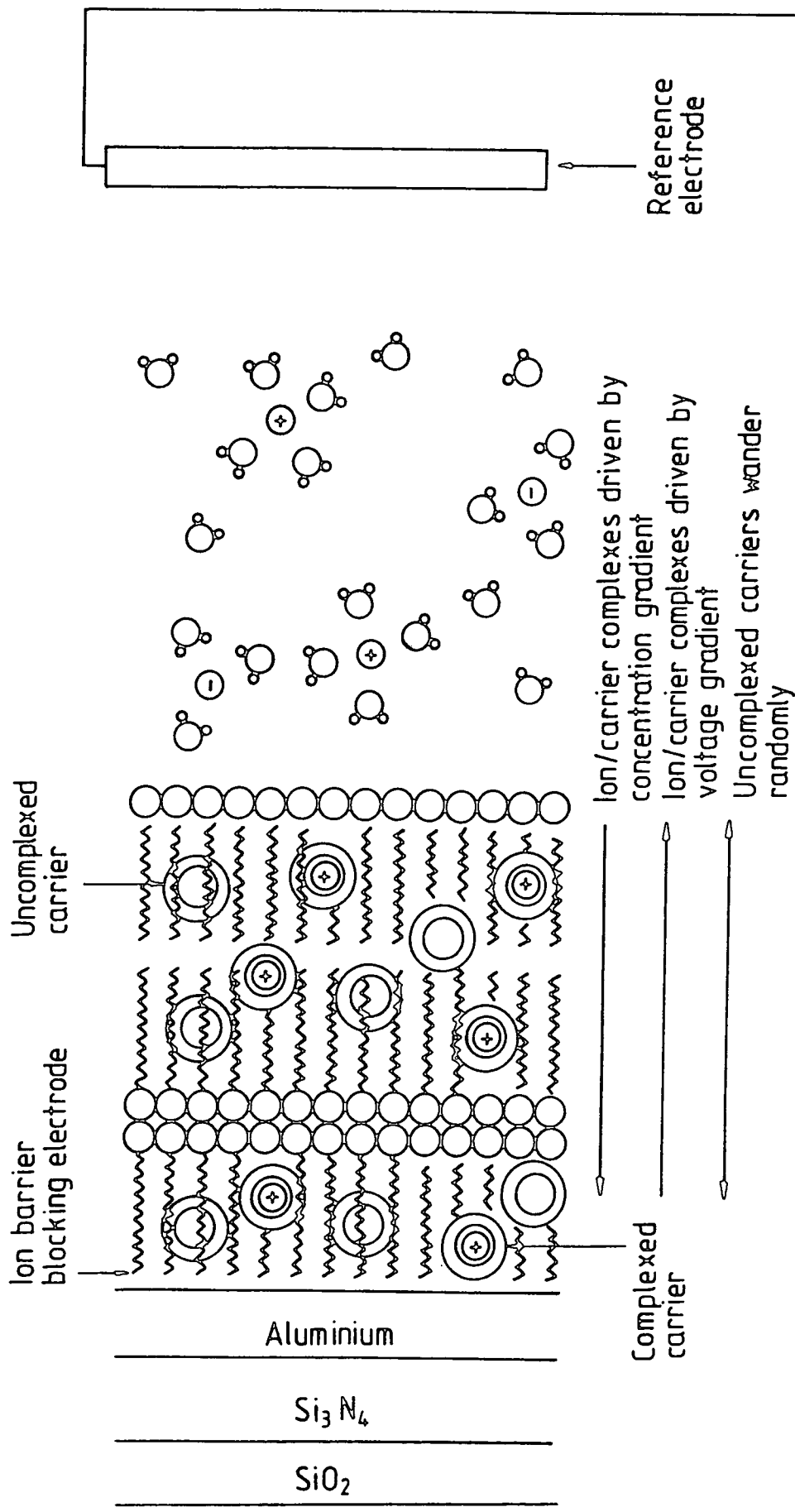
Figure 3.14 The LB film membrane in solution showing the diffusive concentration and electric field gradients (after ref. 17).

Reference electrode

Uncomplexed carrier

Ion barrier blocking electrode

Complexed carrier

Ion/carrier complexes driven by concentration gradient

Ion/carrier complexes driven by voltage gradient

Uncomplexed carriers wander randomly

Si_3N_4

SiO_2
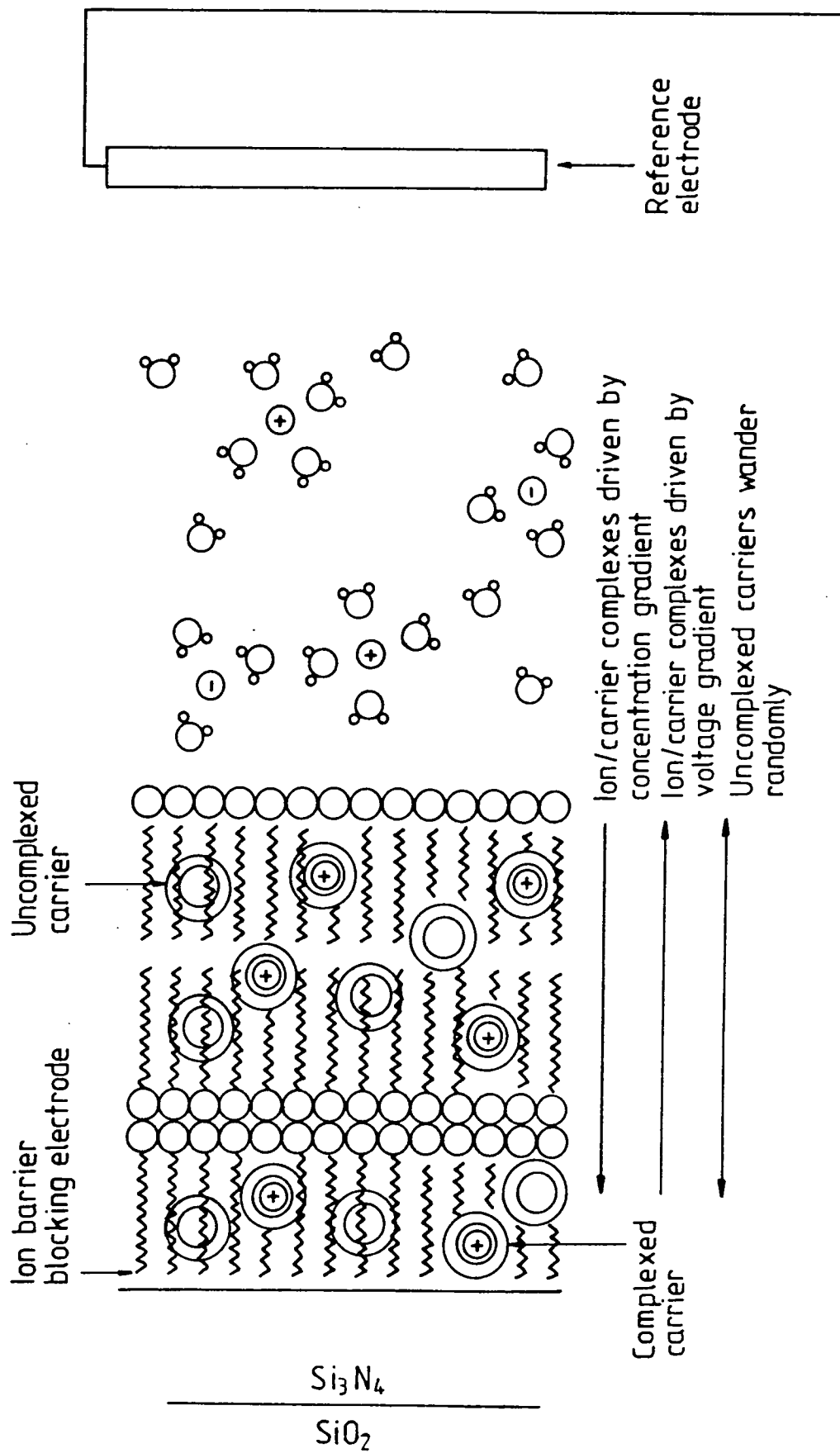
Figure 3.15 The LB film membrane in solution for the system described in this thesis.

reported in this thesis is shown in figure 3.15. The diagram is the same except for the aluminium layer which has been omitted because in the present work the LB film membranes were deposited directly onto the ISFET surface. The origin of the potential in the membrane is as follows. Intially before immersion the membrane contains no ions. However, on immersion the potassium (K^+) and lithium (Li^+) ions feel a diffusive force to enter the membrane. Potassium ions are able to penetrate the valinomycin-doped layer by undergoing complexation (as in the biological membrane), but the lithium ions are prevented from doing so owing to the selectivity of the valinomycin molecule. As each K^+ cation leaves the solution to enter the layer a corresponding counterion (e.g. Cl^- anion) is left behind in solution. In this way charge is redistributed, and an electric field directed out of the layer is established. At some point equilibrium is attained with the electric force on each particle equal and opposite to the concentration gradient-driven diffusive force. Then a surface dipole caused by the adsorption of K^+ ions in the membrane exists and it is this which is measured by the MOSFET system. From this the K^+ concentration in the electrolyte can be derived.

The system of equations describing the device is solved in the following manner. Poisson's equation is solved for each of the three phases which allows the electric field, voltage and charge distribution profiles for each phase to be determined separately as analytic functions (see figure 3.13a, b, and c). However, it is impossible to obtain an analytic expression to describe the entire system. When the device is operated in a circuit with a bias (reference electrode) voltage, a closed voltage loop is formed and according to Kirchoff's voltage law the loop voltage must be equal to zero. It transpires that the voltage across each phase can be expressed as an analytic function of the voltage, V_A at the surface layer/aqueous phase interface as follows

$$V(x = d) = V_A, \quad E(x = d) = E_A = f_1(C_0, V_A)$$

where $C_0 = C_{m0} + C_{m0}^*$ and C_{m0} and C_{m0}^* are the bulk concentrations of the specifically adsorbable ion (K^+) and the non-adsorbable ion (Li^+), respectively.

ψ_1 is the voltage drop across the surface layer and is given by

$$\psi_1 = f_2(E_A) = f_3(C_0, V_A)$$

$E(x = 0)$ is used both to calculate the voltage drop across the aluminium layer and also the surface potential V_S at the silicon/aluminium interface. Hence,

$$E(x = 0) = f_4(C_{m0}, \psi_1, E_A, V_A) = f_5(C_{m0}, C^*_{m0}, V_A)$$

Since the electric field is constant (and equal to $E(x = 0)$) across the aluminium layer the voltage drop can be obtained from the thickness of the layer. Finally the electric field at the silicon/aluminium interface E_S is equal to $E(x = 0)$ from which V_S can be obtained

$$V_S = f_6(E(x = 0)) = f_7(C_{m0}, C^*_{m0}, V_A)$$

The sum of the voltage differences across each phase is therefore also a function of V_A, say, $F(V_A)$ and Kirchoff's voltage law demands that $F(V_A) = 0$. For a given V_A, C_{m0}, C^*_{m0} this equation can be numerically solved for V_A. Back substitution of V_A into the above functions yield the voltages across each phase, from which the electric field and charge distribution profiles may be obtained.

3.9 SUMMARY

In this chapter the basic operating principles of the ISFET have been described in terms of the combination of a MOSFET and an ion sensitive membrane. The operation of the MOSFET is described by standard MOS theory whilst that of the ion sensitive membrane is similar to that of conventional ion-selective electrodes. The pH sensitivity of a Si_3N_4 surface has been analysed in terms of reversible surface reactions between the amphoteric surface hydroxyl sites and the potential determining (H^+ and OH^-) ions in the electrolyte. Similarly, the potassium ion sensitivity of a valinomycin-doped membrane was based on the development of an interfacial potential difference across the layer as a result of a charge redistribution. The following chapter describes the techniques employed for fabricating valinomycin doped Langmuir-Blodgett films to act as the potassium ion sensitive membranes in ISFETs.

CHAPTER 4

EXPERIMENTAL TECHNIQUES

4.0 INTRODUCTION

In this chapter the techniques employed in the fabrication and characterisation of Langmuir-Blodgett (LB) films and ion sensitive field effect transistor (ISFET) devices are described. In section 4.1 all aspects of LB film technology are discussed. Section 4.2 deals with the preparation of LB films and section 4.3 concerns their subsequent deposition. Section 4.4 describes substrate preparation and the fabrication of the ISFET devices. Sections 4.5 and 4.6 present the techniques used for structural characterisation of the LB films and characterisation of the devices, respectively.

4.1 LB FILM TECHNOLOGY

Since the pioneering work of Langmuir and Blodgett [1], developments have led to a number of variations on the original trough, including a circular trough with a radial compression barrier [2] and an alternate layer trough [3] used for the rapid, efficient production of ABAB... type supermolecular non-centrosymmetric LB film structures. These structures are of importance in non-linear optical and pyroelectrical applications. The trough employed for the work described in this project was of the constant perimeter barrier type and is described below.

4.1.1 The conventional Langmuir trough

A conventional Langmuir trough is illustrated in figure 4.1 and a photograph is shown in figure 4.2. The trough itself was made of glass and mounted on a metal platform which could be raised or lowered in order to maintain the height of the water relative to the barriers. When dissolved salts were used at an appreciable concentration (> 0.01 M) in the subphase, a small-volume trough (typically 5 l)
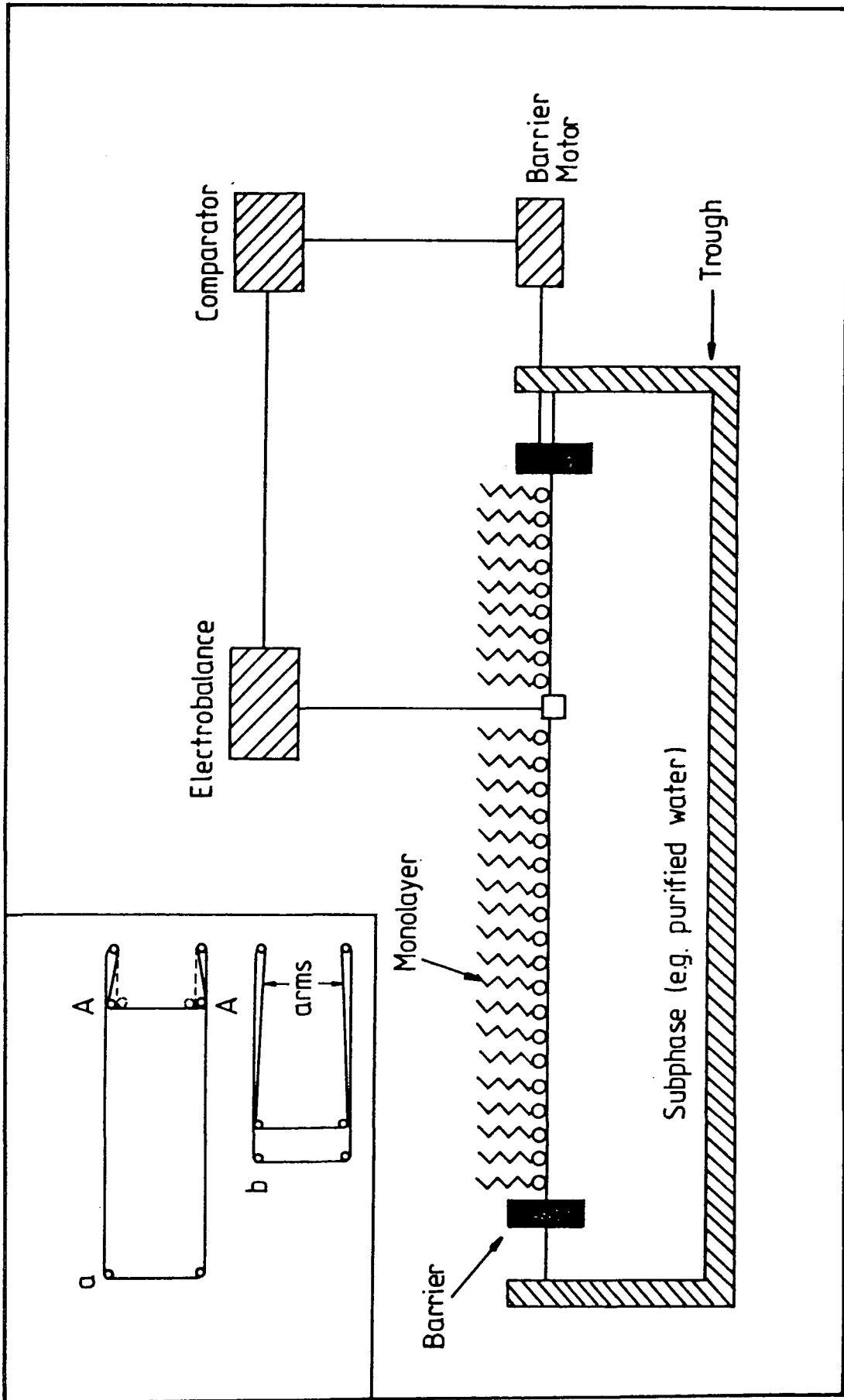
Figure 4.1 Schematic diagram of the constant perimeter barrier Langmuir trough.
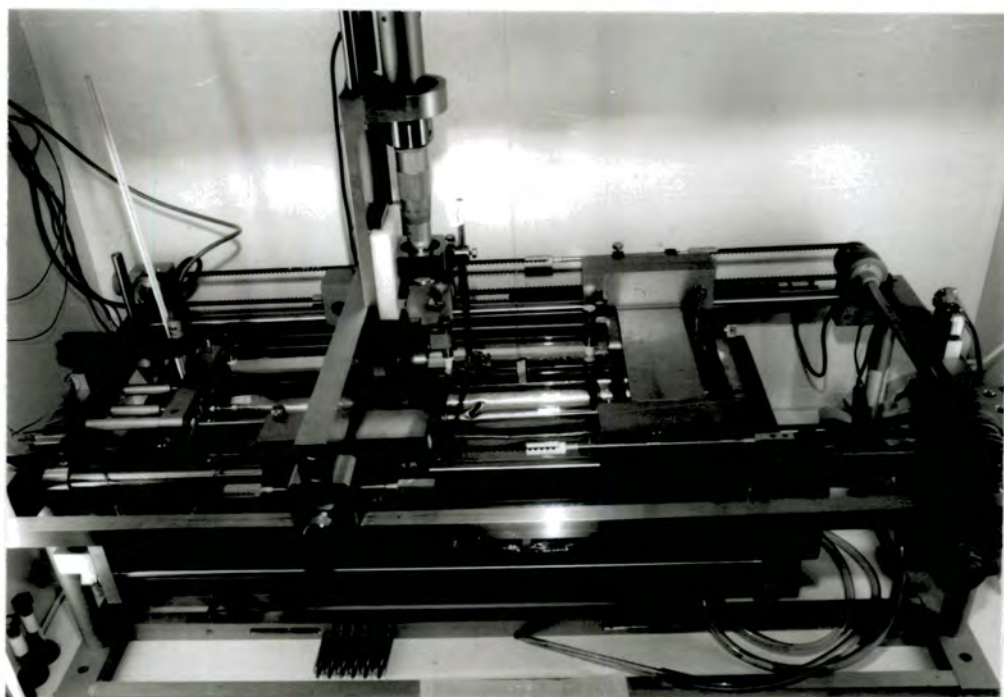
Figure 4.2 Photograph of a conventional Langmuir trough.

constructed entirely from polytetrafluoroethylene (PTFE) was employed for the economical use of expensive, high grade purity chemicals. The barrier used to enclose the LB film material is of the constant perimeter type and consists of a PTFE-coated glass fibre belt, held taut by three pairs of rollers also made from PTFE. These rollers can be seen in the inset to figure 4.1. An undesirable feature of the trough used in the intial stages of the work were the so-called 'arms', labelled in the inset. For the accurate calculation of the molecular area of LB film materials it is important that the precise area occupied by the film is known. Depending on the rigidity of the LB film material used, it may or may not flow into the 'arms' of the trough. This will lead to an uncertainty in the area occupied by the film, especially for small film areas where the 'arms' occupy a large percentage of the total area. During the course of this work the problem was eliminated by moving the pair of rollers marked A outwards, thus pinching of the 'arms'. The original position of this pair of rollers is indicated by the dashed circles. One pair of rollers is attached to a fixed cross-member, whereas the other two pairs are fixed to two moveable cross-members, pulled by toothed rubber belts and driven by an electric motor. In this way the surface area enclosed by the barriers could be continuously varied between the two extremes of surface area shown in figure 4.1.

The dipping head consisted of a motor driven micrometer screw mounted above the water on a moveable crossbeam. The substrates were held by a metal screw clamp attached to the dipping head, and could be raised or lowered at a constant speed in the vertical direction through the air-water interface. The speed of this vertical movement could be continuously varied between 2 mm min^{-1} to 10 mm min^{-1}. The surface pressure (more correctly surface tension) exerted by the film on the water surface is monitored using a Wilhelmy plate suspended in the water by a thread from a microbalance above the trough. The Wilhelmy plate consisted of a 10 mm wide strip of filter paper. The complete system was housed in a glass-doored cabinet mounted upon a Newport XJR pneumatic anti-vibration table. The trough was located in a class 10,000 microelectronics clean room in

41

order to reduce dust contamination.

4.1.2 Instrumentation

A photograph of the instrumentation associated with the trough is shown in figure 4.3. The barrier can be operated via a control box in three different modes; forward, reverse, and control. The manual forward and reverse controls allow the LB film to be compressed or expanded at a continuously, variable preselected speed e.g. during the recording of a surface pressure isotherm. The control mode of operation is normally used during film deposition. During film deposition, material is removed from the water surface and in order to maintain the required dipping surface pressure the barriers must compensate automatically by compressing the film further. This is accomplished using a simple feedback loop with adjustable gain, as shown in figure 4.1. A Beckmann LM6000 microbalance monitors the surface pressure via the force acting on the Wilhelmy plate. A voltage derived from the microbalance is compared with a voltage corresponding to the desired surface pressure which is preselected on the control box. The differential signal controls a motor which activates the barrier. It is important that adjustable gain is allowed for in the feedback loop so that the mechanical properties of different monolayer forming materials can be taken into account.

All movements of the dipping head are dictated by the control box, including its upper and lower limits, and its speed. The required number of dipping cycles can also be preset. High resolution linear potentiometers attached to the barriers and the dipping head allow accurate determination of film area and substrate position, respectively.

Plots of surface pressure (microbalance output) against surface area were obtained on a Bryans 2900 X-Y chart recorder. During film deposition, area and pressure were simultaneously plotted on a Bryans 312 two-channel Y-t chart recorder. A Pye-Unicam PW9409 pH-meter and a mercury thermometer monitored the subphase pH and temperature, respectively.

42
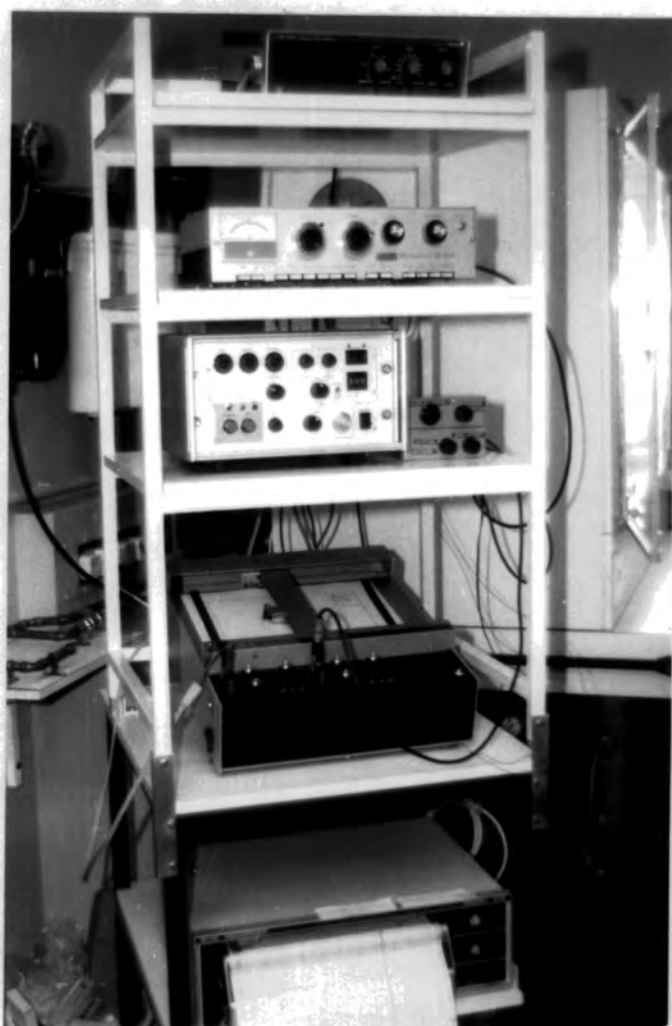
Figure 4.3 Photograph of the instrumentation associated with a conventional Langmuir trough.

4.1.3 Cleanliness

Cleanliness is essential for the production of high-quality LB films. High purity subphase water is vital since any ionic or organic contaminants promote monolayer dissolution and poor deposition. The water used as the subphase and in all cleaning procedures was purified in the following manner. Mains water first passes through a 5 μm filter, then into a Spectrum SC31 reverse osmosis unit and then into a storage tank. From here the water is continuously circulated around a ring main where it undergoes activated carbon organic removal, double-deionisation, membrane filtration, UV sterilisation and finally 0.2 μm filtration. An Anatel in-line monitor confirmed that the total organic carbon content was less than 10 ppb and the resistivity was 17.2 MΩ cm close to the theoretical maximum of 18 MΩ cm. Water is delivered to the trough from the ring main via high quality polypropylene tubing.

Although the water circulating in the ring main is of the highest purity available, degradation occurs whilst it is standing in the trough, for two reasons. Firstly, ions are likely to be leached out of the glass and secondly, bacterial growth is known to occur [4]. Therefore the trough water was changed every three days to reduce this source of contamination. Also at regular intervals a rigorous cleaning procedure was employed in which both barrier and rollers were removed and refluxed in propan-2-ol vapour in a Soxhlet reflux unit for several hours. The trough itself was rinsed with propan-2-ol, chloroform, propan-2-ol and finally purified water. At the same time the Wilhelmy plate was renewed and the instrumentation checked for correct calibration. The subphase surface was cleaned by sweeping it with a fine nozzled glass pipe connected to an aspirator suction pump.

4.2 LB FILM PREPARATION

Before the deposition of a potential LB film material is attempted, its behaviour on the water surface must be assessed. Two important properties that can be studied are its pressure-area relationship and its stability. Once the mate-
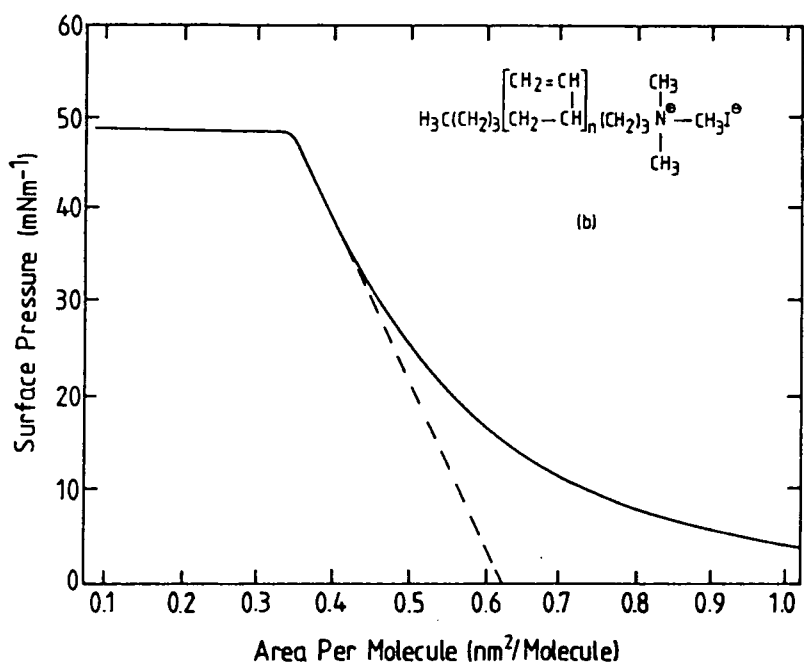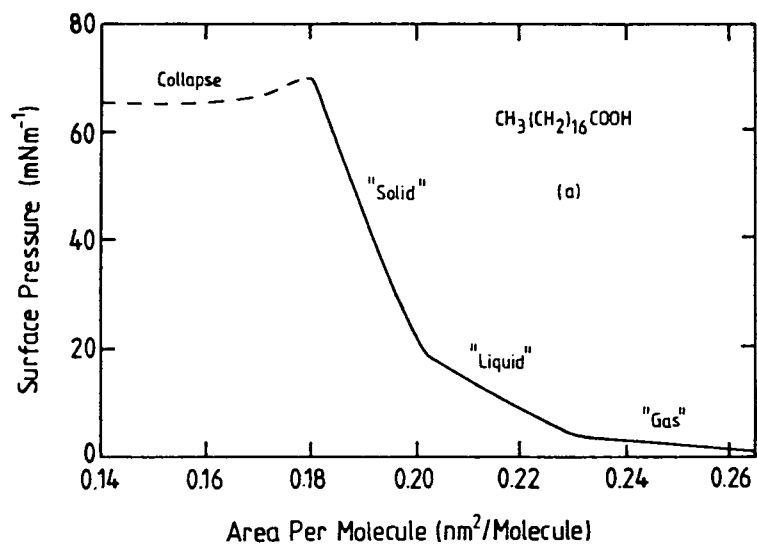
Figure 4.4 Surface pressure-area isotherms for (a) stearic acid, and (b) an ammonium terminated polybutadiene.

rial has been established as a good monolayer film, the conditions for successful deposition can then be addressed.

4.2.1 Pressure-area isotherms

If a material forms an insoluble monolayer at the air-water interface (insolubility in water is a fundamental requirement if the material is to form an LB film), then as the surface area (A) available to the film is reduced so the surface pressure (Π) will increase. The procedure adopted for recording a Π-A isotherm was as follows. The material was first dissolved in an organic solvent (usually "Aristar" grade chloroform) to an accurately known concentration. Then a known volume was deposited on the clean water surface using a Kloehn microlitre syringe. When the solvent had completely evaporated the film was compressed at a fixed, slow rate. By plotting the calibrated output from the microbalance (indicating surface pressure) against that of the barrier potentiometer (giving surface area) a Π-A isotherm is obtained. The surface area (A) of the trough can be converted to surface area per molecule (A_{mol}) if the number of molecules deposited is known. This can be determined from the formula $A_{mol} = AM(cVN_A)^{-1}$ where M is the molecular weight of the material and, c and V are the concentration and volume of the spreading solution, respectively.

A typical isotherm for the classical LB film material, stearic acid is shown in figure 4.4a and the inset shows the molecular formula of the molecule. The isotherm can be divided into four regions. The first three regions correspond approximately to the two dimensional analogues of the "gas", "liquid", and "solid" phases. The fourth region indicates the collapse of the film, that is, a buckling of the film with the molecules moving on top of each other, causing the monomolecular property to be lost. The steep, linear, "solid" portion indicates the molecules have formed a condensed layer of low compressibility. Traditionally, the solid line can be extrapolated down to the A_m axis; the point of intersection A_{mol}^o is taken as the area per molecule in the condensed state. Comparison of this value with

mobile film the barriers respond immediately and smoothly thereby maintaining the preselected pressure. However, in the above case the behaviour of the barriers is delayed and erratic and sometimes oscillatory, and a constant surface pressure cannot be maintained. For the successful deposition of a floating monolayer onto a suitable solid substrate it is important that the molecules are mobile on the water surface. If the film is too rigid; fracturing of the film on withdrawl and failure of the molecules to "flow" into the deposition area may result, causing "holes" in the film to occur. Very rigid monolayers can be made more fluid by mixing with fatty acids or by using slowly evaporating solvents. In the latter case, the solvent provides "lubrication" for the molecules to move more freely in the layer [6].

4.3 LB FILM DEPOSITION

After a II-A isotherm for the material has been recorded and the stability assessed at the desired dipping pressure (usually corresponding to a pressure in the centre of the "solid" phase), a fresh monolayer is spread and compressed in "control" mode. After a few minutes to allow for the surface area to stabilise, deposition can be attempted. The first layer deposited is important for two reasons: firstly, it forms the foundation for subsequent layers and is the only layer directly bonded to the substrate; and secondly any defects in the first monolayer might be propagated into further layers. For these two reasons, particular care was taken in depositing the first monolayer; a low deposition speed (2 mm min^{-1}) was employed followed by a drying time of at least 30 minutes. Subsequent layers were deposited from another fresh monolayer.

Katharine Blodgett postulated three modes in which LB films could be transferred to a substrate and named them X, Y, and Z type, as illustrated in figure 4.5 for amphiphilic type molecules. Most materials deposit in the Y-type manner where transfer of the film onto the substrate occurs on both up- and down-strokes of the substrate. Normally, the fatty acids deposit Y-type and the resulting head-
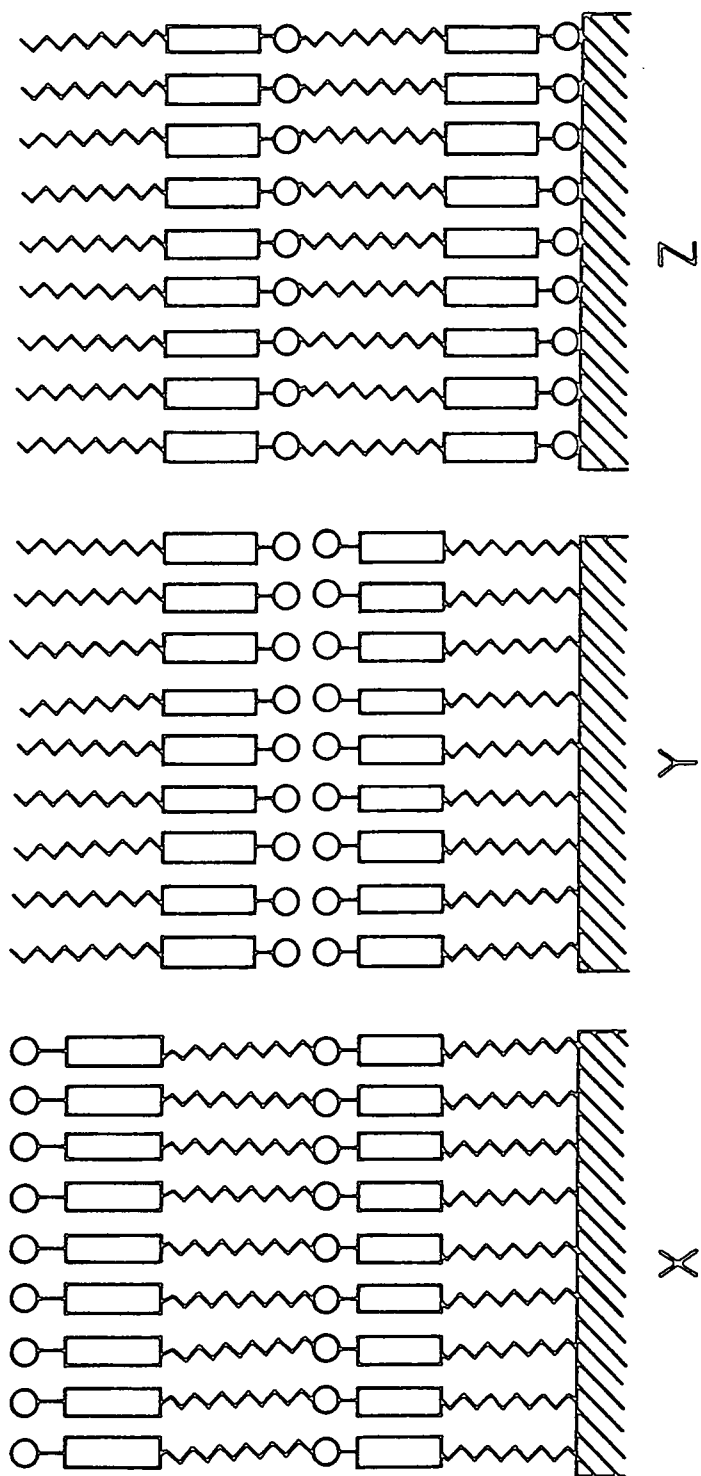
Figure 4.5 Modes of LB film deposition: X, Y, and Z-type.

to-head and tail-to-tail sequence gives a highly symmetrical packing arrangement. Y-type pick up begins on the first downstroke for a hydrophobic substrate and on the first upstroke for a hydrophilic substrate.

X-type deposition is characterised by material transfer only on the downstroke. The fatty acid esters such as ethyl stearate [7] and vinyl stearate [8] have been shown to deposit X-type. Also, unusually, at very high pH levels X-type deposition of fatty acids has been observed. This mode of deposition is energetically unfavourable and X-ray evidence supports molecular rearrangement during or shortly after deposition to give an essentially Y-type structure [9].

Finally, Z-type deposition refers to transfer on the upstroke only. Z-type dipping has been observed in lightly substituted anthracene derivatives [10], porphyrins [11,12], and for the phthalocyanines [6]. These molecules are very different from the classical fatty acids which possess clearly defined hydrophobic and hydrophilic regions of the molecule and this may be one reason for their unusual deposition. The physical processes and molecular interactions involved in the different modes of film transfer have not yet been completely explained.

An important parameter used to characterise the LB film deposition whilst in progress is the transfer ratio. It is defined as the ratio of the change in surface area to the area of the substrate per traversal of the air-water interface. Thus, a transfer ratio of unity and zero indicate complete and zero coverage of the substrate, respectively.

4.4 DEVICE FABRICATION

4.4.1 Substrate Preparation

(a.) Silicon

Silicon wafers were used as substrates for infrared spectroscopy, electron microscopy, ellipsometry and X-ray diffraction experiments. Two types of silicon wafer were used: n-type silicon of either {100} or {111} orientation. The wafers were cleaned in hot propan-2-ol liquid and vapour for several hours in a Soxhlet

reflux unit. In this way the silicon surface was hydrophilic due to its native oxide. A hydrophobic silicon surface was produced by subsequently refluxing in a Soxhlet system containing 2% dichlorodimethylsilane in 1,1,1 trichloroethane. Finally, after rinsing the wafers in pure water to remove the hydrochloric acid formed in the treatment, they were again refluxed in hot propan-2-ol. The single crystal silicon ATR crystals for the infrared spectroscopy (see section 4.5.2) were treated in exactly the same manner as the silicon wafers. However, in the latter case, it was often required to remove a hydrophobic surface to yield a hydrophilic surface. This was done by treatment with a buffered hydrofluoric acid etch (1 part HF to 8 parts ammonium fluoride (NH_4F)) for one minute, followed by thorough rinses in deionised water, and finally, a propan-2-ol reflux.

(b.) Glass

Spectrosil B vitreous silica slides were used as substrates for optical absorption measurements allowing transmission well into the ultraviolet (down to 180 nm). A rigorous cleaning procedure was adopted as follows: particulate matter was first removed by wiping with a lens tissue soaked in propan-2-ol and then the slides were ultrasonically agitated in a 5% Decon 90 alkaline soap solution. Following several rinses in fresh, ultrasonically agitated, deionised water the slides were refluxed in boiling propan-2-ol for several hours. Hydrophobic silica slides were obtained by the dimethyldichlorosilane treatment described for silicon, as in (a.).

4.4.2 Mounting, bonding and encapsulation of ISFET devices

Custom designed printed circuit boards (PCBs) (18 mm x 120 mm) were used as mounting substrates. An array of conducting copper tracks was printed on the PCB. In the vicinity of the chip mounting area the copper tracks were gold plated to ensure reliable wire bonding, and a centrally located recess (5 mm x 2 mm, 0.5 mm deep) was milled out to locate the IC. The latter was mounted using Epo-Tex H54 epoxy (Alpha Metals Ltd.) which was oven cured at 90°C for 1 hour. The substrate-IC assembly was then cleaned. Cleanliness is of the utmost importance

Area
Dipped
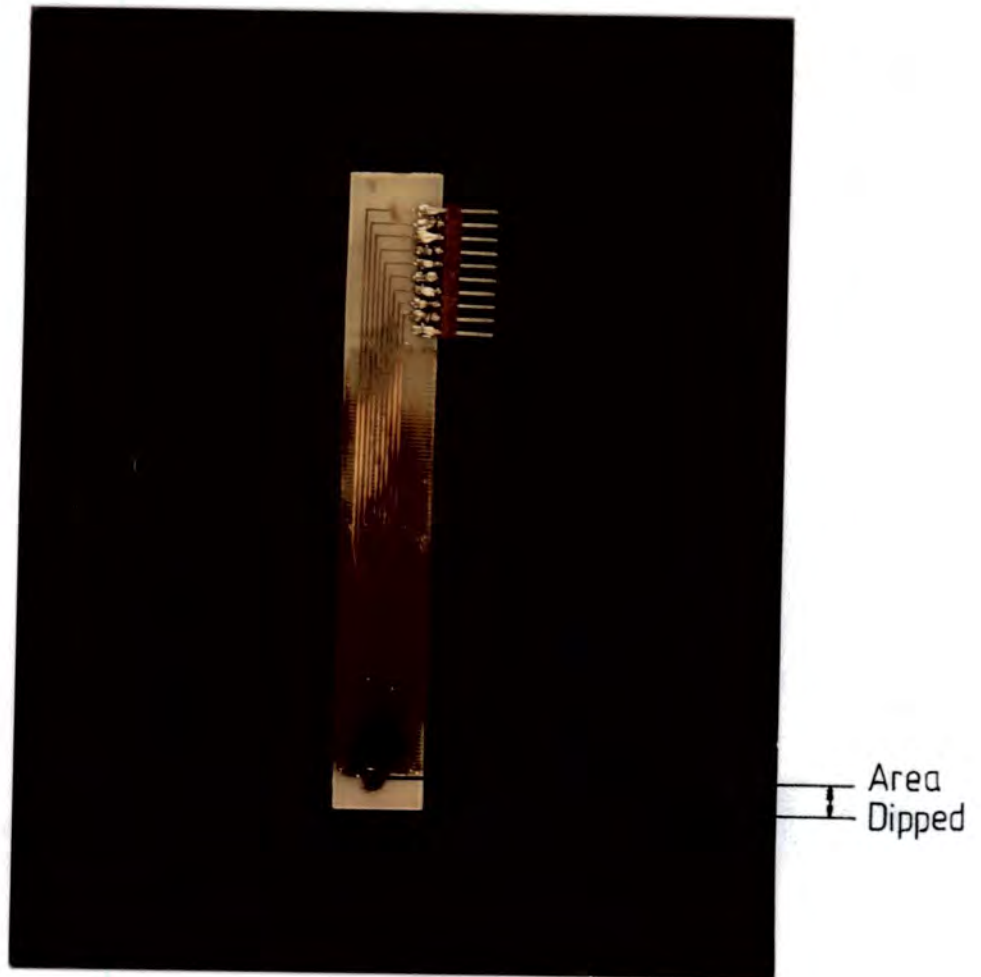
Figure 4.6 A photograph of a mounted encapsulated ISFET.

for successful encapsulation and the following ultrasonic cleaning procedure was adopted: detergent (5% Decon 90 alkaline soap solution), deionised water (x2), propan-2-ol. After cleaning, the IC connections are gold wire bonded to the PCB gold-plated track tips with 25 μm gold wire using a gold wire bonder (Kulicke and Soffa Ind.). Next these connections were secured using a small amount of epoxy which was subsequently cured under the conditions above. Finally, the bond wires, metal pads and the exposed tracks were coated with epoxy and cured. Before making measurements with the ISFETs they were treated in a buffered hydrofluoric acid etch (1 part HF to 8 parts NH_4F) for 30 seconds. A photograph of the mounted ISFET, complete with encapsulation and edge connector, is shown in figure 4.6.

4.5 STRUCTURAL CHARACTERISATION

4.5.1 Reflection High Energy Electron Diffraction

Reflection high energy electron diffraction (RHEED) is a technique which can be used for the rapid identification of the structure of an LB film [13-17]. It is a convenient method and requires minimal sample preparation. From the RHEED diffraction pattern, information concerning the amount of crystalline order, the direction of preferred orientation of crystallites relative to the substrate surface, and interplanar spacings can be deduced.

In the RHEED technique, a mono-energetic beam of electrons (for example of energy 100 keV, λ=0.01 nm) is used to obtain diffraction from the atomic planes constituting the specimen surface. Diffraction will occur according to the Bragg relationship, $\lambda = d_{hkl} \sin\theta$ where d_{hkl} is the interplanar spacing and θ is the Bragg angle. For most metals d_{hkl} is of the order 0.2 nm and the Bragg angle varies from about 1.5° to 0.5°. In RHEED, the electron beam strikes the surface at grazing incidence and consequently only those crystal planes inclined at less than a few degrees to the surface will cause diffraction.

A JEM transmission electron microscope operated at 100 kV was used in the

(a)

3.1nm

θ

5.9 nm
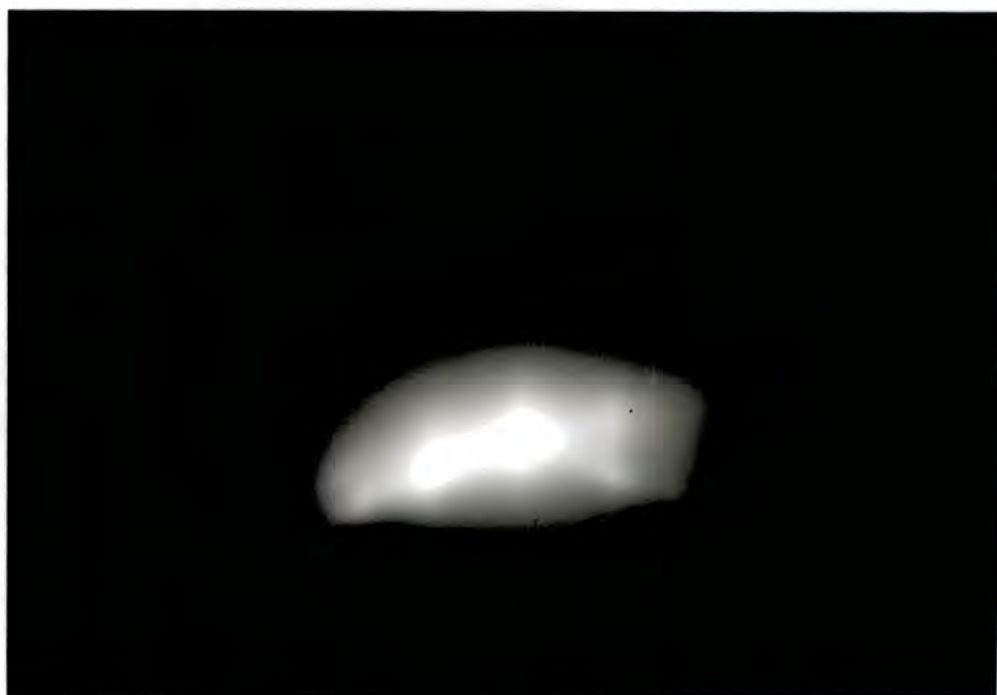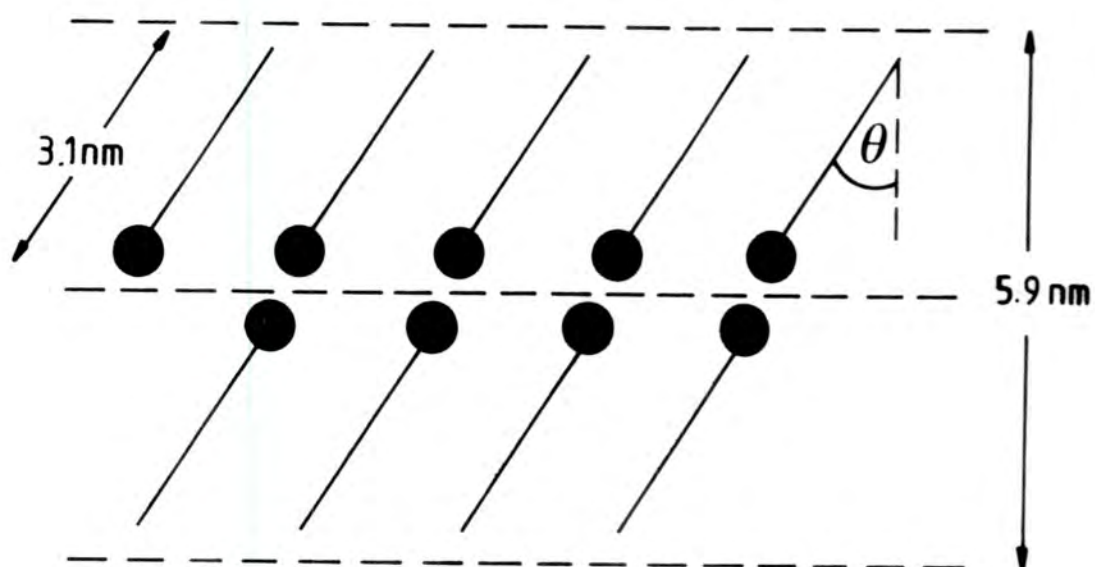
(b)

Figure 4.7 (a) A RHEED pattern from a 6 layer film of ω-tricosenoic acid on a hydrophobic silicon surface, and (b) tilting of the molecules, $\theta = 20°$.

RHEED studies. The specimen was held below the projector lens on a goniometer stage which allowed for grazing incidence; and rotation, tilt and translation of the sample so that the Bragg condition for diffraction could be satisfied. The diffracted beam was allowed to fall on either a fluoresecent screen, or a photographic plate for recording the RHEED pattern.

RHEED has been widely used to examine LB films of the long chain fatty acids. As a result of these investigations it has been established that the structure of fatty acid LB films is granular in nature i.e. the films are comprised of many crystallites. The molecules in each crystallite are inclined at approximately the same angle to the substrate surface. A typical RHEED pattern for six layers of ω-tricosenoic acid prepared on a hydrophobic $\{100\}$ silicon surface taken with the electron beam perpendicular to the direction of dipping is shown in figure 4.7a. The RHEED pattern exhibits the so-called arcs of intensity [18] consisting of a set of diffraction spots. The diffraction spots originate from the C_2H_4 repeat units of the hydrocarbon chains of ω-tricosenoic acid. The angle the diffraction arc makes with the shadow edge of the sample indicates the angle between the molecules' preferred orientation in the crystallite and the sample normal. In the case of ω-tricosenoic acid this is approximately 20°, illustrated diagrammatically in figure 4.7b.

4.5.2 Attenuated total reflection (ATR) Fourier transform infrared spectroscopy

The atoms within a molecule are never stationary but are constantly undergoing pure vibrational, pure rotational and rotational-vibrational modes of oscillation. Infrared spectroscopy provides a means of studying the energy changes associated with these modes. Changes in vibrational energy of a molecule are normally observed in the infrared region of the electromagnetic spectrum. If the absorption of IR radiation is to produce a change in vibrational energy, interaction may only take place provided that there is a change in the electric dipole moment

Laser Reference
Interferometer

Moving Mirror

Infrared
Interferometer

Fixed Mirror

Detector

IR
Source

Sample

Detector
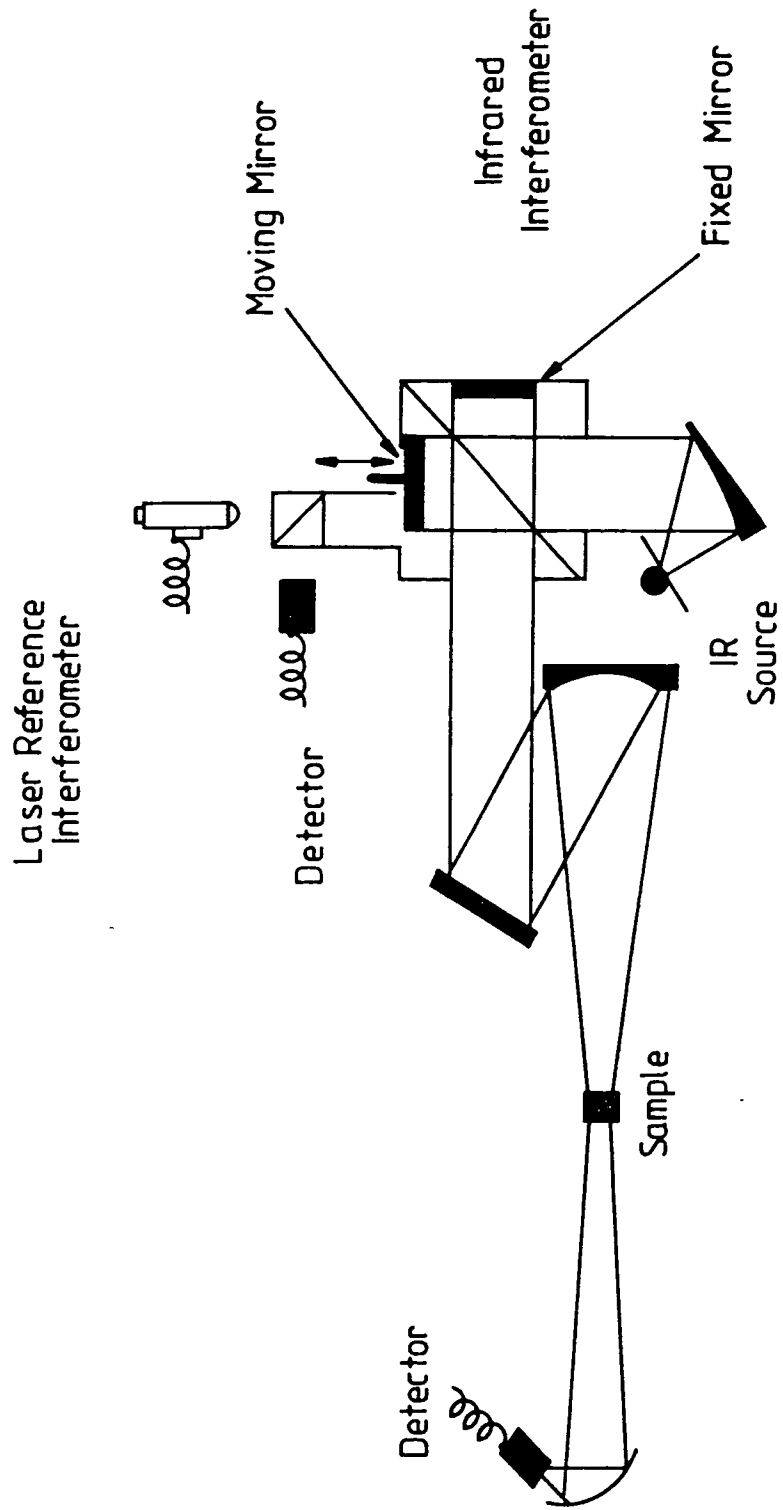
Figure 4.8 The Michelson interferometer.

of the vibrating unit during the vibration. Only then will there be a resonant transfer of energy from the oscillatory electromagnetic field to the molecule. The greater the change in dipole moment associated with a vibration mode, the more intensely it will interact with the radiation. Each type of band is characterised by a particular frequency which depends on the atomic masses involved in the band and the force constant of the bond. The local environment of the bond also affects this frequency and it is this dependence which has been used in the study of valinomycin containing Langmuir-Blodgett films.

Fourier transform infrared (FT-IR) spectroscopy has certain advantages over conventional grating spectroscopy. In the latter, light from a broad band infrared source is passed through the sample onto a grating. The beam is dispersed by the grating, and light of a selected narrow frequency band is directed to the detector. By varying the frequency selected, a direct plot of detector response versus wavelength is obtained. The real advantage of an FT-IR spectrometer results from the use of a Michelson interferometer (shown in figure 4.8) rather than a grating. Collimated light from an infrared source is incident on a beam splitter, part going to the moving mirror and part to the fixed mirror. The return beams recombine at the beam splitter undergoing interference and then the reconstructed beam is directed through the sample and focused on the detector. The motion of the mirror results in a signal at the detector which for a given wavelength λ varies with frequency $\omega = V_m \lambda^{-1}$ (or $\omega = V_m \bar{\nu}$), where V_m is the velocity of the mirror. A laser beam undergoing the same changes in optical path as the infrared beam forms a laser reference interferometer which serves to reference the position of the moving mirror. The collection of data points from the signal of the infrared detector at uniform intervals of mirror travel forms an interferogram, i.e. a record of the detector signal as a function of the difference in path (retardation) for the two beams in the interferometer. One interferometer scan producing one interferogram is performed rapidly (a few seconds each). Normally, approximately 2000

Source ✳ ——— → Detector

LB Film

Si Substrate

(a)

IR Beam   LB Film

Si ATR Crystal
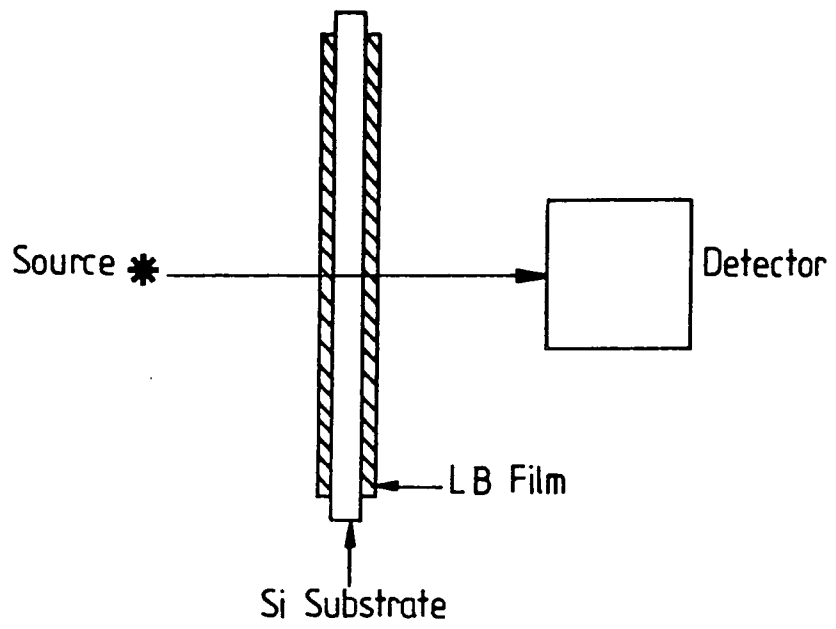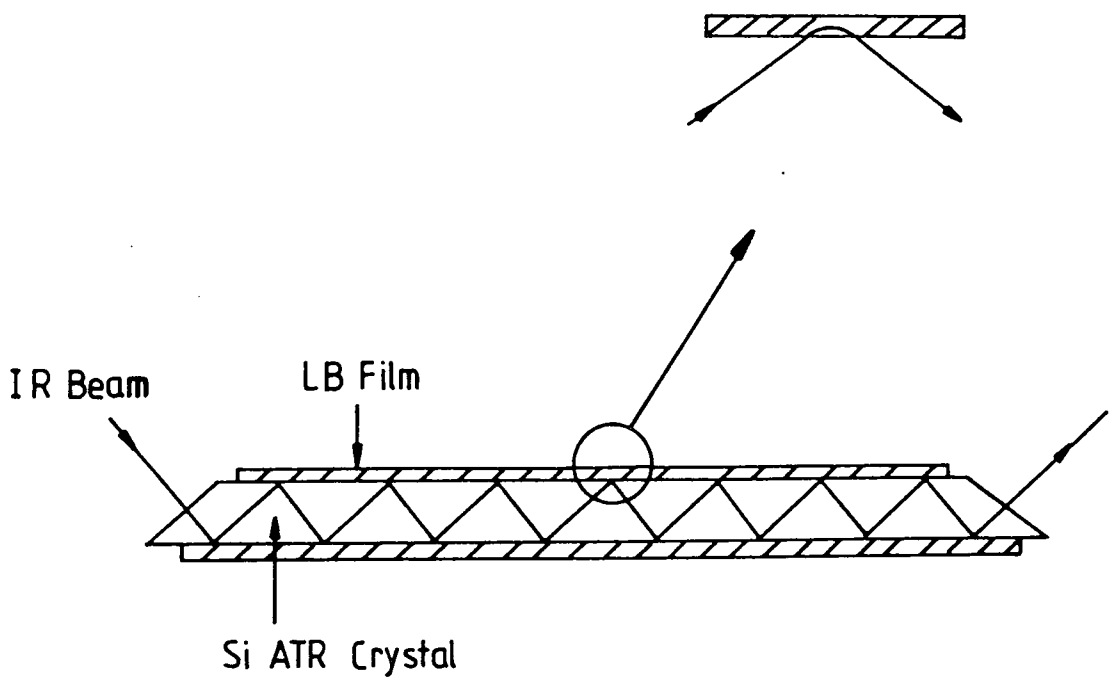
(b)

Figure 4.9 IR spectroscopy, (a) transmission, and (b) attenuated total reflection (ATR).

scans are co-added to improve the signal-to-noise ratio. The Fourier transform

$$S(\overline{\nu}) = 2 \int_0^\infty I(x) \cos(2\pi\overline{\nu}x) \, dx$$

where x is the retardation, converts the signal as a function of retardation (i.e. the interferogram $I(x)$) to a signal as a function of frequency (i.e. the spectrum $S(\overline{\nu})$). The FT-IR spectrometer offers improved signal-to-noise ratios compared to the grating spectrometer because of a higher optical throughput, shorter scanning time, and concurrent observation of all the infrared frequencies.

Attenuated total reflection (ATR) spectroscopy [19] was used to investigate the LB films produced in this work because it has the extremely high sensitivity required to study monomolecular films [20]. The principles of the technique are illustrated in figure 4.9. The LB film specimen under examination is deposited onto the surface of a trapezium-shaped (in cross-section) silicon crystal which in this work was cut from a commercially available silicon wafer. The bevelled surfaces are at an angle of 45° and are highly polished, as are both surfaces of the crystal. IR radiation from the beam splitter enters the crystal and is multiply internally reflected within the crystal until it exits and passes into the detector. When radiation propagating in an optically more dense medium is totally internally reflected at an interface with an optically more rare medium an evanescent field penetrating the rarer medium exists. The evanescent field is a nontransverse wave having components in all spatial directions and decays exponentially with distance from the silicon/sample interface. The IR radiation interacts with the sample via this evanescent wave. The key to the enhanced sensitivity of the ATR spectroscopy compared to conventional transmission spectroscopy lies in the number of multiple reflections within the crystal. The absorption of the IR radiation in the ATR case is increased by a factor equal to the number of reflections, compared to the simple transmission case and when examining samples of equal thickness.

Infrared spectra were obtained on a Mattson Sirius 100 Fourier transform spectrometer equipped with a liquid nitrogen cooled cadmium mercury telluride

detector. All data was collected at a spectral resolution of 4 cm^{-1}. A 1 x 20 x 10 mm silicon crystal was used to obtain the ATR-IR spectra.

4.5.3 Ellipsometry

Ellipsometry is a technique which can measure film thicknesses at least an order of magnitude smaller than can be measured by other methods, such as interferometry. Furthermore, it can make measurements in optically-transparent environments such as air and does not require special conditions. For these reasons ellipsometry is a valuable technique for the rapid determination of the thickness of LB films [21,22]

An ellipsometric measurement involves irradiating a sample with a collimated beam of monochromatic light having a known, controllable state of polarisation and determining the difference between the states of polarisation of the incident and the reflected beams. From this measurement various properties can be computed concerning the reflecting surface. In this project these were: (a) the optical constants of the substrate i.e. the real part NS and the imaginary part KS of the refractive index, NS+iKS; and (b) for a substrate with known optical constants (determined in (a)) and covered with a single transparent film, the film refractive index N and the film thickness T were computed. The electric fields of the incident and reflected beams can be resolved into two orthogonal, linearly polarised components, the s and p components. When polarised light is reflected from a surface, generally the relative amplitudes and phases of the p and s components will change. These changes determine two angles, Δ(delta) and Ψ(psi). The derivation of the equation of ellipsometry is beyond the scope of this thesis but, to underline the relationship between Δ and Ψ and the changes in the p and s components, it is quoted here. The basic equation of ellipsometry is

$$\rho = \tan \Psi e^{i\Delta}$$

where ρ is the ratio of the complex reflection coefficient of the p component to that of the s component.
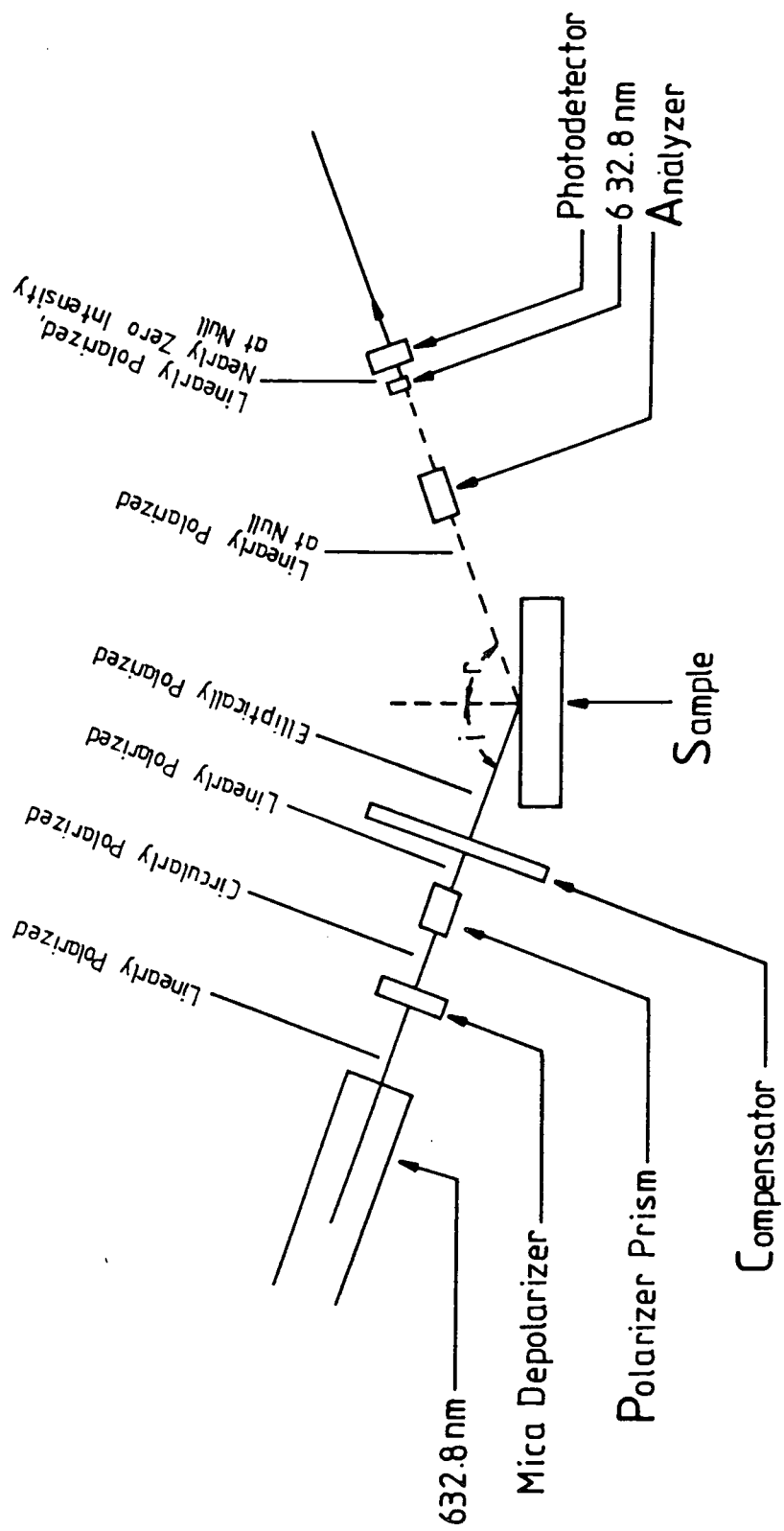
Figure 4.10 PCSA optical configuration of the ellipsometer used.

A Rudolph Research Auto EL-IV nulling ellipsometer was employed during the work. The ellipsometer basically consists of two parts: (1) an optical system for the determination of the angles Δ and Ψ and (2) a dedicated computer to convert these values into physical film parameters. Figure 4.10 illustrates the optical configuration known as the **PCSA** configuration, short for, Polariser, Compensator, Sample, Analyser which describes the passage of light from the source to the detector. The compensator is fixed and there exists some position of the polariser at which the reflected beam is linearly polarised, so that complete extinction can be obtained by orienting the analyser with its transmission axis at 90° to the linearly polarised reflected beam. With the Auto EL-IV the ellipsometric measurement is totally automated and is achieved by alternately adjusting the polariser and analyser until there is a true extinction of the reflected beam. At this null the positions of the polariser and analyser are recorded and they are a measure of Δ and Ψ, respectively.

Conversion of Δ and Ψ to physical parameters is performed by an on-board dedicated computer. For the bare substrate, Fresnel showed that Δ and Ψ were functions as expressed in the equations:

$$\Delta = f_1(\Phi, \lambda, NA, NS, KS)$$

and

$$\Psi = g_1(\Phi, \lambda, NA, NS, KS)$$

where λ is the wavelength of light, Φ is the angle of incidence of the incident beam and NA is the refractive index of the ambient medium. These equations can be solved uniquely for NS and KS. For transparent films on substrates, Drude proposed that:

$$\Delta = f_2(\Phi, \lambda, NA, NS, KS, N, T)$$

and

$$\Psi = g_2(\Phi, \lambda, NA, NS, KS, N, T)$$

54

These equations can be numerically inverted and N and T can be calculated from the results of a single Δ, Ψ measurement.

4.5.4 X-ray low angle diffraction

X-ray low angle diffraction has been used to study single component (e.g. fatty acid salts) as well as alternate layer Langmuir-Blodgett films [23-26]. The technique provides a determination of the d-spacing and also in-plane structural information concerning these films.

X-ray diffraction follows the Bragg law. The wavelength of radiation used was 0.154 nm, and since typically the d-spacing in LB films is 5-6 nm, the criterion for observing diffraction is that the radiation should strike the sample at grazing incidence.

The X-ray measurements were undertaken at the Institute of Crystallography in Moscow. A purpose-built position sensitive small angle X-ray diffractometer was used. A collimated, nickel filtered beam of Cu K_α X-ray radiation (λ=0.154 nm) impinged on the LB samples which were slowly rotated at about 20° per hour in vacuo. The diffracted beam was located with the aid of a position sensitive detector. An angular resolution of approximately 0.01° was realised using a sample-to-detector distance of 74.0 cm. Several scans were recorded and summed for each sample.

The X-ray spectra obtained consisted of a series of Bragg reflections from the (001) planes. For each reflection, θ can be read, and using the Bragg equation $\lambda = 2d\mathrm{l}\sin\theta$, d can be calculated. The d-spacing which is an averaged value corresponds to the dimensions of the unit cell perpendicular to the substrate. Another important parameter called the radius of correlation, R_c, can be calculated from the width of the reflections and it provides information about the long-range structural order in the film.

4.5.5 Ultra-violet spectrophotometry

Optical absorption measurements were made on a Cary Model 2300 UV-visible spectrophotometer. The ultraviolet or visible spectrum could either be taken of; a very dilute solution, contained in quartz cuvettes, or of LB films deposited on Spectrosil B vitreous silica slides. Two equal beams of ultraviolet or visible light are passed, one through the sample and the other through the reference solution or slide. The intensities of the transmitted beams are compared over the whole wavelength range, and the spectrum is plotted automatically as $log_{10}(I_o/I)$ on the ordinate versus wavelength, λ, on the abscissa. A baseline correction for the particular reference material was also recorded.

4.6 ISFET CHARACTERISATION

The electrical characterisation of the ISFET devices included the measurement of the I_D/V_G threshold characteristic, the I_D/V_{DS} output characteristics, and the determination of the athermal drain current for use in the pH measurements. The pH responses of the ISFET devices were evaluated by recording surface potential versus pH curves.

4.6.1 Electrical characterisation

The electronic circuitry used in both the electrical characterisation and pH response evaluation of the ISFETs is shown in figure 4.11. It is the well-known constant current operating configuration for the ISFET which allows the direct determination of surface potential as a function of pH to be made [27]. For measuring the I_D/V_{DS} output characteristics (for various V_G) the feedback loop is disconnected and V_G is applied from a voltage calibrator output. Similarly, the I_D/V_G threshold characteristic can be obtained. Both transistor characteristics were obtained with the devices in a pH 7.0 buffer solution after a 24 hour exposure to solution. Measurements were made at room temperature.

MOS device characteristics are temperature dependent and an athermal drain
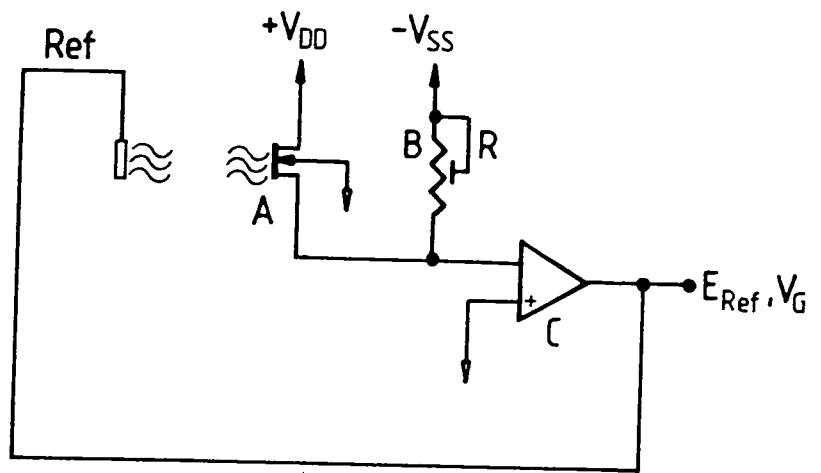
Figure 4.11 ISFET operating mode at constant drain current.

current must be selected for the operation of the ISFET in constant current mode. That is to say, a drain current which is not significantly dependent on temperature. The athermal value was determined from a family of I_D/V_G curves, each at a different temperature. Typically the curves intersect at one point corresponding to an athermal value for the drain current. Once this has been determined pH response measurements can be undertaken.

4.6.2 pH response characterisation

The simple feedback circuit shown in figure 4.11 was used for the pH measurements. Chemically induced changes in I_D (resulting from a change in pH) are automatically offset. For example, if the device is transferred to a solution of greater pH, the interfacial potential at the ISFET surface decreases, and therefore E_{ref} increases to maintain I_D. This means that changes in the surface potential are measured directly as changes in the output voltage E_{ref}.

The surface potential versus pH measurements were recorded as follows: 50 ml solution containing 0.01 M citric acid, 0.01 M phosphoric acid, 0.02 M boric acid and 0.1 M NaCl was titrated with a solution of 0.1 M HCl + 0.1 M NaCl until pH 2.0 was reached. A pH electrode calibrated with two standard buffers and an ISFET operating in constant current mode was placed in this solution, which was stirred thoroughly using a magnetic stirrer. A 0.1 M NaOH solution was then titrated, and the surface potential differences (measured as differences in reference electrode potential) were recorded as a function of pH. The drain current was set to its athermal value. The reference electrode operating in conjunction with the devices was of the saturated calomel type. A typical recording scan from pH 2.0 to pH 11.0 was approximately 30 minutes allowing the ISFET to stabilise for about 3 minutes at each pH value. After each scan, the solution was replaced with the starting mixture and another scan was recorded. Data presented are typically an average of ten scans.

4.6.3 Potassium response characterisation

The measurement of surface potential against potassium concentration were performed in exactly the same manner as in 4.6.2 except the starting solution was 50 ml 0.1 M LiCl and 10^{-5} M KCl. Titration of solutions of 0.1 M LiCl but with varying concentrations of KCl allowed the pK concentration to proceed at unit intervals from pK 5 to pK 1. During the pK response evaluation, the calomel reference electrode was replaced by a double junction reference electrode incorporating an outer cell filled with NaCl. Unfortunately during the titration, it was not possible to monitor the potassium concentration. Consequently, a dummy titration was performed with no ISFET in solution. Every 0.5 pK unit, 10 ml of the solution was removed and placed in a 10 ml volumetric flask. The set of solutions were subsequently analysed by atomic absorption flame spectrophotometry [28] in order to determine their potassium concentration. In this way the potassium concentrations of all starting solutions could be checked, and the progression of potassium concentration during the titration was known.

4.7 SUMMARY

The fabrication and characterisation of Langmuir-Blodgett (LB) films and ion sensitive field effect transistor (ISFET) devices have been described. The techniques of reflection high energy electron diffraction, Fourier transform infrared spectroscopy and X-ray low angle diffraction which are used to obtain structural and chemical information concerning the films are outlined. The methods used for the evaluation of the pH and potassium responses of the ISFET devices have been demonstrated. The next chapter concerns how the techniques of this chapter are combined to fabricate the LB film coated-devices, and describes their subsequent evaluation.

CHAPTER 5

ISFET AND LB FILM-ISFET CHARACTERISATION

5.0 INTRODUCTION

This chapter concerns the characterisation of the ISFET devices with and without a deposited LB film. Section 5.1 describes the characterisation of the virginal ISFET devices. This includes determination of the I_D/V_{DS} output characteristics and the the I_D/V_{GS} threshold characteristic. A family of the latter curves obtained at different temperatures allows the choice of the athermal operating current for the ISFET to be made. Section 5.2 demonstrates the pH response of the devices and the effect of a buffered HF etch on this response. Section 5.3 deals with the characterisation of ISFET devices coated with an LB film. The effect on the pH response as a function of the number of monolayers deposited, and the LB film material is investigated. The pH sensitivity of the ISFET is redundant as far as potassium sensing is concerned and an attempt to reduce it using a plasma polymer overlayer deposited onto the Si_3N_4 ISFET gate is outlined in section 5.4. Finally, section 5.5 describes potassium sensing experiments performed with valinomycin-containing LB films deposited onto the ISFET.

5.1 CHARACTERISATION OF VIRGINAL ISFET DEVICES

5.1.1 Preliminary device assessment

After the ISFET chips had been mounted onto the printed circuit boards, gold wire bonded and encapsulated they were subsequently immersed in a buffered HF solution. This was followed by a "conditioning" period during which the device was exposed to a buffer solution of pH 7.0 for 24 hours.

Before any characterisation was attempted, the suitability of a device to provide reproducible results was determined. The main criterion for this assessment was the determination of a leakage current for the device, that is, with the ISFET

immersed in a pH 7.0 buffer solution and the source and drain terminals short circuited , the current through a picoammeter between the source and ground was measured. This current consists of contributions from the current flowing through the gate insulator which is normally insignificant and, more importantly, from the leakage currents due to poor encapsulation. Poor encapsulation includes inadequate insulation of the device's electrical connections from the solution, and the substrate from solution. For devices used in the early stages of this project, encapsulation of bonding wires, metallisation and the chip periphery was a problem, and a number of devices were fabricated in an intially "leaky" condition. These devices were characterised by leakage currents of around a few tenths of a μA. The high leakage currents were associated with the poor encapsulation of the chip periphery, and hence of the substrate. However, with the arrival of the silicon-on-sapphire (SOS) ISFET devices [1], the proportion of faulty devices was reduced substantially. The improvement in encapsulation as a result of the sapphire isolation of the substrate from solution was evident from leakage currents of less than 10 pA. "Leaky" devices were immediately discarded with no further use. Devices which showed currents of less than 10 pA over the entire bias range (-5 to +5 V) were deemed suitable for further characterisation.

5.1.2 I_D/V_{GS} and I_D/V_{DS} ISFET characterisation

The I_D/V_{GS} (threshold) and I_D/V_{DS} (output) characteristics for the ISFET devices have been obtained using the electronic circuitry shown in figure 4.11. In both cases the feedback connection of figure 4.11 was disconnected. The two characteristics obtained in a pH 7.0 buffer solution at 25°C are shown in figures 5.1 and 5.2, respectively. The curves are identical in form to the output characteristics of an MOS transistor (as they should be if the electrolyte-reference electrode combination of the ISFET system is considered to be equivalent to the metal component of the MOS structure). The results illustrated in figures 5.1 and 5.2 are typical of the SOS ISFET device used in this work. An indication of the
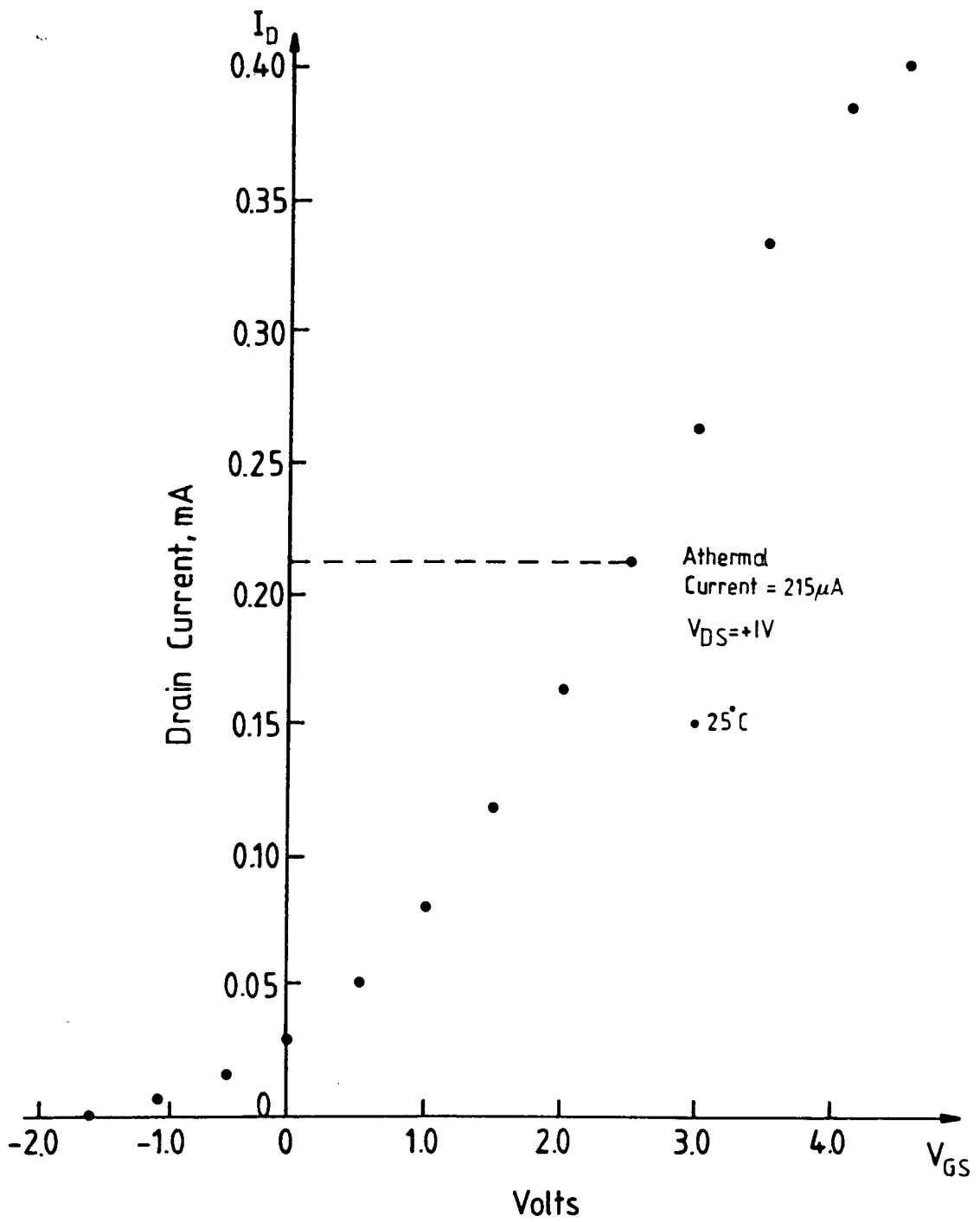
Figure 5.1 The I_D/V_{GS} threshold characteristic for an SOS ISFET device at pH 7.0 and 25°C.
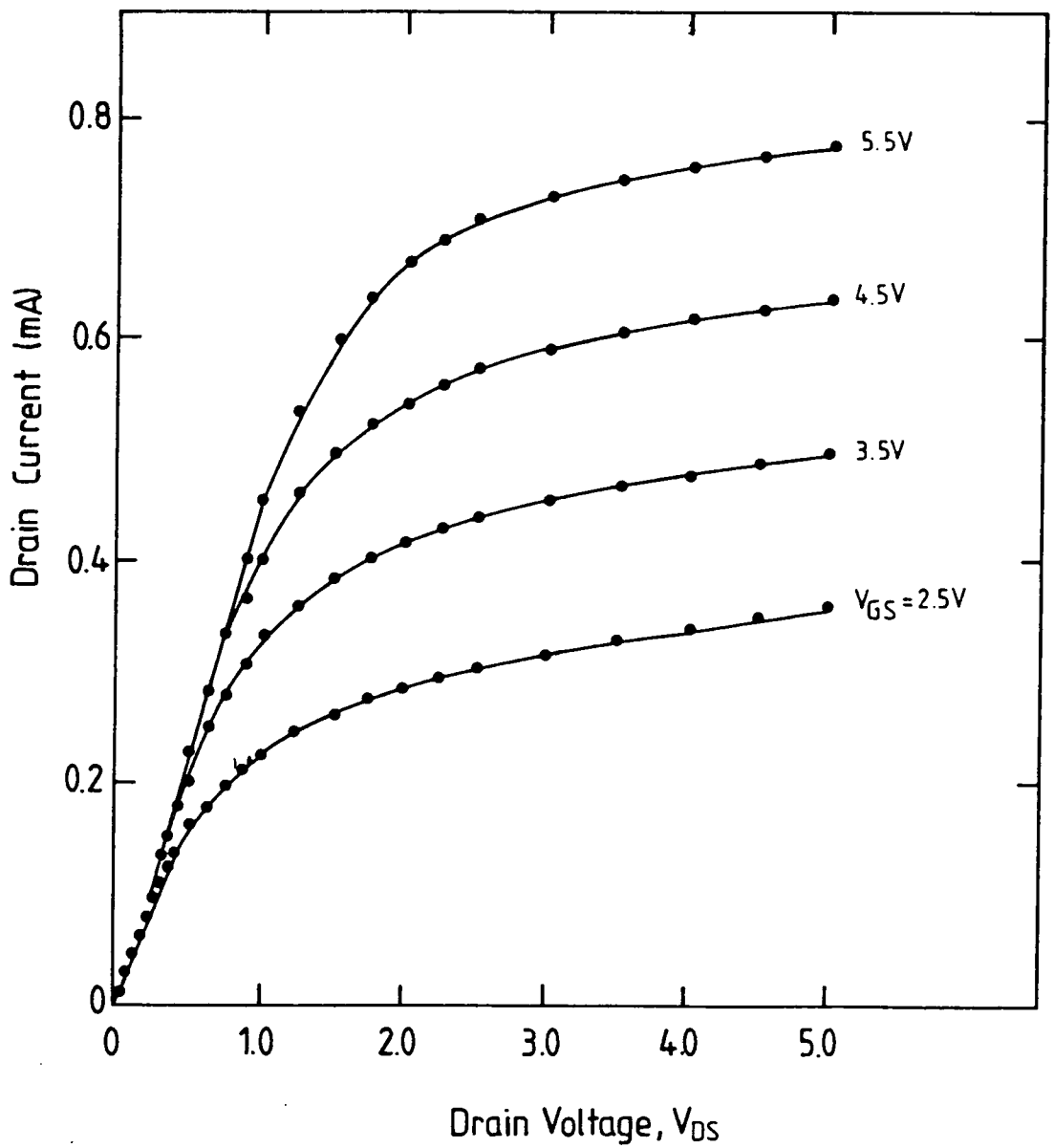
Figure 5.2 The I_D/V_{DS} output characteristics for an SOS ISFET device at pH 7.0 and 25°C.

reproducibility of these curves is given by the threshold voltage V_T obtained from the I_D/V_{GS} characteristic. A value of -1.5 ± 0.05 V (for a pH 7.0 buffer solution) was obtained for most devices studied in this work that had been treated with HF and conditioned in solution.

5.1.3 Effect of a pH change on the I_D/V_{GS} characteristic

The effect of the changing pH of the buffer solution on the I_D/V_{GS} characteristics for a constant V_{DS} is presented in figure 5.3. Clearly the effect is a change in threshold voltage V_T for the characteristic. The shape of the curve remains the same but its position along the V_{GS} axis shifts according to the pH change. The determination of V_T from these curves is difficult because its definition is not precise, but an approximate value for ΔV_T per pH unit (i.e a decade change in H^+ concentration) of 50-55 mV is obtained. The pH response is therefore almost ideal or Nernstian (58.6 mV per decade for a monovalent ion at 298K). This method of determining the change ΔV_T per pH unit, as well as being inaccurate, is laborious since an I_D/V_{GS} characteristic must be plotted for each pH solution used. A more elegant technique which allows ΔV_T to be monitored directly utilises the constant current mode of operation for the ISFET. For precision measurements, the inherent thermal sensitivity of the ISFET devices was taken into account and operation in constant current mode was performed at the athermal current.

5.1.4 ISFET athermal characteristics

The influence of temperature on the MIS device characteristics has been investigated by Vadasz and Grove [2,3]. The threshold voltage V_T and the inversion layer-charge (electron) mobility μ are the most significantly affected terms in the drain equation (equation (1), section 3.1). The results of Vadasz [3] suggest that over a wide temperature range (-55°C to 125°C) typical MIS device characteristics show a locus of minimum $\delta I_D/\delta T$. For biomedical applications, which are performed over a restricted temperature range (15°C to 40°C) the locus can be
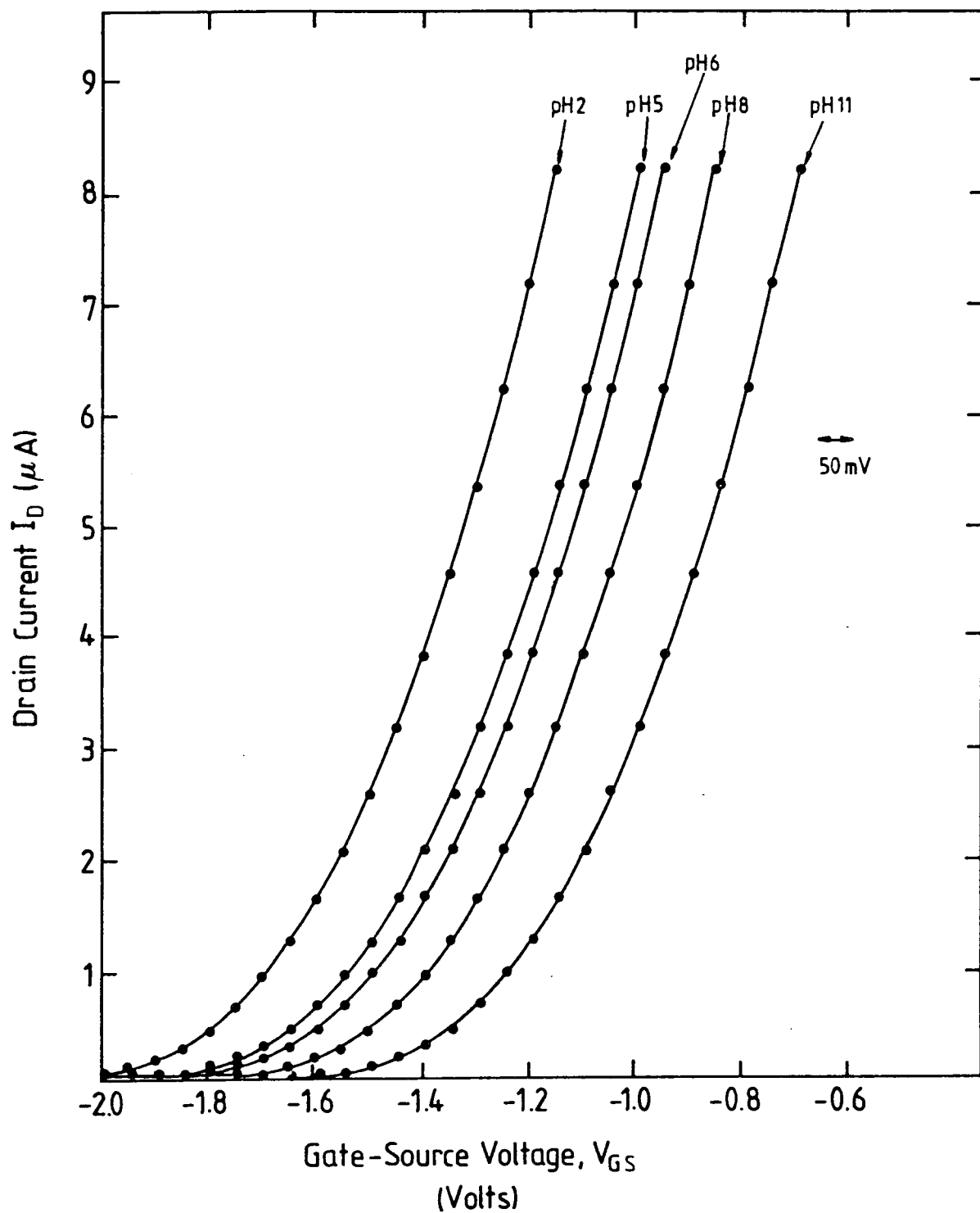
Figure 5.3 The effect of an electrolyte pH change on the I_D/V_{GS} threshold characteristic of an SOS ISFET device at 25°C.
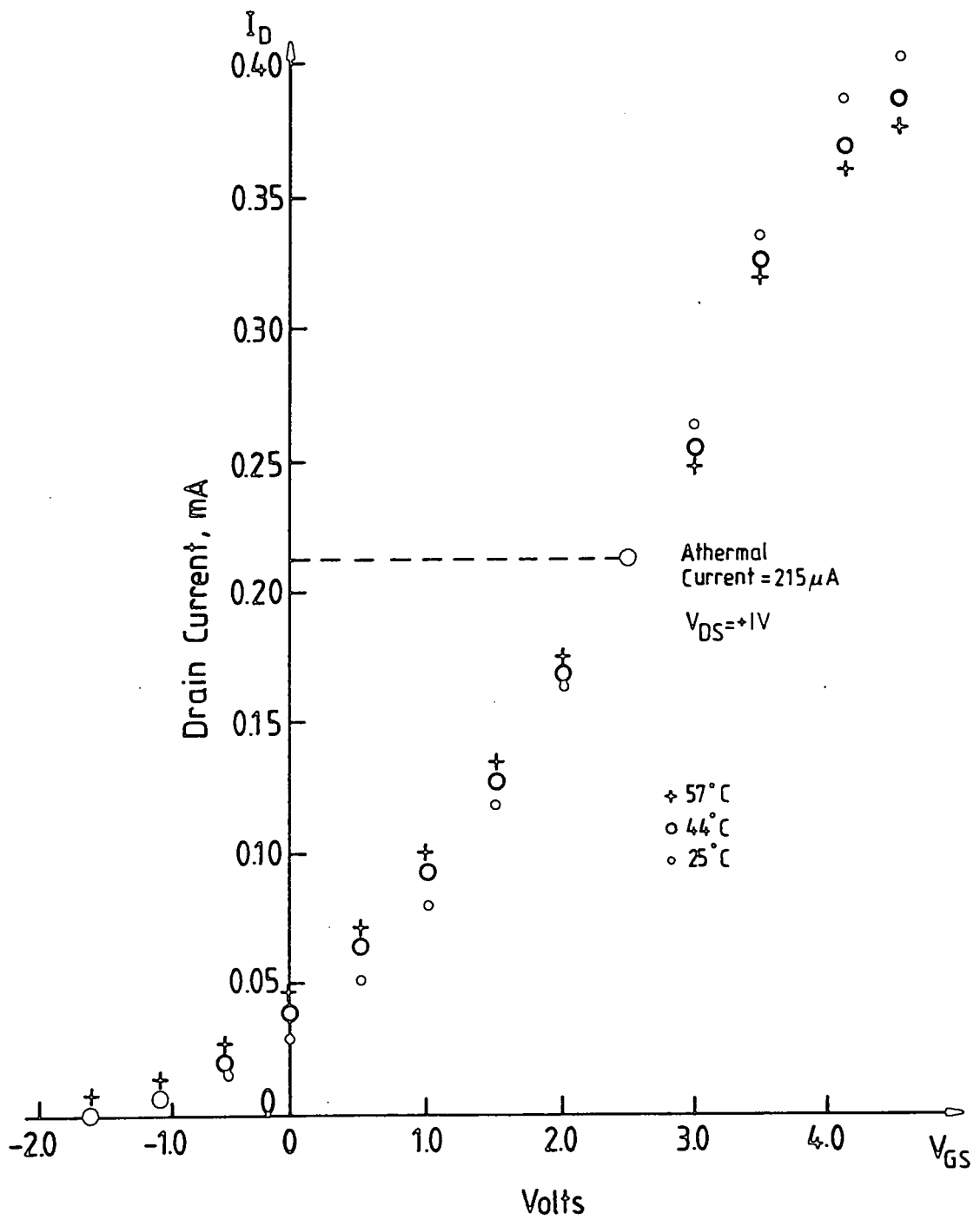
Figure 5.4 Athermal characteristics of an SOS ISFET device at a pH 7.0 for three temperatures.

considered as an athermal point, a point where the drain current is not significantly thermally dependent.

The athermal drain current (or point) is determined by plotting the I_D/V_{GS} characteristics over a temperature interval. The thermal characteristics for the ISFET devices used in this work are shown in figure 5.4 for three different temperatures. The athermal I_D value can be read of as 215 μA. For the devices used in this project athermal current values fell in the range 215 $\pm$ 10 μA. With the drain current set at its athermal value the pH response of the devices could be evaluated.

5.2 EVALUATION OF THE PH AND K^+ RESPONSES OF THE ISFET DEVICES

5.2.1 pH response

Before pH measurements were made the device was conditioned in a pH 7.0 buffer solution (with the ISFET in constant current mode) for 24 hours. This was necessary to allow the Si_3N_4 surface to hydrolyse completely. When the Si_3N_4 gate surface is intially immersed in water, the dangling Si bonds react with the water molecules forming silanol SiOH groups. Until the surface has fully hydrolysed (i.e. until the above process has reached an equilibrium) the bias voltage, E_{ref}, applied to the ISFET continually drifts. Only when the drift is less than 1 mV/hour were pH measurements undertaken. Large drift values are also an indication of poor encapsulation of the ISFET device.

The pH response of the ISFET with no preliminary HF etch of the gate surface is shown in figure 5.5. It can be seen that the response is far from Nernstian, typically 35-40 mV per pH unit. This has been attributed to the formation of a silicon dioxide (SiO_2) film on the nitride surface. It is known that SiO_2 also exhibits an inherent pH sensitivity but lower than that of Si_3N_4 because of a reduced surface site density. After the SiO_2 layer is removed with an HF etch, a near Nernstian response is achieved over the range of pH 4 to pH 9. Most devices
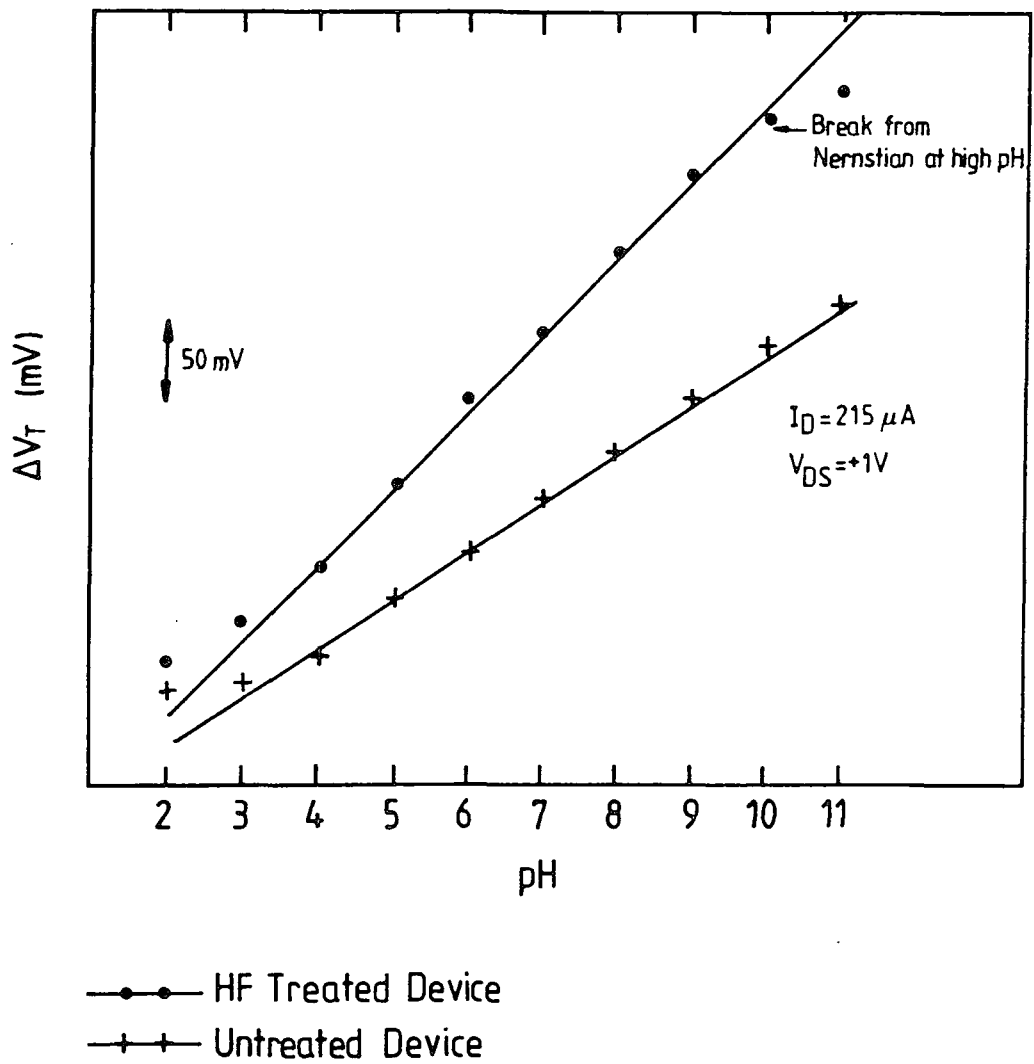
Figure 5.5 pH response of an ISFET device before and after an HF etching treatment.

exhibited response in the range 50-57 mV per pH unit.

5.2.2 Cation (Na^+, K^+) response of the ISFET

It is well known that the pH-responsive surfaces such as Si_3N_4 and SiO_2 also exhibit a response to the alkali-metal cations [4]. For example, in addition to the potential determining ions (H^+ and OH^-) exchanging with SiOH sites on the Si_3N_4 surface, it is possible for a monovalent counter ion such as sodium to also participate thus

$$SiO^- + Na^+ \rightleftharpoons SiONa \tag{1}$$

Therefore the cation responses of the ISFETs were measured. Figure 5.6 illustrates the effect of Li^+, K^+ and Na^+ concentrations on the threshold voltage of the devices (the titration solutions consisted solely of the cation ion under investigation). For all cations no response is observed until the concentration changes from 10^{-2} M to 10^{-1} M where a sharp shift in ΔV_T occurs. This effect is partly due to the participation of the surface reactions of the type described in equation (1) but is also a direct result of the total ionic concentration in solution. From equation (21) of chapter 3 the surface potential is not only determined by the parameters K_1, K_2 and N_S, but also by the magnitude of the Helmholtz capacitance, C_H. The latter depends on the total ionic concentration, C, in the solution. If the titration of, for example, K^+ is carried out in a 0.1 M LiCl solution the device response is shown by the dashed line of figure 5.6. The change in V_T from 10^{-2} M to 10^{-1} M is now much reduced because C has only changed by a factor of approximately two, compared to ten for the single-ion titration. The inherent sensitivity of the device to K^+ is important when the LB film-coated device response is assessed. For all cations little or zero response is obtained in the 10^{-5} M to 10^{-2} M range.
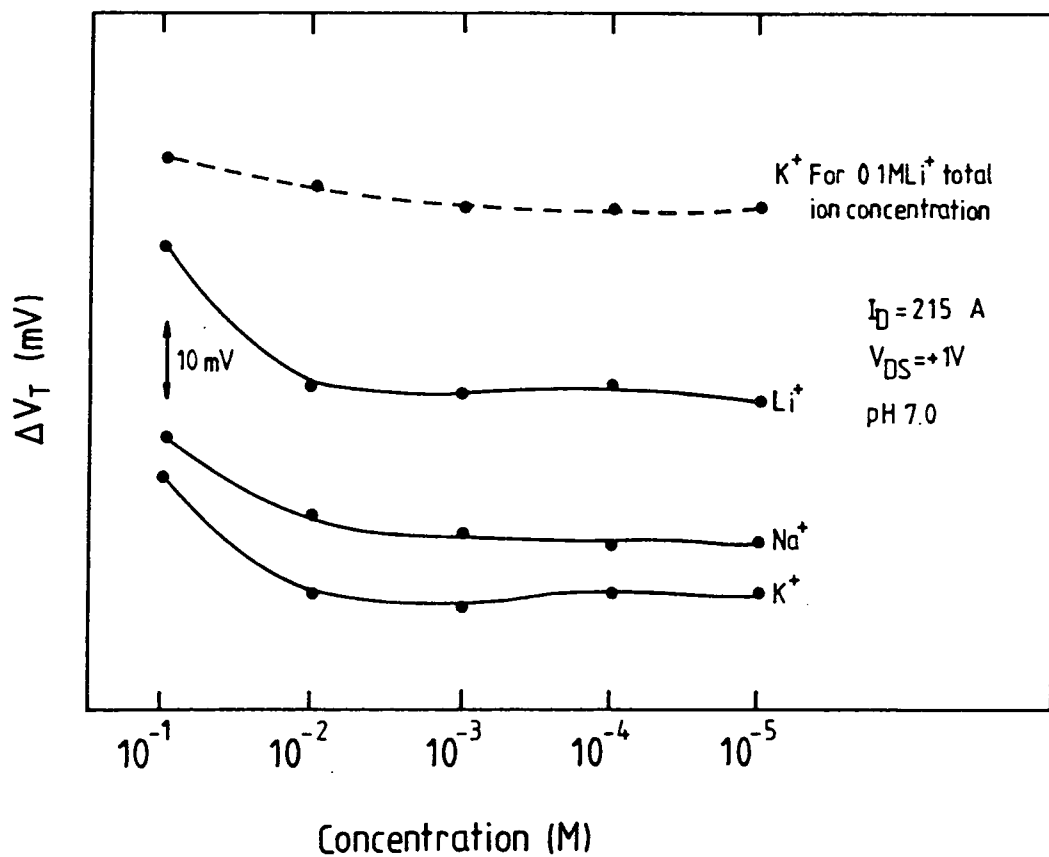
Figure 5.6 Cation (Li$^+$, Na$^+$ and K$^+$) response of an HF treated device.

5.3 ISFET CHARACTERISATION WITH DEPOSITED LB FILMS

5.3.1 Use of IR transmission spectroscopy to examine

the ISFET surface

The early stages of the project were concerned with dipping mixtures of fatty acids and valinomycin onto the ISFET surface. A technique based on IR spectroscopy for determining whether or not an LB film had been transferred onto the ISFET surface was devised. The region of the printed circuit board (PCB) (onto which the ISFET had been previously mounted) that was coated with the LB film is indicated in figure 4.6 of chapter 4. Monitoring the surface area of the film as a function of time during the dipping process provides little evidence for successful transfer of the film onto the ISFET itself. This is because of its relatively small surface area. Instead, exposing the underside of the ISFET chip (by boring a small hole in the reverse side of the PCB) allowed an IR beam to be transmitted through the ISFET. The IR spectrum of any material deposited onto the chip surface could then be analysed to identify not only the presence of the two components but also to provide an indication of the reproducibility of the deposition. Preliminary work was carried out using ω-tricosenoic acid (ω-TA)/valinomycin mixtures. The deposition conditions for a 10:1 mixture were a surface pressure of 23 mN m^{-1}, a pH of 5.8, a dipping speed of 3 mm min^{-1} and a temperature of 21°C. The spectrum for a cast film (deposited from a microsyringe) of a 10:1 mixture is shown in figure 5.7, with the bands due to each component labelled. This was used to identify the mixed LB film on the ISFET. The IR spectrum for 100 layers deposited onto the ISFET is shown in figure 5.8. Comparison of figures 5.7 and 5.8 shows that all the valinomycin bands are present. Valinomycin is unmistakably present on the ISFET surface. The NH band (approx. 3300 cm^{-1}) in the spectrum of figure 5.8 is obscured by the OH band of water vapour; and also the CH$_3$ band is inexplicably absent. By calculating the ratios of the intensities of certain valinomycin bands (ester; amide I, and II) to those of ω-TA in the mixed films for various numbers of layers deposited, yields a constant value. This
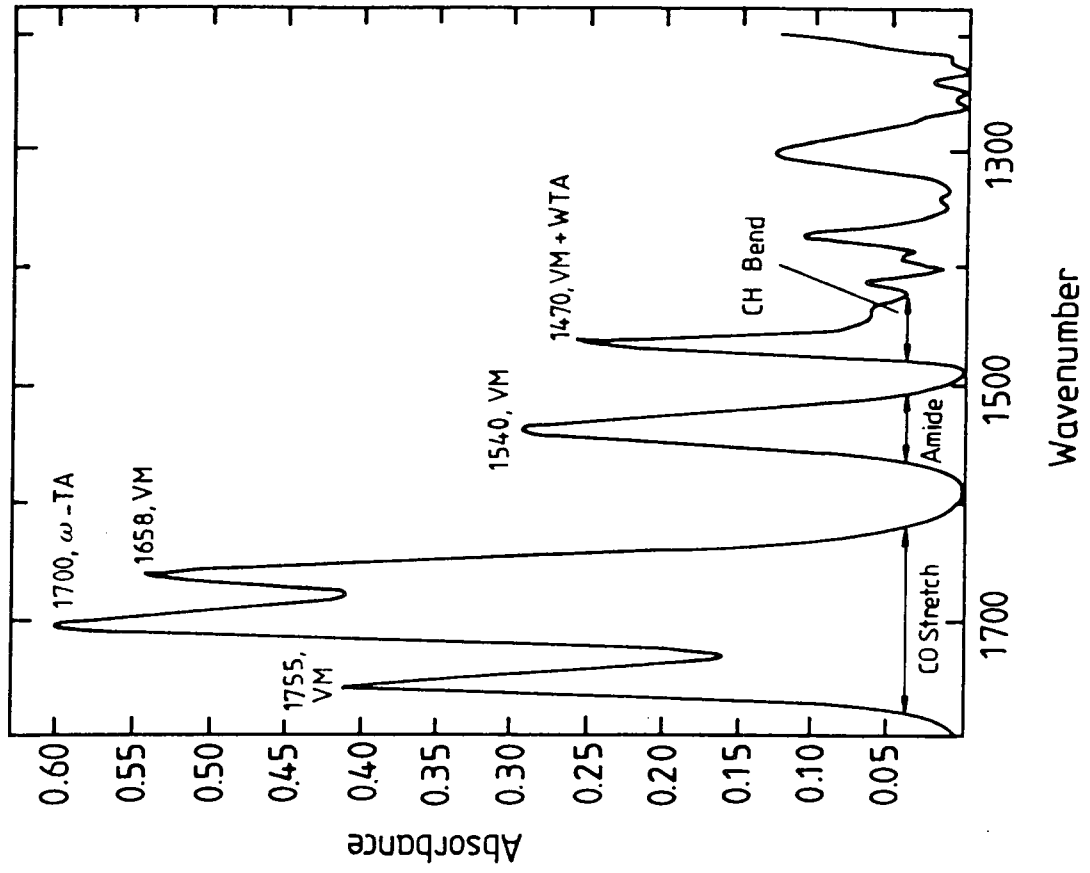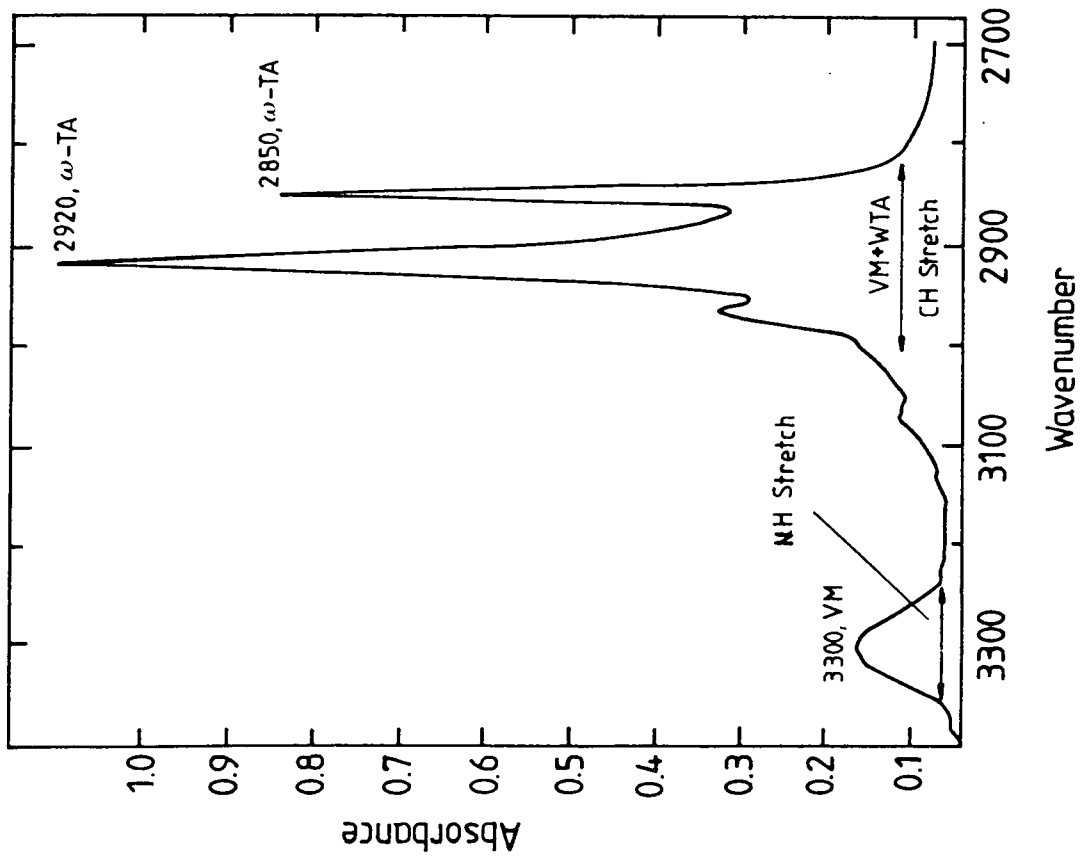
Figure 5.7 ATR-IR spectrum for a cast film of a 10:1 (molar) mixture of ω-tricosenoic acid and valinomycin.
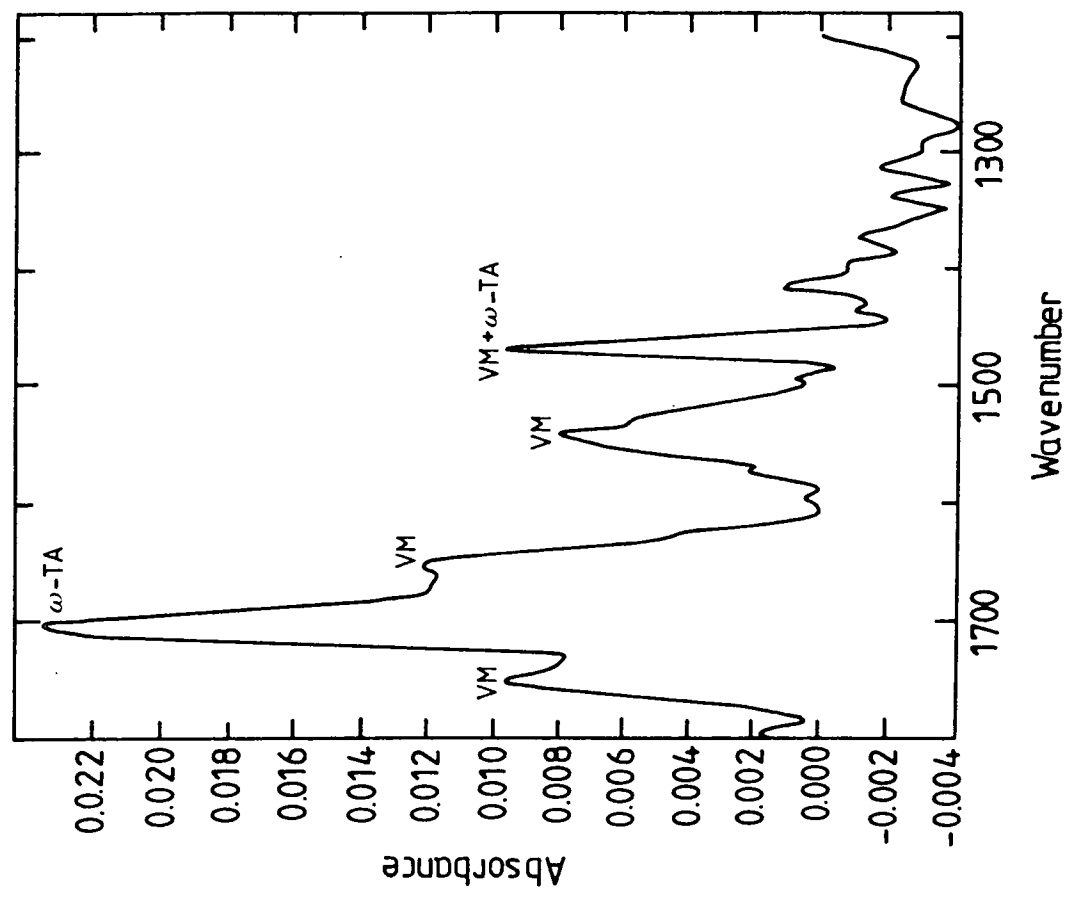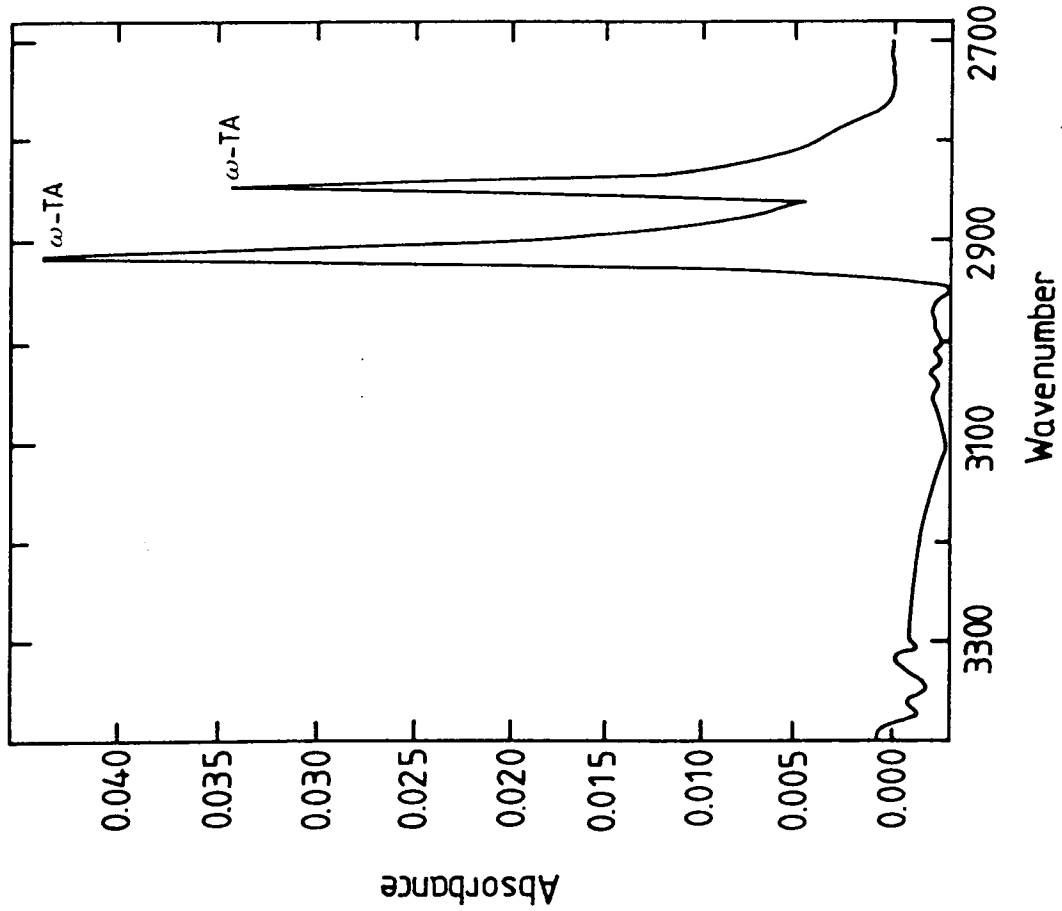
Figure 5.8 Transmission IR spectrum for 100 layers of a 10:1 (molar) mixture of ω-tricosenoic acid and valinomycin deposited onto the ISFET surface.

suggests that the deposition is reproducible and that valinomycin is still being deposited at a large number of layers.

The use of this technique has highlighted a potential advantage of the SOS ISFETs over those ISFETs having exposed substrates. In the case of the latter devices, it was necessary to encapsulate the chip periphery. To achieve this efficiently resulted in a rim of epoxy running around the entire periphery of the ISFET enclosing the gate surface. The rim of epoxy was raised above the flat surface of the PCB and hence the ISFET gate formed the bottom of a well-type hole. On withdrawl of the PCB from the subphase during the dipping process, water was retained in the well. On the subsequent downstroke the trapped water rejoined the subphase; consequently, little or no film was deposited. IR spectroscopy from such a dipped sample showed the presence of a small quantity of material and observation under a microscope revealed a poor, non-uniform film. However, the SOS ISFETs (which required no substrate encapsulation) could be mounted on the PCB in such a way that the ISFET surface was flush with the PCB surface. This provided a level surface onto which LB films could be readily deposited. The results of spectroscopy, and ellipsometry of LB films coated onto mounted SOS ISFET chips, revealed an excellent reproducibility for the deposition.

5.3.2 Fatty acid and fatty acid salt films deposited onto ISFET

Langmuir-Blodgett films of a variety of fatty acids and their salts were deposited onto the gate surface of the ISFET and the effect on the pH response was investigated. The experimental procedure was as follows. Intially, the virginal pH response was determined followed by the deposition of the LB film onto the ISFET and its IR characterisation. Then the pH response was again determined. In order to evaluate whether any film had been lost during the titration, both a visual and an IR examination of the LB film were performed after completion of the pH titrations. Finally, the LB film was removed using Aristar chloroform and the pH response was again recorded.

$\Delta S = $ Change in pH response with addition of 50 layers of LB film

Material	pH Response (mV/Decade)	ΔS Before	ΔS After	Percentage Loss During Immersion
Arachidic Acid	50±2	0	0	<10%
Cadmium Arachidate	52±2	0	0	<5%
Stearic Acid	52±2	0	0	<10%
Cadmium Stearate	50±2	0	0	<5%
ω - TA	55±2	0	0	<10%
Cadmium ω-Tricosenoate	55±2	0	0	<5%

(a)

Polymerised Diacteylene	50±2	0	0	0
Silicon Phthalocyanine	50±2	0	0	<5%

(b)

Table 5.9 (a) The effect of LB films (50 monolayers in thickness) on the pH response of the ISFET device for both fatty acids (and their salts) and (b) the effect of silicon phthalocyanine and polymerised diacetylene LB films.

The fatty acids and their salts deposited onto the ISFET and their effect on the pH response are tabulated in Table 5.9a (the table is for 50 layer films). It is clear from these results that the LB film has no significant effect on the pH response of the ISFETs. The "super" pH response reported by Moriizumi [5] for an SOS ISFET coated with cadmium arachidate was not observed. Furthermore, there is still no effect on the pH response as the number of monolayers is varied. Up to 100 monolayers of cadmium stearate have been deposited and no significant changes in ΔS were observed. The results also indicate that the adhesion of the LB films of the cadmium salts of the fatty acids, upon immersion in aqueous solution, is better than that of the acids. This can be associated with the improved lateral cohesion in the salt films due to the presence of the divalent cadmium ions. For all the salt films, less than 5% of the material was lost for an immersion period of 2 hours. Furthermore, the threshold voltage V_T of the ISFET device did not change when an LB film was coated onto the gate surface. There are two possible interpretations for the results described above. Firstly, and most likely, the LB film does not present a barrier to the potential determining H^+ and OH^- ions and the surface reactions on the Si_3N_4 surface proceed as if no film were present giving an identical pH response. Secondly, it is feasible that the fatty acid and fatty acid salt LB films are taking part in proton exchanging reactions with the electrolyte thus leading to an identical pH response to that produced by the gate surface.

A material which was expected not to undergo proton exchanging reactions with the electrolyte was silicon phthalocyanine [6]. The effect of the number of monolayers on the threshold voltage and the pH response was evaluated. The effect on the pH response for 50 monolayers of this material is shown in Table 5.9b. Again no significant effect is apparent on both the pH sensitivity and the threshold voltage. Adhesion of the film to the ISFET surface was however excellent with almost no loss of material. This concurs with the excellent dipping properties reported in the literature for this material [6]. This result reinforces

the first hypothesis based on the permeability of the LB film to the potential determining ions probably due to pin-hole defects in the LB film or possibly due to ions creeping around the edges of the LB film. In order to provide a structure less permeable to hydrogen ions monolayers of a diacetylenic acid [7] were coated onto the ISFET. The material used was $C_{17}H_{25}-C\equiv C-C\equiv C-(CH_2)_8-COOH$ and the deposition conditions were: a surface pressure of 15 mN m^{-1} and a pH of 6.5. The LB film was subsequently UV-polymerised using an EPROM eraser. The resulting disordered cross-linked structure was expected to be less permeable to the H$^+$ and OH$^-$ ions than the ordered fatty acid structures. The results of Table 5.9b suggest, however, that the pH sensitivity and threshold voltage are unchanged i.e. the same result as for no LB film.

From these experiments it can be concluded that the LB film is no barrier to the H$^+$ and OH$^-$ ions. Furthermore, the cation responses of the ISFET were also found to be unchanged by the addition of an LB film.

5.4 PLASMA POLYMER MEMBRANE COATING FOR THE ISFET

From the point of view of the potassium ion-sensing application it is the MIS structure of the ISFET which provides the mechanism for transducing the equilibrium potential produced across the sensitive membrane. The surface potential is changed which alters the degree of surface inversion, and hence the drain current (or threshold voltage). The intrinsic pH sensitivity of the Si$_3$N$_4$ gate insulator plays no role (and although its elimination is unnecessary because, in the research environment, potassium ion-sensing experiments can be carried out at constant pH) a practical working potassium sensor which is independent of pH is desirable. Towards this aim, an attempt was made to reduce the pH sensitivity of the gate surface.

Preliminary investigations, using the silanising agent dimethyl- dichlorosilane to remove the pH-sensitive silanol groups showed that the pH response could be reduced to approximately 25 mV pH^{-1}. Complete elimination was not possible
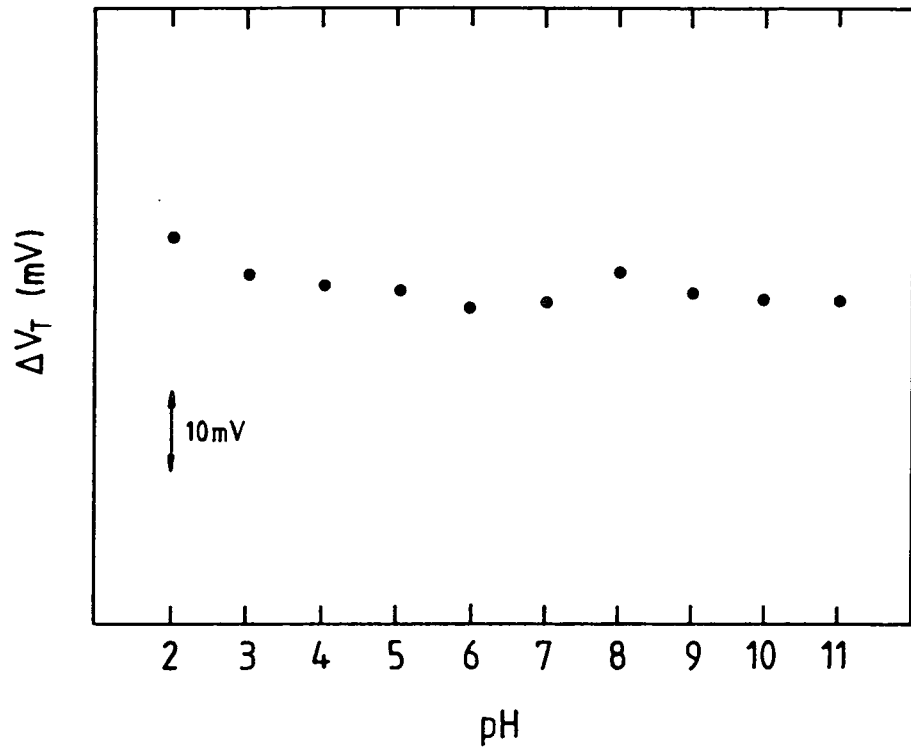
Figure 5.10 The pH response of an ISFET coated with a thin plasma-polymer film of benzene.

and Van den Berg et al [8] have attributed this to the fact that such a direct chemical modification of the silicon surface still leaves residual surface silanol groups to participate in proton exchanging surface reactions.

Next, the deposition of a polymeric layer on top of the gate was attempted. Previous reports in the literature concern the deposition of polyvinylchloride (PVC) [9], poly-p-xylylene (Parylene) [10] and Teflon [11] polymeric films. Such hydrophobic films are essentially site-free (10^{13} cm^{-2} as compared to 10^{15} cm^{-2} for the hydrophilic Si_3N_4 surface) and provide non-Nernstian responses. Plasma polymerisation (in which there is a strong research interest at Durham University) was used to deposit the polymeric layer in the following manner. The plasma polymerisation was carried out with the mounted ISFET placed in the centre of a tubular-shaped pyrex reactor. The system was evacuated to a base pressure of 3 x 10^{-2} torr, and then benzene vapour was introduced and allowed to flow through the system at a pressure of 0.1 torr. Radio frequency power(20 W) was inductively coupled to the system through an externally wound copper coil. When the plasma was ignited a thin polymeric layer was deposited on all surfaces in contact with the plasma.

Intial experiments performed with plasma polymer films of benzene, typically 100 nm in thickness showed the the desired reduction in pH sensitivity (the thickness of the plasma polymer films was obtained by ellipsometry on a silicon test sample placed next to the ISFET in the plasma discharge tube during deposition). Unfortunately, the lifetimes of these films were short (a few hours). This was caused by the formation of micro-cracks in the polymer film which could easily be examined under the optical microscope. Upon re-immersion, the pH response had changed markedly and increased with time; approaching that of the bare Si_3N_4 device. Clearly this indicates the silanol groups had become exposed to the solution and again were contributing to the pH sensitivity.

The above problem was overcome by the use of thinner polymer films, 30-50 nm in thickness. A typical pH response for an ISFET coated with 30 nm of

a plasma polymer of benzene is shown in figure 5.10. The change in threshold voltage ΔV_T as a function of pH is now no longer monotonic, and the maximum pH slope is 5 mv pH^{-1}. Clearly a substantial reduction in pH sensitivity is obtained, and this can be attributed to the essentially site-free surface. However, the results of figure 5.10 were obtained taking into account a relatively large, constant drift in the threshold voltage at a rate of approximately 5 mV per min. This should be contrasted to a rate of drift of 1 mV per hour for the Si_3N_4 surface. The cause of this drift in V_T was associated with the plasma polymer. Removal of the plasma polymer with a short ultrasonic agitation in acetone resulted in a reduction of the drift value to that of the bare Si_3N_4 surface. The large drift values can be attributed to the movement of ions in the polymer (introduced during the deposition process) under the influence of the electric field applied across the polymer-oxide sandwich.

Furthermore, investigation of the deposition process of fatty acids onto a benzene plasma polymer coated glass slide revealed that the unreactive surface of the polymer (as well as providing a pH insensitive surface) also made the transfer of monolayers inordinately difficult. For these reasons, the plasma polymer idea was abandoned and it was decided to perform potassium sensing experiments at constant pH.

5.5 ISFETS COATED WITH LANGMUIR-BLODGETT FILMS

In order to develop a potassium sensor, the next step was the deposition of Langmuir-Blodgett films containing the ionophore onto the gate surface of the ISFET.

5.5.1 Pure valinomycin films

Firstly, pure LB films of valinomycin were investigated. In order for pure films to be deposited onto a substrate, the substrate first of all needed coating with a few layers of cadmium stearate (this deposition procedure is described more fully in chapter 6). Although it could not be proved experimentally, it was assumed
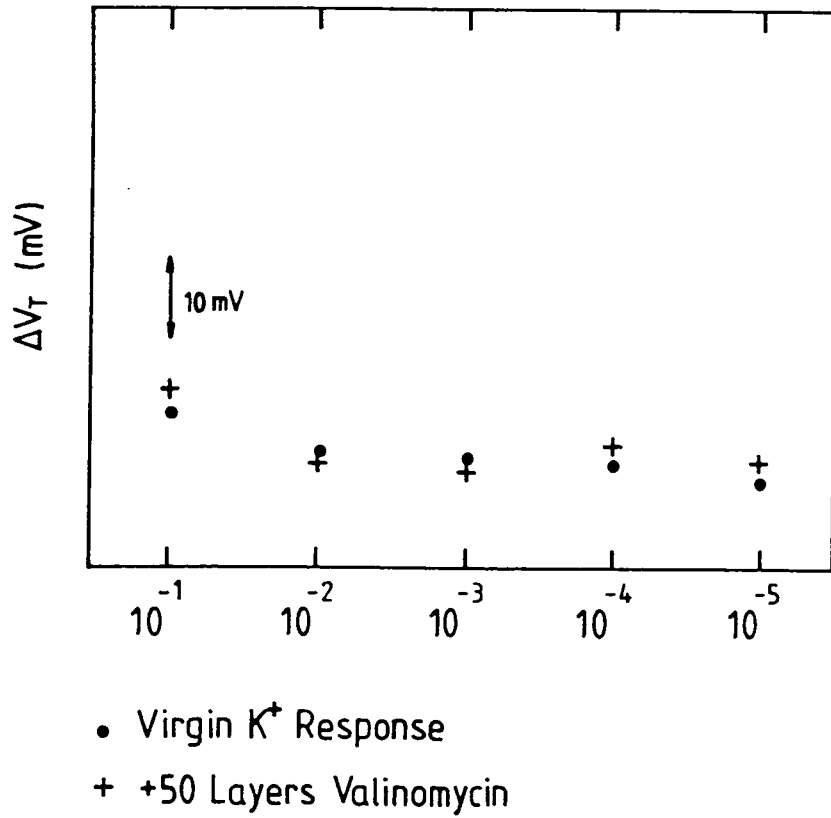
Figure 5.11 The K^+ response of an ISFET device before and after the deposition of an LB film of pure valinomycin. The film was 50 monolayers in thickness and K^+ was varied at 0.1 M LiCl.

that either one (for one deposition cycle) or three (for two cycles) monolayers of cadmium stearate were transferred to the Si_3N_4 gate surface (under the assumption that the silanol groups form a hydrophilic surface). For films greater than 20 monolayers thick, reproducibility of the deposition could be checked by using transmission IR spectroscopy.

The experimental procedure adopted to determine the K^+ response of these films was as follows: firstly, the K^+ response of the bare Si_3N_4 surface was determined; secondly, the response with the cadmium stearate base layer; thirdly, with the LB film of pure valinomycin and finally that of the bare gate surface again (after removal of the films with chloroform). The responses for a typical device coated with 50 monolayers of valinomycin are illustrated in figure 5.11. No significant differences are apparent. All curves exhibit the shift in threshold voltage between 10^{-2} M and 10^{-1} M potassium concentrations (associated with the change in total ion concentration) but below 10^{-2} M, where the affect of the valinomycin should be evident, no response to potassium ions is observed. There is also no change in K^+ (relative to that of the Si_3N_4 surface) as a function of the number of monolayers of valinomycin deposited or as a function of the thickness of the cadmium stearate base layer. Furthermore, the threshold voltage did not shift when an LB film was deposited.

A number of explanations are possible. Firstly, loss of material into the electrolyte must be considered. This cannot be checked for multilayers which have been directly deposited onto the ISFET and are less than 20 monolayers in thickness. However, the results of experiments concerned with immersing an ATR crystal coated with less than 5 monolayers into aqueous potassium solutions suggests no material loss. Also transmission IR spectroscopy performed on the 50 layer samples deposited onto the ISFET indicated only a 5% loss of material during the pH scanning (1 hour). Therefore loss of material as the cause can be eliminated. However, the results of attenuated total reflection IR studies performed on LB films of pure valinomycin (described in detail in chapter 7) suggest that
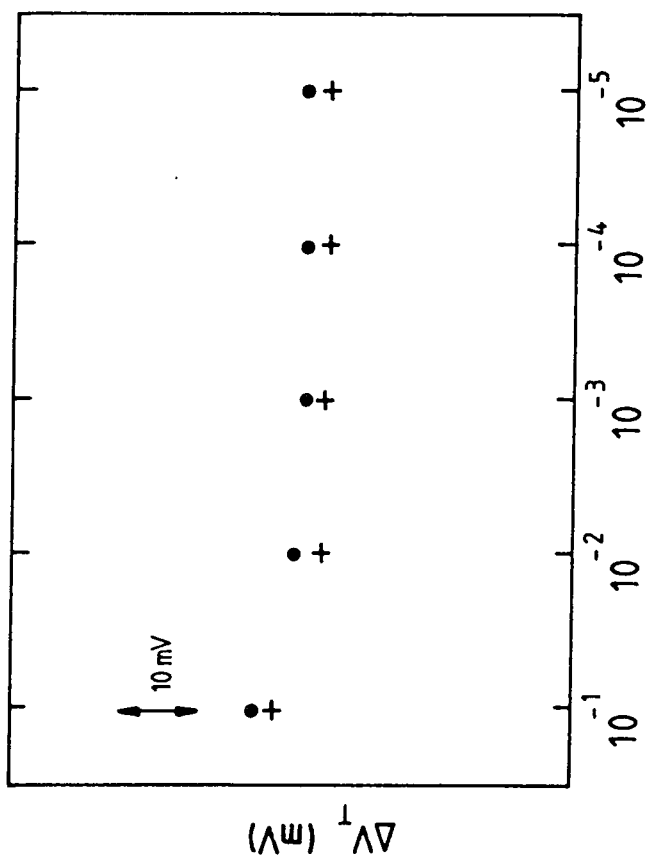
Figure 5.12 The K+ response of an ISFET device before and after the deposition of a mixed LB film of arachidic acid and valinomycin. The film was 50 monolayers in thickness and K+ was varied at 0.1 M LiCl.

these films do not complex with potassium ions. This implies that an equilibrium potential due to complexation will not be observed across a pure valinomycin film, and therefore this is a possible explanation for the lack of a K^+ response from the ISFET measurements.

5.5.2 Arachidic acid/valinomycin films

The effect on the K^+-response of depositing mixed LB films of arachidic acid and valinomycin onto the ISFET gate surface was also investigated. The deposition conditions for the mixed films are outlined in detail in Chapter 6. The experimental procedure used to evaluate the K^+-response of these films is exactly the same as that described in section 5.5.1 for the pure valinomycin films.

The responses for a typical device coated with 50 monolayers of a 10:1 (molar) LB film are illustrated in figure 5.12. Again no significant differences are observed. There is also no change as a function of the mole-fraction of valinomycin in the mixed films.

Loss of material into the electrolyte was considered but again this theory was rejected on the evidence obtained from transmission IR spectroscopic studies. However, the results obtained from a detailed study of the interaction of mixed LB films with potassium containing solutions (presented in Chapter 7) suggest a possible explanation for the lack of response. In such films, the formation of the valinomycin-K^+ complex occurs, however, its dissociation does not take place. In order for a device to exhibit a K^+-response, an equilibrium potential dependent on the potassium ion concentration is necessary. For an equilibrium potential to be set up across the LB film both processes, formation and dissociation, need to occur. The absence of the latter process in the mixed arachidic acid/valinomycin system implies that an equilibrium potential will not be generated. Hence, complexation of the valinomycin in the LB film will continue until saturation occurs, and therefore the device will not exhibit a response that is dependent on the K^+ concentration.

5.6 SUMMARY

SOS ISFETs have been mounted and encapsulated onto dip-type printed circuit boards for laboratory appraisal. The threshold and output characteristics have been presented. The devices, after a preliminary etch in a buffered HF solution, exhibited a near Nernstian response. An attempt to eliminate the pH response using a site-free plasma polymer was successful. However, subsequent problems were encountered with the deposition of LB films onto this surface, which meant that the polymer could not be incorporated into the device. The deposition of a variety of LB films and, in particular, both pure valinomycin and mixed arachidic acid/valinomycin LB films onto the gate region of the ISFET has been demonstrated. Unfortunately, these films do not exhibit a response to potassium ions. A possible explanation has been proposed based on the results of IR studies presented in chapter 7.

CHAPTER 6

DEPOSITION AND CHARACTERISATION OF LB FILMS CONTAINING VALINOMYCIN: RESULTS AND DISCUSSION

6.0 INTRODUCTION

This chapter concerns the preparation and characterisation of pure valino-mycin and valinomycin-containing LB films. Section 6.1 describes studies per-formed on floating Langmuir monolayers of valinomycin, such as their stability; the effect of pH and subphase ion concentration; and the special conditions required for the successful deposition of valinomycin multilayers. Section 6.2 presents the characterisation of these multilayers using various spectroscopic techniques. The interaction between mixed valinomycin/arachidic acid LB films and potassium ions is discussed in detail in chapter 7, and section 6.3 includes a study of these mixtures with a view to using them as potassium sensitive membranes for the ISFET application. Section 6.4 concludes the chapter, describing LB films of the phospholipid molecule, L-α-phosphatidic acid dipalmitoyl.

6.1 LANGMUIR-BLODGETT FILMS OF VALINOMYCIN: DEPOSITION

6.1.1 Π-A isotherm for valinomycin

The Π-A isotherm for valinomycin on unbuffered water (i.e. no subphase ions present) at pH 5.8 and at a temperature of $21 \pm 2°C$ is shown in figure 6.1. The subphase is slightly acidic owing to the carbon dioxide absorbed from the atmo-sphere during storage. The isotherm can be divided into three sections labelled A, B and C. Region A is analogous to the gaseous phase with the valinomycin molecules far apart and contributing to very little pressure development as the film is compressed. Region B (up to approximately 2 nm^2) is a region of roughly constant slope and represents the molecules gradually approaching each other,
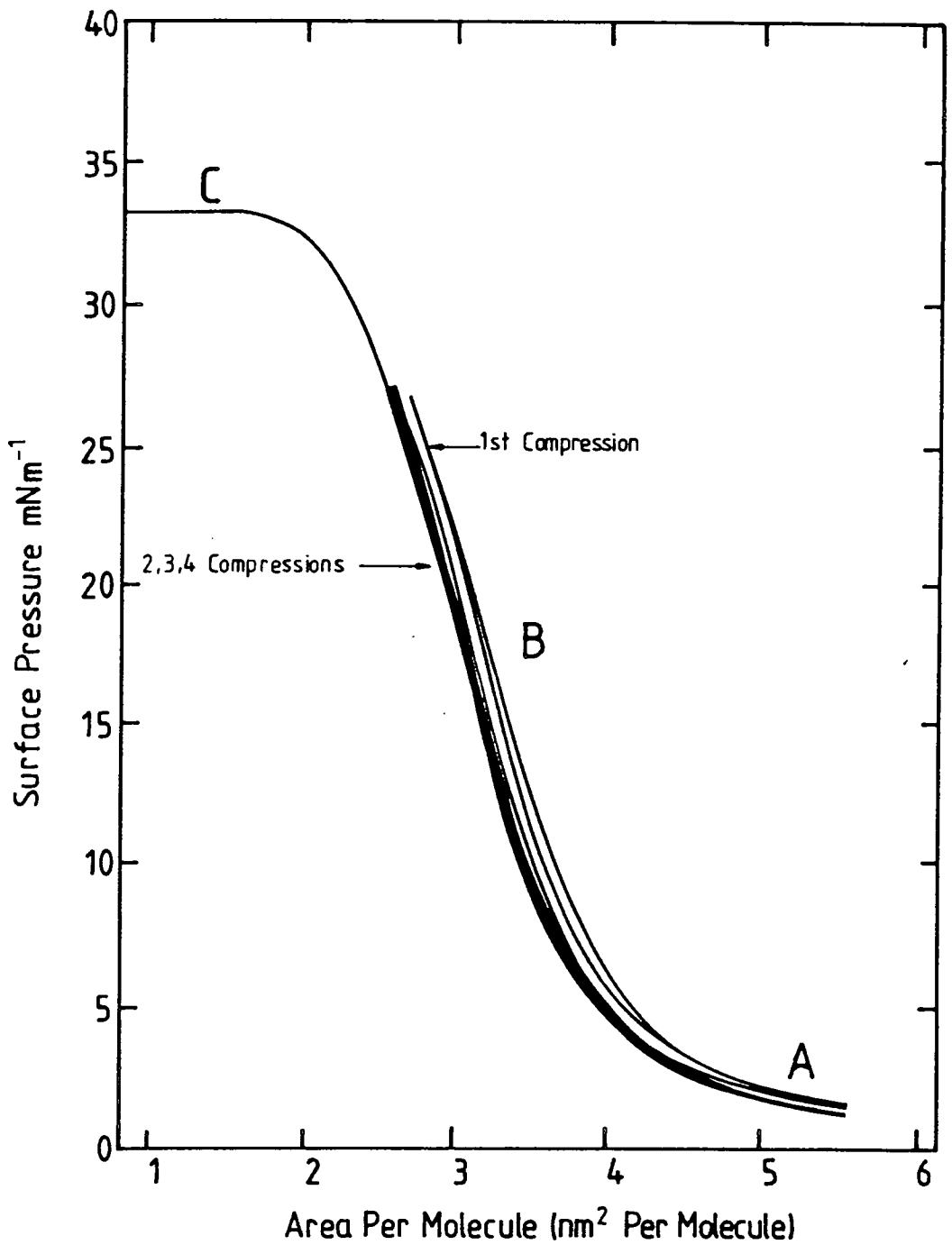
Figure 6.1 Surface pressure-area isotherm for valinomycin on unbuffered water at pH 5.8 (for area per molecule > 1.0 nm^2 per molecule). Also showing the isotherm reproducibility for compressions below the plateau region.
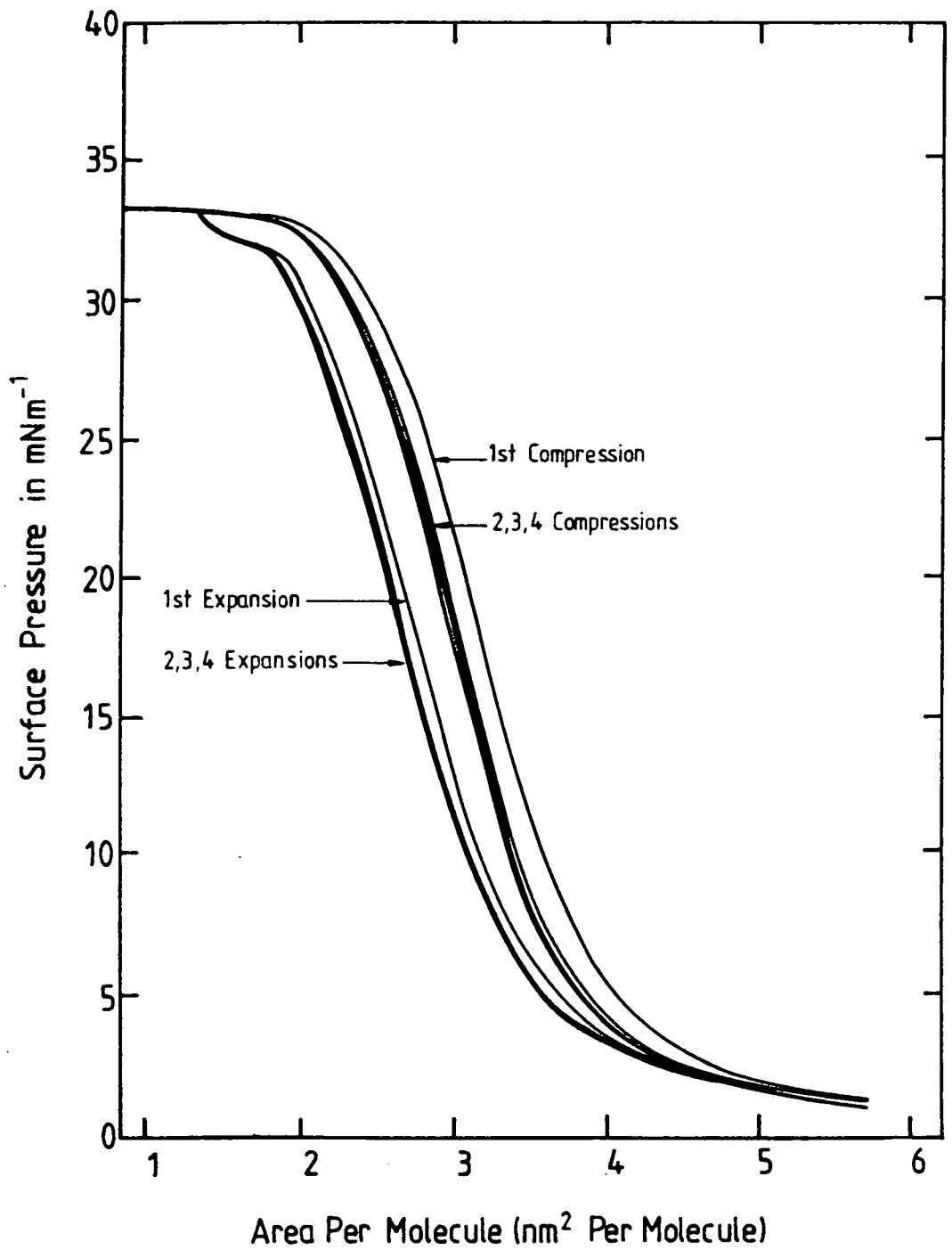
Figure 6.2 Hysteresis of the valinomycin surface pressure-area isotherm for compressions into the plateau region (< 2 nm^2 per molecule).

coming into close contact and forming a condensed monolayer. At an average area of approximately 2 nm^2 the Π-A isotherm starts to curve towards the pressure axis and this corresponds roughly to the hard core area of the uncomplexed molecule [4,6] (if not a little greater assuming there is some area lost in packing). The plateau region C at a surface pressure of 32.5 mN m^{-1} extends beyond 2 nm^2.

Provided that the valinomycin film is not compressed into the plateau region, the isotherm is highly reproducible (figure 6.1). This demonstrates the great mobility of the valinomycin molecules on the water surface. Also the stable intial and final pressures, and the evidence of little hysteresis indicates the water insolubility of valinomycin. This leads to the formation of highly stable floating Langmuir monolayers (see section 6.1.2).

However, the reproducibility only holds below 2 nm^2. For example, if the monolayer is compressed into the plateau region, hysteresis is evident and this is illustrated in figure 6.2. A large hysteresis is observed between the first compression and the first expansion. The second compression-expansion cycle does not follow the first but is shifted to a smaller average area per molecule and also exhibits the same degree of hysteresis. Successive compression-expansion cycles follow the second cycle but still show a constant hysteresis. All compressions and expansions were carried out at the same rate of 2 cm^2 s^{-1} and a time interval of a few minutes was allowed between compression and expansion in order for the film to stabilise. It is worth noting that large hysteresis effects are apparent in isotherms recorded at high rates of expansion. This arises from the fact that such an expansion is a non-equilibrium process, that is to say, if a film is expanded rapidly to, and held at a particular area, the surface pressure gradually increases until a stable value is attained. To record a true Π-A isotherm, expansion and compression should take the Langmuir layer through a series of successive states of equilibria with little change in surface pressure being evident when, for example, a particular area is held. Expansion and compression rates of 2 cm^2 s^{-1} were found to satisfy this condition.

Hysteresis effects can also be caused by the dissolution of the material into the subphase. However, this is not the case for valinomycin monolayers which form highly stable Langmuir films (see section 6.1.2). It is therefore proposed that the large hysteresis effect observed in the compression-expansion isotherms of valinomycin is due to an entirely different effect, and is associated with the formation of aggregates or "islands" in the film.

When the compression continues into the plateau region it is believed that the molecules are sliding on top of each other providing for a large change in area with little surface pressure change. On expansion the molecules remain associated with each other to form aggregates. These aggregates may be confined to the horizontal plane or might be stacked vertically. The aggregates cause a reduction in the effective number of "molecules" in contact with the water surface. This is observed as a shift of the isotherm towards the left i.e. to a smaller average area per molecule. On recompression the isotherm lies between the intial compression and expansion indicating that some aggregation is still present. The next expansion follows the preceding one and from this point onwards the expansions and compressions are reproducible exhibiting a constant hysteresis. This indicates that aggregates which are retained for most of the expansion dissociate at large areas per molecule and then reform on the following compression.

A comparison of the isotherm illustrated in figure 6.1 with other valinomycin isotherms reported in the literature is shown in figure 6.3. The isotherms are similar in form but show a large variation concerning the plateau pressure and the surface area at which concavity towards the pressure axis commences. It is true that none of the isotherms illustrated in figure 6.3 were performed under exactly the same experimental conditions, but the differences (occurring in pH, subphase ion concentration) have in this work (see section 6.1.3) been shown to have a negligible effect on the Π-A isotherm. Therefore no explanation at present is available to explain these discrepancies.

The plateau region C at a surface pressure of 32.5 mN m^{-1} extends beyond
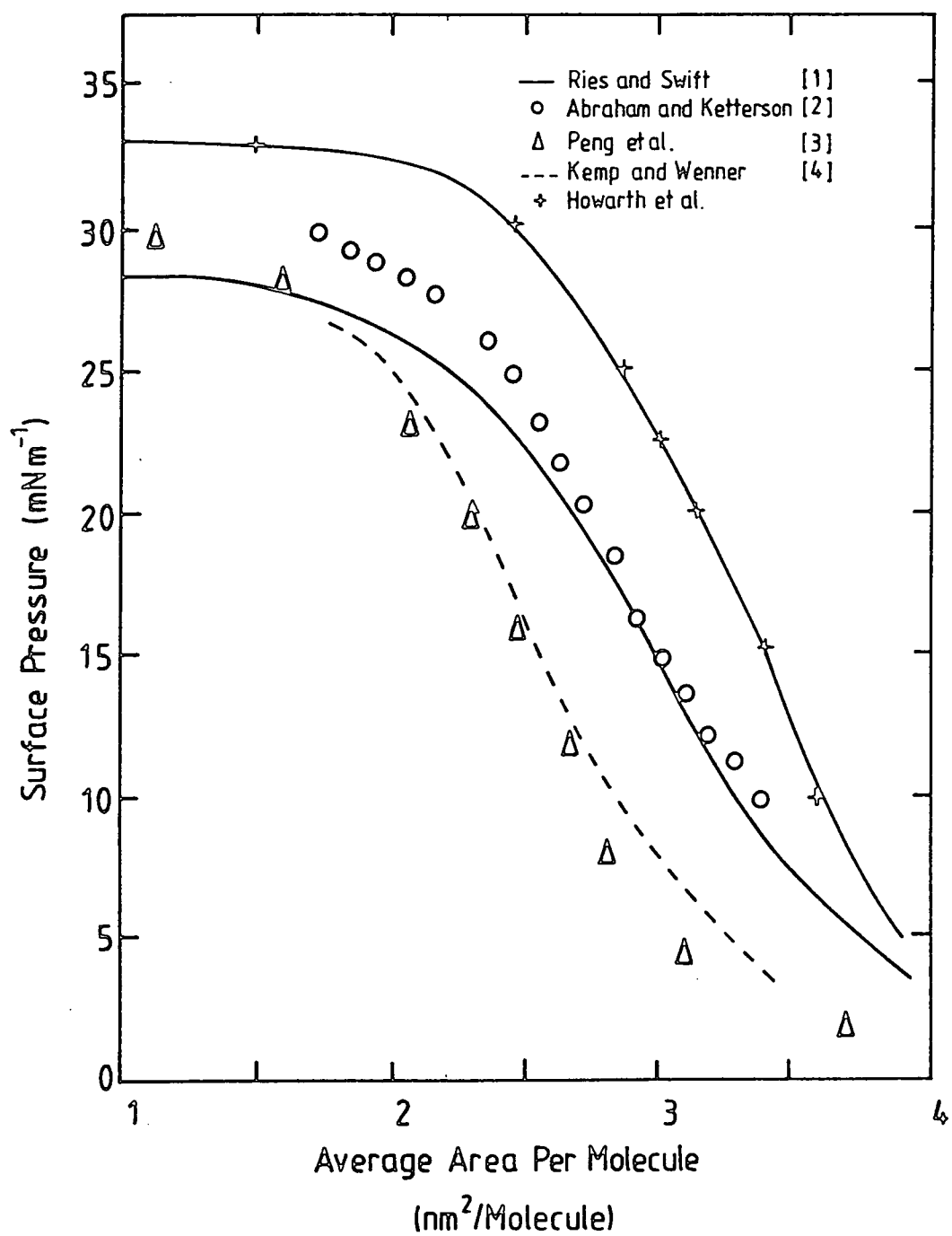
Figure 6.3 Comparison of the surface pressure-area isotherms for valinomycin in the literature.
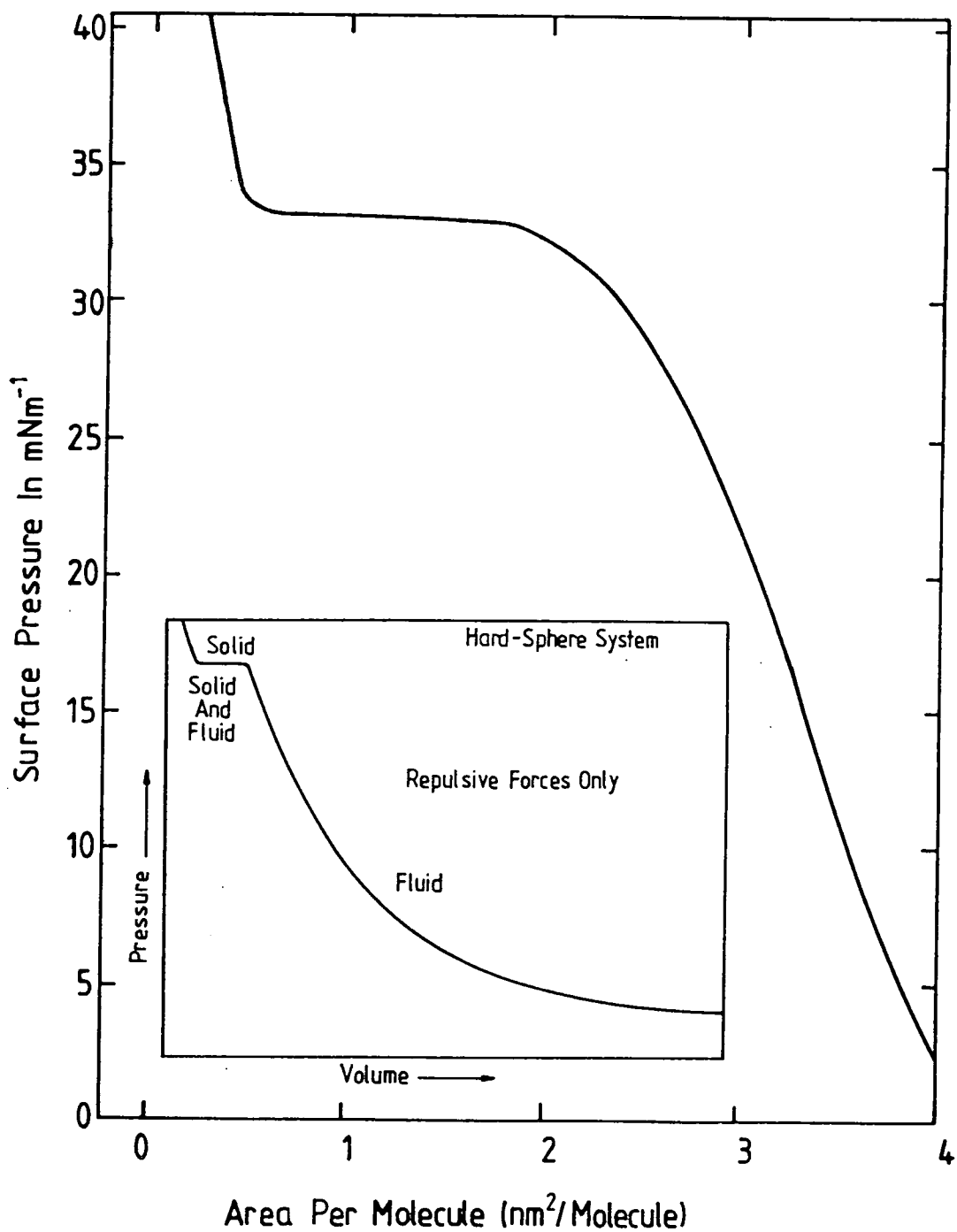
Figure 6.4 The complete isotherm for valinomycin showing the behaviour and indication of a highly incompressible phase below 1.0 nm^2 per molecule.

2 nm^2 and clearly as this represents an area less than the molecular area of even the most compact (complexed) conformation of valinomycin, the film is no longer monomolecular in nature. The film is now composed of stacks of molecules possibly with some of their planes parallel to the water surface and others perpendicular to it. Other workers have compressed their valinomycin films to an average molecular area of around 1- 1.5 nm^2; only Ries and Swift [1] have continued the compression below 1.0 nm^2. The work reported here continues the compression below 0.5 nm^2, and the complete isotherm is illustrated in figure 6.4. A sharp rise in surface pressure is obtained characteristic of the solid portion of the classical fatty acid isotherm. Intially, this portion of the valinomycin isotherm was attributed to an impurity in the spreading solution. However, this theory was dismissed by preparing solutions made from valinomycin and chloroform obtained from different sources (Sigma, Aldrich, Koch and Light, and BDH, respectively). All isotherms obtained were identical. The "solidus" at 40 mN m^{-1} corresponds to an average area per molecule of 0.25 nm^2. This area is evidently much smaller than either that of a plan or a side projection of the molecule, and from this it can be concluded that a stacked array of molecules exists in the film. The steep portion of the isotherm represents a solid-like, highly incompressible phase compared to the highly compressible phase represented by the plateau region. A possible explanation for the onset of this region is as follows, and a schematic diagram of a possible molecular re-arrangement is illustrated in figure 6.5. In the plateau phase the valinomycin film is "buckling" with either the molecules sliding on top of each other or being forced to stand edge on (figure 6.5b) with the plane of the molecule perpendicular to the water surface. The film is composed of vertically oriented molecules and stacks of horizontally oriented molecules and is shown in figure 6.5c. On further compression of the film, the horizontally oriented stacks of valinomycin molecules are forced to orient vertically shown schematically in figure 6.5d. This increases the proportion of vertically oriented molecules and at the same time contributes to an increase in the film's incompressibility. Eventually

Onset of concavity
of isotherm towards
pressure axis, approx.
'hard-core' area of
molecule.

(a)

(b)

(c)

(d)
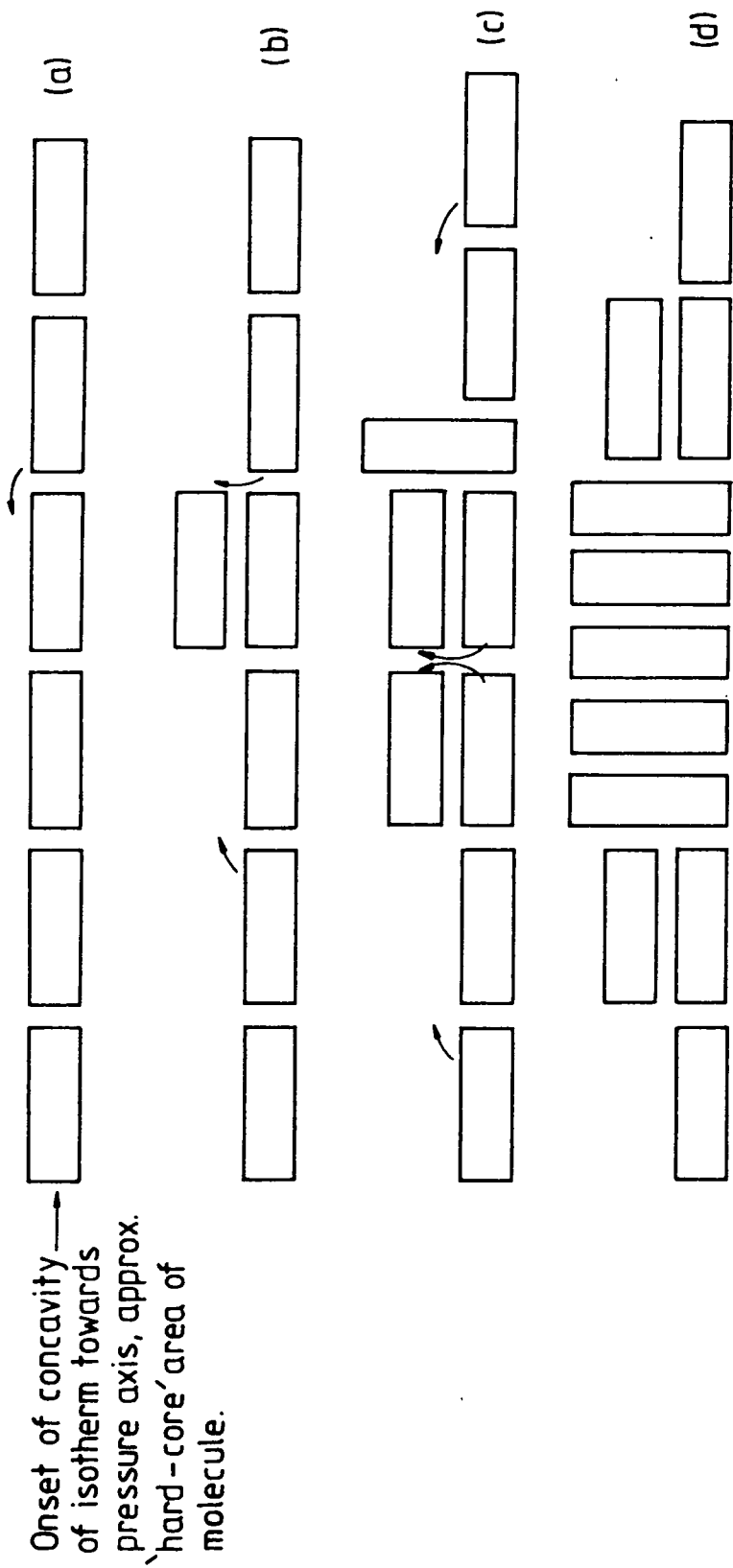
Figure 6.5 Schematic diagram showing the proposed molecular rearrangement of the valinomycin molecules for compressions continuing into the plateau region.

most of the molecules become oriented vertically and the incompressibility rises sharply. This system of vertically oriented molecules shows a lower compressibility because "buckling" of this structure (with molecules moving on top of each other) is energetically more difficult than for the "buckling" of the horizontally ordered system.

It is interesting to note that the Π-A isotherm for valinomycin is similar to the pressure-volume relationship (shown as an inset to figure 6.4) of a model system of hard spheres where interaction takes place by repulsive forces only. The plateau region here represents the solid fluid transition with the substance separating into two distinct phases. These two phases could probably be seen as analogues to the horizontally and vertically oriented valinomycin molecules.

Traditionally, the steep, linear part of the isotherm which represents a solid phase is extrapolated to zero pressure to yield the limiting area per molecule, a_m^o. In the condensed state the film structure changes very little for relatively large fluctuations in surface pressure, that is to say, the area per molecule is constant and meaningful. For example, a_m^o values obtained from the near vertical isotherms of classical fatty acids and their salts correspond extremely well with the molecular areas derived from CPK packing models. For the case of the valinomycin isotherm, a_m^o obtained for the high pressure region C is meaningless as the film is not monomolecular in nature. Extrapolation of the intial part of the isotherm (region B in figure 6.1) yields a value for a_m^o of approximately 4.0 nm^2. However, in this region the area per molecule is varying, indicating that the film structure is changing and hence the value is also meaningless. Indeed, it does not correspond at all with dimensions of the molecule obtained from X-ray studies which suggest an area for the most expanded (uncomplexed) conformation of the molecule of only 1.9 nm^2. Furthermore, Abraham and Ketterson [2] have represented the Π-A isotherm of valinomycin by the two dimensional analogue of the ideal gas law modified to incorporate the "hard-core area", a, of valinomycin i.e. $\Pi(A - a) = kT$. They obtained an average value for a of 2.7 nm^2, and clearly even

this does not fit with the observed X-ray data. The Π-A isotherm of valinomycin offers little detailed information concerning the orientation of the molecule on the water surface.

6.1.2 Stability

The rate of dissolution or collapse of a monolayer on the water surface is an important parameter in determining whether or not a material will be of any practical use in LB film formation. Ideally, at the deposition surface pressure this rate should be zero, but if it is not too great deposition is still possible. In some cases the parameter can be reduced by carefully optimising the subphase conditions and also by a correct choice of the deposition surface pressure. For example, the rapid collapse of a stearic acid monolayer can be reduced to approximately zero by introducing 2×10^{-4} M $CdCl_2$ into the subphase.

In order to assess the stability of a floating monolayer at particular surface pressure and for a set of subphase conditions, the monolayer area as a function of time was recorded. Temperature; compression rate to the desired dipping pressure; and the period of solvent evaporation were all standardised when recording monolayer area decay curves or isotherms.

For valinomycin monolayers, subphase conditions such as pH and ionic concentration had no effect on the area decay curve (and also no effect on the isotherm, see section 6.1.3) indicating little interaction between the valinomycin molecules and the ions present in the subphase. Figure 6.6 illustrates the monolayer area decay curves as a function of surface pressure. Curves (a) and (b) correspond to pressures in region B of the isotherm and indicate that extremely stable monolayers are being formed on the water surface. Therefore these pressures can provisionally be deemed suitable for deposition. In contrast, however, curve (c) at a surface pressure of 30 mN m^{-1} shows a dramatic decay in area . Clearly this pressure is unsuitable for deposition. At a surface pressure of 30 mN m^{-1} concavity of the isotherm towards the pressure axis has already commenced and it is
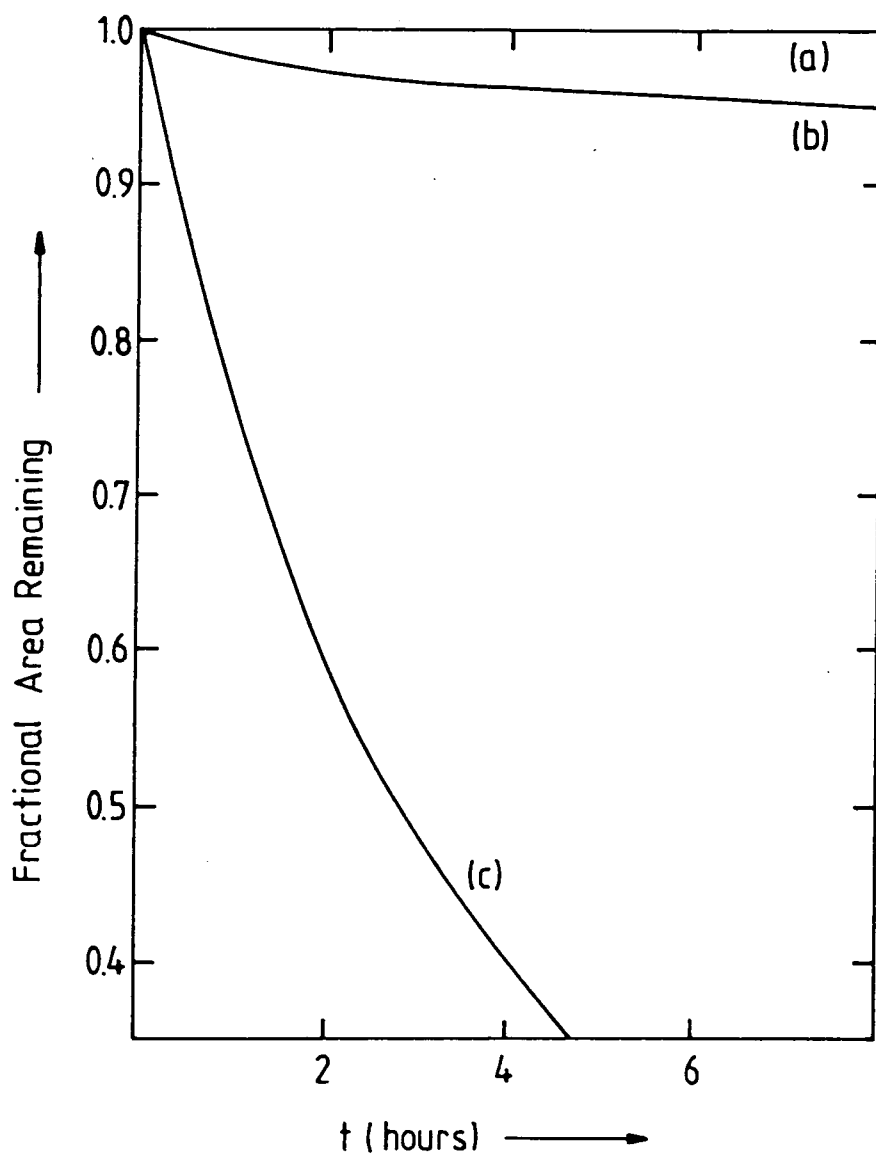
Figure 6.6 Monolayer area decay curves. For pure valinomycin monolayers (solid lines) at (a) 10 mN m^{-1}, (b) 23 mN m^{-1}, and (c) 30 mN m^{-1}.

likely that the processes responsible for collapse at this pressure are the same as those occurring in the plateau region described in the previous subsection.

6.1.3 Effect of pH, and nature and concentration of subphase ions

Figure 6.7 shows the effect of pH on the isotherm of valinomycin. The pH was adjusted using hydrogen chloride and ammonium hydroxide solutions. Within experimental error there is no difference between any of the isotherms and it can be concluded that there is no interaction between hydrogen ions in the subphase and the valinomycin molecules on the water surface. This is consistent with the fact that valinomycin shows no selectivity for hydrogen ions.

Furthermore, no change in the isotherm is observed for buffered subphases (unbuffered water with a tris buffer) added at varying pH. Also for subphases containing divalent calcium ions (up to 1 M) and monovalent sodium ions (again up to 1 M), the isotherms are identical to those on an unbuffered subphase. Valinomycin shows no selectivity for divalent cations and the selectivity coefficient for the sodium ion is low.

Upon complexation with a potassium ion there is a change in the conformation of the valinomycin molecule which produces a change in its area from 1.90 nm^2 (uncomplexed) to 1.50 nm^2 (complexed). It might be expected that such a change could be observed on a macroscopic scale from the Π-A isotherm. Surprisingly such an effect is not observed. The isotherms remain unchanged when potassium chloride is introduced into the subphase up to concentrations of 1 M (shown in figure 6.8). There is no evidence for the expected 0.40 nm^2 per molecule decrease. These results are consistent with those published by Abraham and Ketterson [2] but not with those of Kemp and Wenner [4]. The isotherms obtained by the latter workers for 0.2 M and 1 M KCl subphases are illustrated by the dashed lines of figure 6.8. For the 1 M KCl subphase, the plateau region occurs at a reduced surface pressure of about 22 mN m^{-1}, and as the subphase K^+ concentration was increased further the plateau pressure decreased further. None of these features
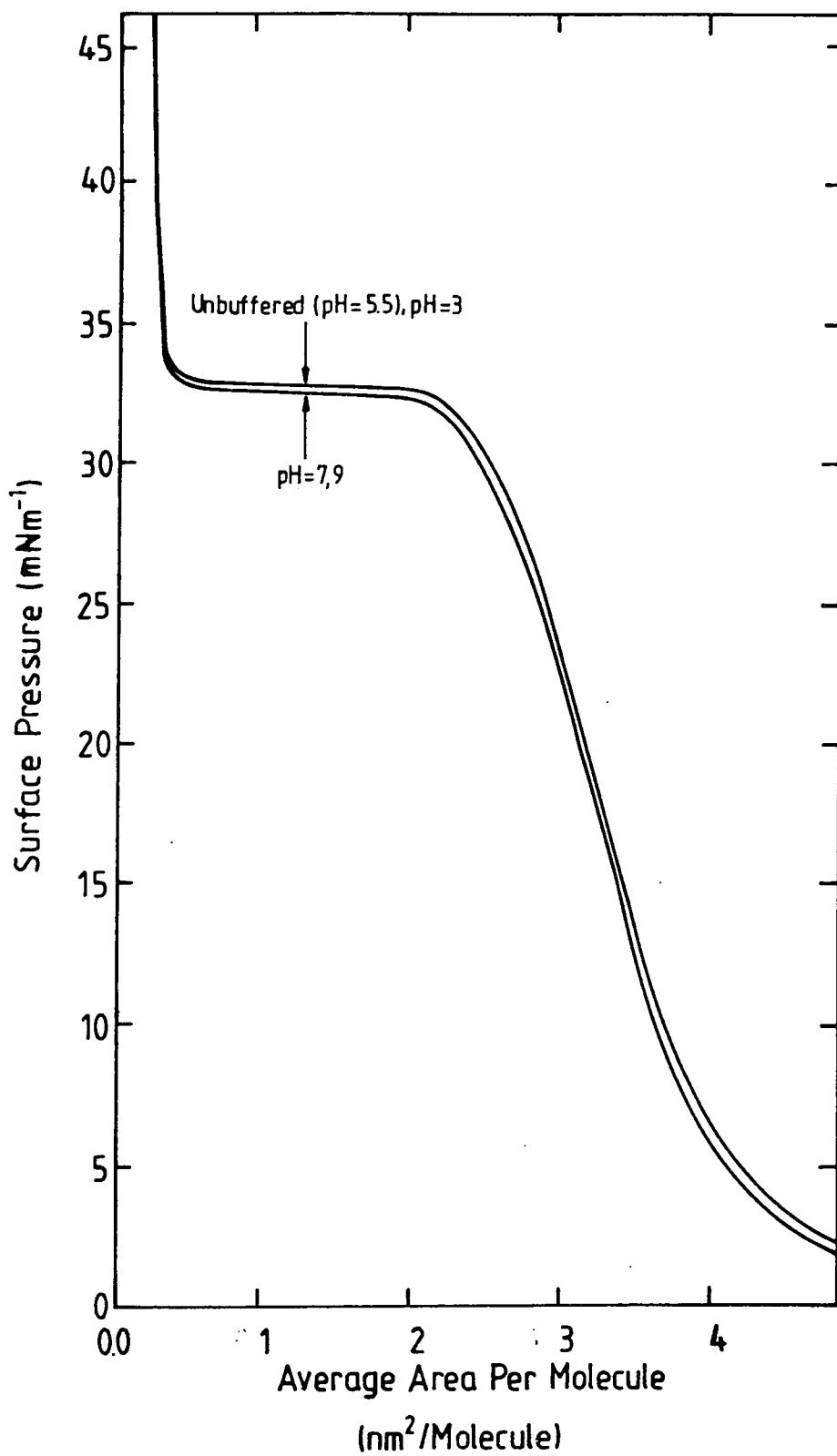
Figure 6.7 The effect of the subphase pH on the surface pressure-area isotherm of vali-
nomycin.
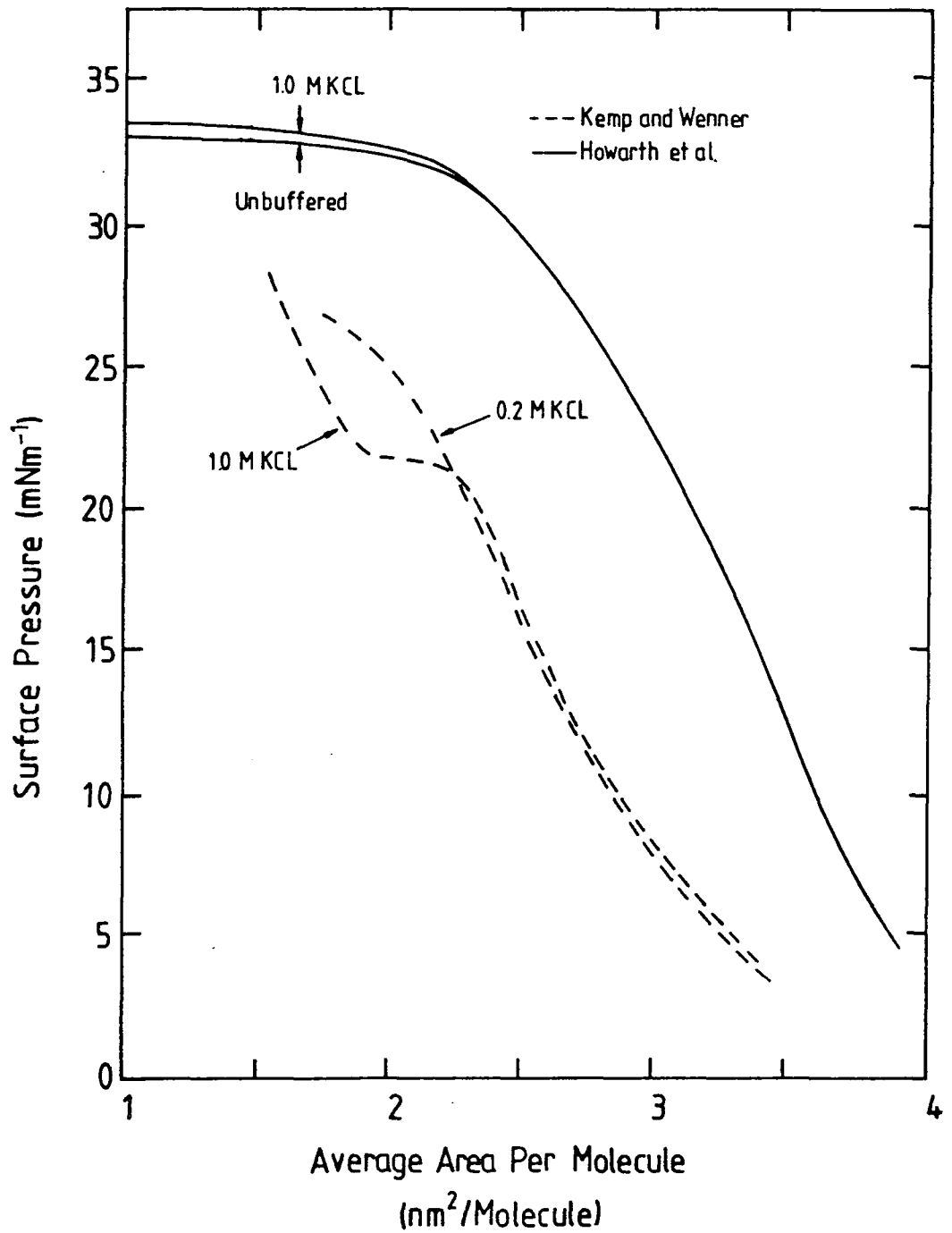
Figure 6.8 The effect of the subphase KCl concentration on the valinomycin Π-A isotherm. Solid lines (Howarth *et al.*) and dashed lines (Kemp and Wenner after ref. 4).

were observed in the work reported in this thesis and an explanation for the differing results, in particular, the premature pressure saturation of the isotherm, is not forthcoming. However, it is worth noting that the results described here and those of Abraham and Ketterson are consistent with the infrared spectroscopic measurements performed on pure valinomycin films outlined in chapter 7.

6.1.4 Deposition of valinomycin: monolayer and multilayer formation

Having assessed the stability of the valinomycin monolayers on the water surface over a range of surface pressures, deposition could be attempted. A provisional deposition pressure of 23 mN m^{-1} was selected. Single-crystal silicon and quartz were used as substrates. Transfer ratios in the range 0- 0.1 indicating poor pick-up were obtained for valinomycin deposited onto hydrophobic substrates. Multilayer formation was therefore not attempted. Preliminary attempts to deposit multilayers of valinomycin onto hydrophilic substrates failed, because on each insertion into the subphase the monolayer that was deposited on the preceding withdrawl peeled off. Only a monolayer could therefore be deposited onto such substrates; deposition occurring only on the first withdrawl. The deposition ratio was approximately unity. Monolayers deposited in this way are of some interest. For example, if deposited onto a silicon ATR crystal, IR spectroscopy can reveal information concerning the interactions between the monolayer and the substrate. These interactions are important because they are the basis for a multilayer structure. The fact that material transferred on the upstroke of the deposition cycle rejoined the floating layer on the succeeding downstroke was clear from two pieces of evidence. Firstly, the record of surface pressure against time (shown in figure 6.9) exhibited an increase during every upstroke indicating that material was peeling off the substrate. Secondly, IR spectroscopy performed after every deposition cycle revealed valinomycin IR band intensities of the same magnitude as those expected for a single monolayer.
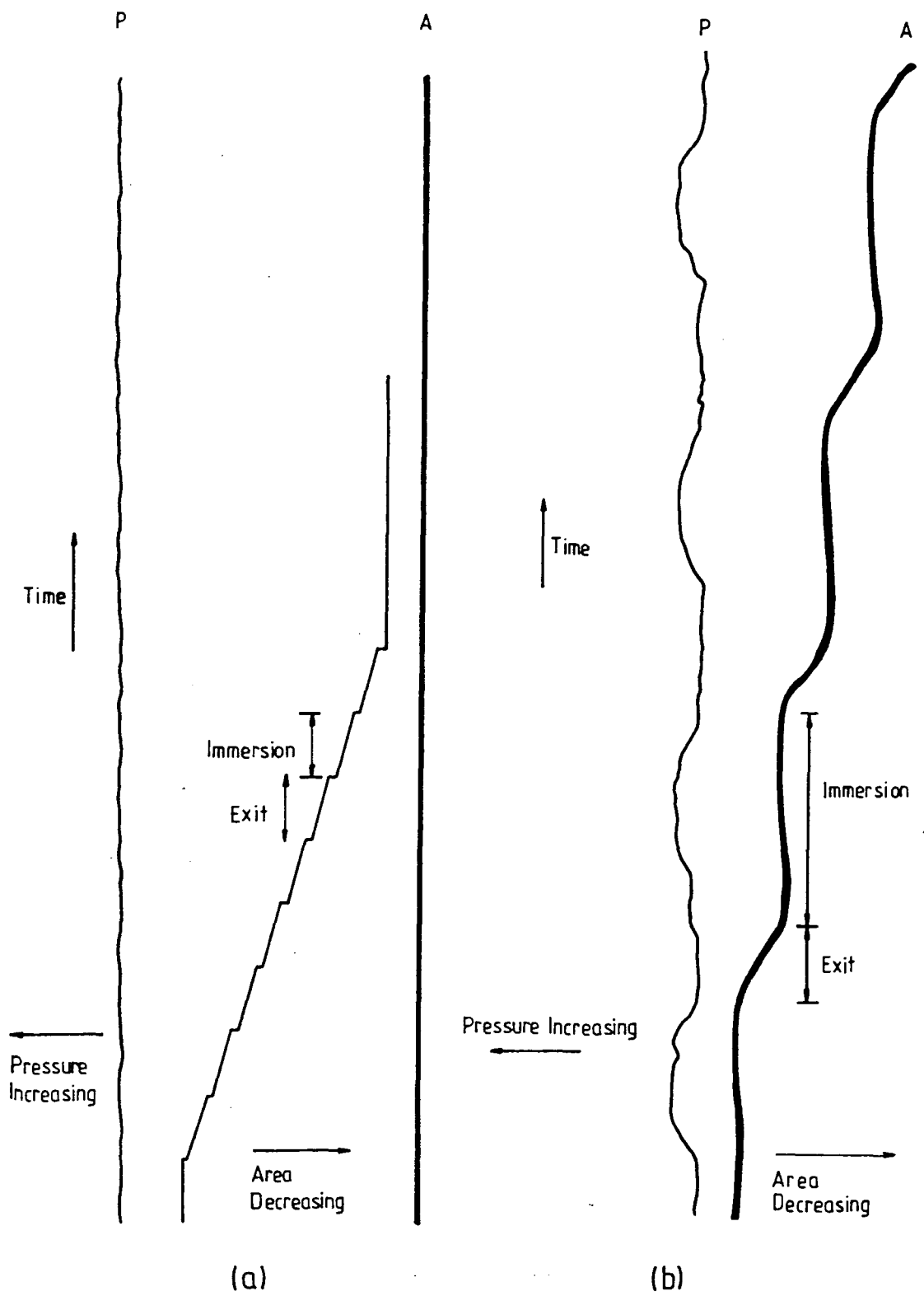
Figure 6.9 Surface area versus time and surface pressure versus time records for (a) ω-tricosenoic acid and (b) valinomycin showing the poor Z-type deposition for the ionophore (the exit speed equals three times the immersion speed).

PAGINATION ERROR

F 6·10 MISSING

However, multilayer deposition was possible if the substrate was first coated with a few fatty acid layers. Using this technique, it was possible to obtain deposition onto both hydrophilic and hydrophobic silicon wafers, and also onto quartz. Multilayer deposition was obtained using base layers of stearic acid, tricosenoic acid or their cadmium salts. Stearic acid and tricosenoic acid were both deposited at a surface pressure of 30 mN m^{-1} (unbuffered subphase) and their cadmium salts were deposited at the same pressure but using a subphase at pH 6.0 and a cadmium ion concentration of 2 x 10^{-4} M. Valinomycin multilayers could subsequently be deposited onto this base layer at a pressure of 23 mN m^{-1}, the first layer being transferred at a substrate speed of 4 mm min^{-1} and subsequent layers at 9 mm min^{-1}. Y-type deposition was obtained with all types of base layer. The deposition ratios were 1.0 ± 0.1. In most cases the valinomycin was transferred onto a hydrophobic silicon wafer which had been coated previously with four layers of the fatty acid; thus the ionophore was deposited onto the alkyl chain surface of the base layer. However, Y-type deposition has also been obtained by transferring monolayers of valinomycin onto the carboxylic head groups of the fatty acid. To accomplish this, the hydrophobic silicon substrate was left submerged after being coated with three layers of the fatty acid; the fatty acid monolayer was then removed from the water surface and replaced by the valinomycin. The substrate was then finally withdrawn through the compressed layer. Hsu and Chan [8] have suggested, from the results of nuclear magnetic resonance studies, that valinomycin can interact with both the polar and the hydrophobic (non-polar) regions of certain phospholipids. These effects may well be of significance for the successful LB film deposition of the ionophore.
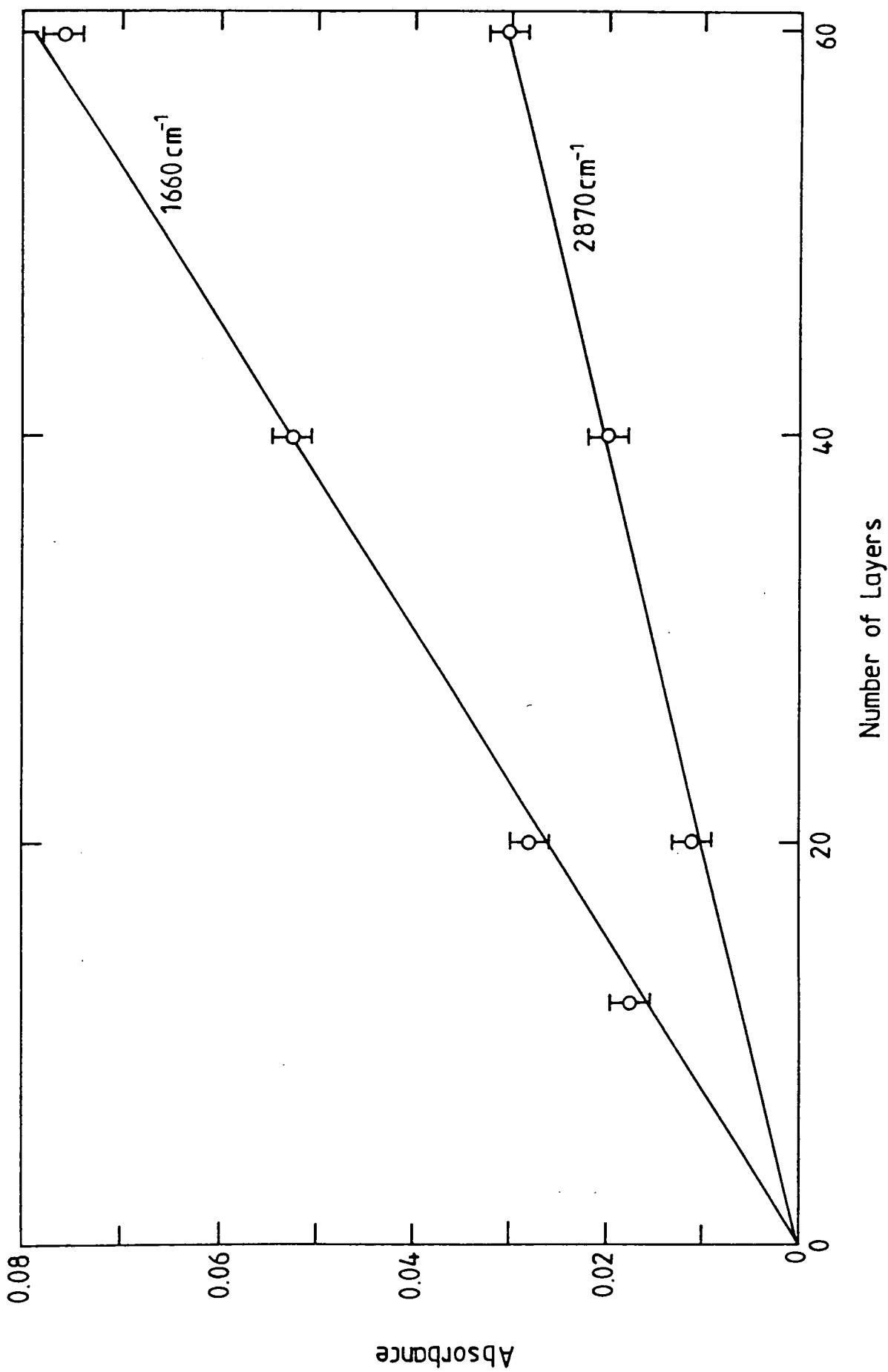
Figure 6.11 Relative IR band intensities versus number of LB layers of valinomycin

stretching and NH bending modes. By plotting relative band intensities (measured by peak heights) versus number of layers, an indication of the reproducibility of the Y-type deposition can be obtained. This is shown in figure 6.11 for two bands, the amide I band and a CH stretching band (not shown in figure 6.10) at 2870 cm^{-1}. Good reproducibility up to 60 layers is suggested.

6.2.2 UV spectrophotometry

By depositing a two-step (2.0 cm per step) multilayer structure on Spectrosil quartz slides with three monolayers of cadmium stearate, the UV absorption spectrum of multilayers of valinomycin could be obtained; 20/30, 40/50, and 60/80 layer structures of valinomycin were deposited. The bulk spectrum of valinomycin (not shown) reveals a shoulder at 215 nm. In the LB film UV spectra of up to 80 layers (the 50 layer spectrum is shown in figure 6.12a) this feature is not easily discernible. The optical density at a wavelength of 215 nm versus number of layers is shown in figure 6.12b. These data imply reproducibility up to 60 layers; however at 80 layers there is a marked reduction from the expected absorption.

6.2.3 Ellipsometry

Detailed ellipsometric measurements were made in order to ascertain the thickness of the valinomycin films. The measurements were performed for different numbers of valinomycin layers deposited onto hydrophobic silicon that had been previously coated with four layers of cadmium stearate. The data were taken at a wavelength of 632.8 nm where the ionophore could be considered to be non-absorbing. Preliminary results indicated that the thickness of the multilayers varied from one end of the substrate to the other in the direction of dipping. Therefore it was decided to investigate this thickness distribution by taking measurements at 5 mm intervals along the length of a 2 cm substrate. The experiment was conducted in the following manner: first, the optical constants of the silicon plus base layer were recorded; 20 layers of valinomycin were then deposited, and

83
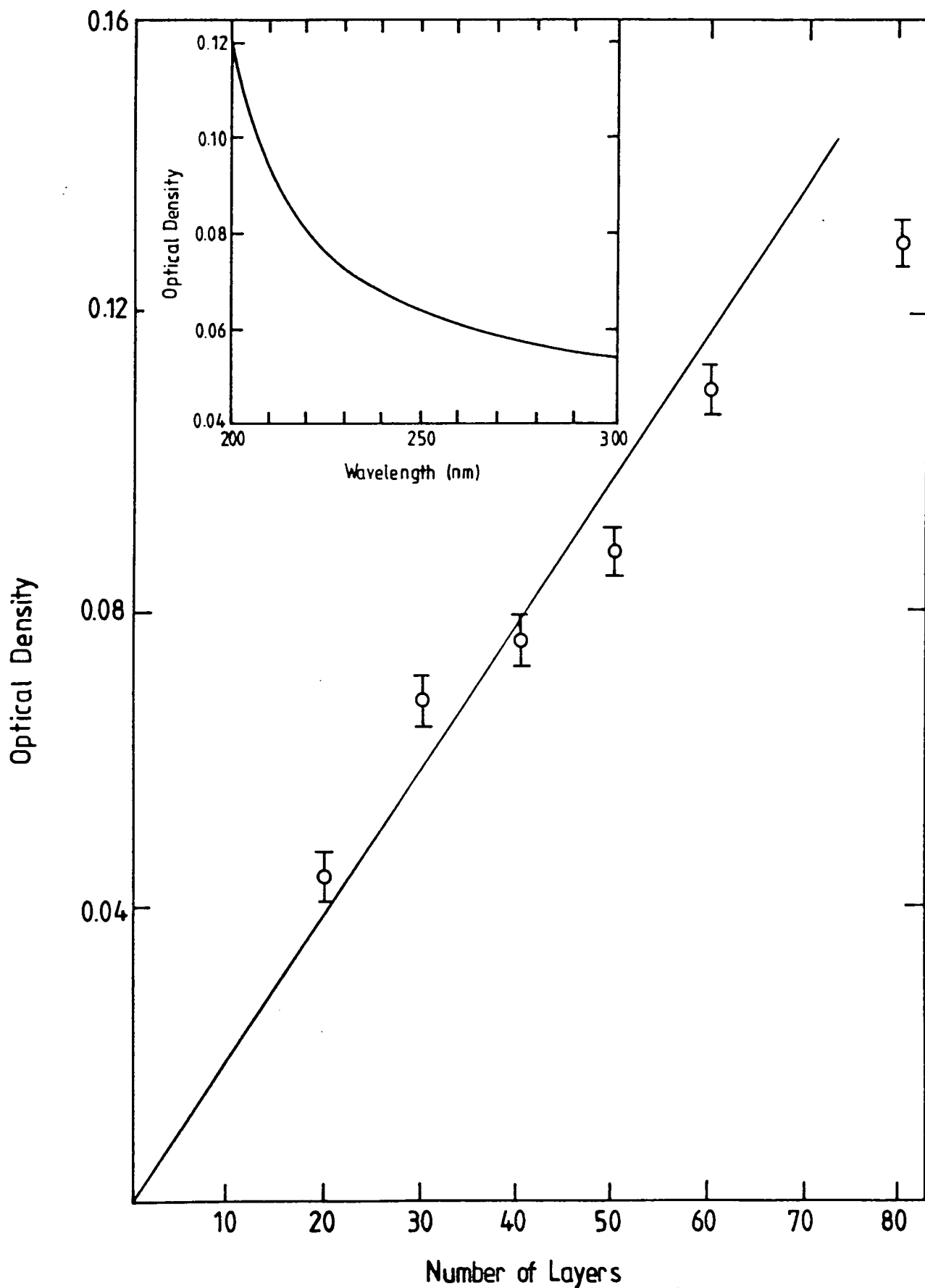
Figure 6.12 UV optical density at 215 nm versus number of LB layers of valinomycin. The inset shows the UV-spectra of a 50 layer sample.

the ellipsometry measurements retaken; another 20 layers of valinomycin were deposited and the experiment was repeated. In this manner a total film thickness of 60 layers was investigated.

The results of this study are presented in figure 6.13, the substrate configuration is also shown. At a particular y-coordinate (along the dipping direction), it is apparent that the thickness scales linearly, indicating good reproducibility. However, as the y-coordinate changes, the thickness per monolayer varies from 0.66 nm to 0.40 nm in a monotonic fashion. The thickest part of the film is obtained at the top end of the substrate. In contrast, results obtained in the x-direction show that the film thickness is highly uniform.

The precise origin of the thickness profile effect is unknown. The ellipsometric values indicate that the disc-shaped valinomycin molecules are being transferred with their large-area faces parallel to the surface [1]. It is of interest to note that the thickest area of the film (i.e. near the top of the substrate) is that which has been in the subphase for the least time during the deposition. The transferred valinomycin layer may well be reorganising (or even being removed from the substrate) while under water, but it is difficult to visualise processes of this nature that would lead to the thickness profile and reproducibility that is observed. The UV experiment probed a relatively large area (compared to that in the ellipsometry and IR experiments) and therefore does not generally show the thickness profile effect. In the case of the IR studies, the profile effect is not observed because the ATR crystal was coated in such a way that a constant y-coordinate on the substrate was addressed during the measurement.

6.3 MIXED LB FILMS OF VALINOMYCIN AND ARACHIDIC ACID

The mixed system of valinomycin and arachidic acid can be treated as a simple model for the biological membrane. LB films of valinomycin/arachidic acid mixtures were investigated with the aim of utilising these films as the ion-selective membranes for ISFETs.

Figure 6.13 LB film thickness, determined using ellipsometry, versus number of layers of valinomycin; the measurements were taken at different positions along the substrate, as indicated in the diagram.
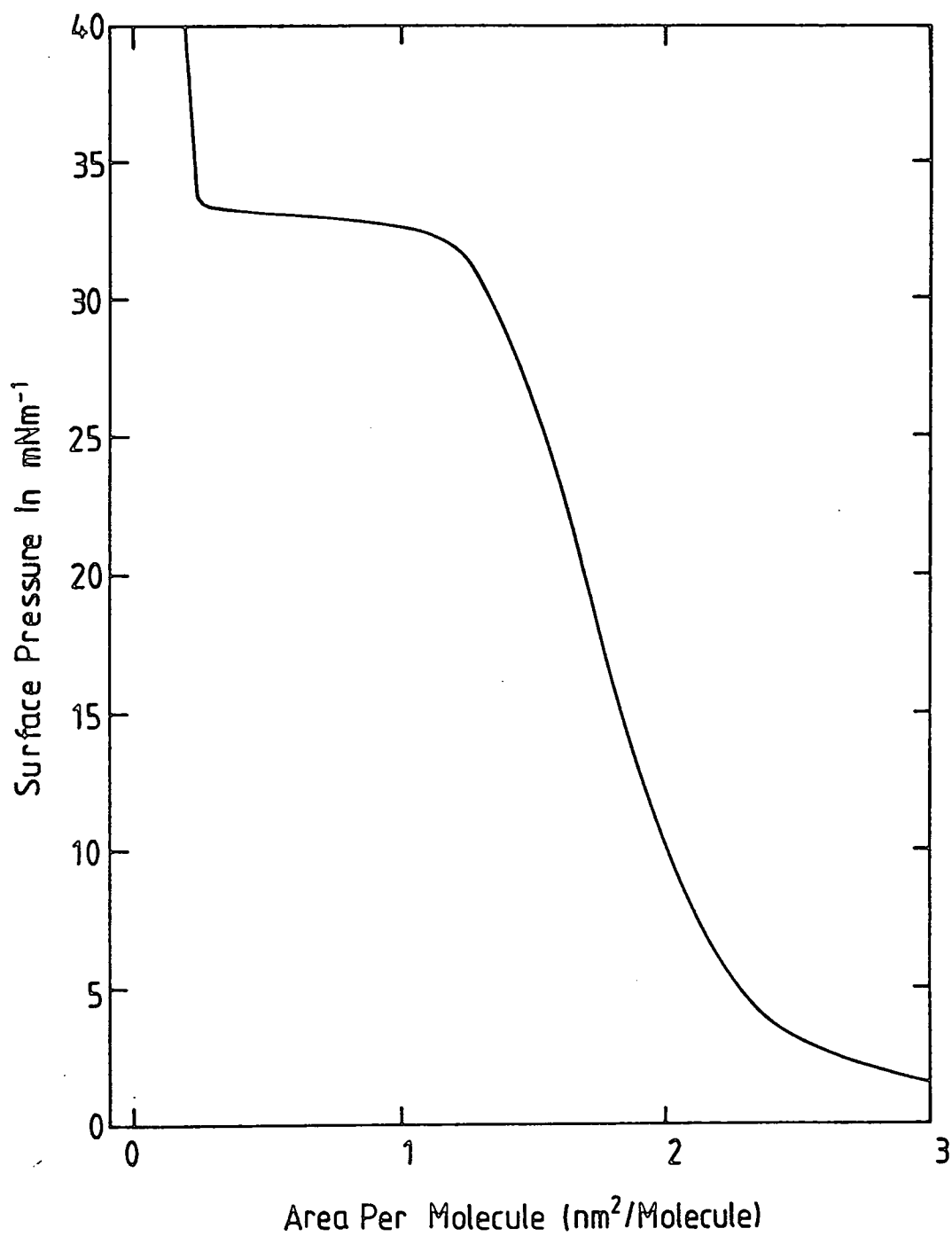
Figure 6.14 Surface pressure-area isotherm for an equimolar mixture of valinomycin and arachidic acid recorded on a pure water subphase at pH 5.8.

6.3.1 Isotherms and deposition conditions

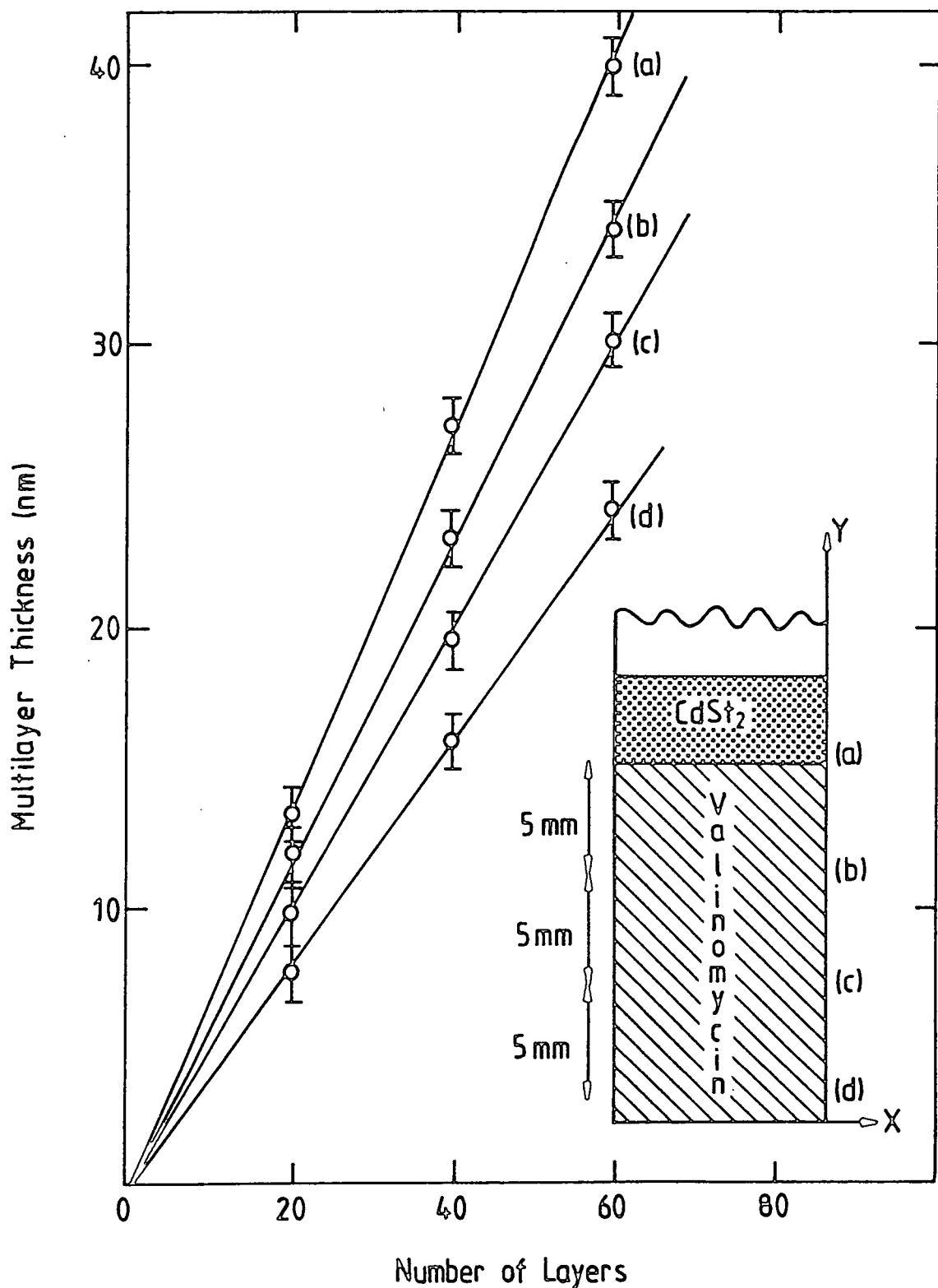LB films of the mixtures were spread from a chloroform solution containing both components. The mixed solution was prepared from individual solutions of the two components, and in this way, mixtures over a range of mole-fractions could be prepared. The isotherm for an equimolar mixture at a temperature of 20°C on an unbuffered subphase, and recorded at a compression rate of 2 cm^2 s^{-1} is shown in figure 6.14. The isotherm is similar to that of pure valinomycin. This is to be expected because although the mixture is equimolar, in terms of film area occupied by each component, the valinomycin molecules dominate. This is because they have a larger molecular area (approx. 1.9 nm^2) compared to the smaller arachidic acid molecules (approx. 0.20 nm^2). However, in this case the steep portion of the isotherm extrapolates to an area of 0.20 nm^2. This corresponds approximately to the projected molecular area of an arachidic acid molecule. Hence it can be conclude that, at high surface pressures, the valinomycin is squeezed out of the film, with only acid molecules contacting the water surface. The valinomycin might lie above or below the arachidic acid monolayer possibly interleaved with water molecules. It is interesting to note that if deposition is attempted in this high pressure region a pure arachidic acid film is the result. IR spectroscopy of such deposited films reveals no valinomycin component. Presumably with the valinomycin not forming an integral part of the film it is free to re-join the floating layer on each deposition cycle.

By varying the mole-fraction of arachidic acid in the mixture, the average area per molecule (at a selected surface pressure) can be plotted as a function of mole-fraction. This type of plot gives an insight into how the two components are mixing. Such a plot for two selected surface pressures is shown in figure 6.15. The straight lines are the theoretical areas versus mole-fraction (and are calculated based on a simple addition of the total area components of both molecules and using the average area per molecule in the pure films at the specific surface pressure). For both surface pressures the experimental data fit well. It appears

85
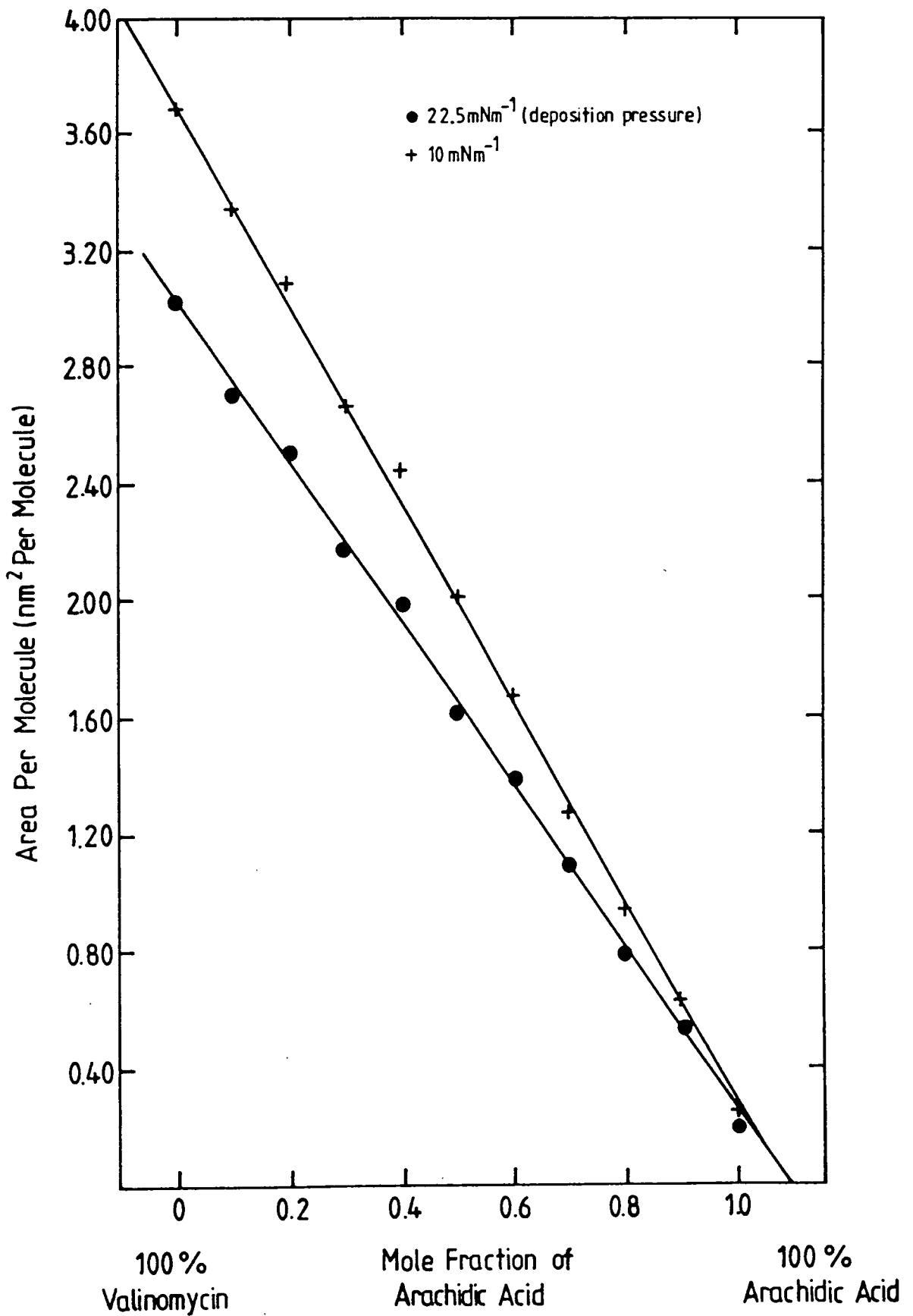
Figure 6.15 Average area per molecule in mixed arachidic acid/valinomycin monolayers as a function of the mole-fraction of acid, plotted for two values of surface pressure.
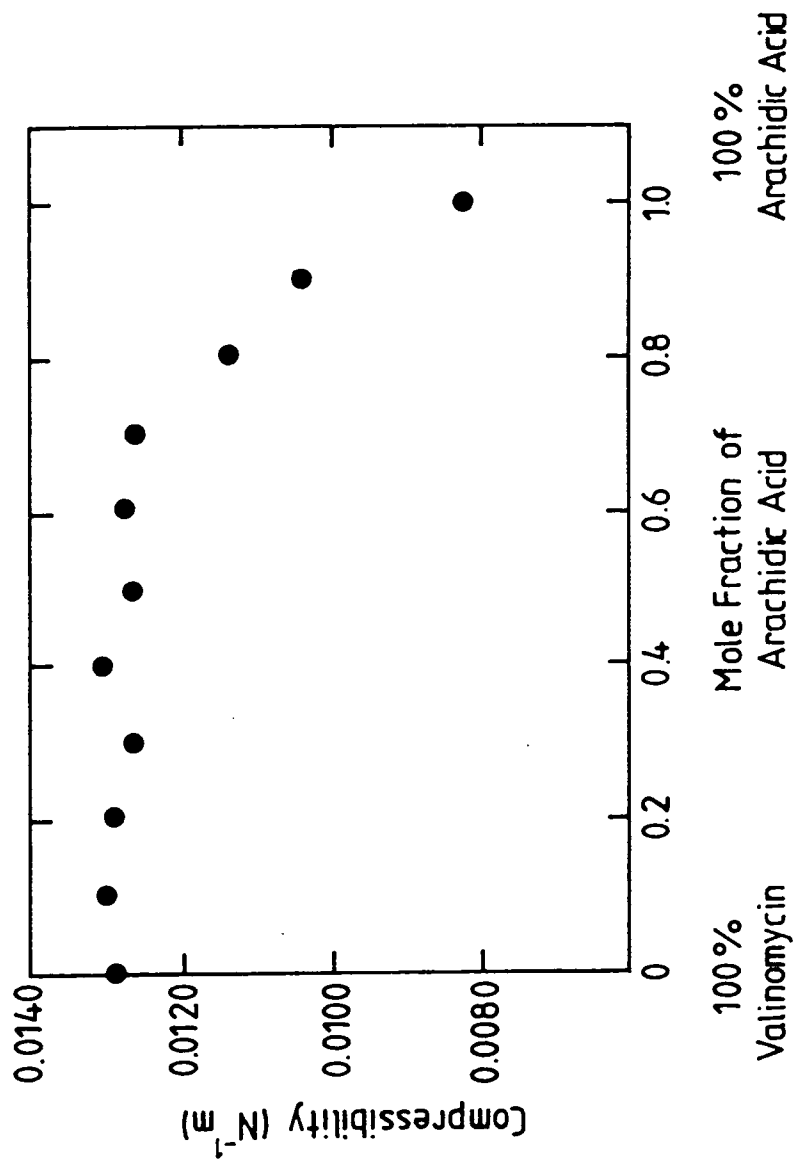
Figure 6.16 Compressibility of mixed arachidic acid/valinomycin monolayers as a function of the mole-fraction of acid.

therefore that the mixed system is behaving ideally and there is little observed expansion or contraction of the film over the entire mole-fraction range. This is in marked contrast to the considerable condensation effects observed by Ries and Swift [1] for their valinomycin/stearic acid and valinomycin/cholesterol mixtures. Their experimental isotherms were markedly displaced to smaller areas per molecule relative to a theoretically calculated average isotherm. The interpretation was of an interaction between the hydroxy group of cholesterol (or the carbonyl oxygen of stearic acid) with the polar inner ring of valinomycin with stabilisation taking place through hydrogen bonding. If these groups are drawn into the polar ring a condensation effect would be produced. No such effects can be inferred from figure 6.15, and it can be concluded that valinomycin and arachidic acid probably do not form miscible monolayers at the air-water interface. Instead, the film probably consists of aggregates or "islands" of each component. The mixed system of aggregates gives the theoretical molecular area since each aggregate is itself ideal. The system can simply be thought of as consisting of fewer molecules ("islands") with a larger area per molecule ("island").

The aggregate nature is revealed if a molecular property of the film, such as the compressibility, is considered. Compressibilities for the mixtures studied in figure 6.15 have been calculated and are plotted as a function of mole-fraction in figure 6.16. The compressibility for each mixture has been calculated using the constant slope region of the isotherm between the surface pressures of 22.5 mN m^{-1} and 10 mN m^{-1}. The compressibility, K, was defined as

$$\frac{(A_0 - A_1)}{A_0 F_1} \quad N^{-1}m$$

where A_1 is the molecular area at pressure $F_1 = 22.5$ mN m^{-1} and A_0 is the extrapolated area at zero surface pressure, defined by the slope of the line between the two surface pressures. From figure 6.16, it is clear that for mole-fractions less than 0.8 the mixed film has a compressibility essentially equal to that of a pure valinomycin film indicating that the valinomycin component is dominating

86

the properties of the film. For mole-fractions greater than 0.8, the effect of the arachidic acid is observable, and this mole-fraction coincides with each component occupying approximately equal areas within the film.

Reproducible Y-type deposition of the mixtures was obtained onto a variety of substrates. The reproducibility was enhanced (especially for mixtures of low mole-fraction) if a base layer of fatty acid (similar to that required for the successful deposition of pure valinomycin multilayers) was first of all deposited. Presumably for the low mole-fraction mixtures, this base layer helps to anchor the valinomycin component of the film.

6.3.2 X-ray structure analysis of LB films of mixtures of arachidic acid and valinomycin

Sixty layer LB film samples of mixtures of arachidic acid and valinomycin were deposited onto 1 cm^2 hydrophobic silicon substrates and subsequently analysed using small-angle X-ray diffraction. The intensity curves are shown in figure 6.17. The non-Bragg maximum at $2\theta = 0.6°$ is associated with the edge of total reflection of the X-rays from the surface. The maxima for all samples are identical and coincide at the same angle of 2θ. The first three orders of diffraction are shown. For pure arachidic acid (curve 1) the Bragg reflections are sharp. However, as the proportion of valinomycin in the mixed film increases (curves 2 to 4) the peaks become smoother and smoother. At the same time the reflections are shifted to smaller angles. The pure valinomycin film (curve 5) exhibits no diffraction peaks. The d-spacings were calculated from the Bragg equation $2d\sin\theta = n\lambda$ were 2θ is the scattering angle, n is the order of reflection and $\lambda = 0.154$ nm. The long range order parameter is $R_c = (\Delta S)^{-1}$, where $\Delta S = 2\Delta\theta\lambda^{-1}$ and $\Delta\theta$ is the width of the reflection at half maximum height.

The pure valinomycin film produced no Bragg reflections of the order (001) indicating that there is no ordering from layer to layer. Given that the deposition ratio for this film was 1.0 ± 0.1 and that the ellipsometric measurements indicate
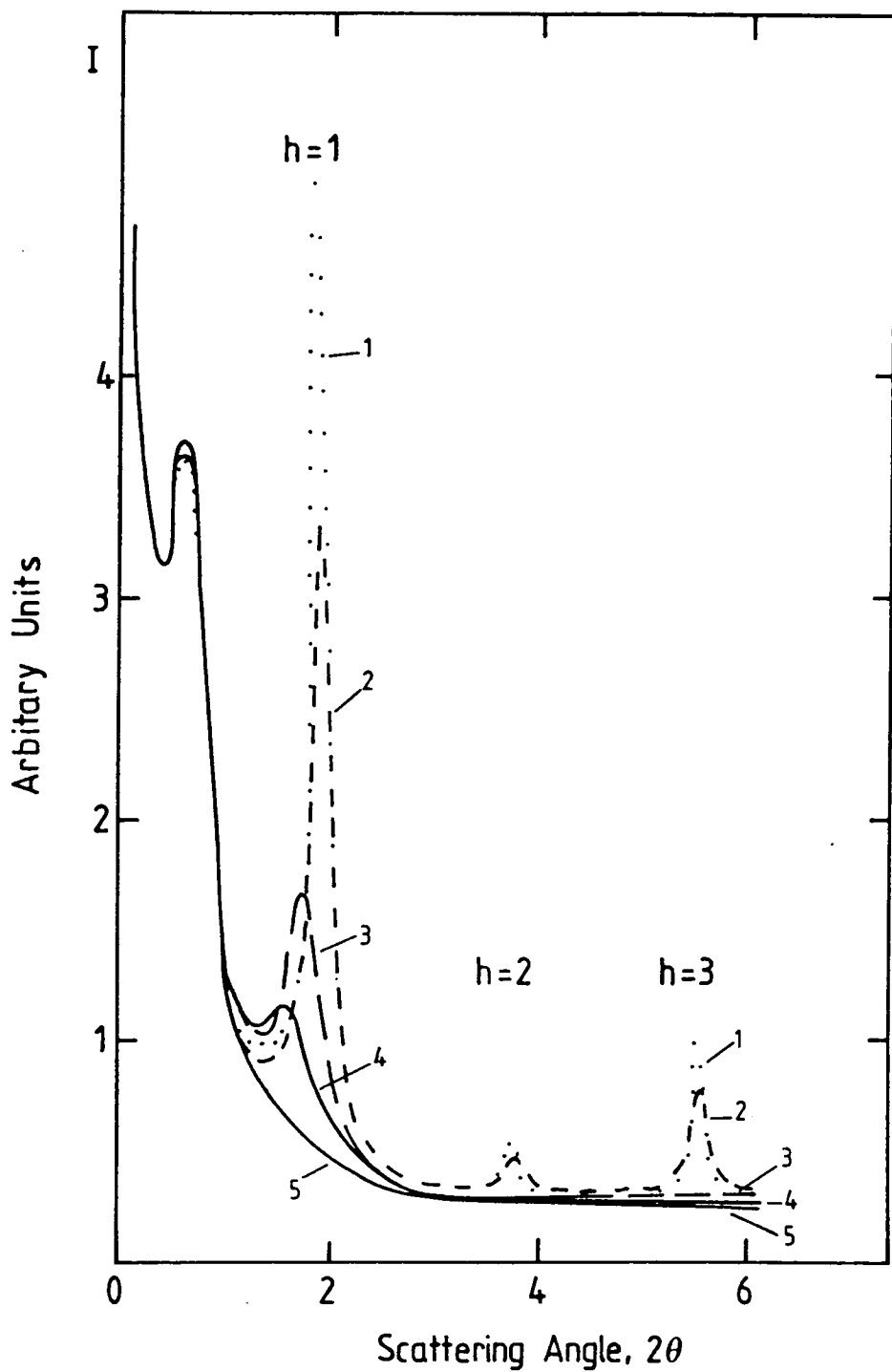
Figure 6.17 Small angle X-ray diffraction intensity curves for 60 layer mixed LB films of valinomycin and arachidic acid for varying mole-fraction (1) pure arachidic, (2) 100:1, (3) 10:1, (4) 1:1 (molar) arachidic acid/valinomycin and (5) pure valinomycin.

Mole Fraction of Arachidic Acid	1	100:1	10:1	1:1	0
$D, nm, (\pm 0.04)$	4.64	4.64	4.90	5.90	-
$R_c, nm, (\pm 3.0)$	74.0	50.0	28.0	25.0	-

Pure Arachidic Film → (points to column "1")

Pure Valinomycin Film → (points to column "0")

Table 6.18 D-spacings and the order parameter, R_c, calculated for the mixed arachidic acid/valinomycin mixtures whose X- ray intensity curves are shown in figure 6.17.

that the valinomycin molecules are depositing with their planes parallel to the substrate, the lack of a diffraction pattern is surprising. A possible interpretation is that shortly after deposition the film reorganises, possibly due to the formation of aggregates or crystallites, and consequently the regular LB layer structure is lost. The first report in the literature of the lack of a layer structure in a LB film was by Tredgold *et al* [9]. They proposed the explanation above to account for the absence of Bragg reflections in their X-ray diffraction patterns of the Ag(II) and Au(III) complexes of mesoporphyrin IX dimethyl ester. More recently Petty *et al* [10] have described similar results for the material ytterbium bisphthalocyanine. It is interesting to note that all these molecules are macrocyclic in nature.

From the intensity curves in figure 6.17, the d-spacing, D, and R_c for each of the mixed LB films have been calculated and are shown in Table 6.18. From the table, two trends with increasing valinomycin content of the mixed film are apparent, and these are illustrated in figures 6.19 a and b. Firstly, an increase in the d-spacing i.e. an increase in the multilayer period (this can be deduced from the shift of the reflections to smaller angles), and secondly, a decrease in the parameter R_c (this can be deduced from the fact that the peaks are becoming broader). As the valinomycin content increases, the film is approximating more closely to a pure valinomycin film which exhibits no order. Hence the decrease in R_c can be immediately interpreted as due to the increasing presence of valinomycin reducing the order in the film.

The reason for the increasing multilayer period is less obvious but might be related to the tilting of the arachidic acid molecules. The chain length of an arachidic acid molecule, determined from a CPK molecular model, is approximately 2.8 nm. The d-spacing of the pure arachidic LB films is 4.6 nm and this is slightly less than twice the molecular chain length. This indicates that bilayers, characteristic of a Y-type film, are present. However, the molecules are tilted at a angle, θ, to the substrate normal, and the structure is illustrated in figure 6.19c. The angle, θ, can be calculated by using simple geometry and is found to be equal
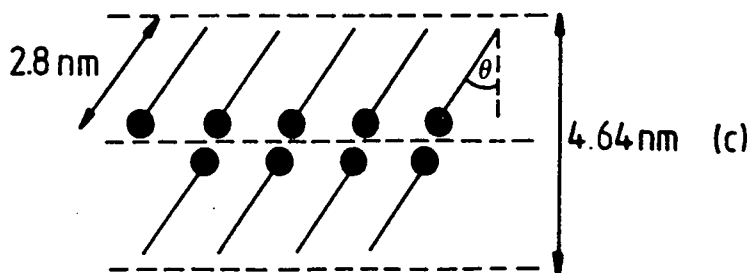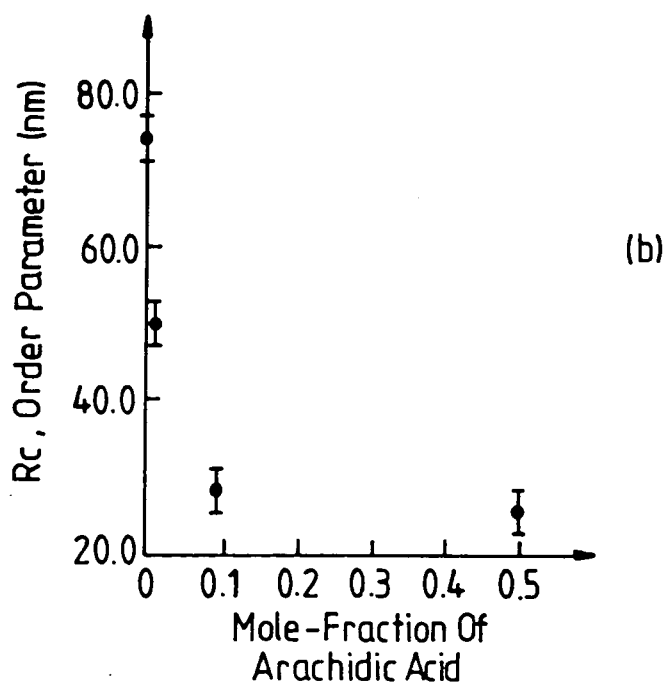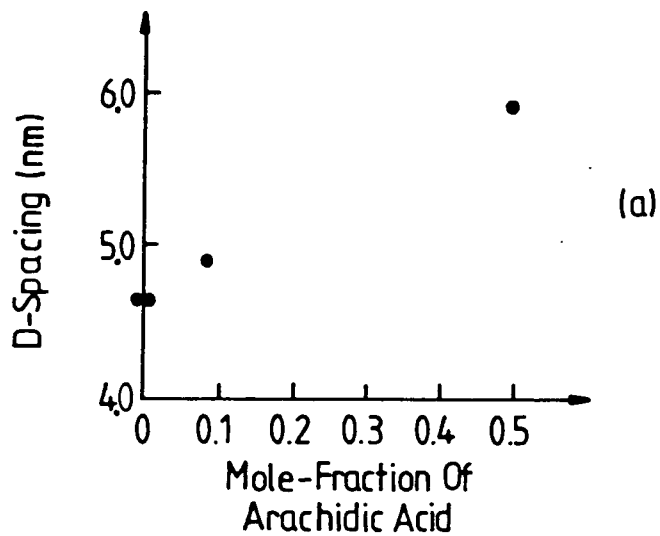
Figure 6.19 (a) d-spacing and (b) the order parameter, R_c, as a function of the mole-fraction of valinomycin, and (c) a schematic representation of the tilt of the arachidic acid molecules in the pure LB films, $\theta = 34°$.

to 34°. The origin of this tilting effect is not fully understood, but is possibly related to the hydrodynamic forces exerted by the meniscus on the amphiphilic arachidic acid molecules [11].

The valinomycin molecule can be thought of as a disc, with an area of 2.0 nm^2 and a thickness of 0.5 nm, whereas the arachidic acid molecule projects an area of only 0.2 nm^2 and has a chain length of 2.8 nm. Considering these differences in shape and molecular dimensions, it is difficult to envisage how the two molecules would be arranged in and LB film, and how successive monolayers would be co-ordinated with each other. The d-spacing for the 100:1 (molar) mixture is the same as that for the pure arachidic acid LB films indicating that the fatty acid molecules (possibly in the form of aggregates) are still tilted in the mixed film. However, referring to figure 6.19b, the reduced R_c value indicates that this film is more disordered because of the presence of the valinomycin. The 10:1 mixed film exhibits an increase in d-spacing and this can possibly be interpreted in terms of a smaller angle of tilt for the arachidic acid molecules (a d-spacing of 4.9 nm corresponds to an angle $\theta = 29°$). For this mixed system, the molecular components occupy roughly equal areas in the film. The hydrodynamic forces acting on the arachidic acid molecules will be different from those during deposition of the pure film, because of the presence of the ionophore, which does not possess the amphiphilic nature of the fatty acid. Therefore, it is likely that the arachidic acid molecules will be constrained by the valinomycin molecules to adopt a different tilt angle. In the 1:1 mixed film, the valinomycin molecules now occupy an area ten times that of the fatty acid molecules. The d-spacing of 5.9 nm cannot be attributed to tilting because it represents more than twice the chain length of the arachidic acid molecule. At present, the only interpretation is that there are regions of the LB film consisting of arachidic acid bilayers interleaved with valinomycin molecules.

6.3.3 Reflection high energy electron diffraction

In this RHEED investigation, the LB films were deposited onto hydrophobic silicon wafers of the {100} orientation. Examinations were undertaken with the electron beam perpendicular to the direction of dipping. For reference, the RHEED diffraction patterns from LB films of pure valinomycin and pure arachidic acid are also included in this section. The quality of a diffraction pattern deteriorates as the film thickness increases because of an accumulation of charge, and therefore an optimum thickness of six monolayers was adopted for these investigations.

Figure 6.20a illustrates the diffraction pattern from a pure arachidic acid LB film consisting of six monolayers. The rows of diffraction spots are typically tilted at ~ 30° with respect to the shadow edge, indicating that the hydrocarbon chains are inclined at a similar angle to the substrate normal. The reflection pattern consists of two rows of spots, inclined at the same angle, but in an opposite sense, to the substrate normal. From this it can be concluded that the structure is composed of grains in which the molecular chains are all inclined at an angle of about 30° to the substrate normal, but the sense of this tilt (either upwards or downwards from the substrate normal, with respect to the dipping direction) varies from grain to grain throughout the film. This type of structure has also been reported in the literature for thin LB films of ω-tricosenoic acid deposited onto silicon substrates [12].

Figure 6.20b shows the diffraction pattern obtained from six monolayers of a pure valinomycin LB film. The diffuse pattern of figure 6.20b indicates that there is no crystalline order and the structure can be described as amorphous. Thus the RHEED data is consistent with the low-angle X-ray data described earlier, which showed no diffraction peaks and hence no order. Finally, the RHEED pattern for six layers of an 11.75:1 (M) arachidic acid/valinomycin LB film is illustrated in figure 6.20c. The pattern is now characterised by blurred arcs of intensity. The spot pattern (characteristic of order within the arachidic acid film) is now less
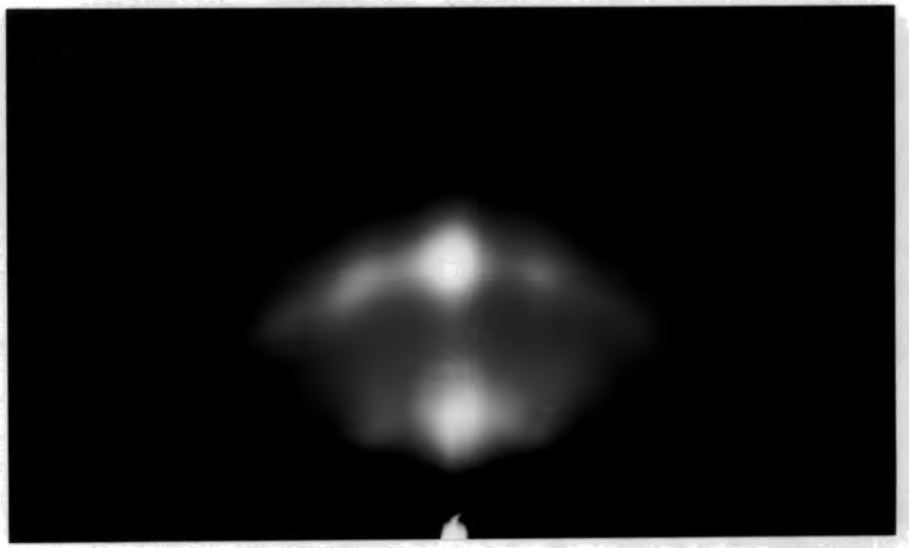
(a)
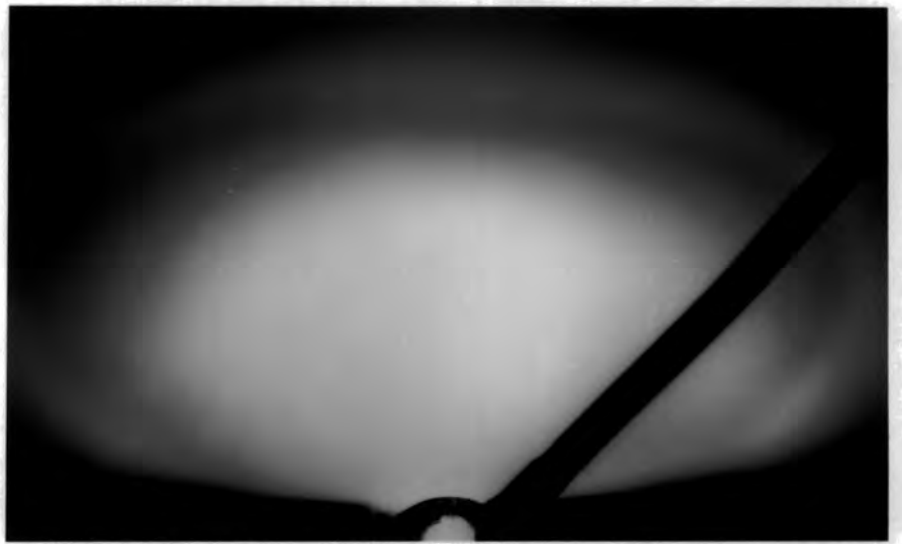
(b)
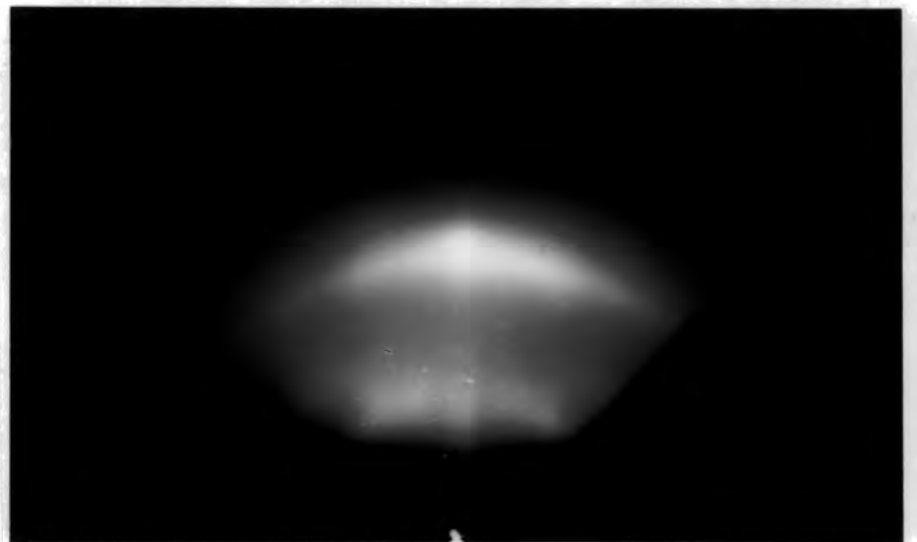
(c)

Figure 6.20 RHEED patterns from six layer LB films of (a) pure arachidic acid, (b) pure valinomycin and (c) an 11.75:1 molar arachidic acid/valinomycin mixture, all on hydrophobic silicon and with the electron beam perpendicular to the dipping direction.

discernible. The arcs of intensity indicate that the arachidic acid component of the film is still ordered within each grain, that is, with the chains tilted at about $\sim 30°$ to the substrate normal. However, the azimuthal direction of this tilt is now random, and varies from grain to grain. The diffuseness of the arcs of intensity arises from the presence of the valinomycin.

6.4 DEPOSITION AND CHARACTERISATION OF LB FILMS OF L-α-PHOSPHATIDIC ACID DIPALMITOYL

6.4.1 Deposition

Due to the inordinate difficulties in preparing multilayer LB films of the phospholipid molecules DPPE and DPPC (see chapter 7), deposition of the phospholipid L-α-phosphatidic acid dipalmitoyl (DPPA) was attempted. The unsuitability of DPPE and DPPC for LB film deposition was attributed to their bulky head groups and it was decided to attempt the deposition of DPPA because it is the simplest of the phospholipid molecules having the smallest head group. The motivation for forming LB multilayers of DPPA was to then proceed and prepare mixed LB films of DPPA and valinomycin. This system represents a simple artificial biological membrane.

Figure 6.21 shows the pressure-area isotherm obtained for the DPPA at a temperature of 20°C and a compression rate of 3 cm^2 s^{-1}; the molecular structure and schematic diagram of the molecule are shown as an inset. The subphase was buffered to pH 6.4 and contained calcium acetate at a concentration of approximately 2×10^{-4} M. Addition of calcium acetate to the subphase causes the calcium salt of DPPA to form at the water surface. It has been recently reported [13] that calcium ions induce the DPPA to form a very highly ordered, close-packed phase and this fact is emphasised by the steepness of the isotherm. Extrapolation of the condensed phase to zero pressure yields an average area per molecule of 0.42 ± 0.02 nm^2. This agrees well with a calculated projected area from a CPK packing model (shown in Plate 6.22) of 0.38 ± 0.04 nm^2.

Figure 6.21 Surface pressure-area isotherm for L-α-phosphatidic acid dipalmitoyl (DPPA) on a subphase containing 2×10^{-4} M calcium acetate at pH 6.4.

Plate 6.22 A CPK packing model of L-α-phosphatidic acid dipalmitoyl (DPPA) showing the two hydrocarbon chains and the phosphate head group.
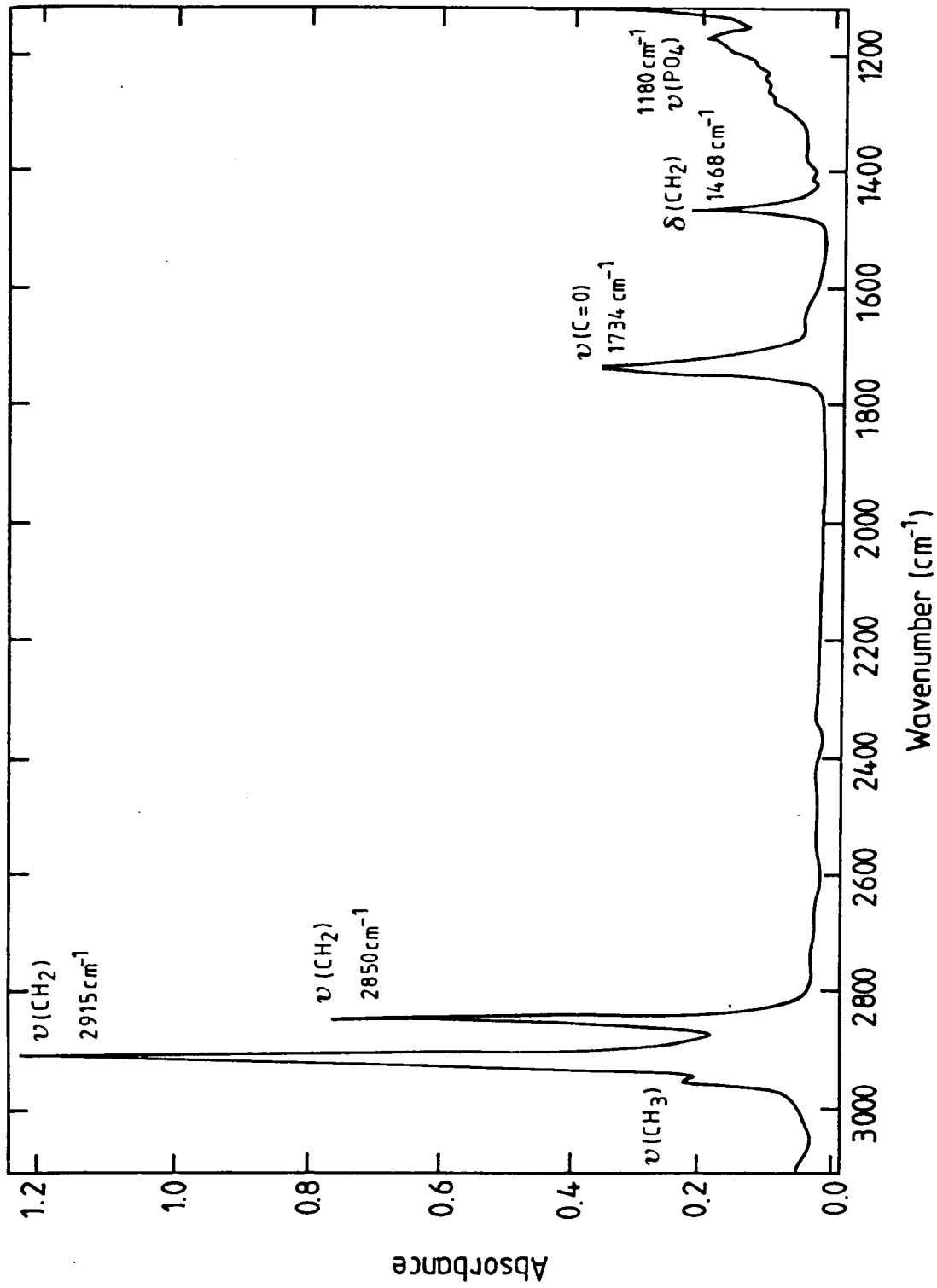
Figure 6.23 ATR-IR spectrum for 16 layers of DPPA.

Deposition of DPPA onto hydrophilic surfaces was possible although it exhibited a poor transfer ratio of less than 0.3. However, excellent Y-type deposition was obtained onto hydrophobic silicon surfaces with a transfer ratio of approximately unity. Deposition was possible at a range of surface pressures with little change in the transfer ratio. However, considering the ultimate aim of preparing a mixed DPPA/valinomycin film, a deposition surface pressure of 23 mN m^{-1} (to coincide with that of pure valinomycin) was selected.

6.4.2 Characterisation

The ATR-IR spectrum of 16 layers of DPPA in the wavenumber range 1100 to 3000 cm^{-1} is presented in figure 6.23. The assignment of the absorption bands are described below. The bands at 2915 cm^{-1} and 2850 cm^{-1} are readily assigned to the antisymmetric and symmetric CH stretching vibrations, respectively. The band at 2955 cm^{-1} is associated with the antisymmetric stretch of the methyl group and the C=O stretching vibration is evident at 1734 cm^{-1}. The CH$_2$ scissoring mode (δ(CH$_2$)band) is observed at 1468 cm^{-1}. Finally, the band 1180 cm^{-1} may be assigned to a ν(PO) vibration of the PO$_4^{2-}$ phospholipid (salt) head group [14].

Characterisation of the multilayer DPPA films has been carried out using transmission IR spectroscopy and ellipsometry. Band intensities (measured by peak heights) as a function of film thickness for wavenumbers of 1734 cm^{-1}, 2850 cm^{-1} and 2915 cm^{-1} are plotted in figure 6.24. Reproducible deposition is inferred. Also, the results of ellipsometric measurements (shown in figure 6.25) at a wavelength of 632.8 nm indicate high quality deposition. The slope of this graph gives an average thickness per monolayer of 2.7 nm. This values agrees with that taken from a CPK packing model of DPPA and it can be inferred that the CH$_2$ chains are oriented normal to the substrate surface. The large (absolute) intensities of the ν_a(CH$_2$) and ν_s(CH$_2$) bands also support such an arrangement because ATR is sensitive to transition dipoles which are parallel to the substrate. For
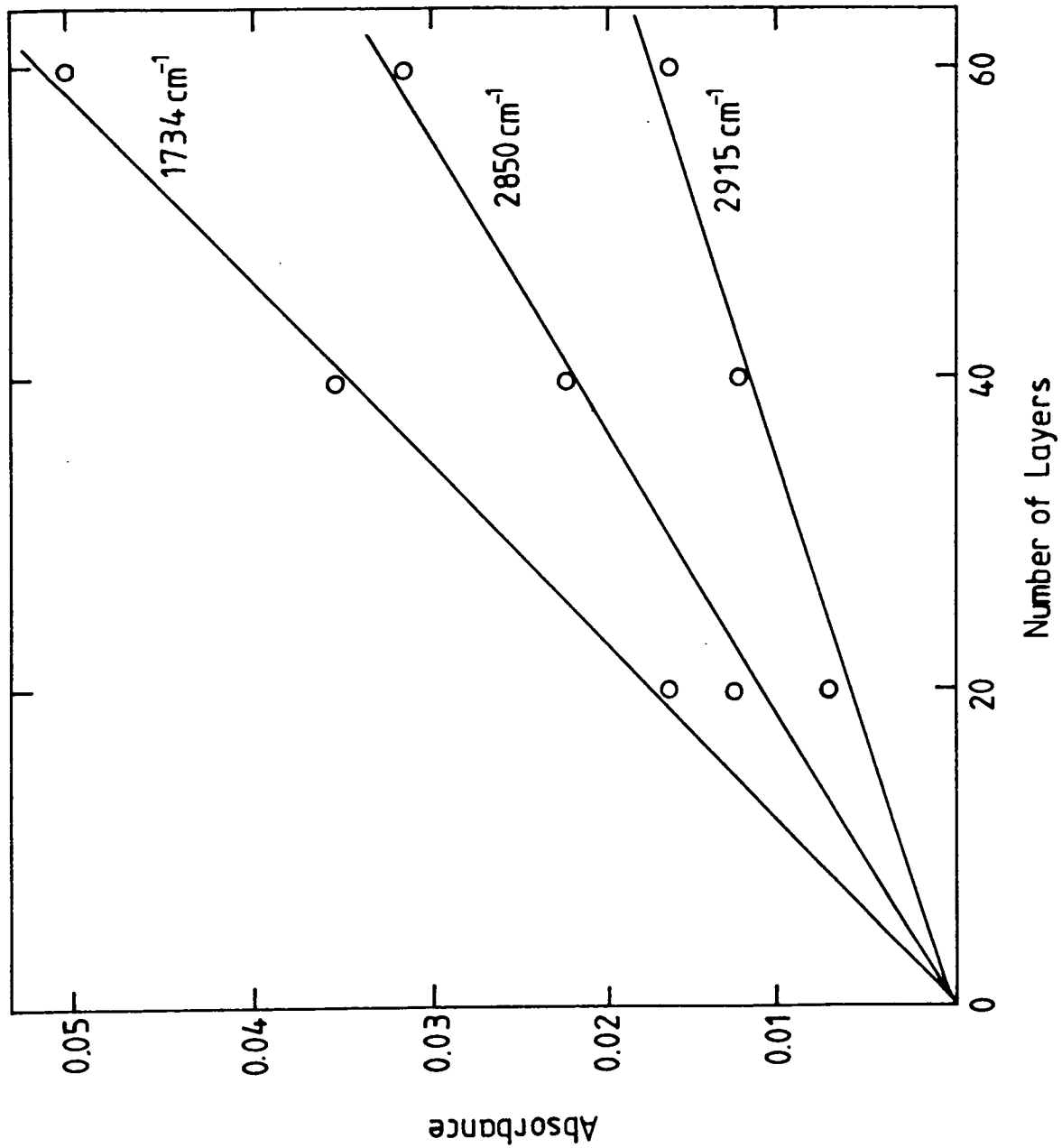
Figure 6.24 Relative intensities (as measured by peak heights) as a function of film thickness for 1734, 2850 and 2915 cm^{-1} bands.
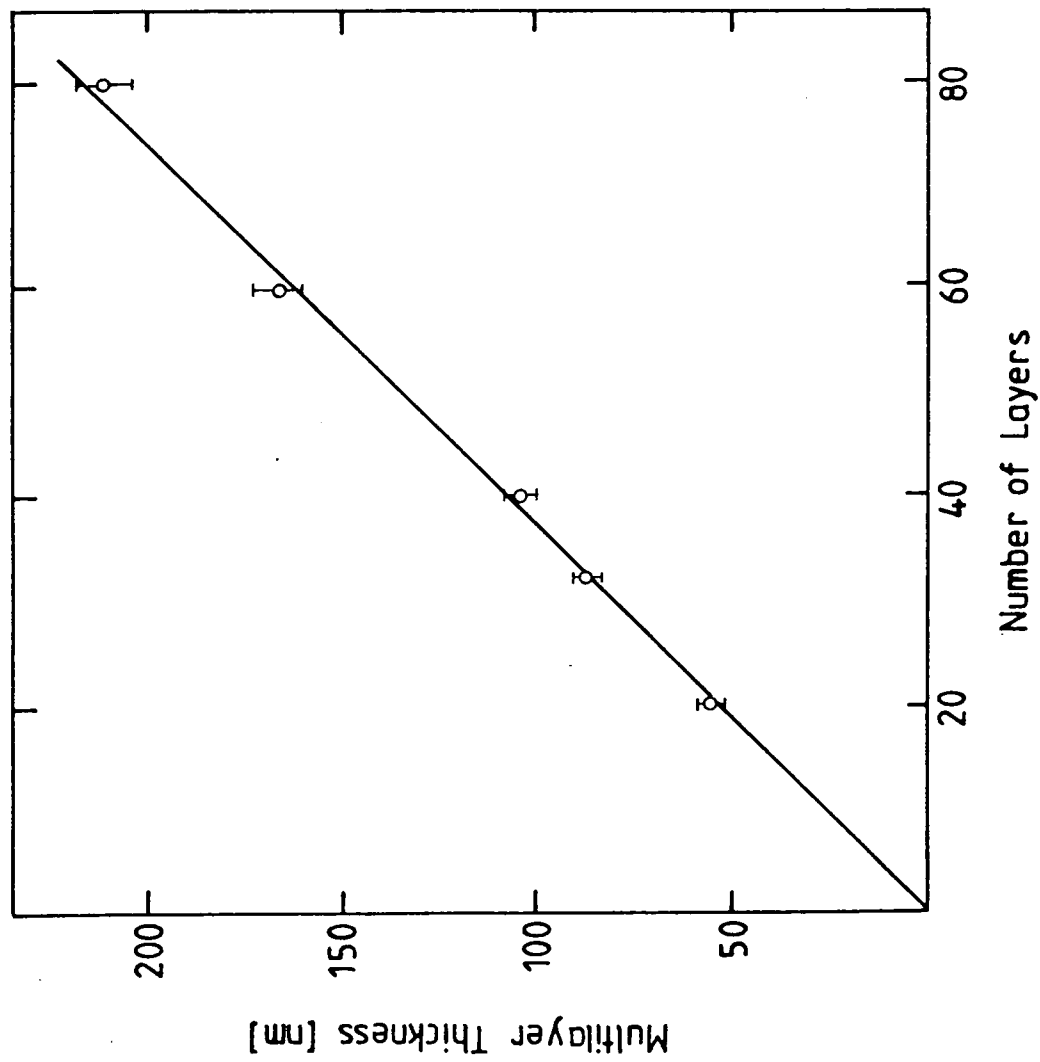
Figure 6.25 Thickness of multilayer DPPA LB films versus number of layers as determined by ellipsometry at 632.8 nm, indicating a thickness per monolayer of 2.7 nm.
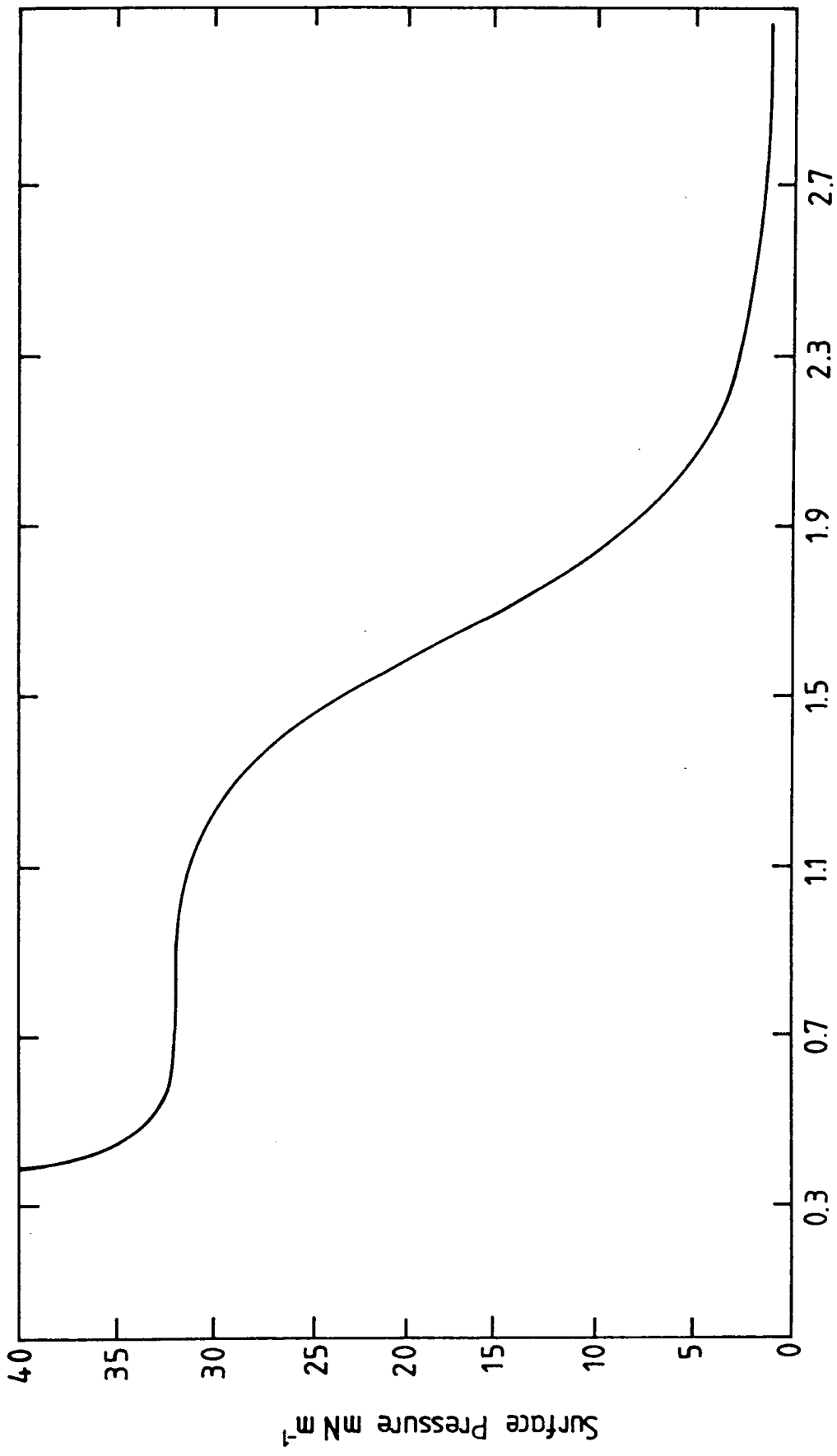
Figure 6.26 Surface pressure-area isotherm for an equimolar mixture of valinomycin and DPPA on a subphase containing 2×10^{-4} M calcium acetate at pH 6.4.

normal orientation of the hydrocarbon chains, the CH_2 transition dipoles are also parallel to the substrate [15].

6.4.3 Deposition of the mixed DPPA/valinomycin system

Figure 6.26 shows the pressure versus area isotherm, measured at $21 \pm 2°C$ and a compression rate of 3 cm s^{-1} for a 1:1 molar mixture of DPPA and valinomycin. The plateau region observed at 32 mN m^{-1} corresponds to that observed for pure valinomycin monolayers. The floating monolayer mixtures could readily be transferred to the hydrophobic silicon ATR crystal at a surface pressure of 23 mN m^{-1}; the deposition was Y-type and a transfer ratio of approximately 1.0 was obtained.

6.5 SUMMARY

The preparation and characterisation of pure valinomycin and valinomycin-containing LB films have been described. The valinomycin isotherm is unusual in that it exhibits a plateau region separating a highly incompressible phase from a compressible phase. It is proposed that during compression through the plateau region the orientation of the majority of the valinomycin molecules is changing with their planes becoming perpendicular to, rather than parallel to, the water surface. The formation of multilayers of the pure ionophore is only possible if the substrate is intially coated with a base layer of a fatty acid or a fatty acid salt. In this case deposition of valinomycin proceeds in a Y-type fashion and is reproducible. Deposition onto both the hydrocarbon chain and the carboxylic head group is possible.

Mixtures of the ionophore and arachidic acid have also been investigated. It is apparent from monolayer studies of these mixtures on water that the two components are immiscible, with the film exhibiting an aggregate nature. Reproducible Y-type deposition of the mixtures is possible onto a variety of substrates. X-ray analysis of the films suggests that as the mole-fraction of valinomycin increases

the d-spacing increases and, at the same time, the long range order in the film decreases. It is likely that the arachidic acid hydrocarbon chains are tilted at an angle to the substrate.

Excellent deposition characteristics for the phospholipid molecule L-α-phosphatidic acid dipalmitoyl are described. This makes possible the fabrication of LB multilayers of the mixed valinomycin/DPPA system. Both this phospholipid based system and the arachidic acid/ valinomycin system represent simple models for the biological membrane. The interaction of these model systems with potassium-containing solutions is described in detail in the next chapter.

CHAPTER 7

INFRARED INVESTIGATIONS OF
VALINOMYCIN-CONTAINING LB FILMS

7.0 INTRODUCTION

It has already been shown in chapter 6 that valinomycin may be deposited as either a pure material or in a mixture with a fatty acid using the LB technique. This chapter describes the results of experiments concerned with the exposure of these films to an aqueous environment containing potassium ions. A study of the interaction between valinomycin-containing LB films and potassium solutions might well provide an insight into the behaviour of the ionophore in this artificially engineered environment, and also be of relevance to potassium-ion sensing applications. Fourier transform attenuated total reflection (ATR) infrared spectroscopy [1] was chosen as the probe for these investigations because it has the extremely high sensitivity required to study ultra thin films [2], and also because the valinomycin potassium (VM/K^+) complex has already been well characterised by IR techniques [3-6]. Section 7.1 presents the ATR-IR spectra for cast films of uncomplexed and complexed valinomycin and the band assignments are described. Section 7.2 discusses the spectra of LB films of valinomycin dipped on both pure water and potassium chloride subphases. The spectra of mixed LB films of valinomycin and arachidic acid dipped on both pure water and potassium chloride subphases are presented, and the differences discussed, in section 7.3. With the potassium sensing application in mind, section 7.4 includes a description of the observation of complexation and the structural changes occurring in the mixed films when they are exposed to potassium containing solutions. Finally, sections 7.5 and 7.6 conclude the chapter with a description of the effects observed in various mixed phospholipid/ionophore systems.

7.1 CAST FILMS OF VALINOMYCIN: UNCOMPLEXED AND COMPLEXED

7.1.1 The valinomycin IR spectrum

The complete IR spectrum of valinomycin is shown in Figure 7.1. A broad band centred at 3300 cm^{-1} wavenumber can be assigned to an NH stretching mode and the CH stretching region is observed between 2800 cm^{-1} and 3100 cm^{-1}. The CH stretching region can be divided into two, those modes associated with the isopropyl residues and those with the methyl groups (the two modes are labelled in figure 7.1). Below 1800 cm^{-1}, the CO stretching region is evident. The bands in this region are as follows: the ester carbonyl band, ν (C=O) at 1755 cm^{-1}; the amide I band (approximately ν (C=O)) at 1660 cm^{-1}; the amide II band (a combination of primarily in-plane NH bending and NC stretching) at 1540 cm^{-1}; the CH bending region consisting of antisymmetric and symmetric modes at 1470 cm^{-1} and 1390 cm^{-1}; respectively; and the amide III band (a combination of primarily NC stretching and in-plane NH bending) at 1246cm^{-1}. Finally, a ν(COC) stretching band at 1183 cm^{-1}(not shown in figure 7.1) is illustrated in figure 7.2.

First of all it was necessary to determine the characteristic changes in the IR spectrum of valinomycin upon complexation. This information would enable the valinomycin complex to be identified in the ATR-IR spectra of LB films of pure valinomycin and in arachidic acid/valinomycin mixtures. A cast film of valinomycin was obtained by depositing valinomycin in an Aristar chloroform solution (using a microsyringe) onto the ATR silicon crystal surface. After the chloroform had been allowed to evaporate the infra-red spectra could be obtained. Similarly, a cast film of complexed valinomycin was prepared from a valinomycin-chloroform solution with a small quantity of potassium chloride added.

The IR spectra of cast films of uncomplexed and complexed valinomycin are compared in Figure 7.2 (with band assignments shown in Table 7.3). The important changes upon complexation with potassium are summarised as follows.
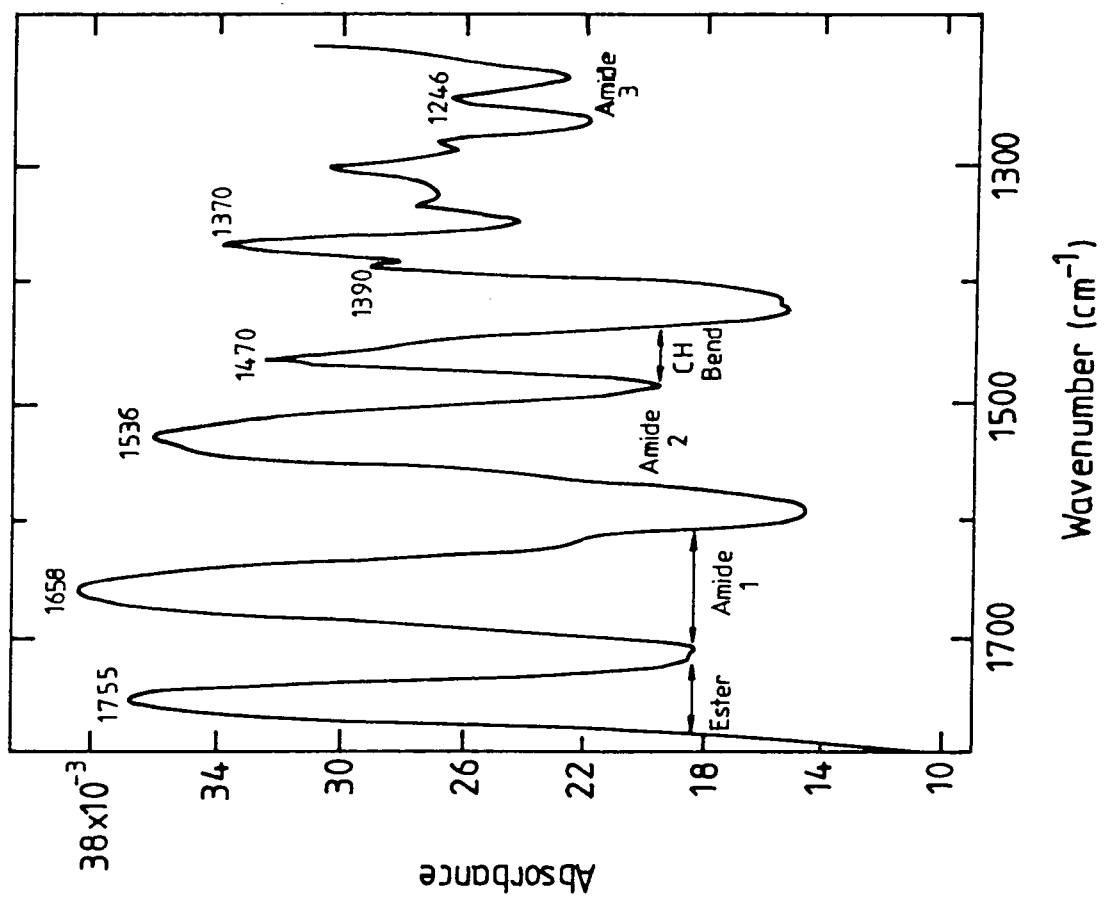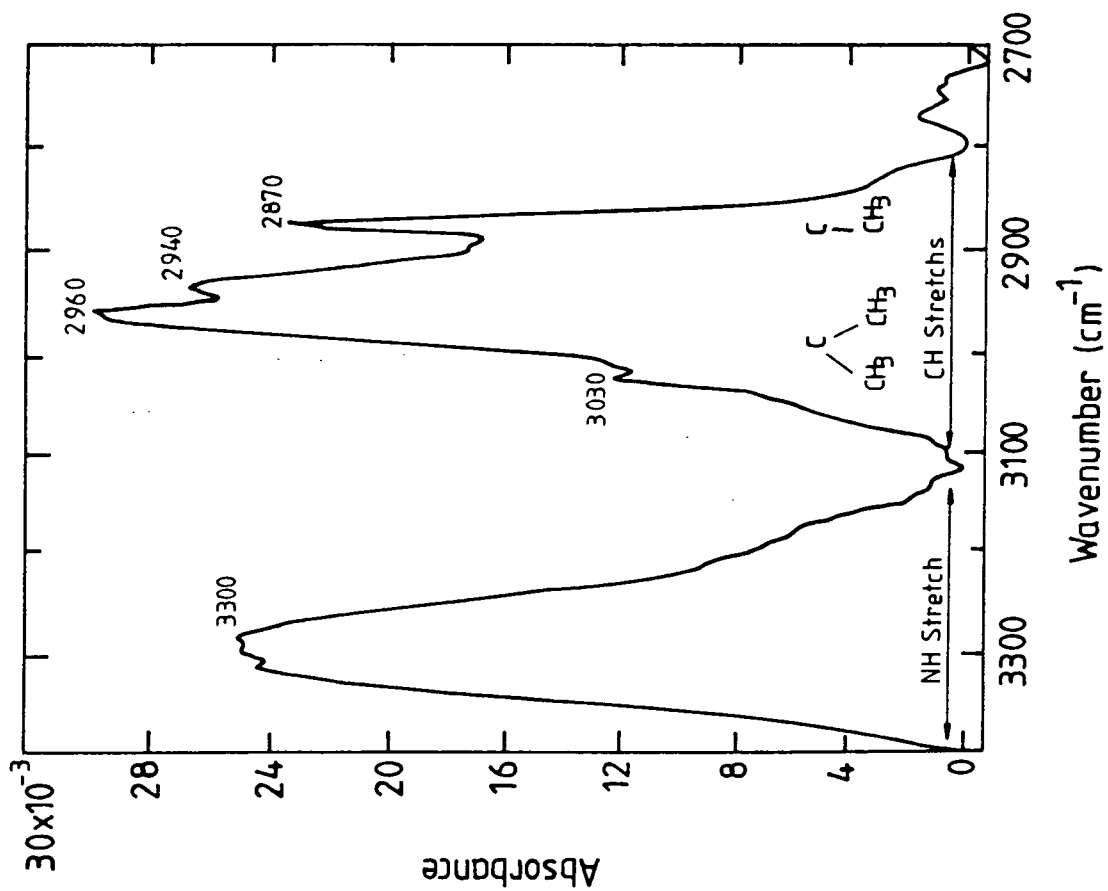
Figure 7.1 The complete IR spectrum for valinomycin.
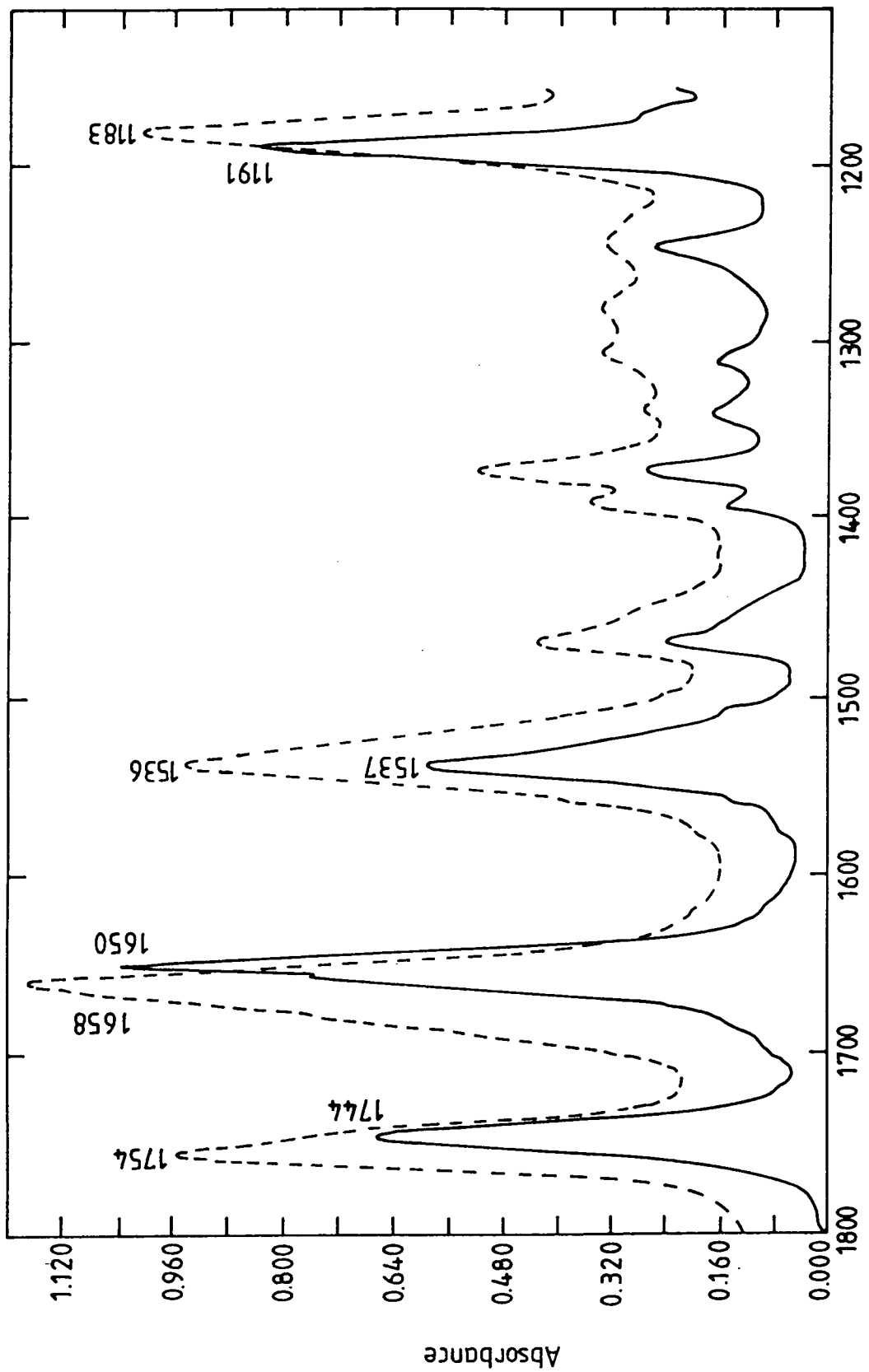
Figure 7.2 ATR-IR spectrum for cast films of uncomplexed (dashed line) and complexed (solid line) valinomycin in the 1800-1100 cm^{-1} region. The films were cast from a solution in chloroform.

Band Assignments for Cast Films of Uncomplexed and Complexed Valinomycin [a]		
	uncomplexed VM	complexed VM
ester, ν(C=O)	1754 (29)	1744 (23)
amide I, ν(C=O)	1658 (35)	1650 (22)
amide II, b(NH$_2$)	1536 (34)	1537 (26)
b(CH$_3$)	1468	1469
	1448 sh	1454 sh
b(CH$_3$)	1390	1393
	1372	1372
amide III, ν(CN)	1246	1248
ester, ν(C-O-C)	1183 (29)	1191 (19)

[a] Full widths at half-maxima (fwhm) are indicated in parentheses.

Table 7.3 Band assignments for cast films of uncomplexed and complexed valinomycin. Full widths at half maximum (fwhm) are indicated in parentheses.

The ester carbonyl band at 1754 cm^{-1} is simultaneously narrowed and shifted to give a more symmetric band at 1744 cm^{-1}. The narrowing suggests that, in the complex, all six ester carbonyls experience a more similar environment; possibly due to ion-dipole interactions with the potassium ion. In the uncomplexed valinomycin the presence of a "hydrogen-bonded" ester ν(C=O) band is indicated by the shoulder at 1739 cm^{-1} and, in addition, a "free" ester ν(C=O) band at 1754 cm^{-1} is observed. A similar shift and narrowing transforms the amide I band at 1658 cm^{-1} into a narrower, more symmetric band at 1650 cm^{-1}. In the complex, all six amide groupings are involved in intramolecular hydrogen bonding [7]. Again, a more uniform environment for the amide groups is implied. The amide II band (approximately b(NH$_2$) at 1536 cm^{-1} is also narrowed; the ν(COC) stretching band is both narrowed and shifted upon complexation to a higher frequency. The CH$_3$ bending modes are not significantly affected by the formation of the complex.

7.1.2 Collapsed film ATR spectra of valinomycin

In order to ascertain whether the IR spectrum of valinomycin from a pure water subphase was different to that of a cast film, and to establish whether complexation of valinomycin on a KCl subphase occurred, preliminary spectra of collapsed films were taken. The valinomycin film was allowed to stabilise on the water surface at the deposition pressure of 23 mN m^{-1} for intervals of between one hour and ten minutes. After this time had elapsed, the film was collapsed by compressing it to the plateau pressure of 32.5 mN m^{-1}. A collapsed film was transferred onto the ATR crystal by skimming it across the water surface.

The spectra of valinomycin from both pure water and KCl subphases (ranging in concentration from 0.05 M to 1.0 M) were identical (in all respects, band positions and widths) to those of the cast film spectra described in the previous section. From this it can be concluded that the valinomycin/potassium complex is not being formed on the water surface. It is conceivable that an interaction

between the ester carbonyl C=O groups and the water molecules prevents their co-ordination with the potassium ion, and therefore complexation does not take place.

7.2 LB FILMS OF PURE VALINOMYCIN

7.2.1 Dipped on a pure water subphase

The ATR spectra of LB films of pure valinomycin are the same as those obtained from cast films and collapsed films. In the ATR spectra of up to 100 LB layers of pure valinomycin, no significant differences could be identified.

7.2.2 Dipped on a KCL subphase

In the ATR spectra of up to 100 monolayers of pure valinomycin dipped on potassium containing subphases (with concentrations varying from 0.05 M to 1.0 M), no evidence for the VM/K$^+$ complex was observed. The spectra were identical to those obtained for valinomycin LB films on a pure water subphase. Furthermore, LB films of valinomycin dipped on a pure water subphase and subsequently immersed in a saturated KCl solution also exhibited no signs of complexation. These results are again consistent with those obtained for collapsed valinomycin films, reinforcing the fact that the VM/K$^+$ complex is not being formed on the water surface. The reason for this is not fully understood at present, but is probably related to the conformation of the valinomycin molecule in these films. The conformation of the valinomycin molecule is strongly dependent on its local environment, for example, the various conformers of valinomycin in non-polar and polar solvents have already been discussed in chapter 2. The local environment of the valinomycin molecule in the films described so far in this chapter is unusual, i.e. its molecular environment is uniformly "valinomycin-like". This environment is unusual when compared to that experienced by the ionophore in the biological membrane and in sensor applications. In the former, valinomycin is surrounded predominantly by the hydrocarbon chains of the phospholipids and, in the latter,

the ionophore is trapped in a polymer (PVC/plasticiser) matrix. Furthermore, the response of pure valinomycin films to potassium ions has not previously been reported in the literature. It is possible that when a valinomycin molecule is surrounded by its neighbours intermolecular or intramolecular interactions between the polar carbonyl groups inhibit the formation of the complex by preventing their coordination with the K^+ ion. To mimic the biological membrane and to try to "activate" the valinomycin molecule, mixed LB films of arachidic acid and the ionophore were prepared. In this system the arachidic acid molecules are representing the phospholipid molecules of the natural environment.

7.3 MIXED LB FILMS OF VALINOMYCIN AND ARACHIDIC ACID

7.3.1 Dipped on a pure water subphase

Using the deposition technique outlined in chapter 6, Langmuir-Blodgett films of arachidic acid/valinomycin (A/VM) mixtures were prepared. The ATR spectrum of a film composed of twenty layers of an 11.75:1 (M) A/VM mixture dipped on a pure water subphase is shown in figure 7.4. The contribution from the cadmium stearate base layer has been subtracted. The spectrum of figure 7.4 reveals a few new bands compared to that of figure 7.1 and these are attributed to the arachidic acid. In the 3300 cm^{-1} region (figure 7.4a) the NH stretching band of valinomycin is obscured by the OH band of water (originating from ice on the CMT detector and because its intensity is continuously varying, it cannot always be completely subtracted). The CH_2 stretching region is apparent between 3000 and 2800 cm^{-1} wavenumbers. This consists of the antisymmetric and symmetric modes at 2915 cm^{-1} and 2848 cm^{-1}, respectively. The CH stretching contribution of the valinomycin is hidden under the arachidic acid bands. Below 1800 cm^{-1} (figure 7.4b) there are several bands associated with the carboxylic acid head group. The intense band at 1702 cm^{-1} is the cyclic acid dimer band originating from the hydrogen bond interaction between the polar head groups of the arachidic acid (the hydrogen bonding scheme is shown as an inset to figure 7.4a).
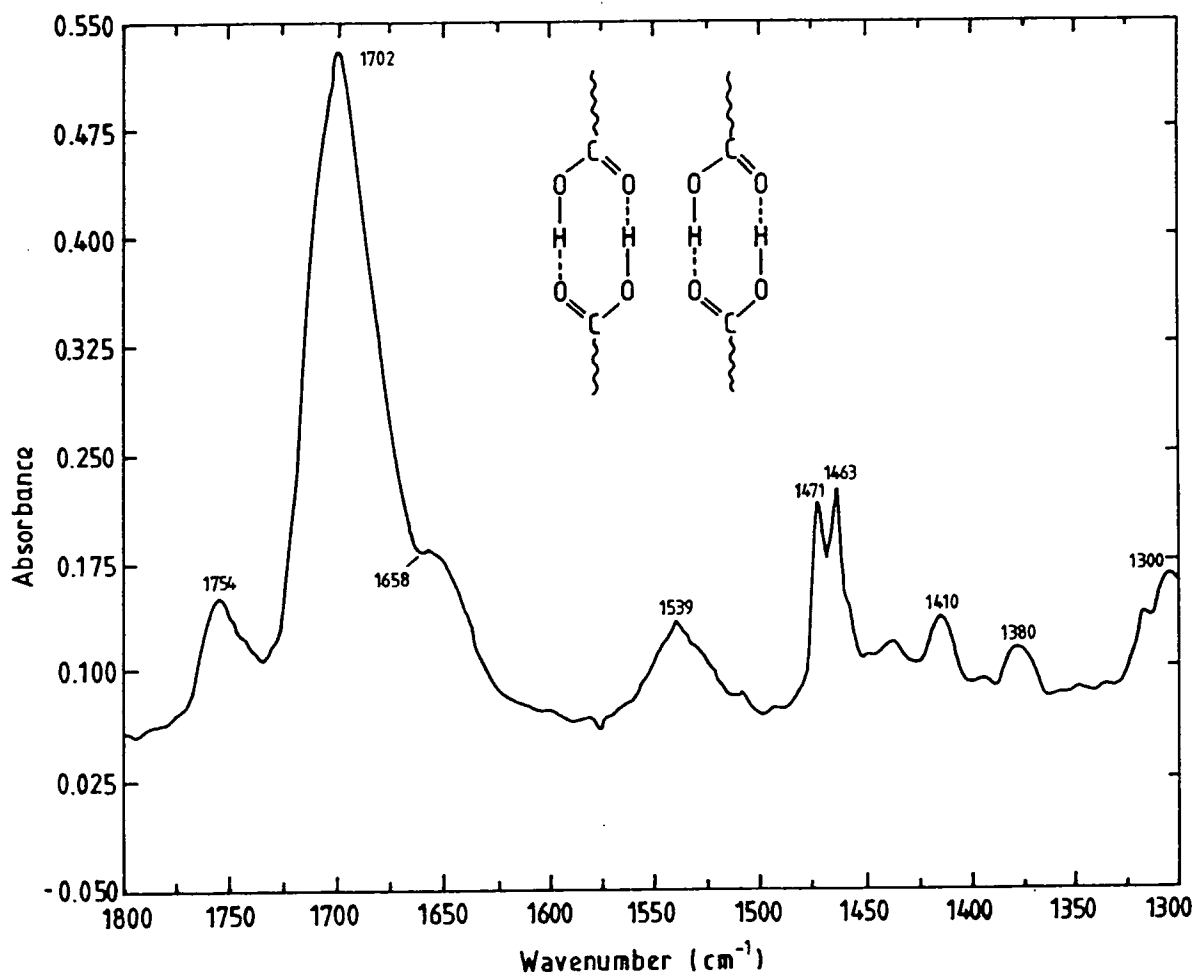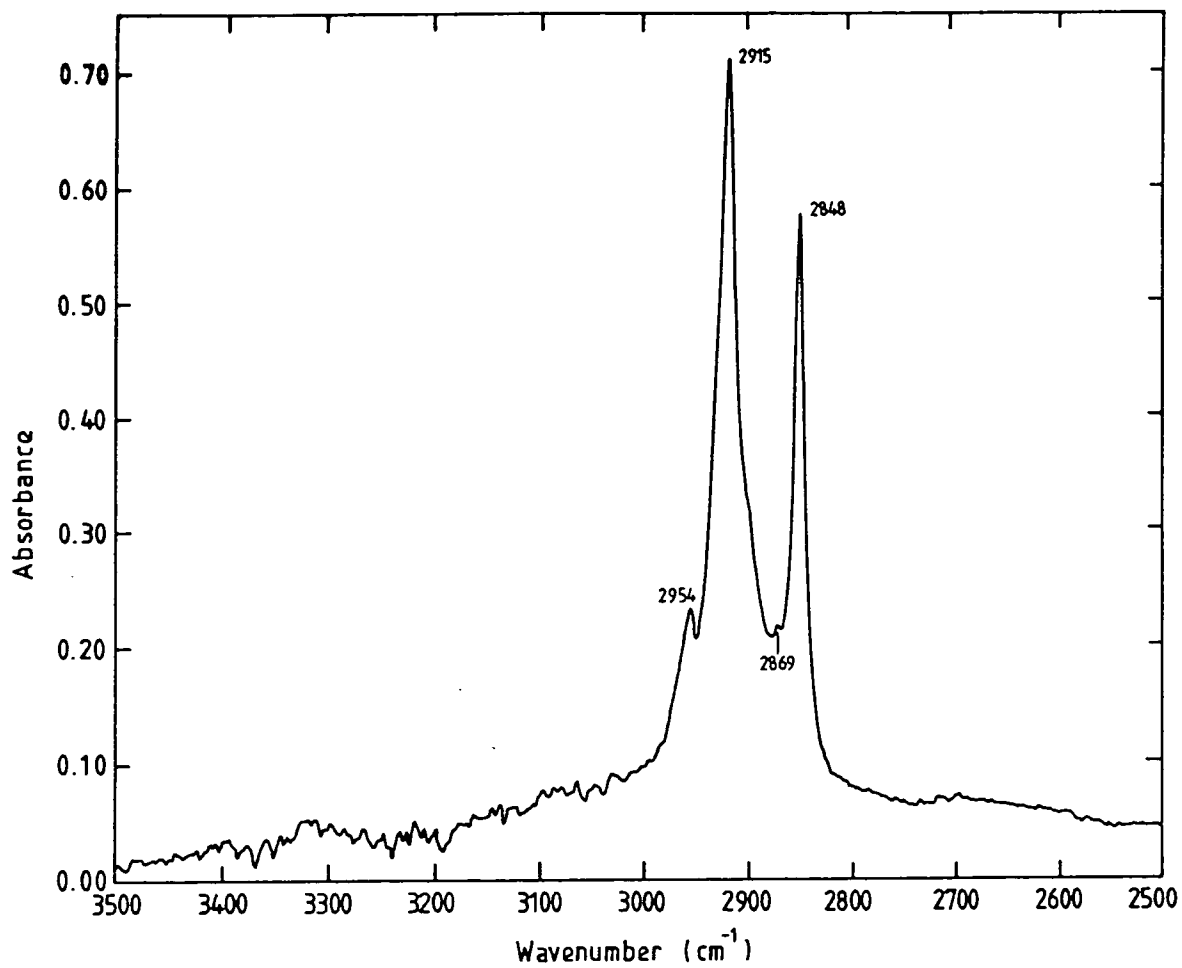
Figure 7.4 The ATR spectrum of a film composed of 20 layers of an 11.75:1 (molar) A/VM mixture dipped on a pure water subphase, (a) 3500 -2500 cm^{-1} and (b) 1800 - 1300 cm^{-1}.

The bands at 1410 cm^{-1} and 1300 cm^{-1} are also due to the acid head group and arise from strongly coupled vibrations involving the in-plane OH deformation, and the C−O stretch, respectively. Normally for fatty acids, the CH bending mode occurring at 1470 cm^{-1} appears as a single band. However, in figure 7.4b this band is split into two, one at 1471 cm^{-1} and the other at 1463 cm^{-1}. This indicates that the CH$_2$ subcells of the arachidic acid are packed in an orthorhombic scheme.

Subtraction of the valinomycin spectrum (figure 7.1) from that of figure 7.4 reveals the arachidic acid spectra with no band shifts being prominent. This can be interpreted as evidence for little interaction between the two molecules in the mixed film and emphasises the aggregate nature of the film with the fatty acid-type molecules closely packed within each aggregate.

7.3.2 Dipped on a KCl subphase

In figure 7.5, the spectrum for an 11.75:1 A/VM LB film dipped on a 0.05 M KCl subphase is shown, and for comparison, the spectrum for the same mixture dipped on a pure water subphase is also shown. The occurrence of two new bands, one at 1742 cm^{-1} and the other at 1650 cm^{-1} indicates the presence of the VM/K$^+$ complex. These two bands correspond to the ester ν(C=O) and amide I bands of complexed valinomycin, respectively (as shown in figure 7.2). From the spectrum it can also be concluded that both uncomplexed and complexed forms of valinomycin are present in the mixed films. This is inferred from the ester ν(C=O) bands at 1754 cm^{-1} and 1742 cm^{-1}, respectively. Thus only a fraction of the valinomycin in the mixed film is in the complexed form (see section 7.4.4). A difference spectrum between an 11.75:1 A/VM mixture dipped on a 0.05 M KCl subphase and the same mixture dipped on a pure water subphase is shown in figure 7.6. Comparison of the band positions and half-widths for this spectrum with those of complexed valinomycin tabulated in Table 7.3 shows a close agreement, indicating that figure 7.6 is, in fact, the spectrum of complexed
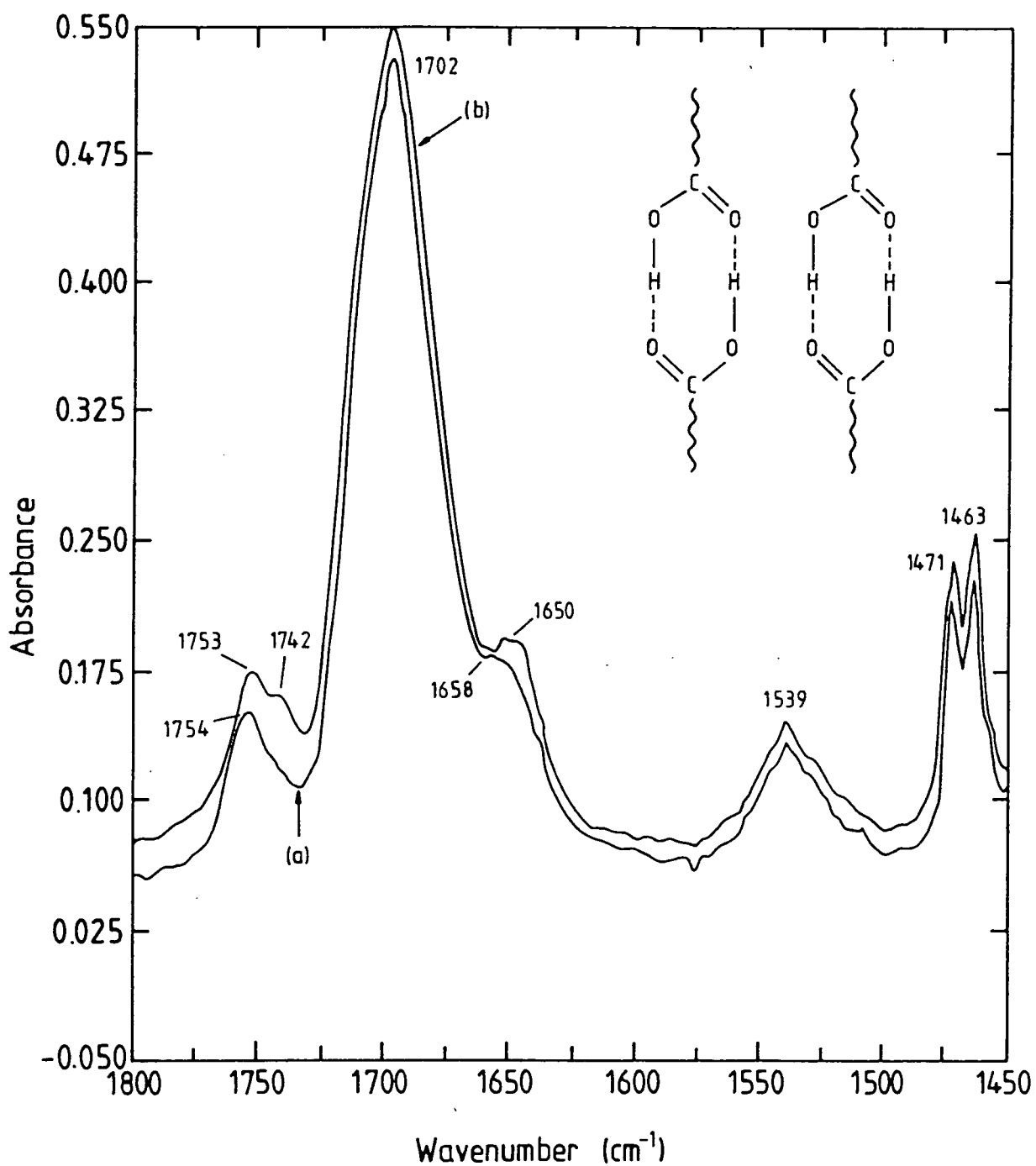
Figure 7.5 ATR-IR spectra for a 20 monolayer thick 11.75:1 (molar) arachidic acid/valinomycin LB film dipped on (a) a pure water subphase and (b) on a 0.05 M KCl subphase.
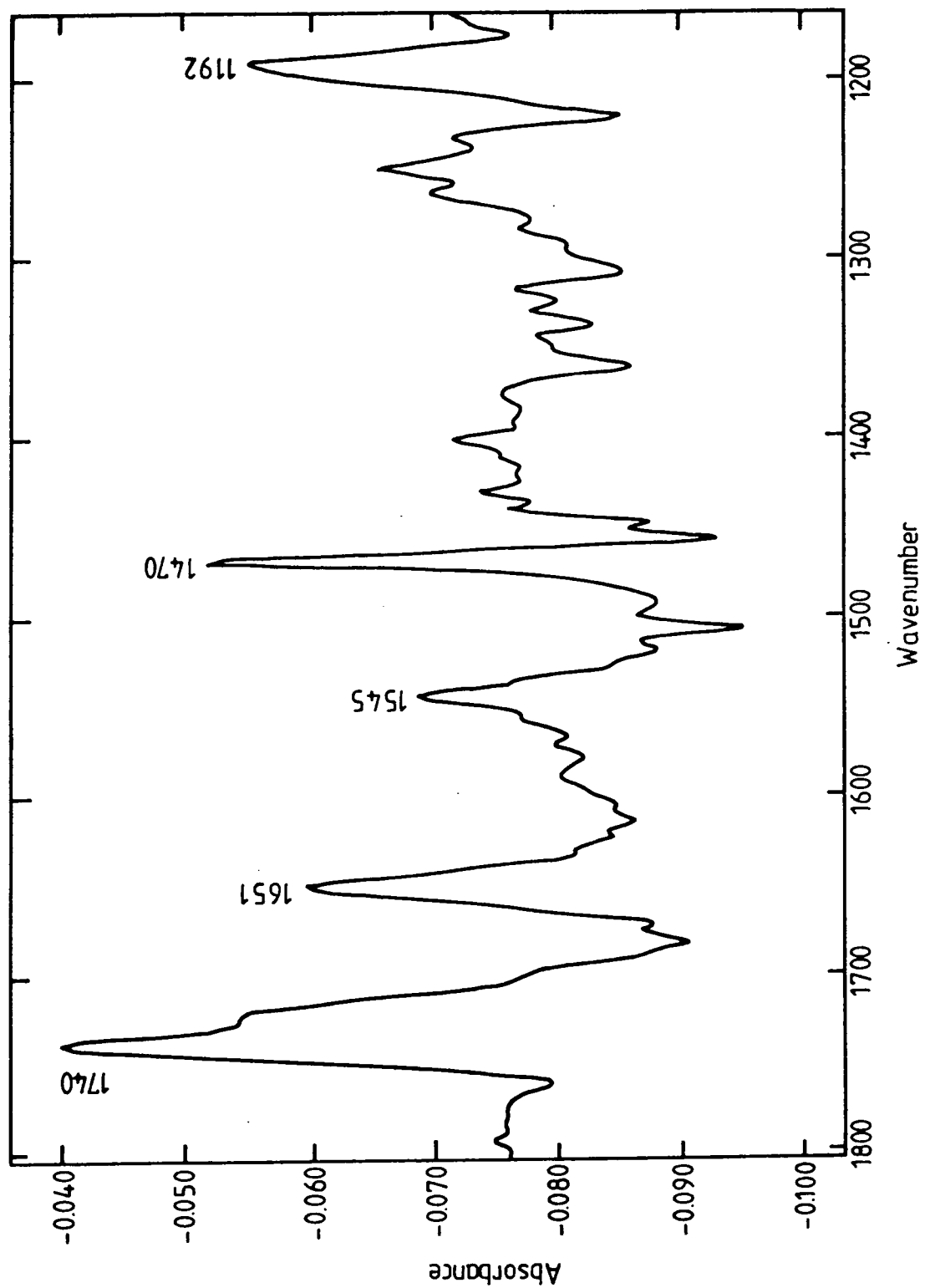
Figure 7.6 Difference spectrum between the spectra of an 11.75:1 (molar) arachidic acid/valinomycin film dipped on a 0.05 M KCl subphase and that of the same mixture dipped on a pure water subphase (shown in figure 7.3).

valinomycin.

The system of arachidic acid and valinomycin is a simple model for the biological membrane and it is encouraging that complexation occurs. The results, however, of the last two sections reveal the more fundamental observation that the presence of arachidic acid is necessary for complexation to take place in the LB film structures. This is possibly related to the hydrophobic environment provided by the arachidic acid. In an 11.75:1 A/VM mixture, the components are approximately occupying equal areas in the film and the arachidic acid may serve to isolate valinomycin molecules from their neighbours. In this way its local environment changes from "valinomycin-like" (cf. pure films of valinomycin described previously) to that presented by the hydrocarbon chains of the arachidic acid. This change seems to "activate" the valinomycin so that complexation can take place. Assuming that the LB film is aggregate in nature then it is also possible to explain why all the valinomycin molecules do not complex. The aggregated valinomycin regions of the mixed film are identical in nature to the pure film. Therefore valinomycin molecules within the aggregate are unable to complex as in the pure films. On this basis it would be expected that as the mole-fraction of arachidic acid in the mixed film increases so also would the proportion of complexed valinomycin molecules. This follows simply because a greater fraction of the ionophoric material will be isolated. Indeed, this relationship is found to hold both for the mixtures described in this section and the next (section 7.4.4).

In view of the potential potassium-sensing application of the mixed films, the following section describes the results of experiments concerned with immersing mixed arachidic acid/valinomycin LB films (in an uncomplexed state) in potassium containing solutions.

7.4 POTASSIUM SENSING WITH LB FILMS OF ARACHIDIC

ACID/ VALINOMYCIN MIXTURES

7.4.1 Observation of the VM/K$^+$ complex

The effect on immersing mixed arachidic acid/valinomycin films in KCl solutions was investigated. These films were deliberately dipped on a pure water subphase so that the valinomycin component would be in the uncomplexed state, and then subsequently immersed in KCl solutions. Using the ATR technique, it was possible to monitor the changes occurring in the LB film as a function of the time immersed in KCl. The spectra were recorded in air after the corresponding immersion period in KCl had elapsed. Normally a few minutes were required to allow the water that had accumulated on the silicon surface to evaporate. In this section, all results are for 14 layer LB samples of an 11.75:1 (M) A/VM mixture.

In figure 7.7, the effects of a total of 10 minutes immersion in a saturated KCl solution on an A/VM LB film are shown. The spectra have been displaced vertically to allow for clarity. A thousand scans were recorded for each spectrum, lasting a total of 10 minutes. After 10s (spectrum not shown in figure 7.7) the spectrum is essentially identical to that of figure 7.5a, and hence the valinomycin is still largely in the uncomplexed state. After 1 min (figure 7.7a), however, a significant amount of complexation has taken place. This is indicated by the ester ν(C=O) and amide I bands at 1744 cm^{-1} and 1653 cm^{-1}, respectively. Uncomplexed valinomycin is evident from the shoulder at 1754 cm^{-1} on the carbonyl band. At 5 min (figure 7.7b) this shoulder is less pronounced indicating that more valinomycin has undergone complexation. From these results it can be concluded that mixed A/VM films (prepared in the uncomplexed state by dipping on a pure water subphase) undergo complexation when immersed in KCl solutions. Hence the potassium ion sensing ability of these films has been demonstrated. For a working sensor, dissociation of the VM/K$^+$ complex is required and this is discussed in section 7.4.3.
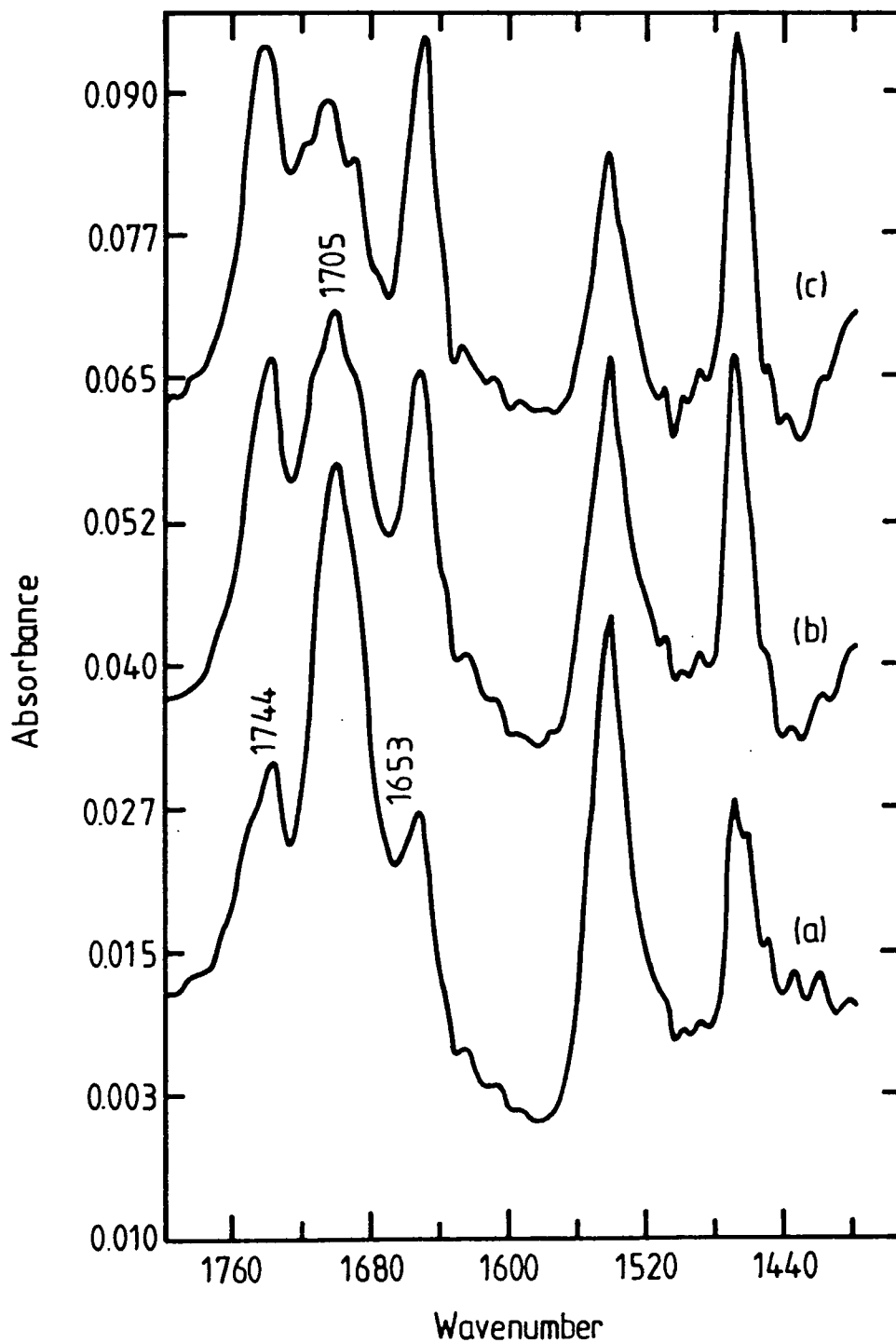
Figure 7.7 Effects of immersion in saturated KCl solution for 14 layers of an 11.75:1 (molar) arachidic acid/valinomycin LB film: (a) after 1 min, (b) after 5 min and (c) after 10 min.

7.4.2 Arachidic acid structural changes

Referring to figure 7.7, a far more profound change in the spectrum after 1 min is the decrease in intensity of the cyclic acid dimer band of the arachidic acid observed at 1705 cm^{-1}. The intensity reduction increases with immersion time and at 10 min (figure 7.7c) a substantial reduction ($>50\%$) is observed.

To interpret this change correctly, it is necessary to look at related changes in the arachidic acid CH$_2$ stretching bands shown in figure 7.8. This is a difference spectrum between the spectra taken before and after a 5 min immersion period in KCl solution. It shows the changes occurring in the arachidic acid structure. Two positive features at 2924 cm^{-1} and 2856 cm^{-1}, corresponding to the antisymmetric and symmetric CH$_2$ stretching modes of the arachidic acid (there are no CH$_2$ groups present in valinomycin). Since ATR is mainly sensitive to dipole changes parallel to the silicon surface, the increase in ν(CH$_2$) band intensities (both of which have there transition dipoles parallel to the surface [8]) can be considered to be a result of the acid chains becoming more perpendicular (i.e. dipoles more parallel) to the surface. The positive changes observed in this region also indicate that material is not disappearing from the LB film (into solution). This is based on the assumption that there are no major changes in extinction coefficients. It is therefore not possible to account for changes in the 1705 cm^{-1} region in terms of loss of material. Another explanation might be the conversion of acid to salt, however, no bands attributable to the salt RCOO$^-$K$^+$ (expected at 1555 cm^{-1}) [9] are observed in the spectra. Instead, it is proposed that the changes in the 1705 cm^{-1} band are due to the acid dimers breaking apart, thus leading to the formation of monomers or sideways dimers. The evidence for this is illustrated in figure 7.7 which shows a relative increase in intensity of the ester carbonyl band with respect to the amide I band (cf. relative intensities in a cast film of complexed valinomycin, see figure 7.1). This implies the existence of another band in the region 1740 - 1750 cm^{-1}, possibly associated with acid sideways dimers.

A control experiment for that described above was also undertaken. This
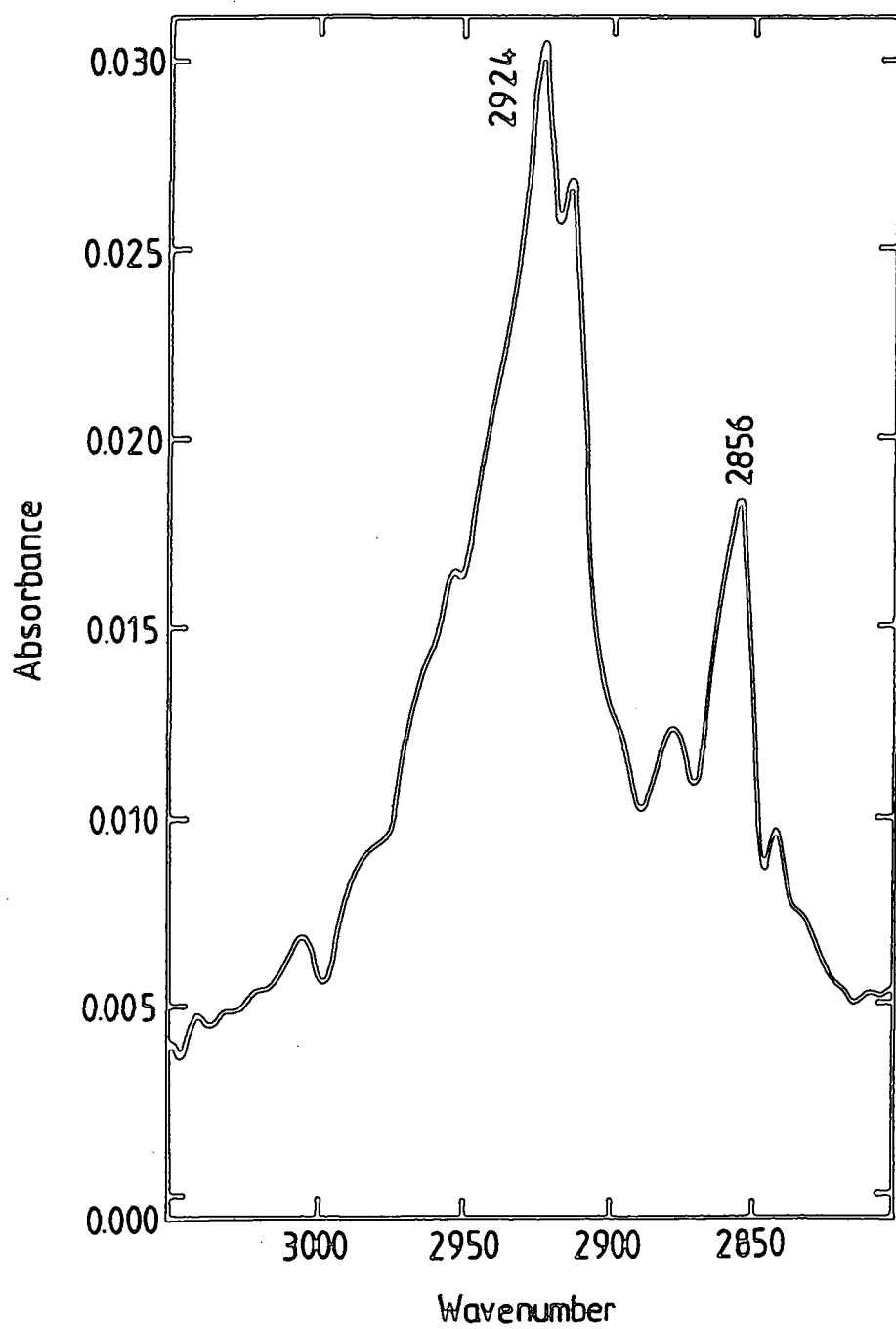
Figure 7.8 Difference spectrum showing the changes occurring in the CH$_2$ stretching region for 14 layers of an 11.75:1 (molar) arachidic acid/valinomycin mixture after a 5 min immersion period in saturated KCl.

involved immersing mixed A/VM LB films in pure water for immersion periods of up to 10 mins. No significant changes in the IR spectra were obtained. No complexation occurred (as there was no KCl present in the water) and also the marked changes in the acid dimer bands were not observed. Thus the changes in the arachidic acid band are related to the complexation process. Furthermore, the structural changes in the acid band are not reversible, i.e. if after immersion in the saturated KCl solution the film is placed in pure water or a KCl solution of a lower concentration, an increase in intensity of the 1705 cm^{-1} band does not occur. This indicates that the dimers have been permanently disrupted.

The structural changes detected in the arachidic acid matrix probably reflect changes in the molecular position of valinomycin molecules in the matrix. Recent NMR work [10] has shown conclusively that, at least for sonicated phospholipid vesicle-based systems, the valinomycin molecule in the uncomplexed conformation occupies an average location in a relatively hydrophobic region (in our case amongst the hydrocarbon chains). However, upon complexation it has a tendency to move to a more polar (in our case nearer to the acid head groups) region. The reason for this is thought [10,11] to be due to the competition for hydrogen bonds on the valinomycin and the presence of a charged (K$^+$) centre. The breaking of the intramolecular hydrogen bonding scheme of the complexed conformation is believed to be responsible for the release mechanism of the cation. Hence, in our model system the following process is envisaged. Intially, the uncomplexed molecule is embedded in the hydrocarbon chain environment. The CH$_2$ chains are aligned so as to best accommodate the much larger (area- wise) valinomycin and it is likely that this arrangement will involve some of the chains being at an angle to the substrate surface. When the A/VM film is immersed in KCl solution, complexation takes place with the conformational reshaping of the ionophore, and the molecules subsequently migrate to the more polar acid head groups. This has two effects, firstly, the extra space now available to the hydrocarbon chains allows them to realign (probably becoming more perpendicular and hence causing the

104

comprises the alkyl chains of the arachidic acid. In the natural membrane the potassium is released at an acid head group-solution interface. An interesting experiment to confirm this idea would be to try to produce a single bilayer or a multilayer with the acid head groups outermost. This could be done in two ways: either using the Schaefer technique [12] to transfer the final layer, or using the method described by Chapman et al [13,14] in which a UV polymerisable matrix (to replace the arachidic acid) is used with the acid head groups of the outermost layer being transferred on the final downstroke.

7.4.4 Effect of mole-fraction of the arachidic acid in the mixed film

An attempt to calculate the amount of complexed valinomycin in the mixed A/VM films has been carried out for both the films reported in this section and those in the previous section. The results presented below are those for the mixed films (of section 7.3) dipped on KCl subphases. Calculations based on the A/VM films of this section indicate a similar trend for the degree of complexation versus mole-fraction but extraction of data from the spectra is difficult owing to the changing acid dimer band.

The basis of a semi-quantitative calculation is shown in figure 7.9. The results are based on the ester carbonyl band. In figure 7.9a, the $\nu(C=O)$ band for the uncomplexed film is shown. Figure 7.9b illustrates that for a partially complexed film; the band shape is a consequence of the superposition of two features, one due to complexed and the other due to uncomplexed valinomycin. The proportion of the complex is given by the ratio D/A. The calculation makes two assumptions that (a) the extinction coefficient of the complex is the same as that of the free valinomycin and (b) the valinomycin band shape in the complex is the same as in the uncomplexed films. If either of these assumptions were wrong it would only influence the magnitude of the ratio and not the relative values. Another problem that must also be taken into consideration is that of the differing baselines for each spectra and consequently baseline-correction of the spectra was employed. Figure

Uncomplexed $\nu(C=O)$ Band

$$\frac{Y}{X} = 0.6$$

X   Y

(a)

Complexed $\nu(C=O)$ Band

$$C = \frac{AX}{Y}$$

A   B   C   D

Band due to complex $D = B - C$

(b)

Proportion of complex $= \dfrac{D}{A}$

(c)

Proportion of Valinomycin in film which has complexed

0.5
0.4
0.3
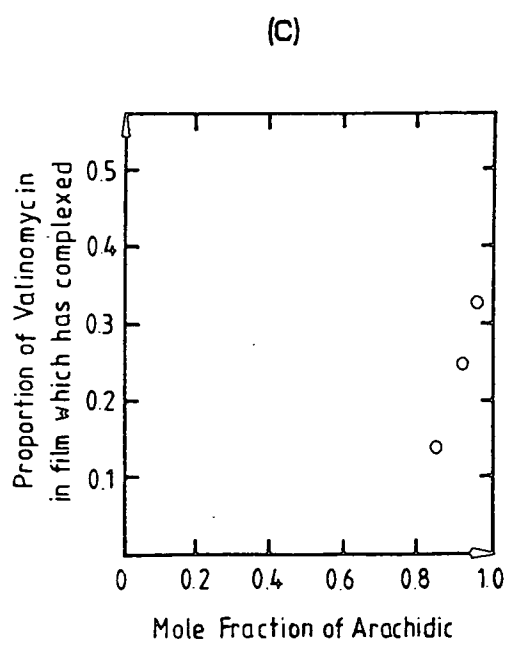0.2
0.1

0   0.2   0.4   0.6   0.8   1.0

Mole Fraction of Arachidic
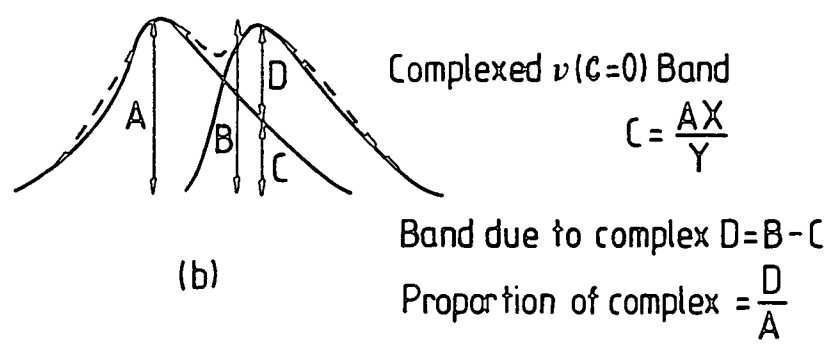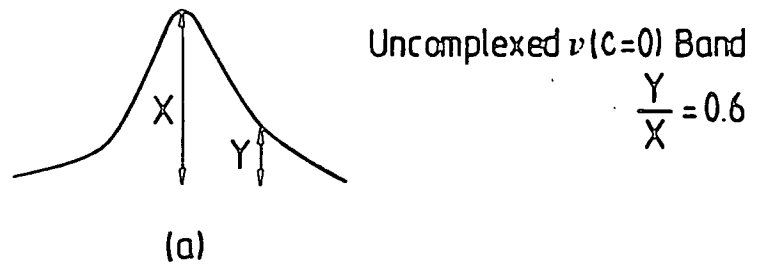
Figure 7.9 Ester carbonyl $\nu(C=O)$ band changes upon complexation. (a) uncomplexed, (b) complexed and (c) a plot of the proportion of complexed valinomycin in the mixed film versus the mole-fraction of acid.

7.9c shows a plot of the proportion of complexed valinomycin in the film versus the mole fraction of arachidic acid. Although only three data points are shown, the trend is obvious, i.e. as the mole-fraction increases so does the proportion of complexed valinomycin. This has already been interpreted in section 7.3.2 as indicating a greater proportion of "active" valinomycin molecules.

7.5 MIXED PHOSPHOLIPID/VALINOMYCIN LB FILMS

The mixed systems of arachidic acid and valinomycin described so far in this chapter are simple artificial membrane structures. In these structures the valinomycin/potassium complex was formed but unfortunately dissociation of the complex did not occur. Also significant structural changes in the fatty acid matrix were apparent. A step closer in modelling the real biological membrane is to replace the fatty acid with a phospholipid molecule. The properties of mixed Langmuir-Blodgett films of a phospholipid and valinomycin are described in the rest of this chapter. Infrared investigations of the interaction of these mixtures with KCl solutions are discussed and compared to those outlined previously.

7.5.1 Choice of phospholipid molecule

Preliminary experiments were performed using the phospholipid molecules L-α-phosphatidylcholine dipalmitoyl (DPPC) and L-α-phosphatidyl ethanolamine dipalmitoyl (DPPE). Before deposition of the mixed systems was attempted it was important to see if it was possible to form good multilayers of the pure material. This was necessary because the phospholipid is acting as the matrix molecule for the valinomycin, and if it deposits poorly in the pure form then deposition of the mixed systems might not be possible.

Previous reports [15-19] in the literature concerning the deposition of these molecules vary from those claiming reproducibility up to 100 layers to others claiming a maximum of only three layers. The isotherms of the two molecules and their molecular structures are shown in figure 7.10a and b, respectively. The isotherm
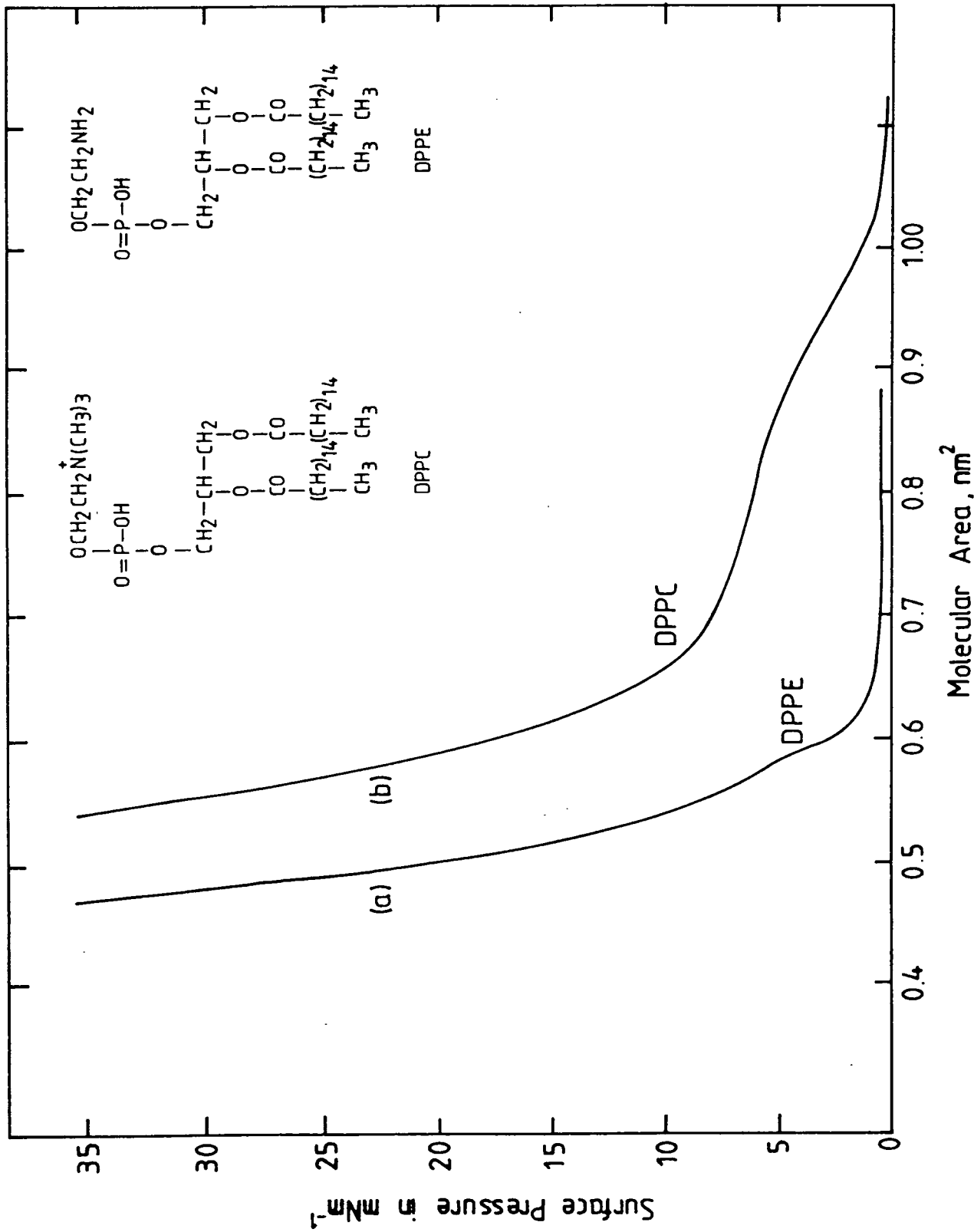
Figure 7.10 Surface pressure-area isotherms for the phospholipids (a) DPPE and (b) DPPC.

of DPPE is much the same as that of the fatty acids. The isotherm of DPPC is quite unique exhibiting a plateau region at about 5 mN m^{-1}, in between the "gas" and "solid" phases. This has been associated with a phase change, related to a conformational change, as the hydrocarbon chains reorient on the water surface. Both molecules exhibit condensed phases and determination of the molecular area per molecule at a surface pressure of 40 mN m^{-1} (well into the condensed phase) coincide with areas obtained from CPK packing models. The area of the DPPC molecule (0.53 ± 0.02 nm^2) is larger than that of the DPPE (0.46 ± 0.02 nm^2) molecule owing to the more bulky phosphate head group of DPPC. Monolayer spreading solutions were produced by dissolving DPPC in chloroform, and the DPPE in a 4:1 (by volume) mixture of chloroform : methanol.

On the deposition of the DPPC [15,16], an excellent monolayer could be transferred onto a hydrophilic substrate with a transfer ratio of about unity . However, on the following downstroke, the water meniscus contact angle immediately changed direction from down to up, and consequently the monolayer was completely removed. This demonstrates that the polar head group of DPPC is extremely hydrophilic preferring to interact with the water molecules (rather than itself or the OH groups of the Si substrate). Therefore multilayer deposition was found to be impossible. For a hydrophobic substrate, on the first two traversals of the air-water interface, poor deposition was obtained, and on the second downstroke, monolayer peeling was observed as described above.

In the case of DPPE [16-19], a maximum of three monolayers could be deposited onto a variety of substrates. However, the deposition was not reproducible. Because of the difficulties in preparing simple multilayers of these pure phospholipids, another phospholipid was chosen, L-α-phosphatidic acid dipalmitoyl (DPPA). This is the simplest of the phospholipids with the smallest head group and the molecule plays a key role in the biosynthesis of most glycerophospholipids. It occurs at a low level (1- 5% of total phospholipids) in many tissues. The deposition and characterisation of multilayers of DPPA (in fact the calcium salt of this

acid) has already been described in chapter 6. Excellent results were obtained, and hence DPPA was deemed suitable as the phospholipid matrix molecule for the mixed phospholipid/valinomycin systems.

7.6 ATR-IR SPECTRA OF MIXED PHOSPHOLIPID/IONOPHORE SYSTEMS

The behaviour of the phospholipid/ionophore system on exposure to potassium solutions is now described. All the potassium sensing experiments described in this work were performed using 10-layer LB samples.

7.6.1 Observation of complexation

The ATR-IR spectrum for a 10-layer 1:1 DPPA/valinomycin LB sample is shown in figure 7.11, curve (a). For all the spectra reported, unless otherwise stated, the DPPA spectrum has been subtracted from that measured, in order to reveal the features due to the valinomycin. The prominent peaks in curve (a) at 1756 cm^{-1} and 1662 cm^{-1} correspond to the ester ν(C=O) band and the amide I ν(C=O) band, respectively. These bands are approximately those for the cast film of valinomycin cf. 1754 cm^{-1} and 1658 cm^{-1}, respectively. Spectrum (b) of figure 7.11 shows the effect of immersing the LB membrane in a solution of 0.1 M KCl for 10 minutes (the spectrum was measured in air after exposure to KCl and, again, the phospholipid spectrum has been subtracted). There is little change in position of either of the two main IR bands after 10 minutes in solution. However, after a total of 30 minutes exposure (spectrum (c)) a distinct shoulder has appeared in the ester band at 1746 cm^{-1}. This is accompanied by a small shift to a lower wavenumber of the amide I band to 1658 cm^{-1}. These effects are evidence for the formation of the valinomycin/potassium complex. The amount of complexation is small due to the small shift of the amide I band. The small absorption at approximately 1724 cm^{-1} in spectra (b) and (c) of figure 7.11 could possibly be assigned to a perturbation of the ester ν(C=O) groups of the DPPA by
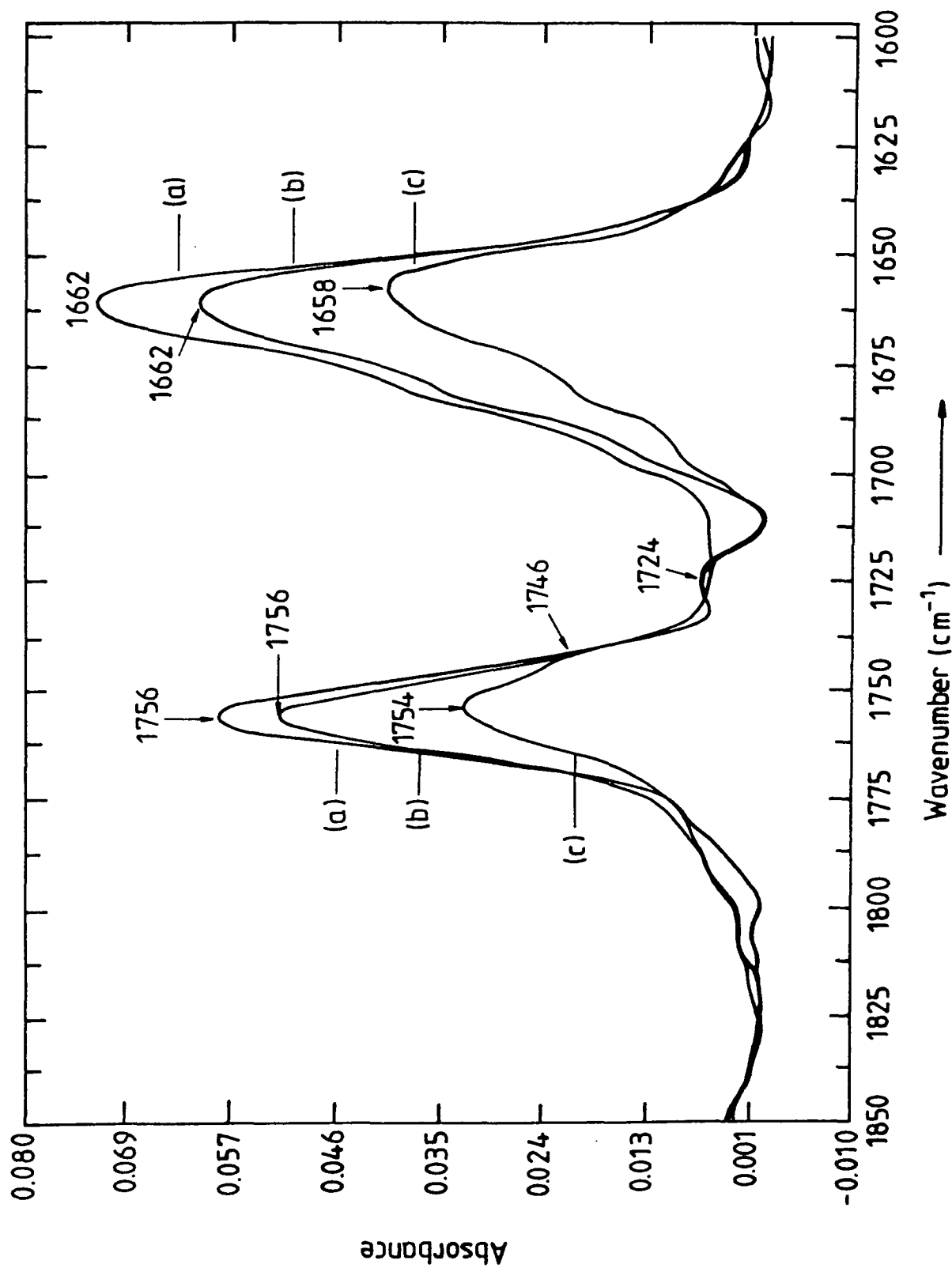
Figure 7.11 Effects of immersion in KCl solutions on 10 layers of a 1:1 (molar) DPPA/valinomycin
LB film: (a) as dipped, (b) after 10 min in 0.1 M KCl and (c) after a further 20 min.

interaction with, (or rearrangement due to) the valinomycin/potassium complex.

If the LB sample is further immersed in 1.0 M KCl, the complexation is now clearly seen. Figure 7.12, spectrum (d), was obtained after 10 minutes in the more concentrated potassium solution. The presence of two distinct peaks in the ester $\nu(C=O)$ region shows that both complexed and uncomplexed valinomycin are present in the film. At this stage it is interesting to note the effect of KCl concentration on the rate of valinomycin complexation. From the intensity of the band at 1746 cm^{-1} it is clear that more complexation occurred in 10 min in 1.0 M KCl than occurred in a 30 min immersion in 0.1 M KCl, and empirically increasing the KCl concentration increases the rate of valinomycin complexation.

7.6.2 Observation of dissociation

The final spectrum, curve (e) of figure 7.12, shows the result of a subsequent period of 10 minutes immersion in deionised water. The effect is marked, the band at 1746 cm^{-1} has now disappeared and furthermore the amide I band undergoes a small shift to a greater wavenumber. From these two pieces of evidence, it can be concluded that the potassium complex has dissociated. The only ester $\nu(C=O)$ band evident is that representing uncomplexed valinomycin at 1753 cm^{-1}. The shift is not completely back to 1756 cm^{-1} indicating that complexed material remains. This result is in contrast to the previous work described on valinomycin/arachidic acid mixtures, in which dissociation was not observed. The mixed phospholipid/ionophore system is behaving as a real biological membrane with both association and dissociation of the complex occurring. The reversibility of the mixed system is attributed to the more flexible nature of the phospholipid matrix. It is suggested that a simple fatty acid or fatty acid salt film will hold the valinomycin complex rigidly and thus not allow the dissociation to take place. When the potassium selectivity of valinomycin is exploited, the ionophore is cast in a polymer matrix that contains a considerable proportion of plasticiser (which presumably allows for microscopic flexibility of the matrix).
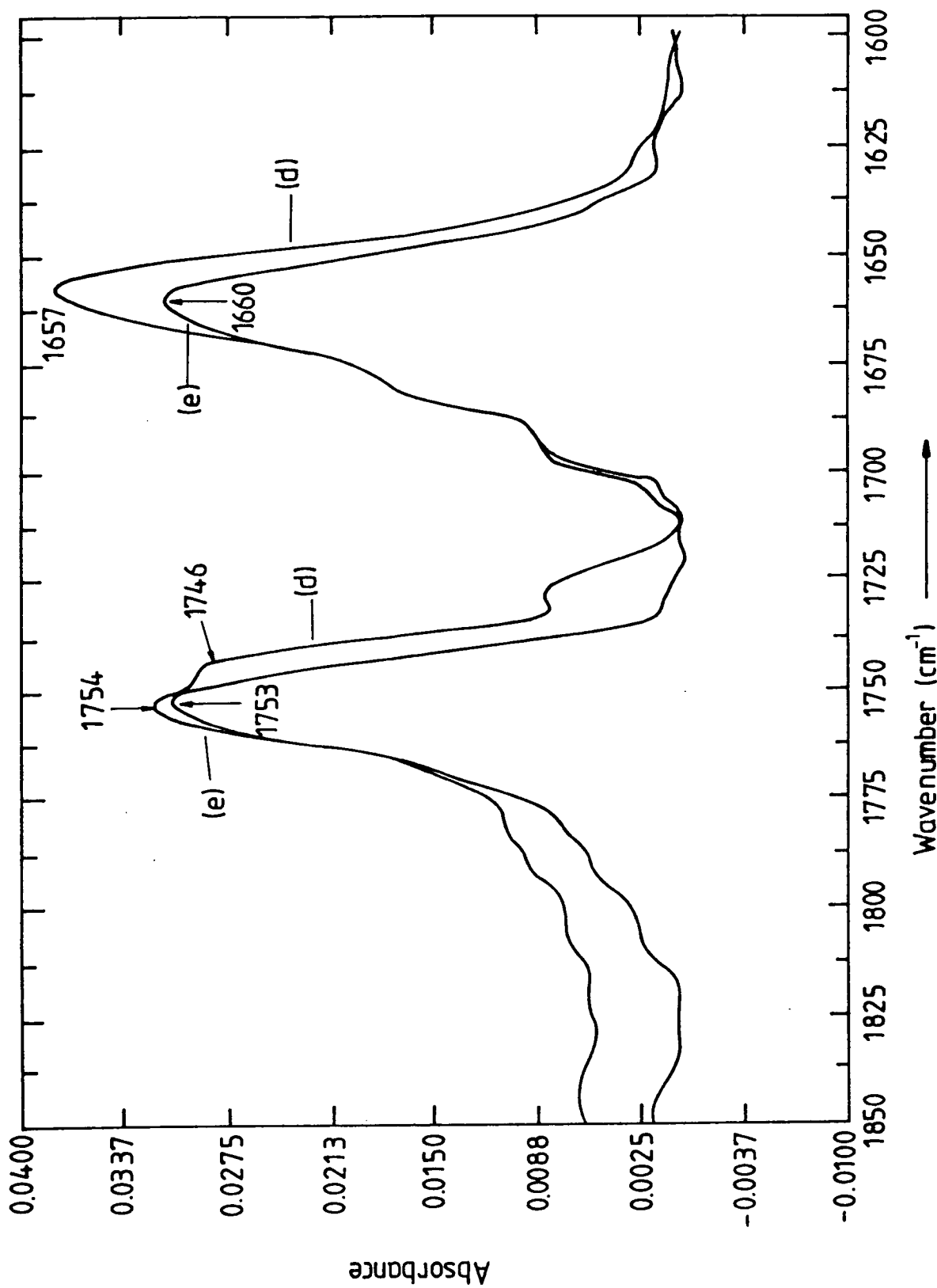
Figure 7.12 Continuation of figure 7.11, (d) after a further 10 min in 1.0 M KCl and (e) after a subsequent period of 10 min in deionised water.

7.6.3 Other mixed phospholipid/valinomycin systems

Figure 7.13 shows the changing valinomycin spectra when 10 layers of a 10:1 DPPA/valinomycin mixture is exposed to first of all 0.1 M KCl and then subsequently to deionised water. Spectrum (a) represents the state of the LB film after dipping, and the valinomycin ester $\nu(C=O)$, and amide I bands are evident. After 5 minutes immersion in 0.1 M KCl (spectrum (b)), complexation has occurred and this is indicated by the appearance of a band at 1747 cm^{-1}. The shoulder at 1754 cm^{-1} indicates that uncomplexed material still remains. From this data, the effect of the mole-fraction of DPPA on the rate of complexation is clear (compare figure 7.11, spectrum (b) which represents the 1:1 mixture in 0.1 M KCl for 10 min). As with the arachidic acid/valinomycin mixtures, increasing the mole fraction of the matrix molecule increases the rate of complexation. After 5 min in water (spectrum not shown), no decomplexation has occurred. However, after a period of 20 min (spectrum (c)) dissociation is now observable with the increase in intensity of the 1754 cm^{-1} band.

Hence, both association and dissociation of the complex appear to occur in both the 10:1 and 1:1 mixed phospholipid/valinomycin systems. However, it is apparent from figures 7.11, 7.12 and 7.13 that the intensities of the ester and the amide I bands decrease as the LB membrane is left in either the KCl solution or the water, indicating a loss of the ionophore. Furthermore, less of the DPPA needs to be subtracted from the measured IR spectra to reveal the valinomycin bands. This implies the phospholipid is also disappearing from the film. In the studies of the arachidic acid/valinomycin mixtures, although structural changes in the fatty acid occurred, no loss of material of either component was observed.

Therefore, in an attempt to prevent the DPPA (and valinomycin) leaving the film, a three component DPPA/arachidic acid/valinomycin mixture was prepared. The films were deposited at a surface pressure of 23 mN m^{-1} on a calcium ion (Ca^{2+}) containing subphase, and therefore the film is composed of the Ca^{2+} salts of the fatty acid-type components.
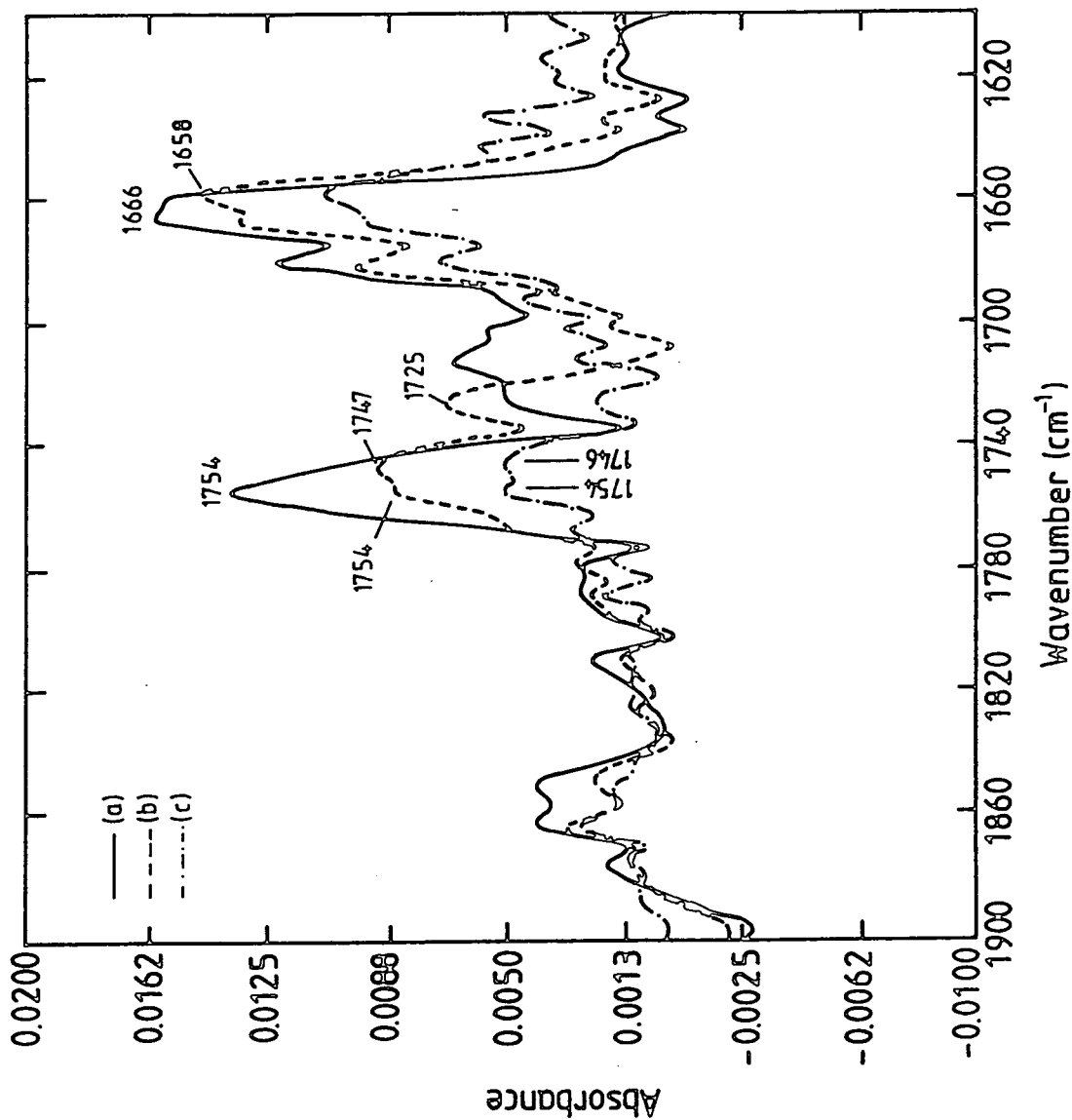
Figure 7.13 The changing valinomycin spectra when 10 layers of a 10:1 (molar) DPPA/valinomycin LB film is exposed to KCl solutions: (a) as dipped, (b) after 5 min in 0.1 M KCl, and (c) after a subsequent period of 20 min in water.

Figure 7.14, spectrum (a) is the ATR-IR spectrum for a 10:5:3 DPPA/A/valin-omycin mixture immediately after dipping. In such a film approximately equal areas are occupied by the "fatty acid-type" molecules and the valinomycin molecules. Furthermore, the number of arachidic acid molecules is twice that of the phospholipid molecules to take into account their relative molecular areas. After 10 seconds in 0.1 M KCl (spectrum (b)), the complexation is advanced and easily observed from the shift of the ester and amide I bands. After a further 15 min (spectrum not shown) no further complexation has taken place. Furthermore, there is no loss in intensity of the valinomycin bands as a function of time and this is clear evidence that the ionophore is not being lost from the film. However, after 5 min in pure water (spectrum (c)), there is a dramatic loss of both components (DPPA and valinomycin). A small amount of dissociation has also occurred but this is only fleetingly observed due to the sudden loss in material. The intensity of the calcium arachidate band (which has been subtracted from figure 7.14) remained constant during both KCl and water immersions indicating that no loss of fatty acid material occurred. This is consistent with the results on the A/VM mixtures described previously.

In conclusion, this three component mixed system exhibits complexation and dissociation. However, compared to the two component system there is reduced dissociation because of the deleterious effect of the addition of the fatty acid component. Furthermore, the loss of both DPPA and valinomycin is reduced on complexation but both components are substantially lost during the immersion in water. The band at 1727 cm^{-1} (which is present in all the spectra obtained from the phospholipid/ionophore systems) again appears upon complexation.

Preliminary work on a further system has also been undertaken. A cross-section through the LB structure is shown in the inset to figure 7.15. In order to trap the DPPA and valinomycin, two layers of arachidic acid were deposited on top of the 10 layers of a 5:1 DPPA/valinomycin mixture. Figure 7.15 also presents the relevant spectra. Spectrum (a) represents the as-dipped sample with
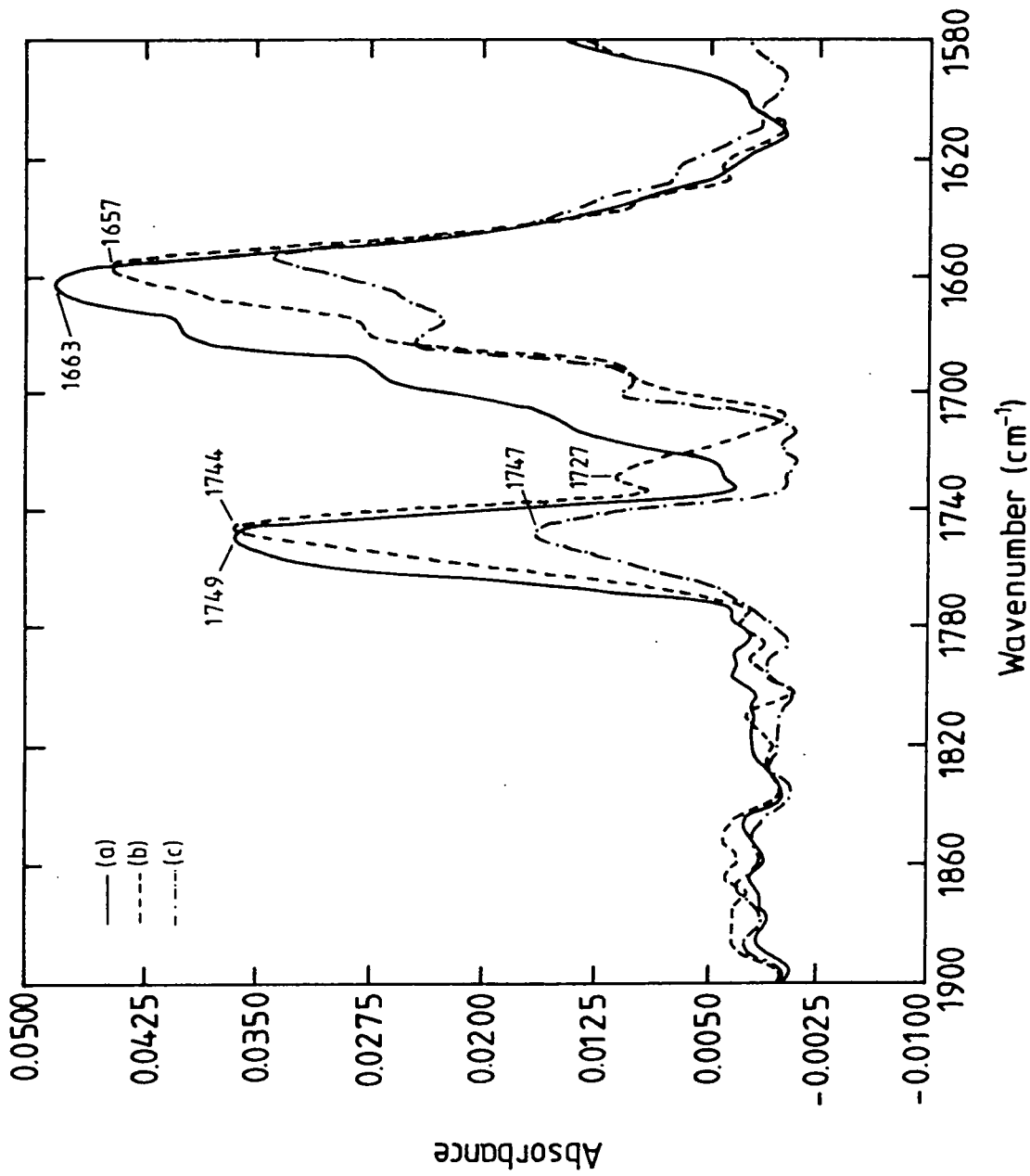
Figure 7.14 The valinomycin spectra for a 10:5:3 arachidic acid/DPPA/valinomycin mixture: (a) as dipped, (b) after 10 seconds in 0.1 M KCl and (c) after a subsequent immersion for 5 min in deionised water.
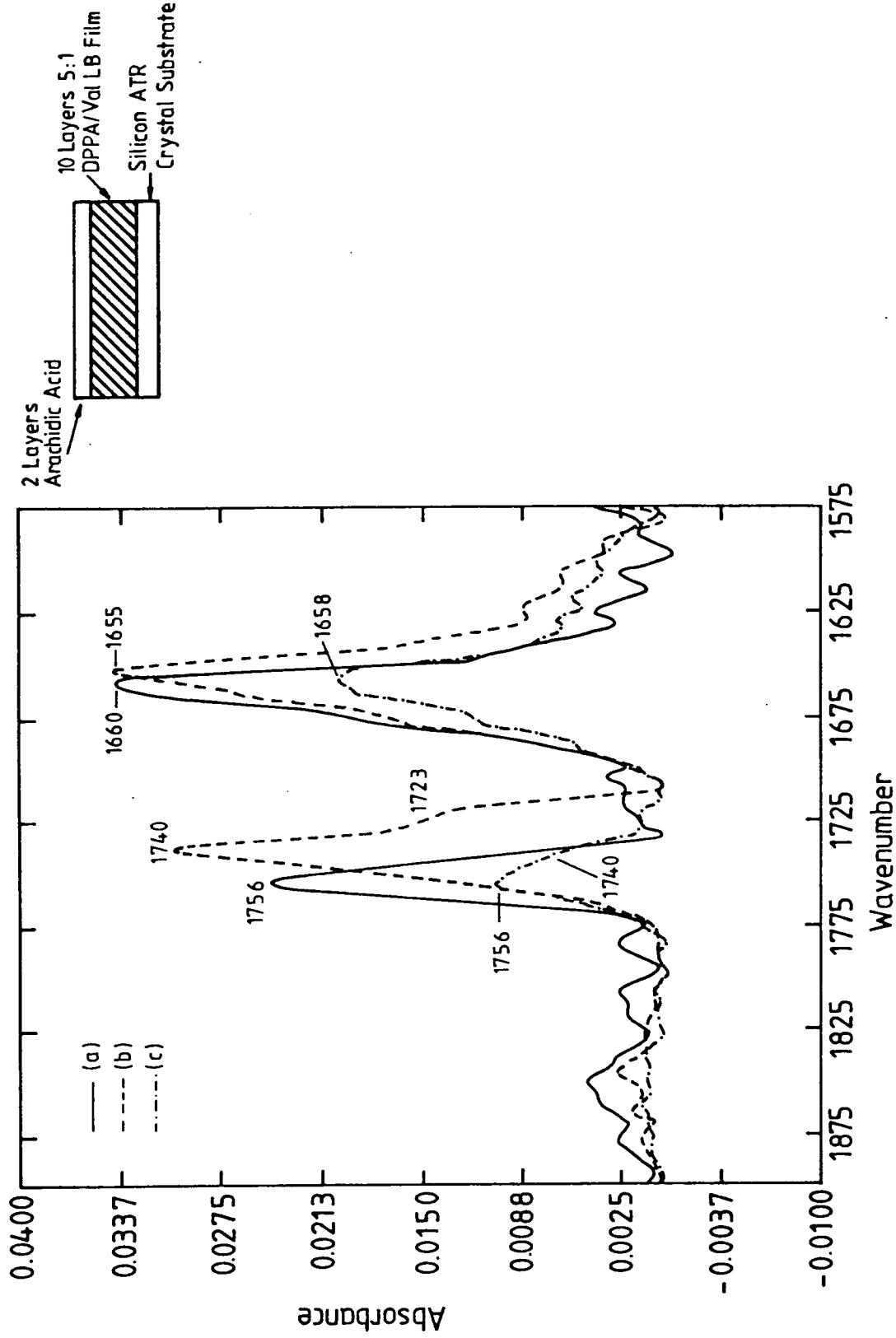
Figure 7.15 A 5:1 (molar) DPPA/valinomycin system capped with 2 layers of arachidic acid. The spectra are as follows: (a) as dipped, (b) after 1 min in a 1 M KCl solution and finally (c) after a subsequent period of 5 min in pure water. The inset shows the cross-section through the LB film structure.

both the DPPA and the arachidic acid spectra subtracted for clarity. After a total of 2 min immersion in 0.1 M KCl (spectrum not shown), no complexation is evident. After a subsequent immersion of 1 min in a 1 M KCl solution (spectrum (b)), the complexation is advanced. Finally, after 5 min in water (spectrum (c)), an advanced state of decomplexation (compared to the mixed three-component system) is observed. However, there is still a marked reduction in the intensity of the valinomycin bands suggesting loss of the ionophore. DPPA is also lost from the film.

Therefore, in this system, as well as in the mixed three-component system, the loss of DPPA and valinomycin upon complexation is reduced. However, upon immersion in water the loss of material is just as great. An advantage of this system is that, with the arachidic acid being removed from the mixture, decomplexation is once again favoured. On the other hand, addition of two layers of arachidic acid as a trapping layer hinders the complexation process. Experiments with arachidic acid layers up to 20 monolayers in thickness suggest that there is no material loss for immersions in KCl. The results also suggest that the complexation process becomes slower as the thickness of the capping layer increases.

It is evident from the ATR spectra of these phospholipid/valinomycin mixed LB systems that as the mole-fraction of DPPA increases so does the amount of spectral noise. The noise has been linked to the presence of trapped water in the LB film, and hence, this demonstrates the affinity of DPPA for water. It is therefore quite conceivable that upon complexation, as the valinomycin adopts its tighter conformation, the film is "opened-up". The resulting "open" structure might easily be penetrated by water molecules (attracted by the DPPA head groups) leading to a less stable LB film. If the phospholipid/valinomycin mixed LB systems in their uncomplexed state are first of all immersed in water, no degradation of the film is observed. A rapid loss of both components is only observed when an LB film in the complexed state is immersed in deionised water. The loss of material is therefore intimately related to the decomplexation process.

At the present time, the processes responsible for the loss of organic material are not fully understood.

7.7 SUMMARY

In conclusion, valinomycin-containing Langmuir-Blodgett films have been prepared. The structural changes occurring in these films when they are exposed to KCl solutions have been analysed using Fourier transform infrared ATR spectroscopy. Pure valinomycin films, either of the Langmuir-Blodgett type or the cast type do not undergo complexation. A detailed examination has revealed that, in order to complex with potassium ions, valinomycin must be mixed with a secondary component, e.g. arachidic acid. Significant complexation occurred after 1 min, but more interesting and profound structural changes in the arachidic acid matrix have been inferred from the IR spectra. A marked decrease in intensity of the acid dimer $\nu(C{=}O)$ band and enhancement of the $\nu(CH_2)$ bands suggest structural changes in the arachidic acid hydrocarbon chains and acid head groups, possibly reflecting the migration of valinomycin molecules towards the polar acid head groups. The connection with potassium transport is obvious and demonstrates the close resemblance of the mixed LB film system with the biological membrane. However, an important distinction is that dissociation of the VM/K^+ complex does not occur in the mixed arachidic acid/valinomycin system.

To model the biological membrane more closely, the fatty acid (arachidic acid) component was replaced by the phospholipid molecule L-α-phosphatidic acid dipalmitoyl (DPPA). This molecule was chosen for its superior dipping properties compared to other phospholipid molecules. The properties of this mixed system are also described. Infrared spectroscopy reveals that the VM/K^+ is formed and in contrast to the above system, dissociation of the complex was also observed. However, for this two-component system a significant loss of both components occurs when the films are immersed in KCl solutions and water. The loss of material in KCl can be reduced by the introduction of arachidic acid to form a

three-component system. However, this has a deleterious effect on the dissociation of the complex. Incorporating the arachidic acid as a capping layer on top of a two-component (phospholipid/valinomycin) LB system enhances the decomplexation but hinders complexation, presumably by preventing the penetration of potassium ions into the potassium-selective portion of the structure. The loss of material in these systems has been linked to the process of decomplexation, since uncomplexed films immersed in water show no signs of degradation. Finally, from the work presented here, it is difficult to quantify the degree of complexation (especially in the phospholipid-based systems where the band intensities are changing as a function of material lost) and to establish a time period for complexation. Clearly, both these are important parameters. However, empirically the following trends have been found for all the systems described. Firstly, the speed of complexation decreases as the mole-fraction of valinomycin in the mixed system increases, and secondly, this parameter increases with increasing potassium concentration.

CHAPTER 8

CONCLUSIONS

8.1 SUMMARY

The LB technique has been successfully used to fabricate ultra-thin organic films which are selective to potassium ions. The ionophore used for the potassium sensing was the macrocyclic depsipeptide, valinomycin. The work presented in this thesis has concentrated on two specific mixed component LB systems, namely arachidic acid/valinomycin and L-α-phosphatidic acid dipalmitoyl/valinomycin. The research has highlighted certain advantages and disadvantages of each system.

The deposition and characterisation of Langmuir-Blodgett films of pure valinomycin has been carried out. The isotherm of the pure ionophore is unusual in that it exhibits a plateau region before the onset of a steep solid-like region. It has been proposed that the plateau represents the condensation of a highly incompressible phase from a highly compressible phase in which the majority of the valinomycin molecules are oriented in stacks with their planes perpendicular to the water surface. The deposition of multilayers of valinomycin onto a variety of substrates is possible if and only if the substrate is initially coated with a few layers of a fatty acid or fatty acid salt. Reproducible Y-type deposition was possible onto both the hydrocarbon chain and the carboxylic head group of the fatty acid. FTIR spectroscopy, UV-spectrophotometry and ellipsometry indicate good reproducibility. However, a detailed ellipsometric study of valinomycin multilayers reveals a thickness profile in the direction of dipping. The average thickness per monolayer varies in a monotonic fashion along the substrate. The processes that are responsible for the thickness reproducibility both parallel to and perpendicular to the dipping direction are, at present, not fully understood.

A detailed study of the interaction between valinomycin-containing Langmuir-Blodgett films with aqueous potassium solutions was undertaken. The probe for

116

this investigation was attenuated total reflection Fourier transform infra red (ATR-FTIR) spectroscopy which has been demonstrated to have the required sensitivity to look at ultra-thin films. Thin films (of any kind) of pure valinomycin have not been previously reported in the literature. Therefore it was interesting to investigate the interaction of LB films of the pure ionophore with KCl solutions. Interestingly no complexation with potassium ions was observed for these films (as well as for cast films). The reason for this is possibly related to the fact that the valinomycin molecules are surrounded by themselves. This unusual environment might force the ionophore to adopt a conformation which is not suitable for complexation.

The research has revealed that, in order to complex with K^+, valinomycin must be mixed with a secondary component. The arachidic acid/valinomycin system was first of all investigated. Significant complexation was found to occur after one minute. Furthermore, profound structural changes in the fatty acid matrix were also observed. They have been interpreted as possibly reflecting the migration of valinomycin molecules from the hydrophobic regions of the LB structure towards the polar acid head groups. Unfortunately, the dissociation of the VM/K^+ complex was not observed in this mixed system.

The system described above represents a simple model for the biological membrane with the distinction that decomplexation does not occur. To produce a more realistic model the fatty acid was replaced by the phospholipid molecule, L-α-phosphatidic acid dipalmitoyl (DPPA). In this system IR spectroscopy identified both formation and dissociation of the VM/K^+ complex. The disadvantage of this system was the significant loss of both components upon immersion in KCl solutions and water. A number of attempts have been made to reduce this loss. A three component system of arachidic acid, valinomycin and DPPA, was investigated. The loss of material in KCl was reduced, however, the inclusion of the fatty acid had a deleterious effect on the dissociation of the complex. Another system, incorporating an arachidic acid film as a capping layer for the DPPA/valinomycin

structure, has improved the decomplexation properties but, at the same time, the complexation process is hindered.

Deposition of LB films onto the gate surface of an ISFET has also been demonstrated. Reproducible deposition onto the surface of mounted SOS ISFETs is possible, and has been confirmed by infrared transmission spectroscopy. The deposition of a variety of LB films shows no effect on the pH responses of these devices. This has been interpreted as illustrating the fact that LB films provide no barrier to the potential determining H^+ and OH^- ions. They are able to participate in the silanol reactions on the Si_3N_4 surface, which are responsible for the pH response of the device, as if no LB film were present.

Attempts at incorporating the potassium selective LB film systems described above with an ISFET have been largely unsuccessful. Intial experiments, concerned with the pure valinomycin films, exhibited no potassium response that could be associated with the ionophore. The subsequent ATR-IR investigation of the interaction of these films with KCl showed that complexation did not occur, and hence explained the observed ISFET results. Similarly, for the mixed arachidic acid/valinomycin system, no response was observed and a possible reason for this, in terms of the absence of decomplexation in these films, has been proposed. The responses of the ISFET devices coated with the DPPA/valinomycin based systems, at the time of writing, have not been evaluated.

8.1 SUGGESTIONS FOR FURTHER WORK

As a result of the present work, ultra-thin Langmuir-Blodgett films incorporating the ionophore valinomycin have been fabricated, and have been demonstrated to undergo complexation with potassium ions when immersed in aqueous potassium containing solutions. Furthermore, dissociation of the complex occurs when the films are immersed in water, but unfortunately loss of the film into solution occurs. Future work should address this problem. Present thinking suggests that the problem is associated partly with the hydrophilic nature, and partly with

118

the flexibility of the phospholipid matrix. It is proposed that the ionophore requires a flexible matrix in order to dissociate (cf. the rigid arachidic acid-based system) but, at the same time, the flexibility of the phospholipid coupled with its hydrophilic nature leads to an unstable matrix when immersed in an aqueous solution. The problem might be solved using phospholipids that have polymerisable, diacetylene units incorporated into their alkyl chains. This should certainly produce a more stable film when the deposited LB film is cross-linked, however, the effect of the loss in flexibility on the dissociation properties of this system will require investigation.

In addition to investigating the problem of stability of the LB films, future work should also concentrate on the incorporation of the DPPA/valinomycin based systems with the ISFET devices. Once the problem of stability of these films has been solved, the K^+-response of such devices can be evaluated. The optimisation of parameters, such as, the mole-fraction of the phospholipid in the mixed film and the thickness of the arachidic acid capping layer, can be undertaken. The device assessment of these films can be carried out in parallel with the equivalent IR spectroscopic studies.

Furthermore, new materials should be investigated. For example, different ionophores, such as, monensin (which is Na^+ selective) or A23187 (which is Ca^{2+} selective), might be incorporated into LB films, and subsequently integrated with the ISFET device. The possibility exists for immobilising urease and glucose-oxidase in LB film form, thus creating a new type of enzyme sensor. Also, the LB technique might be used to fabricate films of materials which would be difficult to deposit by any other means, such as, antibody/antigen materials and highly specific and reversible receptor proteins.

The present work has also highlighted the technique of ATR-IR spectroscopy for probing ultra-thin Langmuir-Blodgett films. The technique has revealed valuable information concerning decomplexation, and the associated structural changes in valinomycin based systems. Further fundamental work can be carried

out. For example, investigations concerning the following might be undertaken: the molecular interactions responsible for the behaviour of pure valinomycin films, the effect of different matrix molecules, and the behaviour of systems incorporating a hydrophilic acid head group as the outermost layer.

REFERENCES

CHAPTER 1

1. P. Bergveld, IEE Trans., **BME-17**, 70 (1970).

2. P. Bergveld, IEE Trans., **BME-19**, 342 (1972).

3. G. Eisenman, "Glass electrodes for hydrogen and other cations", Dekker, 1967.

4. R. P. Buck and V. R. Shepherd, Anal. Chem., **46**, 2097 (1974).

5. T. A. Fjeldy, K. Nagy and B. Stark, Sens. and Actuators, **3**, 111 (1983).

6. S. D. Moss, J. Janata and C. C. Johnson, Anal. Chem., **47**, 2238 (1975).

7. M. M. Shemyakin, Yu. A. Ovchinnikov, V. T. Ivanov, V. K. Antonov, E. I. Vinogradova, A. M. Shkrob, G. G. Malenkov, A. V. Evstratov, I. A. Laine, E. I. Melnik and I. D. Ryabora, J. Membr. Biol., **1**, 402 (1969).

8. G. G. Stark and R. Benz, J. Membr. Biol., **5**, 133 (1971).

9. R. H. Tredgold, Rep. Prog. Phys., **50**, 1609 (1987).

10. G. G. Roberts, Advances in Physics, **34**, 475 (1985).

11. M. C. Petty in "Polymer surfaces and Interfaces" (Chapter 9), ed. W. J. Feast and H. S. Munro, Wiley (1987).

CHAPTER 2

1. M. Brockman, Ber., **88**, 77 (1955).

2. M. M. Shemyakin, Yu. A. Ovchinnikov, V. T. Ivanov, V. K. Antonov, E. I. Vinogradova, A. M. Shkrob, G. G. Malenkov, A. V. Evstratov, I. A. Laine, E. I. Melnik and I. D. Ryabora, J. Membr. Biol., **1**, 402 (1969).

3. G. Stark and R. Benz, J. Membr. Biol, **5**, 133 (1971).

4. P. Mueller and D. O. Rubin, Biochem. Biophys. Res. Commun., **26**, 398 (1967).

5. G. D. Smith, W. L. Duax, D. A. Lengs, G. T. DeTitta, J. W. Edmonds, D. C. Rohrer and C. M. Weeks, J. Am. Chem. Soc., **97**, 7242 (1975).

6. W. L. Duax, H. Hauptman, C. M. Weeks and D. A. Norton, Science, **176**, 911 (1972).

7. I. M. Asher, K. J. Rothschild, E. Anastassakis and H. E. Stanley, J. Am. Chem. Soc., **99**, 2024 (1977).

8. K. J. Rothschild, I. M. Asher, H. E. Stanley and E. Anastassakis, J. Am. Chem. Soc., **99**, 2032 (1977).

9. K. Neupert-Laves and M. Dolber, Helv. Chem. Acta., **58**, 432 (1975).

10. I. M. Asher, K. J. Rothschild and H. E. Stanley, J. Mol. Biol., **89**, 205 (1974).

11. D. H. Haynes, A. Kowalsky and B. C. Pressman, J. Biol. Chem., **244**, 502 (1969).

12. J. D. Robertson, Ann. N. Y. Acad. Sci., **137**, 421 (1966).

13. D. F. Wallach and P. H. Zahler, Proc. Nat. Acad. Sci. U. S., **56**, 1552 (1966).

14. J. Lenard and S. J. Singer, Proc. Nat. Acad. Sci. U. S., **56**, 1552 (1966).

15. S. J. Singer and G. L. Nicolson, Science, **175**, 720 (1972).

16. B. P. Rosen, "Bacterial Transport" (Chapters 4 and 12), Plenum Press, London and New York, 1978.

17. P. Läuger, Biochem. Biophys. Acta, **552**, 143 (1979).

18. B. C. Pressman, Ann. Rev. Biochem., **45**, 501 (1976).

19. G. G. Stark, B. Ketterer, R. Benz, and P. Läuger, Biophy. J., **11**, 981 (1971).

CHAPTER 3

1. A. S. Grove, "Physics and technology of semiconductor devices", Wiley and Sons (1967).

2. I. Lunström, S. Shivaraman, C. Svensson and L. Lundkvist, Appl. Phys. Lett., **26**, 55 (1975).

3. P. Bergveld, Sens. and Actuators, 8, 109 (1985).

4. P. Bergveld, IEE Trans., **BME-19**, 342 (1972).

5. J. Janata and S. D. Moss, Biomed. Eng. **11**, 241 (1976).

6. J. Koryta, "Ion-selective electrodes", Cambridge University Press (1975).

7. W. M. Siu and R. S. Cobbold, IEE Trans., **ED-26**, 1805 (1979).

8. D. E. Yates, S. Levine and T. W. Healy, J. Chem. Soc., Faraday Trans., **70**, 1807 (1974).

9. K. Dousma, "A colloidal chemical study of the formation of iron oxyhydroxide", Ph. D. Thesis, University of Utrecht (1979).

10. D. L. Chapman, Phil. Mag., **25**, 475 (1913).

11. O. Stern, Z. Electrochem., **30**, 508 (1924).

12. L. Bousse, N. F. de Rooij and P. Bergveld, IEE Trans. **ED-30**, 1263 (1983).

13. A. van den Berg, P. Bergveld, D. N. Reinhout and E. J. R. Sudhölter, Sens. and Actuators, 8, 129 (1985).

14. S. D. Moss, J. Janata and C. C. Johnson, Anal. Chem., **47**, 2238 (1975).

15. A. Sibbald, Proc. IEE I, **130**, 235 (1983).

16. E. J. Fogt, D. F. Untereker and M. S. Norenberg, Anal. Chem., **57**, 1995 (1985).

17. A. D. Brown, Sens. and Actuators, 6, 151 (1984).

CHAPTER 4

1. K. B. Blodgett and I. Langmuir, Phys. Rev., **51**, 964 (1937).

2. P. Fromherz, Rev. Sci. Inst., **46**, 1380 (1975).

3. B. Holcroft, M. C. Petty, G. G. Roberts and G. J. Russell, Thin Solid Films, **134**, 83 (1985).

4. N. Carr, Chemtronics, **1**, 167 (1986).

5. S. Baker, Ph. D. Thesis, University of Durham (1985).

6. S. Baker, M. C. Petty, G. G. Roberts and M. V. Twigg, Thin Solid Films, **99**, 53 (1983).

7. K. Fukuda and T. Shiozawa, Thin Solid Films, **68**, 55 (1980).

8. G. S. Galleti and A. Giuseppi-Elie, Thin Solid Films, **132**, 163 (1985).

9. G. L. Gaines, Jr., "Insoluble monolayers at liquid-gas interfaces", Interscience, New York (1966).

10. P. S. Vincett, W. A. Barlow, F. T. Boyle, J. A. Finney and G. G. Roberts, Thin Solid Films, **60**, 265 (1979).

11. R. Jones, R. H. Tredgold and P. Hodge, Thin Solid Films, **99**, 25 (1983).

12. R. H. Tredgold, S. D. Evans, P. Hodge, R. Jones, N. G. Stocks and M. C. J. Young, British Polymer Journal, **19**, 397 (1987).

13. I. R. Peterson, G. J. Russell and G. G. Roberts, Thin Solid Films, **109**, 371 (1983).

14. G. J. Russell, M. C. Petty, I. R. Peterson, G. G. Roberts, J. P. Lloyd and K. K. Kan, J. Mat. Sci., **3**, 25 (1984).

15. A. Bonnerot, P. A. Chollet, H. Frisby and M. Hoclet, Chem. Phys., **97**, 365 (1985).

16. C. A. Jones, G. J. Russell, M. C. Petty and G. G. Roberts, Phil. Mag. B., **54**, L89 (1986).

17. I. R. Peterson and G. J. Russell, Thin Solid Films, **134**, 143 (1985).

18. G. J. Russell in "Progress in crystal growth and characterization", vol. 5, ed. B. R. Pamplin, Pergamon Press (1982).

19. F. M. Mirabella, Appl. Spectrosc. Rev., **21**, 95 (1985).

20. G. H. Davies and J. Yarwood, J. Spectrochim. Acta, **434**, 1619 (1987).

21. D. den Engelson, J. Opt. Soc. Am., **61**, 1460 (1971).

22. F. Partovi, J. Opt. Soc. Am., **52**, 918 (1962).

23. W. Lesslauer, Acta Cryst. B, **30**, 1927 (1974)

24. M. Pomerantz and A. Segmüller, Thin Solid Films, **68**, 33 (1980).

25. R. H. Tredgold, A. J. Vickers, A. Hoorfer, P. Hodge and E.Khoshdel, J. Phys. D. Appl. Phys., **18**, 1139 (1985).

26. Yu. M. Lvov, D. Svergun, L. A. Feigin, C. Pearson and M. C. Petty, Phil. Mag. Lett., **59**, 317 (1989).

27. A. Sibbald, Proc. IEE I, **130**, 235 (1983).

28. R. D. Beaty in "Concepts, instrumentation and techniques in atomic absorption spectrophotometry, Perkin Elmer Corp. (1978).

CHAPTER 5

1. T. Akiyama, K. Komiya, V. Okabe, T. Sugano and E. Niki, Bunseki Kag., **30**, 754 (1981).

2. A. S. Grove, "Physics and technology of semiconductor devices", Wiley and Sons (1967).

3. L. Vadasz and A. S. Grove, IEEE Trans., **ED-13**, 863 (1966).

4. G. Eisenman, Biophys. J., **2**, 259 (1962).

5. M. Sriyudthsak, H. Yamagishi and T. Moriizumi, Thin Solid Films, **160**, 463 (1988).

6. S. Baker, M. C. Petty, G. G. Roberts and M. V. Twigg, Thin Solid

7. G. Lieser, B. Tieke and G. Wegner, Thin Solid Films, **68**, 77 (1980).

8. A. van den Berg, P. Bergveld, D. N. Reinhout and E. J. R. Sudhölter, Sens. and Actuators, **8**, 129 (1985).

9. T. Matsuo, and H. Nakajima, Sens. and Actuators, **5**, 293 (1984).

10. M. Fujihira, M. Fukui and T. Osa, J. Electroanal. Chem., **106**, 413 (1980).

11. H. Nakajima, M. Esashi and T. Matsuo, J. Electrochem. Soc., **129**, 141 (1982).

CHAPTER 6

1. H. E. Ries, Jr. and H. S. Swift, J. Colloid Interface Science, **64**, 111 (1978).

2. B. M. Abraham and J. B. Ketterson, Langmuir, **1**, 461 (1985).

3. J. B. Peng, B. M. Abraham, P. Dutta, J. B. Ketterson and H. F. Gibbard, Langmuir, **3**, 483 (1988).

4. G. Kemp and C. E. Wenner, Biochem. Biophys. Acta, **282**, 1 (1972).

5. V. A. Howarth, M. C. Petty, G. H. Davies and J. Yarwood, Thin Solid Films, **160**, 483 (1988).

6. G. D. Smith, W. L. Duax, D. A. Lengs, G. T. DeTitta, J. W. Edmonds, D. C. Rohrer and C. M. Weeks, J. Am. Chem. Soc., **97**, 7242 (1975).

7. Yu. A. Ovchinnikov and V. T. Ivanov, Tetrahedron, **31**, 2177 (1975).

8. M. Hsu and S. I. Chan, Biochemistry, **12**, 3872 (1973).

9. R. H. Tredgold, A. J. Vickers, A. Hoorfar, P. Hodge and E. Khoshdel, J. Phys. D: Appl. Phys., **18**, 1139 (1985).

10. M.Petty, by private communication, University of Essex.

11. A. Bonnerot, P. A. Chollet, H. Frisby and M. Hoclet, Chem. Phys., **97**, 365 (1985).

12. C. A. Jones, G. J. Russell, M. C. Petty and G. G. Roberts, Phil. Mag. B., **54**, L89 (1986).

13. A. Boughriet, M. Ladjadj and E. Bicknell-Brown, Biochim. Biophys. Acta., **939**, 523 (1988).

14. L. J. Bellamy, "Infrared spectroscopy of complex molecules", Vol. 1., 348, Chapman and Hall, London (1975).

15. J. F. Rabolt, F. C. Burns, N. E. Schlotter and J. D. Swalen, J. Electron Spectrosc. Relat. Phenom., **30**, 29 (1983).

CHAPTER 7

1. F. M. Mirabella, Appl. Spectrosc. Rev., **21**, 95 (1985).

2. G. H. Davies and J. Yarwood, J. Spectrochim. Acta, **434**, 1619 (1987).

3. I. M. Asher, K. J. Rothschild, E. Anastassakis and H. E. Stanley, J. Am. Chem. Soc., **99**, 2024 (1977).

4. I. M. Asher, K. J. Rothschild and H. E. Stanley, J. Mol. Biol., **89**, 205 (1974).

5. K. J. Rothschild, I. M. Asher, H. E. Stanley and E. Anastassakis, J. Am. Chem. Soc., **99**, 2032 (1977).

6. E. Grell and T. Funck, Eur. J. Biochem., **34**, 415 (1973).

7. M. M. Shemyakin, Yu. A. Ovchinnikov, V. T. Ivanov, V. K. Antonov, E. I. Vinogradova, A. M. Shkrob, G. G. Malenkov, A. V. Evstratov, I. A. Laine, E. I. Melnik and I. D. Ryabora, J. Membr. Biol., **1**, 402 (1969).

8. J. F. Rabolt, F. C. Burns, N. E. Schlotter and J. D. Swalen, J. Electron Spectrosc. Relat. Phenom., **30**, 29 (1983).

9. L. J. Bellamy, "Infrared spectroscopy of complex molecules", Vol. 1., Chapman and Hall, London (1975).

10. P. Meers and G. W. Feigenson, Biochem. Biophys. Acta, **938**, 469 (1988).

11. W. L. Duax, H. Hauptman, C. M. Weeks and D. A. Norton, Science, **176**, 911 (1972).

12. I. Langmuir and V. J. Schaefer, J. Am. Chem. Soc., **60**, 1351 (1938).

13. L. R. McLean, A. A. Durrani, M. A. Whittman, D. S. Johnston and D. Chapman, Thin Solid Films, **99**, 127 (1983).

14. O. Albrecht, D. S. Johnston, C. Villaverde and D. Chapman, Biochem. Biophys. Acta., **687**, 165 (1982).

15. J. P. Green, M. C. Philips and G. G. Shipley, Biochem. Biophys. Acta., **330**, 243 (1973).

16. D. M. Taylor and M. G. B. Mahboubian-Jones, Thin Solid Films, **87**, 167 (1982).

17. R. A. Demel, L. L. M. Van Deenen and B. A. Pethica, Biochem. Biophys. Acta., **135**, 11 (1967).

18. H. Nakahara, K. Fukuda, H. Akutsu and Y. Kyogoku, J. Colloid Interface Sci., **65**, 517 (1978).

19. H. Hasmonay, M. Caillaud and M. Dupreyat, Biochem. Biophys. Res. Comm., **89**, 338 (1979).

APPENDIX 1

PUBLICATIONS

1. V. A. Howarth, M. C. Petty, G. H. Davies and J. Yarwood, "The deposition and characterisation of multilayers of the ionophore valinomycin", Proc. 3rd International Conference on Langmuir-Blodgett films, published in Thin Solid Films, **160**, 483 (1988).

2. V. A. Howarth, M. C. Petty, G. H. Davies and J. Yarwood, "Infrared studies of valinomycin-containing Langmuir-Blodgett films", Langmuir, 5, 330 (1989).

3. V. A. Howarth, D. F. Cui, M. C. Petty, H. Ancelin and J. Yarwood, "Phospholipid-based potassium-selective Langmuir-Blodgett films", Proc. 4th International Conference on Langmuir-Blodgett films (1989), to be published in Thin Solid Films.

4. V. A. Howarth, D. F. Cui, M. C. Petty, H. Ancelin and J. Yarwood, "Structural characterisation of phospholipid Langmuir-Blodgett multilayers containing valinomycin", in preparation.

5. D. F. Cui, V. A. Howarth, M. C. Petty, H. Ancelin and J. Yarwood, "The deposition and characterisation of phosphatidic acid Langmuir-Blodgett films", submitted to Thin Solid Films.